8-2019

In vivo and in vitro approaches to studying the effect of osmolytes on enzymes of the folate pathway

Deepika Nambiar
University of Tennessee, dnambia1@vols.utk.edu

To the Graduate Council:

I am submitting herewith a dissertation written by Deepika Nambiar entitled "In vivo and in vitro approaches to studying the effect of osmolytes on enzymes of the folate pathway." I have examined the final electronic copy of this dissertation for form and content and recommend that it be accepted in partial fulfillment of the requirements for the degree of Doctor of Philosophy, with a major in Biochemistry and Cellular and Molecular Biology.

Gladys Alexandre, Major Professor

We have read this dissertation and recommend its acceptance:

Elizabeth Fozo, Daniel Roberts, Pratul Agarwal

Accepted for the Council:

Dixie L. Thompson

Vice Provost and Dean of the Graduate School

(Original signatures are on file with official student records.)

In vivo and in vitro approaches to studying the effect of osmolytes on enzymes of the folate pathway

A Dissertation Presented for the
Doctor of Philosophy
Degree
The University of Tennessee, Knoxville

Deepika Karunakaran Nambiar
August 2019

DEDICATION

This thesis is dedicated to my parents Mr. Kalikottu Veetil Karunakaran and Mrs. Pushpa Karunakaran. They have always encouraged and supported me to go after what I desire and made me the strong individual I am today. I dedicate this thesis to my sister Mrs. Savitha Vinod, brother-in-law Mr. Vinod Vijayan and nieces Anoushka Vinod and Aadvieka Vinod for their unconditional love and support. I also dedicate this thesis to my advisor and mentor, the late Dr. Elizabeth Howell, who guided me through my graduate school journey not just by guiding me through my research project but also through graduate school life, never giving up on me with her can-do attitude and by constantly making science fun.

ACKNOWLEDGEMENTS

I want to acknowledge my advisor and mentor Dr Elizabeth Howell. Liz had been my greatest supporter in graduate school and was truly inspirational. She helped me maneuver though my graduate life not just by helping me learn and understand biochemistry and the research projects but also by helping me through graduate school life. She always encouraged and supported my extracurricular activities and attended several of my dance shows. She always found time to listen and help me with my research talks to scientific and nonscientific audience. She was great lover of art and an expert in clay work. I have thoroughly enjoyed the clay bowl making sessions during summer semester. Liz passed away on 9th April 2019 and will be missed badly. Liz had a "can-do" attitude and was a huge supporter of women in science and a great mentor. I would like to honor her by learning from her teaching methods and will try to support other curious minds by being a mentor myself.

I would like to acknowledge my chair and committee member, Dr. Gladys Alexandre for stepping in place of Liz. She has taken care of the Howell lab and provided support in times of need. I truly appreciate all the help and guidance I have received for my finishing my PhD work and starting an internship with Unilever. I would like to thank Dr. Elizabeth Fozo along with Gladys for all the helpful suggestions I received for my work on *in vivo* titration of enzymes. Your insights into the microbial world has helped us publish my first PhD paper. I would also like to thank Dr. Daniel Roberts and Dr. Pratul Agarwal for stepping in, guiding and helping me with my graduation work. I appreciate Dr. Agarwal for all the helpful discussion during lab meetings and setting up of dihydropteroate synthase computational work for my thesis.

I would like to thank the Howell lab, Dr. Michael Duff Jr. and Gabriel Fuente for being supportive and friendly. I have enjoyed our scientific discussion and nonscientific banters and all those fun times we had during lab meetings, lunches, get togethers, picnics and holiday celebrations. I would especially like to thank Mike who has been my mentor and has helped me throughout my PhD coursework while answering all my research questions and helping me with my experiments. He has been my greatest supporter when Liz wasn't around. I would also like to thank Mike for his help in setting up and analysis of the MD simulations for Chapter 3. I have had the honor to mentor several undergrads during my PhD. I would like to thank my mentees Robert Shew, Bryan Schwarz, Carla Arrieta, Carolyn Ware, Ojaswini Sharma, Creighton Kellum, Mannal Abbas and Alex for working alongside me and helping me collect some wonderful data.

I would like to thank my friends in Knoxville without whom my PhD life would not have been as interesting. A shout out to Seda Kocaman, Riddhi Shah, Mustafa Murat, Khusbhoo Bafna, Shantanu Shukla, Arkadipta Bakshi, Ishan Gaud, Eshita Kalia, Jennifer Gryder and Tracy Ferrell for all the great fun in Knoxville. I would also like to thank my friends back home in India, especially to Priya Pakhare and Rakesh Nair who have spent sleepless nights helping me and for just being there when I've needed them. I would also like to thank Crossfit Bearden for introducing me to crossfit as a great de-stressor and being a friendly workout community. I would like to thank Unilever Trumbull for believing

in me and giving me the opportunity to intern with them over Summer 2019. It is a great work environment and I have learnt a lot from my short time here.

Most of all, I want to thank my strongest pillar of support - my family. Dad, mom, Savi, Jiju and my two little munchkins, this would not have been possible without you!

ABSTRACT

The cell is a heterogenous, complex environment, while macromolecules are usually studied in dilute solutions. Our lab, as well as many others, has identified several types of weak, solvating, “quinary” interactions that change the behavior of enzymes. One group of molecules that participate in weak interactions are osmolytes. Osmolytes are small molecules involved in osmoregulation in the cell. Previous *in vitro* studies have identified that osmolytes, including trehalose, preferentially interact with folate, thereby reducing the association of the ligand to *E. coli* chromosomal and R67 plasmid dihydrofolate reductases. We have employed vapor pressure osmometry to study the weak interactions of trehalose with different atom types on folate. The study indicated trehalose preferentially interacts with phosphate and amide oxygens, but is preferentially excluded from the other atom types. We were able to calculate the predicted preferential interaction coefficient of trehalose with folate and these results concurred with our experimental results.

The effect of different osmolytes on the affinity of PtPP and pABA for dihydropteroate synthase was measured by isothermal titration calorimetry. Trehalose and sucrose weakened binding of PtPP to DHPS, and tightened pABA binding. The rest of the osmolytes had opposite effects on ligand binding. The data suggested this pattern was due to the preferential interaction of trehalose with PtPP and exclusion from pABA. For the other osmolytes, there was preferential exclusion from pABA, but preferential interaction with PtPP. Weak osmolyte interactions with ligands weakened their binding to DHPS.

We employed an osmotic stress approach to understand the role and relevance of these weak interactions between osmolytes and ligands *in vivo*. The activities of the enzymes R67 dihydrofolate reductase, methylenetetrahydrofolate reductase, serine hydroxymethyl transferase and chorismate mutase could be titrated by increasing osmotic stress. One reason for titration of enzyme activity was that the osmolytes produced in the cell participated in weak interactions with reduced folates, thereby preventing their association to their respective enzyme. Lesser product formation led to decreased cell growth in these auxotrophic cells. The titration of enzyme activity the cell with osmotic stress indicates that the weak interactions between osmolytes *in vitro* may also occur *in vivo*.

TABLE OF CONTENTS

LIST OF TABLES

LIST OF FIGURES

1. INTRODUCTION AND GENERAL INFORMATION

1.1 Folic acid and its importance

Folate (Vitamin B9) is made up of a pteridine ring, a *para*-amino benzoate (*p*ABA) moiety and a glutamate tail (Figure 1.1). Most bacteria, plants and fungi synthesize folates using guanosine triphosphate (GTP) and chorismate as the starting material. Higher animals are unable to produce their own folates, rather they acquire them through dietary intake. Tetrahydrofolate (THF) is a reduced form of folate that goes through a series of one-carbon transfer reactions that leads to the formation of essential amino acids and nucleotide precursors. The enzymes that metabolize folates make up the folate cycle pathway. A deficiency or malfunctioning of this pathway in humans can lead to various diseases such as neural tube defects, cardiovascular diseases and cancer [1]. Since humans do not possess the enzymes to synthesize folates *de novo*, the folate biosynthetic pathway is an attractive candidate for design of antibacterial drugs.

The folate cycle begins with the formation of the pterin ring using GTP as the precursor [2]. The pterin ring undergoes various modifications to create an intermediate, 6-hydroxymethyl-7, 8-dihydropterin pyrophosphate (H_2PtPP). The next step involves the cleavage of the pyrophosphate and joining of the pterin moiety to *p*ABA to form dihydropteroate. This reaction is catalyzed by dihydropteroate synthase (DHPS). Addition of a glutamate tail to dihydropteroate leads to the formation of dihydrofolate (DHF). DHF is reduced to THF through the action of dihydrofolate reductase (DHFR) using NADPH as the cofactor. Other reduced folates are synthesized from THF and they feed into the one carbon metabolic pathway according to the positioning of their carbon groups [2]. Serine hydroxymethyltransferase (SHMT) uses THF to convert serine into glycine along with 5, 10-methyleneTHF. Methylenetetrahydrofolate reductase (MTHFR) catalyzes the reduction of 5, 10-methyleneTHF to 5-methylTHF. Methionine synthase then forms methionine using 5-methylTHF and homocysteine, this is how the folate cycle leads into the methionine cycle [3]. An abbreviated version of the folic acid pathway is shown in Figure 1.2.

1.2 Cellular crowding

My thesis focuses on understanding how the folate pathway enzymes function in the presence of weak interactions *in vivo* and *in vitro*. The cellular environment of E*scherichia coli* is complex, with a concentration of ~300 mg/l of macromolecules, which occupies an estimated 30% of the cell volume [4]. The enzyme kinetics of the folate pathway are typically studied *in vitro* which is very different from the crowded cellular environment. Attractive and repulsive forces between macromolecules exist in the cell and these affect cellular reactions. The magnitude of the effects are strongly dependent upon the relative sizes, shapes, and charges of concentrated crowding macromolecules [5].

Water molecules present at the binding surfaces influence the interactions between macromolecules. Our lab studies the role of water on ligand and cofactor binding to

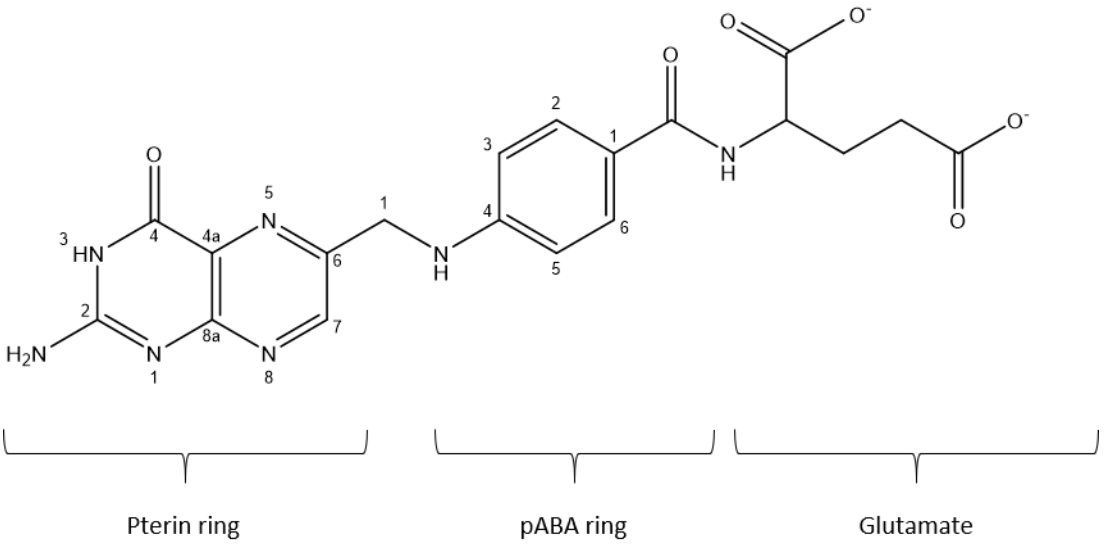

Figure 1.1: Structure of folate

The folate molecule has a pteridine ring, pABA ring and glutamate tail. The folate atoms are numbered as per their position on the pteridine or pABA ring.

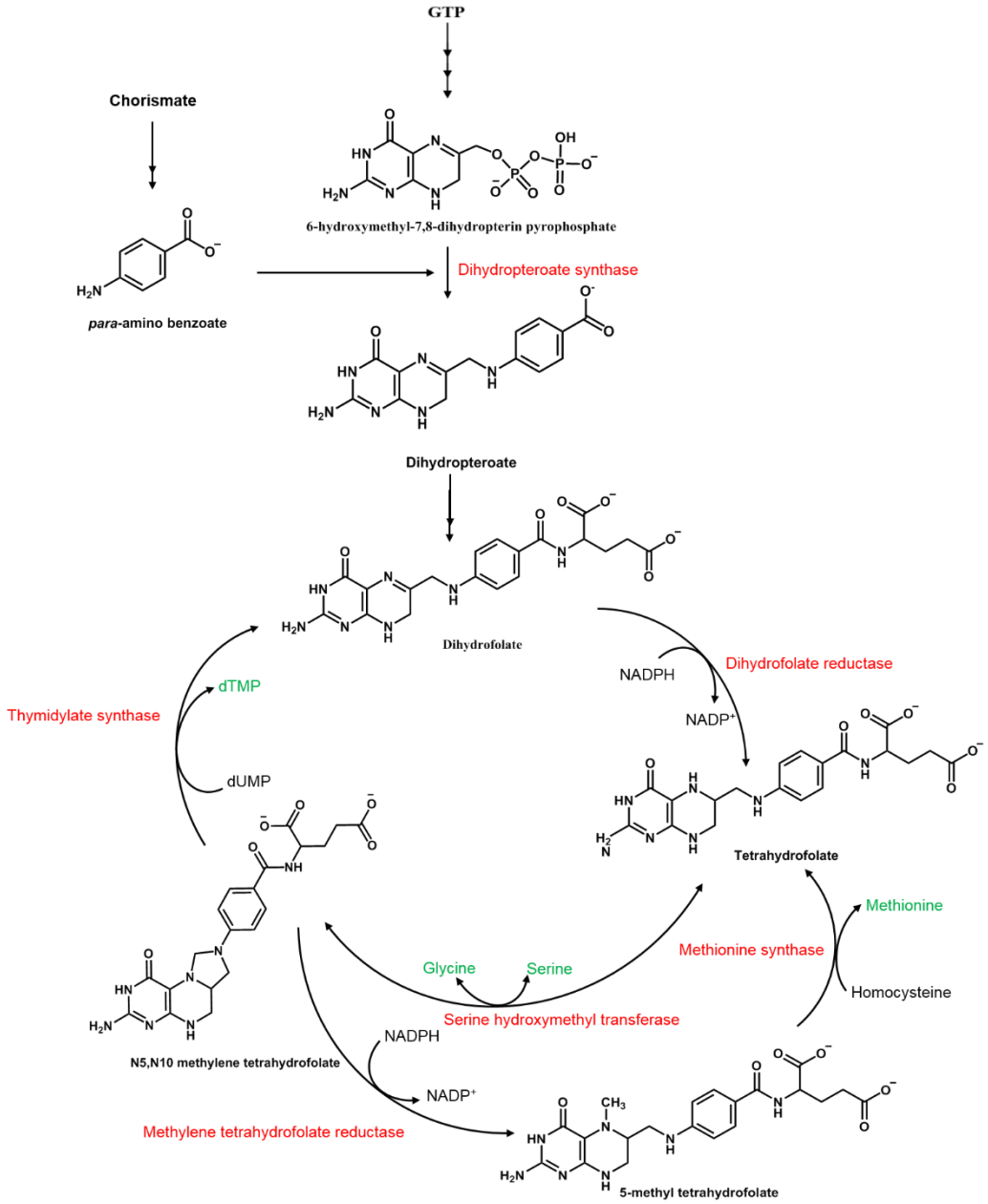

Figure 1.2: The folate pathway

GTP and chorismate serve as the precursors for the synthesis of the pteridine and pABA, respectively. These molecules are fused to form dihydropteroate, to which a glutamate tail is added, leading to the formation of dihydrofolate. Tetrahydrofolate is formed through the reduction of dihydrofolate, and this feeds into the one carbon cycle needed for the synthesis of essential amino acids and nucleotide precursors. The structures of reduced folates are shown in the pathway with the enzymes highlighted in red and products in green.

dihydrofolate reductase by adding osmolytes, small molecules that occupy space and volume in a system, which can perturb water activity. Osmolytes act as a co-solvent and can cause changes in the catalytic efficiency or binding properties of the enzyme. Depending on the size and charge of the osmolyte, they can take up space and participate in interactions. The nature of the interactions are osmolyte specific, for example: betaine will weakly interact by cation-pi interactions whereas trehalose interacts by hydrogen bonding. The shape and size of the osmolyte influences the degree to which the osmolyte occupies volume in the environment. The volume occupied by one osmolyte excludes other macromolecules from occupying the same space causing volume exclusion effects. Volume exclusions influence the interactions between macromolecular species [6]. Increased volume occupancy is predicted to shift the equilibrium towards the bound species. Osmolytes can also weakly interact with the ligands, or the protein surface, and displace the water molecules causing an effect on the binding or catalytic properties.

The cell is composed of several biological macromolecules in a mixture of solutes and water. Increase/decrease in the concentration of solutes (change in osmotic strength) leads to osmosis of water in the direction opposite to the osmotic stress [7, 8]. There are two possible outcomes with the addition of osmotic stress to a hydrated macromolecule. There could be exclusion of the osmolytes/solutes from the exposed macromolecular surface due to preferences of groups/atoms on the protein to interact with water compared to the osmolyte. The osmolytes can also be sterically excluded from cavities, channels and grooves due to size effects, e.g. volume exclusion [6]. These osmolytes thus occupy space in the bulk water solution. An example of this is the preferential exclusion of glycine betaine (also known as trimethylglycine) from the surface of DNA, specifically from the anionic phosphate oxygens [9]. A second scenario is the preferential interaction of osmolytes/co-solutes with the surface of the macromolecule. Water molecules on the surface of the macromolecule are replaced by osmolytes. This leads to an increase in water in the bulk solution. An example of this is the preferential interaction of trehalose with the phosphate oxygens on the lipids in a bilayer [10]. Figure 1.3 shows a representation of the preferential interaction or exclusion of the osmolytes from the protein surface.

1.3 Osmolytes of the cell and their function

Osmotic stress causes a change in the flux of water, cell volume, cytoplasmic membrane tension and biopolymer concentrations in the cell. It also changes the turgor pressure, which is the force exerted by water against the cell wall [11]. Osmolytes, particularly those known as osmoprotectants, are small molecules that are biosynthesized in cells as a response to osmotic stress, as well as against dehydration and heat [12]. There are three classes of osmolytes: amino acids like proline and glutamate; polyols like glycerol, trehalose and sucrose; and methylamines like trimethylamine N-oxide (TMAO) and betaine [13]. Figure 1.4 shows the structures of organic osmolytes present in bacterial cells.

There are various osmolytes present, with differing roles, during osmotic stress. The concentration of osmolytes in the osmotically stressed cell is around 2 µmol/mg dry weight

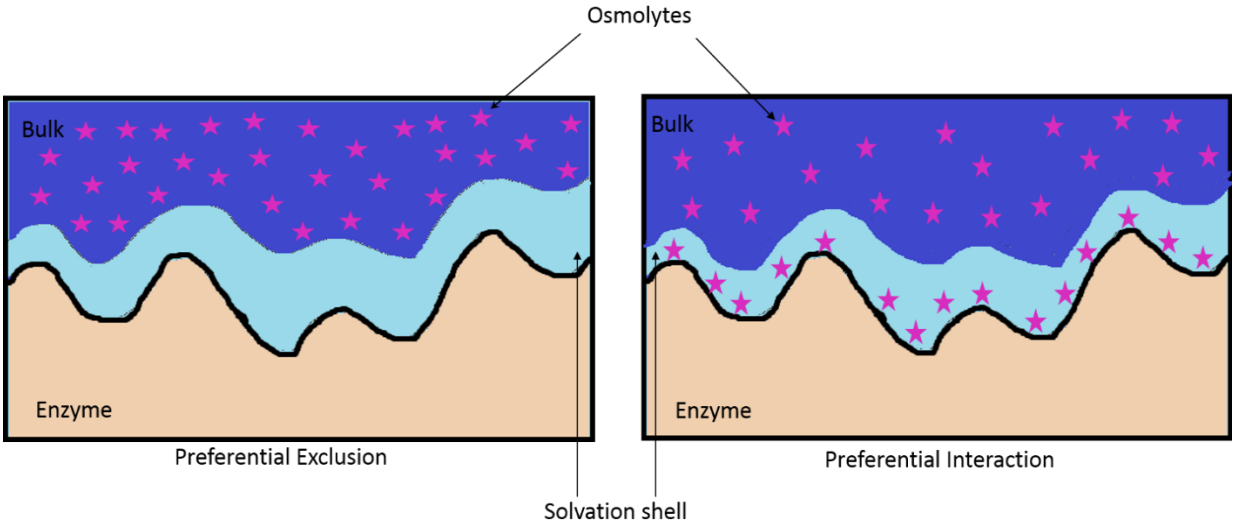

Figure 1.3: Models for preferential exclusion (left panel) and preferential interaction (right panel)

This figure shows a representation of the addition of osmolytes to a solvated enzyme. The solvation layer is shown in light blue and the dark blue represents the bulk water. The enzyme is represented in light orange. Osmolytes (pink stars ★) are excluded from the surface of the enzyme and thus are present in the bulk solution (left panel), whereas if osmolytes prefer to interact with the surface of the protein, then they replace the water molecules in the solvation shell (right panel).

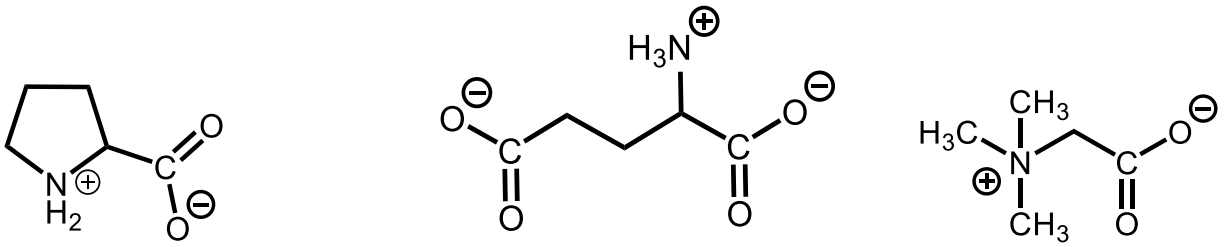

Proline Glutamate Glycine betaine

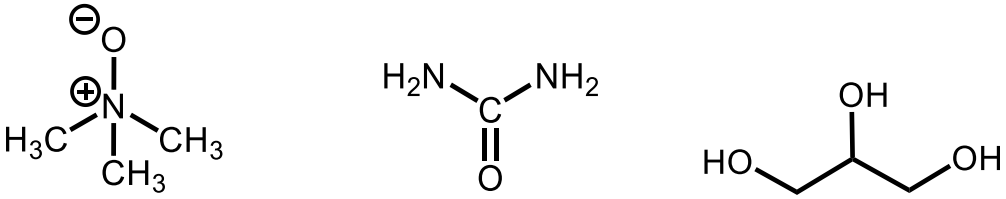

Trimethylamine oxide (TMAO) Urea Glycerol

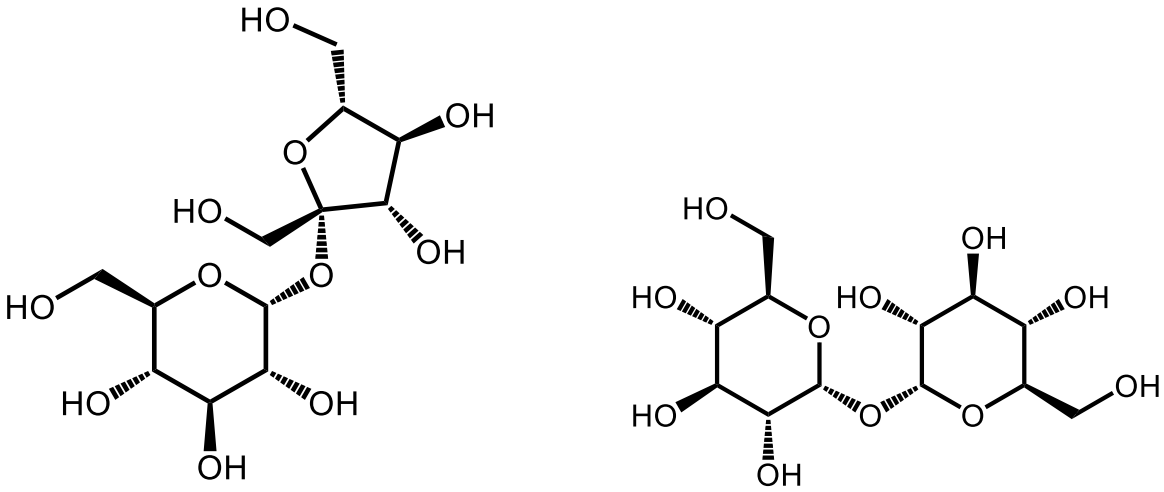

Sucrose Trehalose

Figure 1.4: Biologically relevant osmolytes made in the cell during osmotic stress

The organic osmolytes help maintain turgor pressure during stress conditions preventing the loss of cell integrity. They also help in maintaining the folded and native states of the proteins in the cell. Urea is a protein denaturant that is present in cells.

of the cell [18]. The concentration of trehalose was found to be 0.36 µmol/mg dry weight when it is the predominant osmolyte [18]. Betaine, when predominant was found to be 1.17 µmol/mg dry weight of the cell [18]. In exponentially growing *E. coli,* the intracellular concentration of K^+ ions increase from 0.15-0.55 M when the osmolality of the medium increases from 0.1-1.2 Osm (osmolal / kg of solvent). Excess K^+ in the cell is secreted to the surrounding environment [8]. In gram negative bacteria, glutamate levels increased up to 10% under osmotic stress. *E. coli* has low intracellular proline levels when the medium does not contain proline, but can uptake proline proportional to the osmotic strength of medium [8]. Glycine betaine is the most preferred osmolyte in *E. coli*. It is taken up from the environment with the aid of transport systems [14] or synthesized from externally supplied choline in a two-step reaction [15]. Trehalose and glutamate are the major organic osmolytes when *E. coli* is grown in minimal media with glucose [14]. During osmotic stress in minimal media with glucose as the carbon source, intracellular trehalose concentrations increased about 40-fold in *E. coli* [16]. The intracellular concentration of trehalose in *E. coli* is about 20% of the osmolar concentration of solutes in the growth medium. Mutations that result in a lower trehalose concentrations lead to an increase in sensitivity to osmotic stress [17]. Addition of exogenous glycine betaine and proline leads to suppression of trehalose synthesis [8, 18].

The osmolytes not only help to maintain turgor pressure but also help in stabilizing proteins. Stabilizing osmolytes are excluded from the protein surface forcing the polypeptide to adopt a folded conformation with a minimal exposed surface area [19]. Osmolytes are also capable of reversing protein misfolding and/or aggregation and modulating the activity of molecular chaperones [20]. Most protein concentrations in *E. coli* do not change with osmotic stress; however, MTHFR (an enzyme under study in Chapter 4) does have a two-fold decrease in protein levels [21].

1.4 Osmolyte studies with dihydrofolate reductase (DHFR)

Our lab is interested in studying the role of water in the activity of folate pathway enzymes. If water was involved in binding or catalysis, its perturbation would affect the catalytic properties of the enzyme. To study this, the effect of the addition of small molecule osmolytes that perturb water activity was explored. The initial studies were done with dihydrofolate reductase, the primary enzyme in the folate biosynthesis pathway.

Dihydrofolate reductase catalyzes the reduction of dihydrofolate to tetrahydrofolate using NADPH as the cofactor. Isothermal titration calorimetry (ITC) can be used to study the effect of ligand binding to an enzyme (K_a values), whereas steady state kinetics yields information on how the osmolytes affect the kinetics (k_{cat} and K_M) of the enzyme. Previous studies in our lab found that osmolytes affect ligand binding to three different scaffolds of DHFR (*E. coli* chromosomal DHFR (EcDHFR) [22], R plasmid encoded DHFR (R67 DHFR) [23] and FolM, a pteridine reductase (PTR1) from *E. coli* [24]) as indicated by ITC and steady state kinetics.

The binding of NADPH to apo-R67 DHFR [23] became tighter in the presence of osmolytes, and this effect is independent of the kind of osmolyte used (Figure 1.5A). Osmolytes

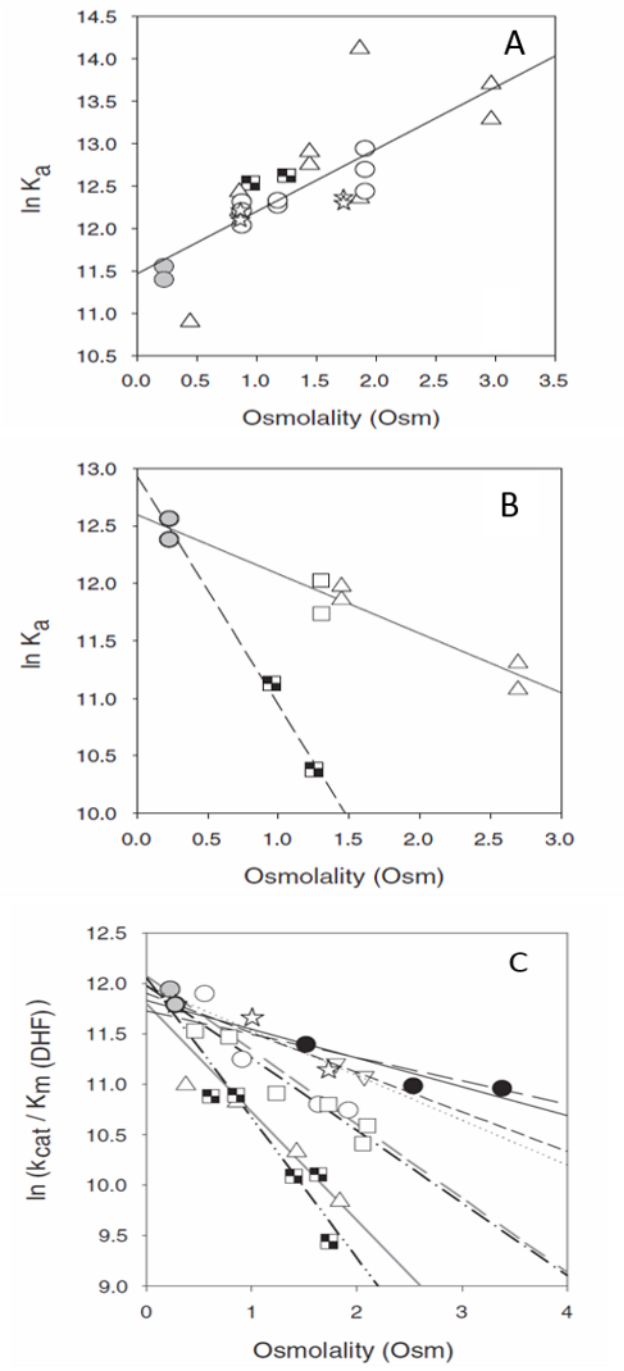

Figure 1.5: Effect of osmolytes on ligand binding to R67 DHFR

A: The association of NADPH to R67 DHFR tightened in the presence of osmolytes as monitored by ITC. B: ITC binding data show that the association of DHF to the R67 DHFR-$NADP^+$ complex weakens in the presence of osmolytes and the effects are dependent on the type of osmolyte. C: Steady state kinetic data of the reduction of DHF by R67 DHFR-NADPH. There is a decrease in the catalytic efficiency of the enzyme with increasing osmolyte concentrations. The osmolytes are shown as buffer (●), glycerol (●), ethylene glycol (✳), TMAO (▽), sucrose (□), glycine betaine (△) and PEG400 (⬓) [23].

prefer to be excluded from NADPH leading to its tighter association with enzyme at low water activity. This has been attributed to the lowering of the desolvation penalty associated with complex formation. On the other hand, weaker binding of the DHF to R67 DHFR occurs with increasing concentration of the osmolyte (Figure 1.5B). Polyethylene glycol 400 (PEG 400) has a steeper slope than the rest of the osmolytes. If crowding or volume exclusion is responsible for these effects, then NADPH binding should be affected in a similar manner. NADPH binding to R67 DHFR tightens in the presence of PEG400, hence ruling out crowding effects. Furthermore, kinetics for the reduction of DHF indicate that the efficiency of the enzyme decreases with increasing osmolyte concentrations, and the effect was dependent upon the osmolyte (Figure 1.5C). Osmolytes did not affect the enzyme catalytic turnover values, k_{cat}s, but the DHF K_Ms increase significantly in the presence of osmolytes.

One possible reason that the osmolytes could be affecting DHF binding to R67 DHFR is by interacting with the enzyme through preferential interactions and changing its properties such as fold, oligomerization state or the stability. R67 DHFR possesses 222 symmetry wherein a single active site pore allows binding of both the ligand and the cofactor. Thus the same site can be occupied by either the ligand or the cofactor [25]. As DHF and NADPH bind to symmetry related residues on opposite sides of the active site pore, if osmolyte were to interact with enzyme at the active site surface, then should have the same effect on both NADPH and DHF binding. Either binding should be weaker for both substrate and cofactor, or binding should get tighter for both ligands. However, osmolytes have opposing effects on the binding of the substrate and cofactor to R67 DHFR. Thus, it was concluded that the effects on ligand binding are not due to the interaction of the osmolytes with R67 DHFR, but due to their interaction with DHF.

Since osmolytes interact with DHF, and hinder its association to R67 DHFR, these effects should hold true for other enzymes that utilize DHF as a substrate. EcDHFR catalyzes the dihydrofolate reductase reaction but has a different sequence and structure than R67 DHFR. ITC measurements of DHF binding to EcDHFR indicate weakened affinity in the presence of osmolytes [22].

Similar results with a pteridine reductase, FolM, which possesses weak DHFR activity, additionally indicate the osmolytes interact with DHF. Methotrexate is an antifolate which binds DHFR and competitively inhibits it. The effects of osmolytes on binding of methotrexate (MTX) to FolM indicates MTX binding is weaker in the presence of osmolytes [24]. In all these dihydrofolate reductases, the K_d for dihydrofolate increases in the presence of osmolytes and supports our model shown in Figure 1.6 where osmolytes preferentially interact with DHF, hindering its association to the enzyme.

These studies lead to the proposal of a preferential interaction model of osmolytes with DHF (Figure 1.6). In this model, osmolytes compete with, and displace, water molecules in the solvation shell of the ligand. If removal of the osmolytes requires more energy than removal of water, this leads to the shifting of the binding equilibrium towards the formation of free enzyme and DHF species. The binding affinity of DHF to dihydrofolate reductase is reduced in presence of osmolytes.

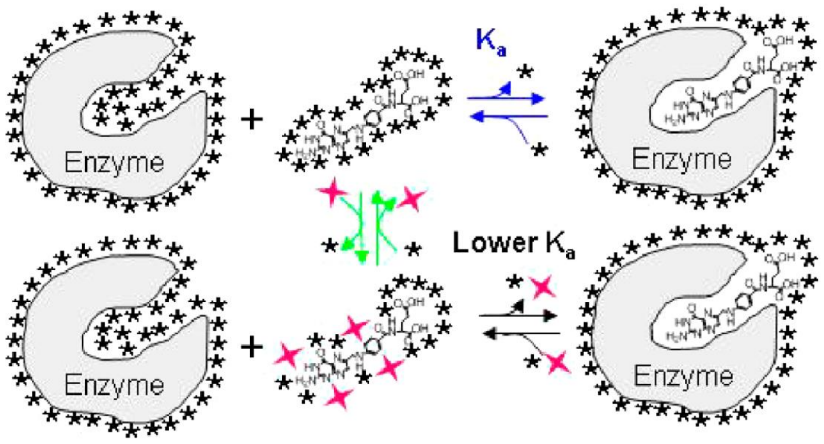

Figure 1.6: Model of the preferential interaction of osmolytes with folate

The top panel depicts the binding of ligand by the enzyme in a dilute buffer condition. The ligand and enzyme are solvated with water molecules (★). In order for the enzyme-ligand complex to form, the water molecules from the interface are removed. The bottom panel depicts the case where osmolytes (✦) interact with specific functional groups on the ligand (shown in our previous osmolyte studies and discussed in section 1.5). There has to be removal of not only the water molecules but also the osmolytes for the complex to form. If the osmolytes bind more tightly than water, this leads to lowering of the association, shifting the binding equilibrium towards the free enzyme and ligand species [24].

1.5 Preferential interactions between folate and osmolytes

Folate has a greater stability than dihydrofolate and it has been routinely used in the biophysical studies in place of DHF. Nuclear magnetic resonance (NMR) and vapor pressure osmometry (VPO) studies have helped explore the interactions of folate with betaine [26,27]. At higher concentrations folate dimerizes in a fully "stretched out" conformation at neutral pH [28]. The pterin ring of one folate and the *p*ABA ring of the second folate participate in π-stacking interactions, whereas the negatively charged glutamate tails move freely in solution away from the complex [28]. The negatively charged carboxyl group of glutamate projects outward preventing formation of higher oligomers [28]. NMR studies indicate that betaine increases the folate dimerization K_d by preferentially interacting with the folate monomer. Nuclear Overhauser effect (NOE) spectroscopy results indicate that the bonds between the pterin and pABA rings are less dynamic in the presence of betaine, which suggests the osmolyte interacting with the pABA benzoyl ring [27].

Deuterated osmolytes are needed to perform NMR experiments, and thus make it an expensive technique to study the weak interactions with folates. Moreover, there are a limited number of protons on the pterin ring in folate that makes it hard to determine the nature of osmolyte-folate interactions. VPO can be used to detect the interactions of co-solvents with compounds containing different functional groups.

This technique predicts if an osmolyte/co-solute prefers to interact or be excluded from a compound, and has been use for the osmolytes: glycine betaine [9, 26] , proline [29], urea [30], glycerol [31] and trehalose [10, 32] .

1.6 Vapor pressure osmometry

The VPO can be used to measure the preference of a compound to interact with osmolyte as compared to water in a three-component solution system: (1-water, 2-compound, 3-osmolyte)[9]. Three different types of solutions are made for measuring the interactions in a three-component system:test compound in water (m_2), osmolyte in water (m_3), mixture of test compound and osmolyte solution (in the same molalities tested in the m_2, m_3 solutions)

There are two possible scenarios that can occur with interaction of osmolyte with the test compound (Figure 1.7 A). If osmolyte prefers to interact with certain functional groups on the compound, the solvating water molecules will be displaced, leading to an increase in the bulk water concentration. This decreases the solution osmolality in relation to the sum of the two component solutions. On the other hand, if osmolyte prefers to be excluded from a certain functional group(s) (or the functional group(s) prefers water over the osmolyte), the osmolyte concentration in the bulk solution will increase. This would increase the osmolality of the three component solution with respect to the two component solutions.

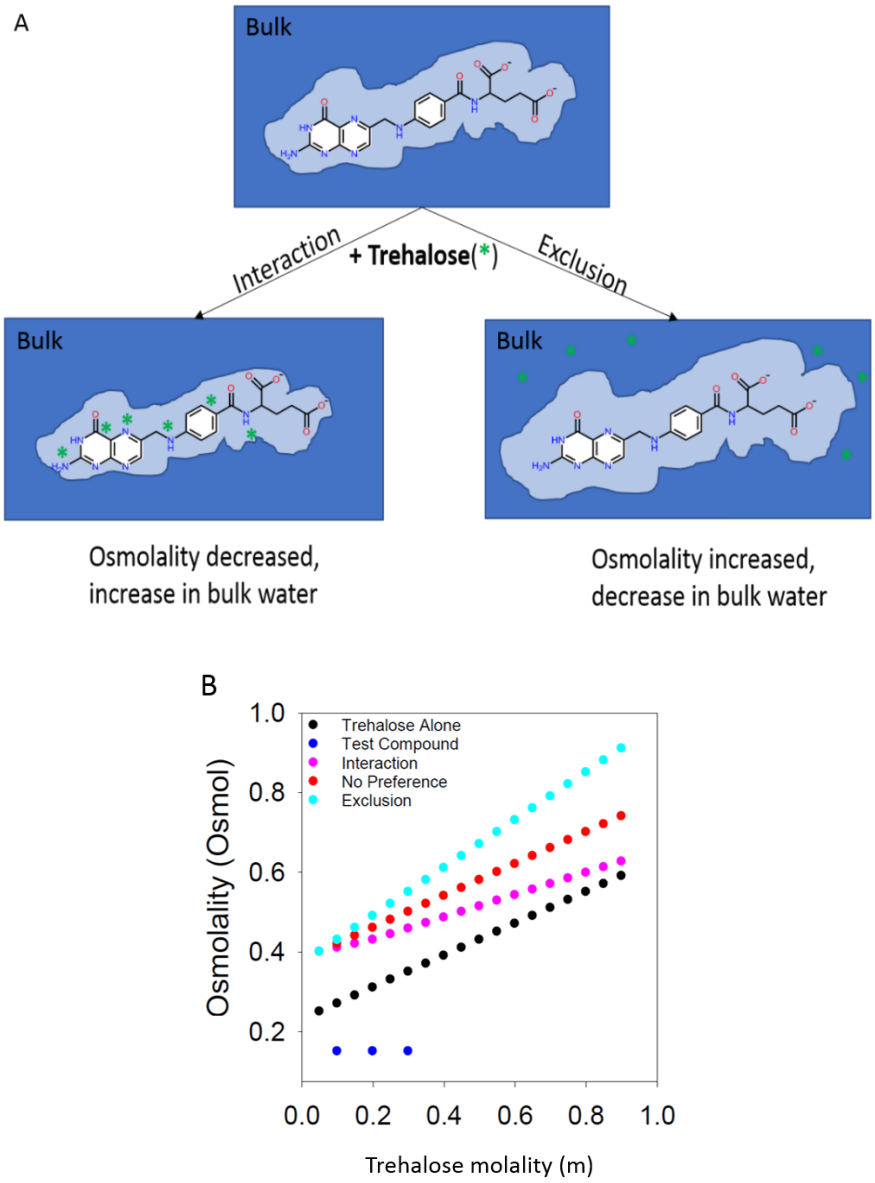

Figure 1.7: Vapor Pressure Osmometry principle

A. Cartoon representation of preferential interaction or exclusion of trehalose (✱) from functional groups on folate. Trehalose molecules can preferentially interact with certain functional groups and displace the water into the bulk solution, decreasing the osmolality of the solution (left). On the other hand, trehalose molecules can be excluded from functional groups on folate, causing a decrease in bulk water concentration and an increase in osmolality (right). B. Change in the osmolality of the two component or three solutions with respect to trehalose molality. Representative plots of trehalose (●) and test compound (●) only solutions are shown. Examples are given of what the VPO data would look like if trehalose preferentially interacts with a small molecule (●), is excluded (●), or there is no preference for the small molecule to interact with trehalose versus water (●).

The two component systems are the contributions to the osmolality from the individual components. The three component system gives the net osmolality taking into account the favorable/unfavorable interactions between osmolyte and test compound. If the osmolality of the three component system is equal to the sum of the osmolalities of both of the two component systems, then there are no net effective interactions. However, if the sum of the two component solutions is different than the osmolality of the three-component solution, then it indicates interaction or exclusion. The osmolalities obtained from the three solutions is then plotted versus the molality of the osmolyte (Figure 1.7B).

To determine if the osmolytes interact with the test compounds, the osmolalities from the three component systems (water, osmolyte, test compound) are subtracted from the osmolalities of the two component systems (osmolyte in water and test compound in water). The difference in osmolality (ΔOsm) is plotted against the product of the molalities of osmolyte and test compound. The slope of the graph is the preferential interaction coefficient

$$\Delta Osm = Osm(m_2, m_3) - Osm(m_2, 0) - Osm(0, m_3) \quad \text{Eq: 1.1}$$

$$\Delta Osm \cong (\mu_{23}RT)m_2m_3 \quad \text{Eq:1.2}$$

where Δ*Osm* is the difference in the osmolalities; m_2 and m_3 are molal concentrations of test compound and osmolyte, respectively; and μ_{23}/RT (the preferential interaction coefficient) is the relative chemical potential of the test compound in osmolyte [9].

During associative interactions between osmolyte and test compound, the osmolality of the three-component solution will be lower than the sum of the osmolalities of the individual component solutions. Thus, the slope of the graph, and μ_{23}/RT value, will be negative. In the case where there are unfavorable interactions, the osmolality of the three-component solution will be higher than the osmolalities of the individual component solutions. The slope, and the μ_{23}/RT value, will be positive. A μ_{23}/RT value of zero indicates that the net effective interactions between osmolyte and test compound are

equivalent, and that water and osmolyte both associate with the test compound to the same extent.

1.6.1 Predicting μ_{23}/RT values

Preferential interaction coefficients of an osmolyte with any compound can be predicted based on the interactions of the osmolyte with a set of test compounds. A set of 20, or more, model compounds with different atom types and functional groups can be used to create a data set of interactions between the osmolyte and each type of atom. The functional groups of the model compounds contain phosphates, amides, carboxylates, hydroxyls, aliphatic and aromatic moieties. Preferential interaction values are additive contributions arising from favorable/unfavorable interactions of each surface exposed atom type with the osmolyte. The interactions of each atom type is dependent upon the solvent exposed surface area of the atom. The accessible surface area of the differential functional groups on the test compound is determined by the Surface Racer program [33]

and the preferential interaction coefficient is deconvoluted into atomistic interaction potential (α values). From these α values, the preferential interaction coefficient can be calculated for any molecule based on its structure.

Atomistic interaction values have been determined most extensively for glycine betaine [9, 26]. Betaine preferentially interacts with aromatic carbons, amide nitrogens and cationic nitrogens and is excluded from carboxylate, phosphate and amide oxygens. This explains why betaine prefers to be away from protein surfaces and helps in maintaining the folded state [9]. VPO studies in our lab added to the Record group study by exploring interactions of betaine with model compounds representing the functional groups on folate. Betaine preferentially is excluded by the nitrogen in the pterin ring but prefers to interact with amine nitrogens off of aromatic rings [26]. Preferential interaction coefficients can be predicted for proline [29], glycerol [31], polyethylene glycols [31], and trehalose [10] as well (Table 1.1).

1.7 Trehalose as an osmolyte

E. coli increase the production of compatible solutes called osmoprotectants under stress conditions [8]. The osmolytes are used, in part, to combat turgor pressure during osmotic stress. Glycine betaine and proline are the predominant osmolytes when they are present in the surrounding environment. But in cases of nutrient limitation, trehalose (a disaccharide composed of two α-(1-1)-α linked D-glucose units) is the predominant osmolyte in the cell [14]. It can form up to 20% dry mass in some organisms and allow them to survive dehydration and metabolic dormant conditions. Trehalose is predicted to form extensive hydrogen bonds (H-bonds) with water, and forms a glass matrix in the cytoplasm which reduces the structural fluctuations of the biopolymers [34, 35]. There are several mechanisms through which trehalose can stabilize proteins. Trehalose increases the surface tension of solutions. Protein-solvent interfacial tension is the change in surface tension of the solvent when a protein molecule is introduced in the system. Trehalose is excluded from the surface of proteins and increases the protein-solvent interfacial tension [34, 36]. In another possible mechanism, trehalose may favor the folded state by increasing the free energy of the denatured state. It is proposed that trehalose interacts favorably with polar side chains of proteins but unfavorably with apolar side chains and the peptide backbone [37]. It is excluded from the surfaces of hydrophobic groups. Therefore, as the hydrophobic core becomes exposed to the solvent upon unfolding, trehalose is excluded from more of the protein surface. This is energetically unfavorable, which decreases the stability of the unfolded state.

Table 1.1 Atomistic interaction coefficients of trehalose, betaine, proline, glycerol, TEG and PEG400 with different atom types.

	α values ($x10^4$ m^{-1} $Å^{-2}$)[a]						
	Trehalose	Betaine	Proline	Glycerol	TEG	PEG400 (ex)[b]	PEG400 (in)[b]
Aliphatic Carbon	22.4 ± 0.8	-3 ± 1	5.3 ± 1.3	0.9 ± 0.2	-5.9 ± 0.5	-0.1 ± 0.1	-1.9 ± 0.2
Hydroxyl Oxygen	-0.8 ± 0.7	7 ± 1	-0.7 ± 1.3	0.5 ± 0.1	14 ± 1	0.4 ± 0.4	4.6 ± 0.2
Amide Oxygen	-19.6 ± 5.4	49 ± 3	14.5 ± 4.5	14 ± 1	50 ± 2	12 ± 1	13 ± 1
Amide Nitrogen	-4.7 ± 2.2	-33 ± 2	-11.8 ± 3.2	-8.3 ±0.6	-28 ± 1	-7.0 ± 0.5	-7.1 ± 0.4
Carboxylate oxygen	-28.2 ± 2.1	28 ± 1	16.6 ± 4.3	7.9 ± 0.1	61 ± 1	6.7 ± 0.4	18 ± 1
Carboxylic acid oxygen	ND[c]	ND	ND	0.8 ± 0.1	-6.9 ± 0.7	0.6 ± 0.6	-2.5 ± 0.2
Cationic nitrogen	12.9 ± 2.1	-14 ± 1	-12.6 ± 4.3	-4.2 ± 0.3	-14 ± 1	-3.5 ± 0.3	-3.4 ± 0.2
Aromatic carbon	5.9 ± 1.5 or -8.9 ± 1.6	-31 ± 1	-9.2 ± 0.9	-7.3 ± 0.2	-45 ± 1	-6.2 ±0.2	-3.1 ± 1
Phosphate oxygen	-59.2 ± 5.1	48 ± 2	18.0 ± 5.2	ND	ND	ND	ND
Amine nitrogen off the aromatic ring	ND	-53 ± 3	ND	ND	ND	ND	ND
Aromatic nitrogen	ND	27 ± 3	ND	ND	ND	ND	ND

The data are compiled from refs [9, 10, 26, 29, 31]

1.8 Clustering behavior of trehalose

Trehalose interacts with the surrounding water molecules primarily via its 8 hydroxyl groups, which may also mediate trehalose-trehalose contacts [34]. Osmometry and molecular dynamics simulation studies by Sapir and Harries look at the effect of increasing trehalose concentration on its self-association in water [38]. Trehalose was found to have a cluster percolation threshold at concentrations above 1.5 *m*. There was positive deviation from ideality which increased with concentration. Trehalose molecules self-associate through intermolecular H-bonds and repel other trehalose clusters via volume exclusion effects [38]. Trehalose is also proposed to associate with water molecules through H-bond networks. The intermolecular H-bonds dominate the trehalose-trehalose attraction, while there is an excluded volume effect that leads to mutual repulsion between clusters of trehalose molecules. Both these forces are responsible for the self-association and clustering behavior of trehalose.

1.9 Osmometry studies with trehalose

Previous osmometry studies to determine the preferential interaction of trehalose with 20 test compounds by Hong et al [10] conclude that trehalose interacts with amides, carboxylates and phosphate oxygens. In contrast, trehalose is preferentially excluded from aliphatic carbon group. The free energy of unfolded state of protein is increased in the presence of trehalose. Also, trehalose is predicted to stay away from hydrophobic groups. This fits in with the predicted preferential exclusion of trehalose from the aliphatic groups. One drawback to this study is that it uses only a few representative compounds for each atom type in this analysis. The results for aromatic carbons, using phenylalanine, sodium benzoate, 4-hydroxylbenzyl alcohol (4BA) and histidine as model compounds, were inconclusive. There is no distinction made between aromatic carbons and aromatic nitrogens. They predict aromatic carbons exclude trehalose on the basis of data from phenylalanine and sodium benzoate. Conversely, they predict aromatic carbons and nitrogens preferentially interact with trehalose based on results for histidine and 4BA. Since the pteridine ring and pABA ring of folate have aromatic groups, we choose to extend their experiments with 50 additional test compounds, with an emphasis on 10 heterocyclic and 9 non-heterocyclic aromatic compounds. We characterize and quantify the weak interactions of trehalose with compounds with varying functional groups (Figure 1.8). The VPO experiment is set up as described above (Section 1.6).

Based on α values, microscopic local bulk partition coefficient of the compound in water and a particular osmolyte is determined [31]. It predicts the accumulation of exclusion of the solution from the surface of a particular functional group. A K_p value of more than 1 is indicative of the osmolyte accumulation around the surface of the compound whereas a value of less than 1 is indicative of osmolyte exclusion from that surface of the compound. The partition coefficient of trehalose and betaine with folate indicate the two osmolytes interact very differently with folate (Figure 1.9).

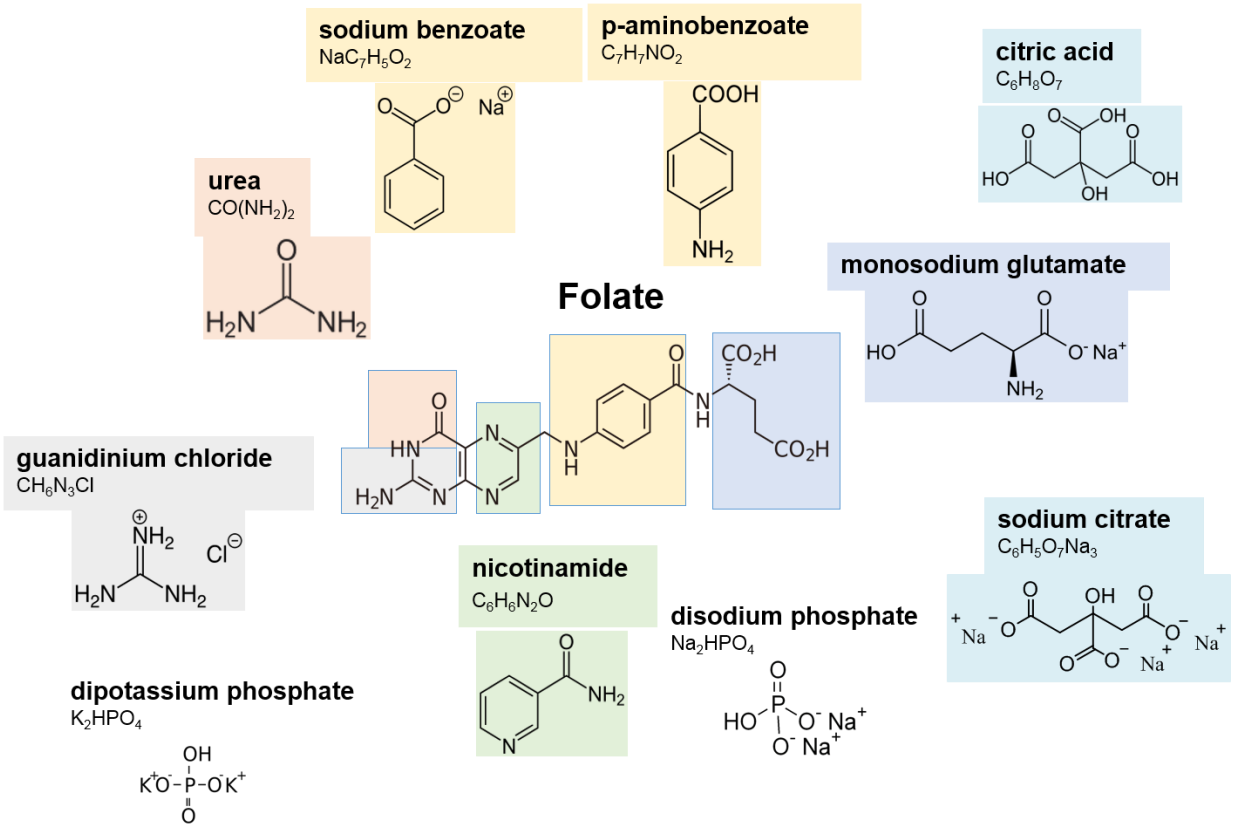

Figure 1.8: Similarity in functional groups between model compounds and folate

Some of the model compounds to be used in our study due to their similarity to functional groups found on the folate molecule. For example, in order to study how trehalose interacts with carboxylate groups present in the glutamate tail in folate, osmometry experiments will be conducted with several amino acids and citrate salts. Some of the test compounds used are color coded to represent the functional groups present on the folate molecule. In order to study the contributions arising from aromatic carbons, sodium benzoate and p-amino benzoate (shown in yellow) were for the osmometry studies.

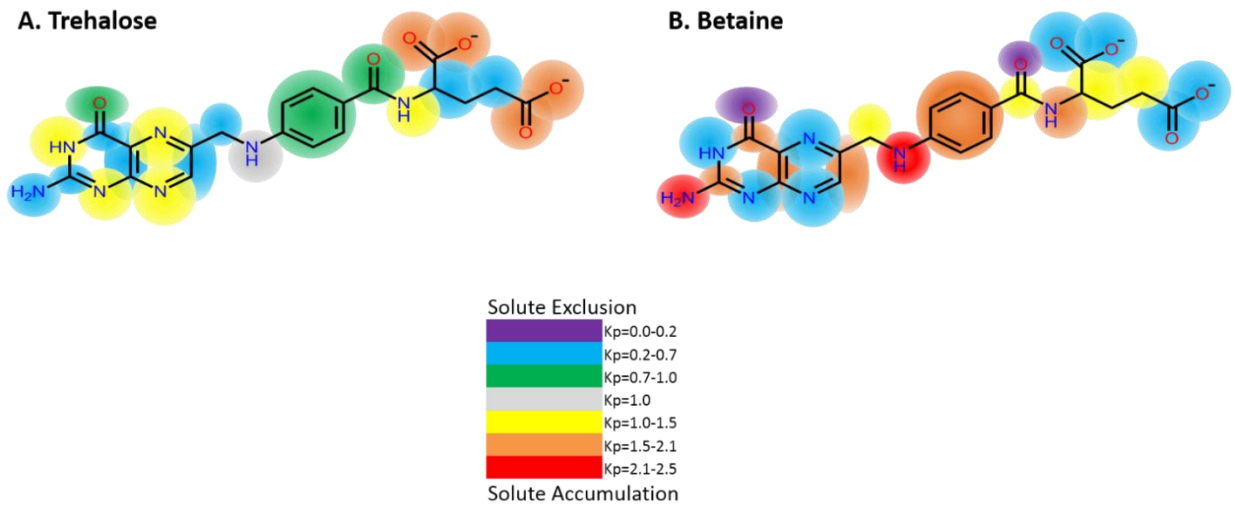

Figure 1.9: Partition coefficient (K_p) values

A: Trehalose and B: Betaine with folate using the atomistic coefficient values from refs [9, 10, 26]. Trehalose preferentially excludes aromatic carbons whereas betaine preferentially interacts with it. Another example being trehalose preferentially interacts with carboxylate oxygens, whereas betaine preferentially excludes it.

1.10 Use of VPO for other osmolytes

VPO has been used to study the interaction of several other osmolytes with sets of model compounds. Urea preferentially interacts with amide backbones and aliphatic and aromatic compounds reflecting on its tendency to denature proteins [30]. Glycerol preferentially excludes aliphatic carbons and amide oxygens and can thus serve as excellent protein stabilizers [31]. PEG400 preferentially interacts with cationic and amide nitrogens and aromatic carbons, but excludes carboxylate and hydroxyl oxygens and aliphatic carbons [31]. On the other hand, TEG preferentially excludes hydroxyl and amide oxygens but interacts with rest of the functional groups. TEG was found to be the only osmolyte that preferentially interacts with aliphatic carbon [31].

1.11 Differential interactions of osmolytes

The atomistic interaction coefficients are derived from the interaction of several osmolytes with compounds containing differential functional groups. A closer look into these coefficients shows that certain functional groups have contrasting effects with different osmolytes (Table 1.1). For example, trehalose prefers to interact with phosphate groups whereas betaine prefers to exclude them [9, 10, 26].

These differential interactions by osmolytes are relevant in the cell since glycine betaine is the preferred osmolyte under stress, but under nutrient limiting conditions, trehalose is the predominant osmoprotectant. Thus changes in the environment outside of the cell would affect the osmolyte concentration and identity in the cell. This may influence the macromolecules and their function depending on the extent of the weak interactions/repulsions. For example, previous studies in the lab have predicted interaction of osmolytes with reduced folates [22-24]. To understand the effect an osmolyte might have on a folate pathway ligand with phosphate groups, we calculate the preferential interaction coefficients for the ligands of dihydropteroate synthase (DHPS). This was done by calculating the solvent accessible surface areas of the functional groups on the ligands and multiplying them with the atomistic interaction coefficients. One of the ligands of this enzyme has a pyrophosphate moiety and we predict that trehalose will weaken its binding to the enzyme, while binding will get tighter in the presence of betaine.

1.12 Dihydropteroate synthase

Dihydropteroate synthase enzyme is needed for the synthesis of *denovo* folates. Pteroate is then glutamylated and enters the folate biosynthesis pathway for the formation of dihydrofolate. Humans do not have the folate synthesis pathway enzymes and hence cannot synthesize folate, and thus DHPS serves as an intriguing antibacterial drug target. Alignment of the DHPS sequences from pathogenic organisms in ClustalW, indicates there is only 40-45% sequence identity amongst them (Figure 1.10). Though, DHPS has

Figure 1.10: Sequence alignment of DHPS from pathogenic bacteria using Clustal W

There is 40-45% sequence identity, but the enzyme fold and ligand recognition sites are conserved amongst these organisms. * represents conserved amino acid residues, - represents gaps in sequences, • represents change of the amino acid seen in one species and **:** is change of the amino acid seen in multiple species.

a conserved structure in most pathogenic microorganisms. DHPS is a dimeric $(\alpha/\beta)_8$ TIM barrel protein (Figure 1.11) [39-44]. Dihydropteroate synthase (DHPS) catalyzes the condensation of 6-hydroxymethyl-7, 8-dihydropterin pyrophosphate (H_2PtPP) and *p*ABA to form dihydropteroate [39]. H_2PtPP binds and forms a cationic pterin intermediate upon cleavage of the pyrophosphate group [41]. Formation of this carbocation intermediate has been reported to be the rate determining step of the reaction [40, 41]. The leaving pyrophosphate group is coordinated with a magnesium ion present in the active site. Formation of this intermediate also leads to a rearrangement of loops 1 and 2, which creates a binding site for *p*ABA. Thus ligand binding occurs in an ordered fashion [41, 45]. The carbocation pterin intermediate reacts with incoming *p*ABA to form dihydropteroate [39, 41].

1.12.1 Bifunctional DHPS

In certain pathogenic bacteria, DHPS is fused to 6-hydroxymethyl-7, 8-dihydropterin pyrophosphokinase (HPPK) [46-48], HPPK catalyzes the previous step in the folate pathway. The pterin recognition site is similar to its monofunctional forms. There are distinct pterin binding sites in both HPPK and DHPS [47, 48]. It is predicted that close proximity of the two enzymes helps transfer the substrates and products to the next reaction [46].

In fungi and *Saccharomyces cerevisiae,* DHPS is fused to two other genes, HPPK and dihydroneopterin aldolase to form a trifunctional enzyme. The DHPS active site structure is similar to that seen in its monofunctional forms [49]. Dihydroneopterin aldolase catalyzes the conversion of dihydroneopterin to 6-hydroxymethyl-7, 8-dihydropterin. The latter is the substrate for HPPK.

1.13 *Bacillus anthracis* DHPS

Bacillus anthracis (anthrax) spores are used as bioterrorism agents and mortality is reported to be around 45% [50]. Antimicrobial therapies are implemented to curb anthrax and extensive efforts are being taken to find new enzymes and pathways to be targeted in this organism. Richard Lee's lab at St. Jude Children's Research Hospital designs drugs against the DHPS enzyme and these studies are discussed in the next sections.

Bacillus anthracis DHPS (BaDHPS) is a classic dimeric $(\alpha/\beta)_8$ TIM barrel structure with β-barrel surrounded by α-helices linked together with loops [39, 41]. The loops form an important part of the structure, which undergo conformational changes when ligands bind. The pterin binds in the active site present in the center of the TIM barrel whereas *p*ABA binds near the C-terminus of the enzyme (Figure 1.12). The loops have highly conserved residues and they are responsible for coordination and/or formation of the active site for the ligands. Loops 1, 2, 6 and 7 are more conserved than loops 3-5. The loops are highly mobile structures.

Arg68 in loop2 fits into the TIM barrel in the absence of the pterin ligand. The terminal guanidinium groups of Arg68 participate in π-stacking interactions with Arg254. Also the

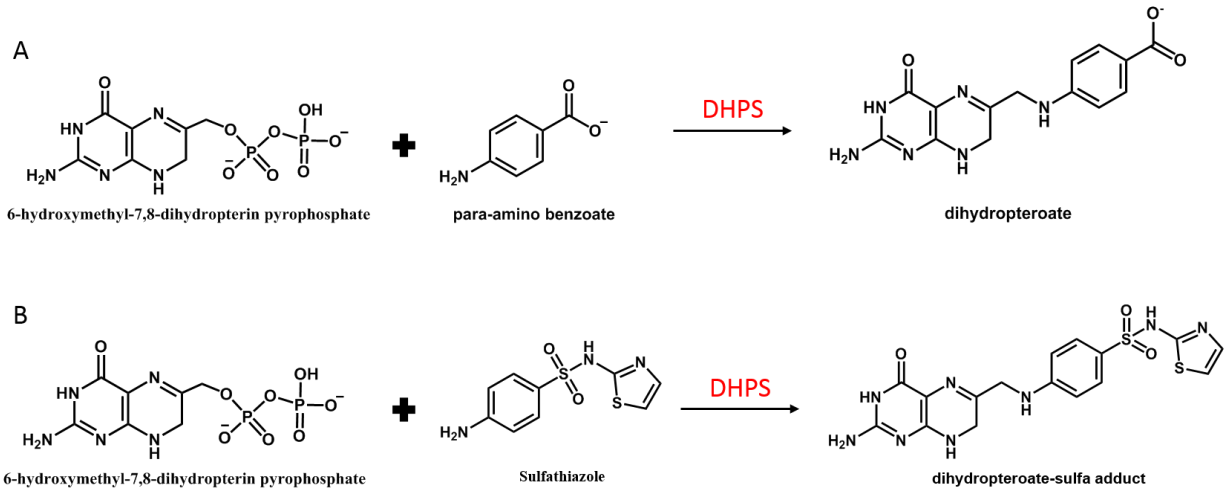

Figure 1.11: Reaction scheme of DHPS

A: H_2PtPP and pABA react to form a molecule of dihydropteroate. B: Sulfathiazole is an analog of pABA and acts as a competitive inhibitor of DHPS enzyme. It reacts with H_2PtPP to make a DHP-sulfa drug adduct.

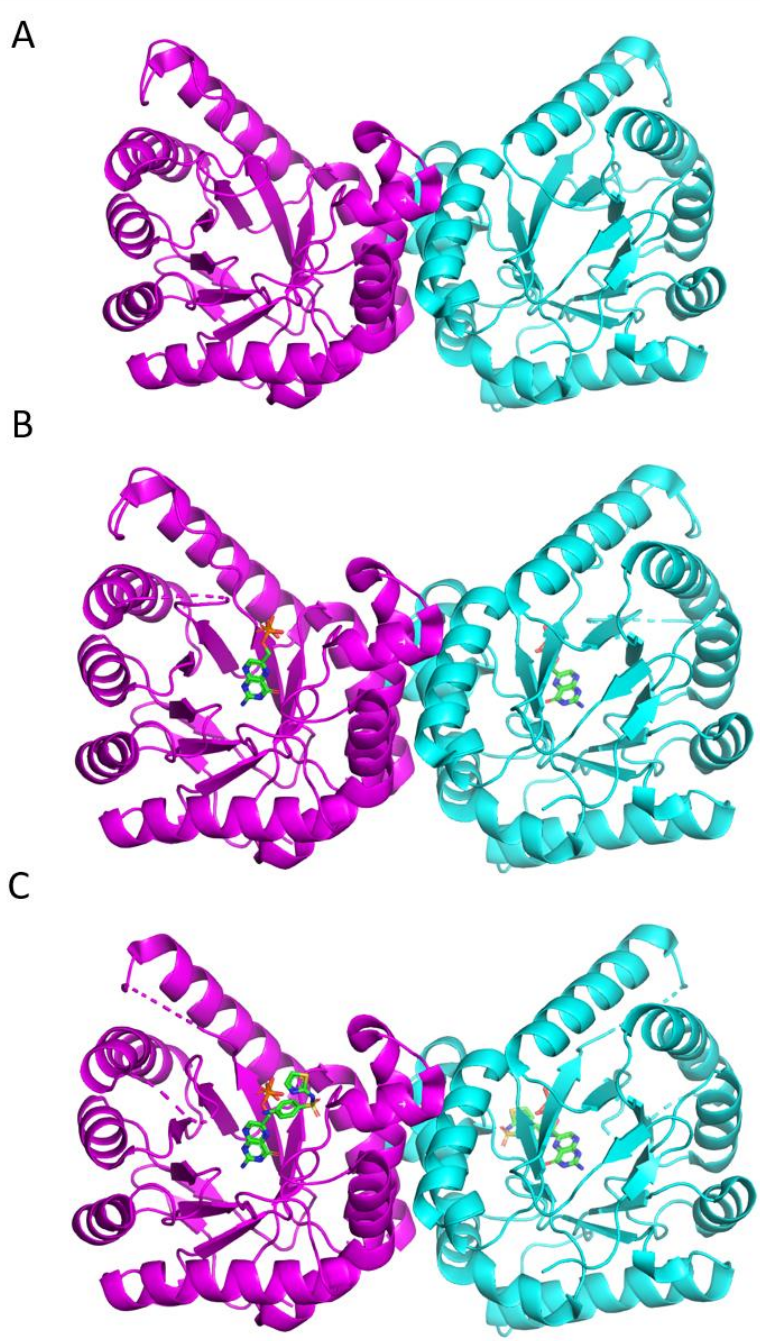

Figure 1.12: The structure of *Bacillus anthracis* DHPS

A: Structure of apo-BaDHPS (PDB ID: 1TWW). The enzyme is a homodimeric 8β-barrel alternating with 8α-helices. B: Structure of binary DHPS complex bound with pteridine pyrophosphate as ligand (PDB ID: 1TWS) C: Structure of ternary DHPS complex bound with cationic dihydropterin intermediate and para-hydroxybenzoate (PDB: 1TWC). (need to add figure for panel C) [39]

guanidinium nitrogens of Arg68 form hydrogen bonds with Asn120 and Asp184. Structures are available for pteridine pyrophosphate (PtPP) and H_2PtPP bound to BaDHPS [39, 41]. PtPP displaces the guanidinium group of Arg68 and interacts with Asn120, Asp184 and Lys220. Mutation in Asp184 abolishes binding of the pterin ligand, while a Lys220 mutant affects binding and k_{cat} of both the ligands since it is important for binding of pteridine and pABA ligands [39, 41].

Thus, in the absence of the ligand, Arg68 blocks the active site of the enzyme. The bound pterin also interacts with Phe189 and Met145 from one side, and Arg254 from the other side. The pyrophosphate groups of the ligand form hydrogen bonds with Arg254 and His256. Conserved residues Pro185, Gly186, Leu187, and Gly188 in loop 6 also interact with the pterin ring [39, 41].

Loop 1 forms a protective lid over the *p*ABA active site. Phe33 from loop 1, Pro 69 from loop 2 and Lys 220 and Phe189 form the *p*ABA binding site after pterin ligand binds to the enzyme [39, 41]. Mutations in the residues of loops 1 and 2 do not change the turnover of the enzyme, but increase the K_M for *p*ABA, while H_2PtPP binding is not perturbed. This indicates that the loop residues are involved in binding of *p*ABA.

1.14 Drugs/inhibitors of DHPS

1.14.1 Sulfa drugs

Sulfa drugs are *p*ABA analogs that are effective inhibitors of the folic acid biosynthesis pathway and are used as antibacterial and antiprotozoal drugs. They are competive inhibitors of pABA, binding near the C-terminus of the enzyme (Figure 1.11). Sulfa drugs deplete/sequester the pterin pool to form sulfa-pterin dead end product conjugate [51, 52]. Sulfamethoxazole (SMX) and sulfathiazole (STZ) are a few examples of sulfa drugs. Resistance to these drugs is attributed to increased drug efflux and/or mutations in the *p*ABA binding site [51]. As mentioned above, the *p*ABA binding site is made up of flexible loop regions and thus can develop mutations that result in increased sulfonamide resistance. The extra rings in the sulfa drugs, like the methoxazole ring in SMX and the thiazole ring in STZ, stick further away from the active site compared to pABA, and are near the loops. Hence mutations in the loops disrupt the drug binding, but do not deter *p*ABA binding [53]. Therefore, there is interest in designing new drugs that target DHPS that will not be affected by mutations in the loops near the pABA binding site.

1.15 Atomistic interaction values for trehalose and betaine used to predict the changes in binding of ligands to DHPS

As mentioned above (Sections 1.11), it is predicted that trehalose preferentially interacts with phosphate groups and betaine preferentially excludes them (Table 1.1). Trehalose

is also predicted to preferentially exclude aromatic carbons, whereas betaine preferentially interacts with them (Figure 1.9). Our previous *in vitro* and *in vivo* studies have predicted that osmolytes can either interact or exclude folate ligands/cofactor, which alters their binding to the folate pathway enzyme. Our current study is unique in that the betaine and trehalose will behave/interact differently with the ligands of DHPS and alter their binding. The effects of the osmolytes on the ligands, and its subsequent effect on their binding to DHPS, is explored using isothermal titration calorimetry. The effects of the osmolytes on the enzyme are also explored using circular dichroism and differential scanning calorimetry. The results of this section are presented in Chapter 3.

1.16 *In vitro* experiments versus the *in vivo* environment

The cell is a complex and crowded environment with the concentration of macromolecules reaching up to 300 mg/ml. Weak interactions of osmolytes with ligands of the folate pathway and their effects have been explored in Chapter 2 and 3 of this thesis. It has been reported that the osmolytes preferentially interact, or exclude, specific functional groups. These functional groups are also present on several macromolecules of the cell. Thus, we predict that the weak, interactions are relevant to the environment inside the cell. Even though the interactions are weak, the high concentrations of macromolecules and osmolytes (at least under osmotic stress) lead to a large number of potential interacting partners with each ligand inside the cell. We hypothesize that the cumulative effect of a large number of weak interactions will cause significant effects inside the cell. These interactions between ligands and small molecule osmolytes and/or macromolecules will also influence enzyme activity *in vivo*. Thus, in Chapter 4, we are specifically looking at how the weak interactions affect the activity of folate cycle enzymes. The effect of weak interactions on the activity of particular folate enzymes can be scored as a function of cell growth.

1.16.1 Osmotic titration studies on R67 DHFR

Previous *in vitro* studies in the lab have established the preferential interaction between osmolytes and folates [22-24, 26, 27]. Therefore, it is important to understand if the weak interactions between osmolytes and folate ligands are relevant inside a cell. Since these interactions are weak, we want to know if there are any net effects of high concentrations of cosolutes on enzyme function in the cell. Thus, *in vivo* osmotic stress titration studies are conducted with the R67 DHFR enzyme [23]. *E. coli* produces osmolytes in response to osmotic stress, and it was hypothesized that the osmolytes affect the functioning of the enzyme[23].

Chromosomally encoded DHFR in *E. coli* cells (EcDHFR) is an essential enzyme in the folate biosynthesis pathway. Osmotic stress studies on R67 DHFR in *E. coli* cells is complicated by effects on both the chromosomal and plasmid encoded DHFRs. In order to study the osmotic effects on only R67 DHFR, the growth of cells in presence of the

antifolate drug, trimethoprim (TMP), is scored. Chromosomally encoded *E. coli* DHFR is inhibited by the antibiotic (K_i=20 pM) [54], but R67 DHFR is resistant to the drug ,with a million fold higher K_i (0.15 mM) [55]. Addition of TMP to the wild type *E. coli* cell inhibits chromosomal DHFR activity leading to arrest of cell growth. However, when complemented with a plasmid vector containing the R67 DHFR gene, bacterial cell growth is restored in the presence of TMP. Osmotic stress titration studies in *E. coli* carrying the wild type (wt) R67 DHFR gene cloned in pUC8 indicated that these cells are capable of growth until 1.95 Osm in presence of TMP. This is similar to osmolality levels tolerated by *E. coli* in absence of TMP after which there is loss of cytoplasmic water leading to growth arrest [18].

Our model (Figure 1.6) predicts that with increasing osmotic stress, osmolytes will interact with free DHF preventing its association with R67 DHFR. However, *in vivo*, no reduction in *E. coli* growth with increasing osmotic stress is observed in the cells carrying the wt R67 DHFR-pUC8 plasmid in the presence of TMP. A high copy number plasmid like pUC8 will yield high concentrations of the rescuing wt R67 DHFR. In other words, it is difficult to titrate cell growth with respect to enzyme activity due to high levels of R67 DHFR. A catalytically less active R67 DHFR variant, Y69L (around 250-fold lower than wt) [56]), is tested. Similar to wt R67 DHFR, cells harboring Y69L R67 DHFR in pUC8 vector are resistant to TMP. Under TMP and osmotic stress treatment, this strain is capable of growth until 0.92 Osm. This is lower osmolality than what was tolerated by wt R67 DHFR. With increasing osmotic stress, the osmolytes weakly interact with DHF, hindering substrate binding to Y69L R67 DHFR. The decreased DHF binding, in addition to low catalytic efficacy of the R67 DHFR mutant, is responsible for lowered osmotic tolerance of the strain. These results support our model (Figure 1.6) and encouraged us to continue with our *in vivo* studies.

Our next step is to devise a system to explore the effect of osmotic stress on different enzymes of the folate pathway. Since folates interact with osmolytes, we predict that the osmotic stress effects are relevant to other enzymes in the pathway. In order to conduct osmotic stress titrations, we need the enzyme levels or activity to be lower than the chromosomal levels. To achieve this, we work with the pKTS vector that produces lowered levels, and reduction of half-life, of the enzyme [57].

1.16.2 The pKTS plasmid lowers the concentration of protein in the cell

In order to achieve lower enzyme levels in the cell, Neuenschwander et al. report the use of a pKTS vector for studies with the enzyme chorismate mutase [57]. The pKTS plasmid is constructed so that expression of the gene of interest is under the control of a tetracycline inducible promoter, and the protein turnover is compromised by the addition of an SsrA degradation tag. Addition of tetracycline leads to the induction of the enzyme with the SsrA tag attached to the C-terminus. In the pKTS expression system (Figure 1.13), the tetracycline repressor encoded by *tetR* is bound to the P_{tet} promoter when tetracycline is absent. Addition of tetracycline leads to the formation of a complex between

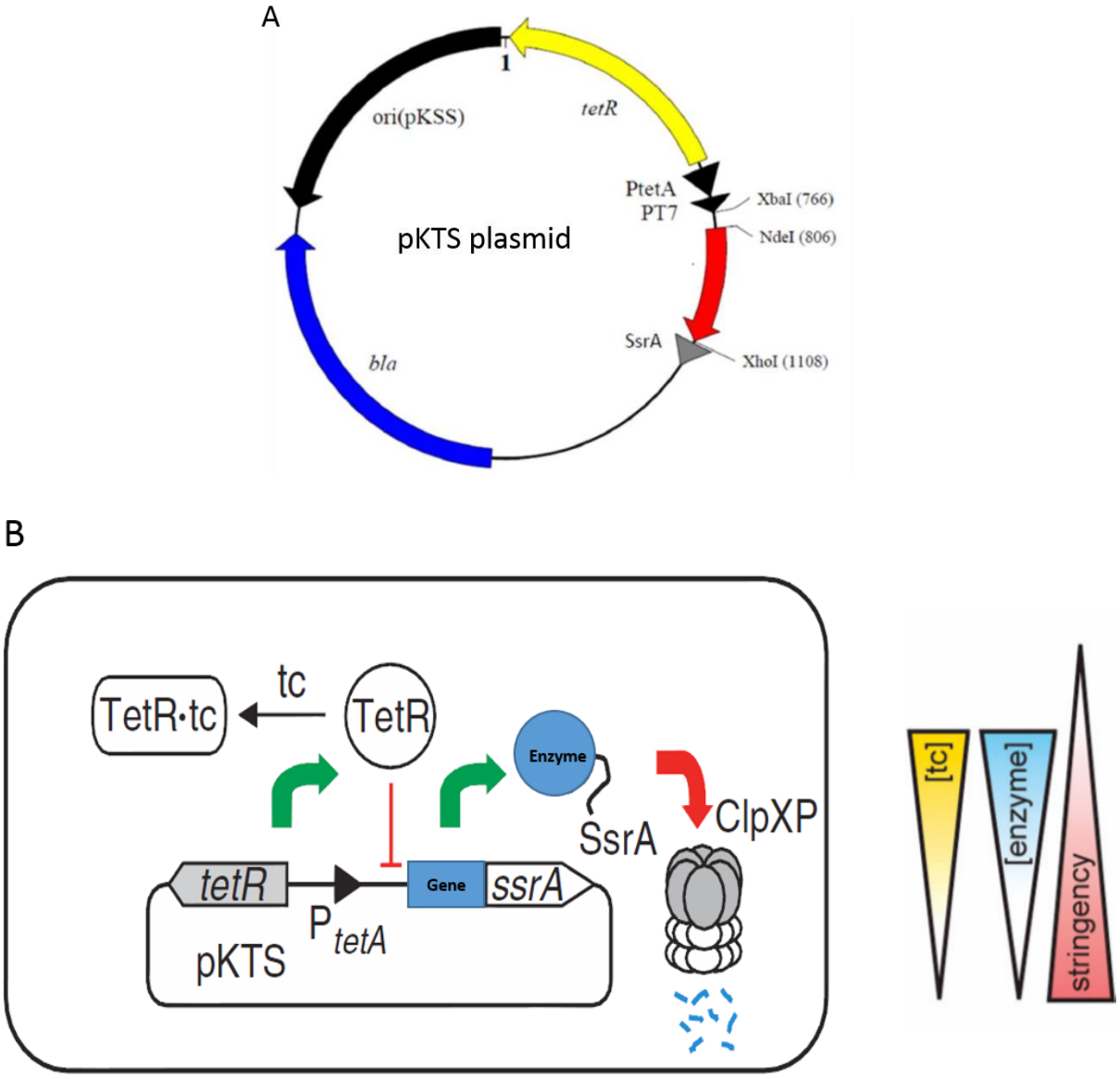

Figure 1.13: The pKTS expression system

A: pKTS as a selection vector. The gene of interest (red arrow) is cloned in between Nde1 and Xho1 restriction sites. When the protein is produced, an SsrA tag is fused to the C-terminal end of the enzyme. The plasmid has a tetracycline induction system, and clones with this plasmid can be selected with ampicillin. B:The tetracycline induction system works with the addition of tetracycline (tc) that binds to the TetR repressor protein leading to its removal from the *tetR* promoter site and allows induction of gene expression. The protein made from this construct is tagged with an SsrA tag at the C-terminus. This tag is recognized by the ClpX protease and is degraded thus lowering the half-life of the enzyme in the cell. Thus as shown in the left arrows, increased tetracycline (yellow bar) increases amount of enzyme (blue arrow) in the cell. Adapted from [57].

tetracycline and the repressor, relieving its inhibition of the promoter. For a non-essential gene in a low copy number plasmid in *E. coli* grown in rich medium, the lowest tetracycline concentrations are estimated to produce basal gene expression of about one mRNA molecule every third generation [58, 59]. Enzyme production is not only under tetracycline control in the pKTS plasmid, but there is also an SsrA tag fused to the C-terminus of the enzyme. Once the protein is synthesized, the tag is recognized by the ClpX protease marking it for degradation. The pKTS plasmid thus controls enzyme levels transcriptionally and through limits of the enzyme half-life.the amount of enzyme in the cell, the lesser would be the stringency of phenotype selection.

Neuenschwander et al. monitored the induction of green fluorescent protein (GFP) from the pKTS vector [57], and found that the protein is induced only under the addition of tetracycline with little to no protein produced in the absence of tetracycline. Flow cytometry analysis shows that GFP with an SsrA tag has lower expression levels than GFP without an SsrA tag. The control of chorismate mutase levels with the use of pKTS vector was also explored by the Hilvert lab [57]. They started with several rounds of mutagenesis that led to the formation of a catalytically inefficient, hexameric enzyme hEcCM. Activity was partially recovered when hEcCM was mutagenized to moderately efficient tEcCM (trimeric chorismate mutase). Cells harboring the wild type and moderately active tEcCM were indistinguishable in cell growth screens due to their high enzyme levels and activities. Thus, the genes for all three variants of the enzyme were cloned into the pKTS vector. At the highest tetracycline concentrations, the wild type and tEcCM cells had similar growth rates whereas hEcCM grew slowly. At intermediate tetracycline levels, tEcCM cells grew slower than the wild type cells. Thus, pKTS is an

efficient system for lowering enzyme levels in the cell and can be used for cell growth assays. The cell growth serves as a readout for enzyme activity/levels. The Hilvert lab used this system to screen libraries for mutant enzymes with enhanced activity in their directed evolution experiments.

1.16.3 Scoring cell growth as a function of enzyme activity/levels

Auxotrophic strains serve as selection platforms for studying enzyme activity as they do not grow unless the missing metabolite is produced by the respective enzyme. This selection is due to the restriction of cell growth as a function of enzyme activity. The maximal activity of the enzyme (V_{max}) is dependent on the concentration of the enzyme (E_{total}) in the cell and its k_{cat} (Figure 1.14). If the activity of the enzyme is essential to the cell, low amounts of protein, or less active protein (black zone), will lead to no growth. On the other hand, high enzyme activity or levels (blue zone) will lead to good growth of the cells. None of these conditions are ideal if cell growth needs to be scored with respect to enzyme function. Protein levels in the selection zone are ideal (highlighted in red) so that any change in enzyme activity gives an observable change in cell growth [60]. Thus, in order to obtain titrable cell growth with respect to enzyme activity, the enzyme levels or activities have to be lower than the chromosomal levels.

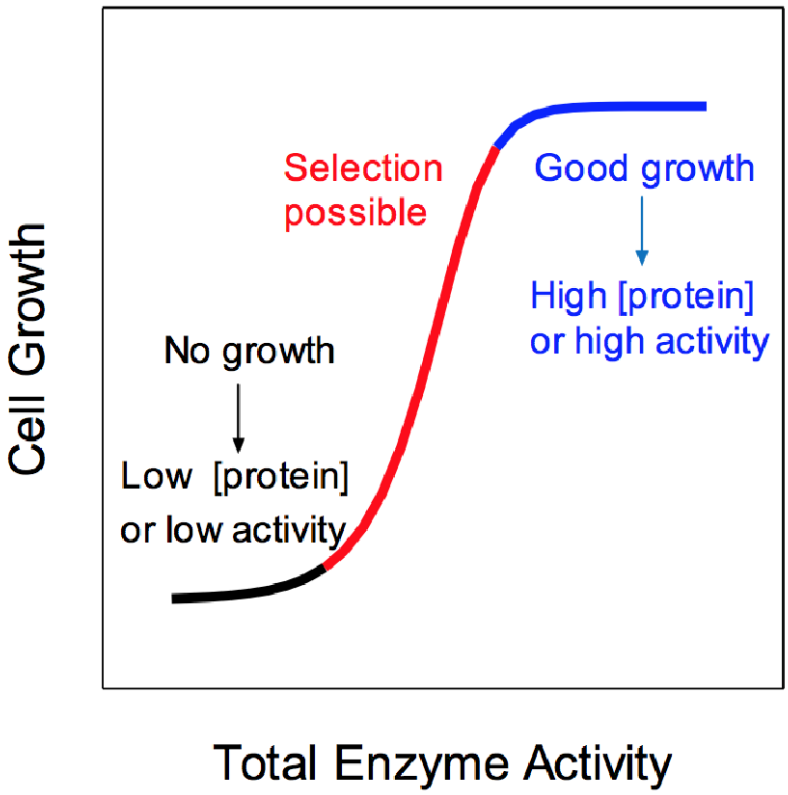

Figure 1.14: Selection conditions where cell growth is dependent on enzyme activity

Auxotrophic cells are capable of growth only when the metabolites of the reaction are supplied during cell growth. In a scenario where there is a low enzyme level or activity, there will be no or negligible cell growth (black line). The other case would be where high enzyme activity or levels leads to good growth (blue line). Selection conditions need to be designed where cell growth is dependent on changes in the enzyme activity (red line). Any small change in the total enzyme activity thus leads to an appreciable change in cell growth. Adapted from [60]

For our *in vivo* titration of enzyme activity using an osmotic stress assay, we work with the deletant strains of the enzymes of the folate pathway. The selected enzymes are essential for the cell. These strains are rescued with the introduction of the respective gene in the pKTS vector. These strains are referred to as rescued or complemented strains. The deletant strain is capable of growth in minimal media supplemented with the folate end product(s). However, the rescued strain is grown in minimal media without supplements and its growth is solely dependent on the enzyme activity. The level of enzyme in the rescued cells is lower than the chromosomal level, and hence cell growth is sensitive to enzymatic activity. Cell growth with increasing osmotic stress in the rescued strain serves as a readout for the enzyme activity and growth of the deletant strain in minimal media with added supplements serves as the control.

The enzymes investigated are narrowed down based on the criteria listed below:

1. The folate pathway enzymes should be essential to the cell. Knockout strains of the enzymes should be auxotrophic and can only grow in minimal media with the addition of respective folate end products.

2. The pKTS vector is designed to add an SsrA tag to the C-terminus of the enzyme. Therefore, the C terminus should not be close to the active site to ensure its proper functioning.

3. A preference is that the K_M of the substrate should be higher than the *in vivo* concentration of the substrate to ensure that the active site is not saturated.

1.17 Enzymes selected for the study

Reduced forms of folate are metabolized by the enzymes of the folate pathway (Figure 1.2). Since our previous studies show that osmolytes preferentially interact with DHF, we predict that osmolytes interact with the other reduced forms of folate as well. The predicted preferential interaction coefficients of two osmolytes, trehalose and betaine,

with DHF, THF and 5, 10-methyleneTHF (as well as other ligands) are listed in Table 1.2. A negative value is indicative of preferential interaction of the osmolyte with the ligand whereas positive value is indicative of preferential exclusion. It is predicted that the reduced folates preferentially interact with osmolytes, and we use osmotic stress titration studies to examine these interactions *in vivo*. Thus, with favorable weak interactions of osmolytes with the ligand, we predict that the ligand enzyme complex will be lowered in the cell leading to lesser activity of the enzyme. On the other hand, unfavorable osmolyte ligand interactions will reduce the desolvation penalty, leading to tighter complex formation and enhanced activity. The enzymes studied were R67 dihydrofolate reductase (R67 DHFR), methylenetetrahydrofolate reductase (MTHFR) and serine hydroxymethyltransferase (SHMT). The presence of the SsrA tag at the C-terminus is predicted to not interfere with the activity of these enzymes. This is inferred by measuring the distance between the active site and C-terminus of the enzyme. The active site is

Table 1.2 Preferential interaction coefficients of betaine and trehalose calculated for the ligands of the folate pathway.

Enzyme	Ligand	Betaine μ_{23}/RT (m^{-1})[a]	Trehalose μ_{23}/RT (m^{-1}) [b]
DHFR	NADPH	0.983	-0.408
	DHF	-0.049	-0.110
	Trimethoprim	-0.744	0.468
SHMT	Serine	0.160	0.018
	Glycine	0.156	-0.038
	THF	-0.112	-0.122
	5,10-methyleneTHF	-0.053	-0.105
	Pyridoxal 5'-phosphate	0.820	-0.676
Chorismate mutase	Chorismate	0.430	0.140
	Prephenate	0.563	-0.006
MTHFR	NADH	0.160	0.277
	5,10-methyleneTHF	-0.053	-0.105
	FAD	0.999	-0.651

a: values calculated from [9, 26]
b: values calculated from [10]

The inhibitors of the enzyme are highlighted in red and substrates are highlighted in blue.

around 20 Å away from the C-terminus for these enzymes.

As the pKTS plasmid from the Hilvert lab had a chorismate mutase insert, we also worked with this enzyme. Its substrate, chorismate, is predicted to be preferentially excluded by both trehalose and betaine as it has a positive μ_{23}/RT value. Low to no effect of osmotic stress on the rescued strain as compared to the deletant strain is expected from the chorismate mutase titration studies.

1.17.1 Plasmid encoded R67 Dihydrofolate reductase (R67 DHFR)

Dihydrofolate reductase catalyzes the reduction of dihydrofolate (DHF) to tetrahydrofolate (THF) using NADPH as a cofactor. R67 DHFR is different in sequence and structure from the chromosomal variant from *E. coli* [61]. EcDHFR is a monomer and is the target of the antibiotic, trimethoprim. In contrast, R67 DHFR is a tetramer [62], and confers resistance to trimethoprim [61]. R67 DHFR's active site is the central pore where both the ligand and cofactor bind [63]. The K_M for DHF is 5.8 µM, while the intracellular concentration of DHF is 51 µM in *E. coli* [64]. Thus, it is predicted that its active site is saturated with the DHF *in vivo*. Another variant of R67 DHFR that is used in our studies is Quad4. The Quad4 gene is a tandem array of four fused R67 DHFR genes and the kinetic parameters of the resulting monomeric protein are similar to those of R67 DHFR [65].

1.17.2 Methylenetetrahydrofolate reductase (MTHFR)

Methylenetetrahydrofolate reductase (MTHFR) is encoded by the *metF* gene in *E. coli* and its enzyme activity is linked to methionine production in the cell. In humans, a deficiency of MTHFR leads to elevated homocysteine levels in plasma and increases the risk for cardiovascular disease and neural tube defects [66]. Methylenetetrahydrofolate reductase is a tetrameric enzyme, which catalyzes the reduction of 5, 10-methyleneTHF to 5-methylTHF using NAD(P)H as a cofactor. The 5-methylTHF product serves as a methyl group donor for the subsequent conversion of homocysteine to methionine by methionine synthase [67]. A FAD cofactor is essential for the activity of the enzyme [67]. The enzyme catalyzes the reaction using a ping-pong Bi-Bi mechanism. The FAD-bound enzyme gets reduced by NADH in the reductive half reaction. In the oxidative half–reaction, the reducing equivalent is transferred to 5,10-methyleneTHF to form 5-methylTHF and FAD gets oxidized [68]. 5, 10-methyleneTHF binding to the enzyme reduces the loss of FAD and stabilizes the enzyme [66].

In *E. coli* K12, the concentration of 5,10-methylene-THF is 22.2 µM [69]. The MTHFR K_M for 5,10-methylene-THF is only 0.5 µM [67], suggesting the enzyme will be saturated *in vivo.* Porcine and plant MTHFRs bind polyglutamylated folates with lower K_M values, however any preference for polyglutamylated substrates is not yet established for the *E. coli* enzyme [70]. However, triglutamylated folates are more effective in preventing loss of FAD from *E. coli* MTHFR compared to monoglutamylated folates, thereby stabilizing the enzyme [66].

1.17.3 Serine hydroxymethyltransferase (SHMT)

There are two major pathways for biosynthesis of serine and glycine. Phosphoglyceric acid is converted to serine which is acted upon by SHMT to make glycine. The second reaction is the synthesis of glycine from threonine by action of threonine aldolase [71, 72].

Serine hydroxymethyltransferase (SHMT) is the enzyme encoded by the g*lyA* gene. SHMT converts serine to glycine using pyridoxal phosphate (PLP) as a coenzyme. It catalyzes the cleavage of PLP-serine to form PLP-glycine along with the condensation of formaldehyde with THF to form 5, 10-methenyltetrahydrofolate [73]. In *E. coli* K12, the THF concentration (in all glutamylation states) is 10.1 μM [69] and the K_M for THF is 25 μM [74]. The K_M is higher than the concentration of the metabolites *in vivo* [69], suggesting we may be able to titrate its activity.

1.17.4 Chorismate mutase (CM)

Chorismate mutase is used as a negative control in our studies. Chorismate mutase catalyzes the intramolecular rearrangement of chorismate to prephenate [75]. Prephenate is responsible for the biosynthesis of aromatic amino acids like phenylalanine and tyrosine [76]. *E. coli* possess two chorismate mutases, each fused to either prephenate dehydrogenase or prephenate dehydratase [77]. Thus a deletant strain of CM abolishes not only the CM activity in this organism, but also the dehydrogenase and dehydratase reactions responsible for aromatic acid biosynthesis. Since this enzyme serves as the metabolic branchpoint, a CM deletant (*aroQ*) strain with an auxillary plasmid (pKIMP-UAUC) [77], which carries the two genes for the dehydrogenase and dehydratase activities is used. Prephenate can thus be converted to tyrosine and phenylalanine. The use of the *aroQ* deletant strain with an auxillary plasmid (pKIMP-UAUC) strain allows us to score the effect of osmotic stress only on CM activity.

1.18 Rationale/aims of this research work

The work in this thesis addresses three main questions:

5. What are the molecular interactions between trehalose and folate? Vapor pressure osmometry (VPO) studies can be used to study the interactions of osmolyte with specific functional groups. Previous work in our lab looked at how betaine interacts with the functional groups on folate. Trehalose is the predominant osmolyte in nutrient limiting conditions, and the osmotic stress experiments in Chapter 4 mimic these conditions. Hence it is intriguing to figure out how trehalose interacts with various functional groups that are present on folate, specifically with heterocyclic and non-heterocyclic aromatic compounds. We use VPO to test for interactions of trehalose with about 50 compounds which have the functional groups of interest. The results of this study are discussed in Chapter 2.

6. Does trehalose and betaine exert opposing effects on ligand/s binding to enzyme DHPS? Our studies in Chapter 2 show that betaine and trehalose have differential interactions with different functional groups. An example of this concerns the phosphate group, which excludes betaine, however phosphate interacts with trehalose. In order to study how these opposing interactions affect ligand binding to the enzyme, we elected to work with the enzyme dihydropteroate synthase (DHPS). One of the ligands of this enzyme, pteridine pyrophosphate, contains phosphate groups. ITC studies are used to understand how betaine and trehalose affect the binding of ligand(s) to enzyme DHPS. This is discussed in Chapter 3 of this thesis.

7. The osmolytes weakly interact with dihydrofolate and hinder its binding to the enzyme DHFR. But does this hold true in an *in vivo* environment? The cellular environment is complex and crowded and the weak interactions studied *in vitro* are also found inside the cells. So, can *in vitro* studies be correlated with the *in vivo* cellular environment? If it does, the osmolytes should interact with folates in the cell and affect the ligand binding to the enzyme. We employ osmotic stress studies in *Escherichia coli* to address this question. This study is discussed in detail in Chapter 4.

My thesis chapters, put together, focus on understanding the effect an osmolyte can exert on the functioning of an enzyme *in vitro* as well as in *in vivo* conditions.

1.19 References

[1] Scott, J. M., and Weir, D. G. (1998) Folic acid, homocysteine and one-carbon metabolism: a review of the essential biochemistry, *J. Cardiovasc Risk 5*, 223-227.

[2] Bermingham, A., and Derrick, J. P. (2002) The folic acid biosynthesis pathway in bacteria: evaluation of potential for antibacterial drug discovery, *Bioessays 24*, 637-648.

[3] E Trimmer, E. (2013) Methylenetetrahydrofolate reductase: biochemical characterization and medical significance, *Curr. Pharm. Des. 19*, 2574-2593.

[4] McGuffee, S. R., and Elcock, A. H. (2010) Diffusion, crowding & protein stability in a dynamic molecular model of the bacterial cytoplasm, *PLoS Comput. Biol. 6*, e1000694.

[5] Zimmerman, S. B., and Minton, A. P. (1993) Macromolecular crowding: biochemical, biophysical, and physiological consequences, *Annu. Rev. Biophys. Biomol. Struct 22*, 27-65.

[6] Minton, A. P. (1981) Excluded volume as a determinant of macromolecular structure and reactivity, *Biopolymers 20*, 2093-2120.

[7] Deardorff, D. L. (1980) Osmotic strength, osmolality, and osmolarity, *Am. J. Health Syst. Pharm. 37*, 504-509.

[8] Csonka, L. N. (1989) Physiological and genetic responses of bacteria to osmotic stress, *Microbiol. Rev. 53*, 121-147.

[9] Capp, M. W., Pegram, L. M., Saecker, R. M., Kratz, M., Riccardi, D., Wendorff, T., Cannon, J. G., and Record Jr, M. T. (2009) Interactions of the osmolyte glycine betaine with molecular surfaces in water: thermodynamics, structural interpretation, and prediction of m-values, *Biochemistry 48*, 10372-10379.

[10] Hong, J., Gierasch, L. M., and Liu, Z. (2015) Its preferential interactions with biopolymers account for diverse observed effects of trehalose, *Biophys. J. 109*, 144-153.

[11] Wood, J. M. (2015) Bacterial responses to osmotic challenges, *The Journal of general physiology 145*, 381-388.

[12] Yancey, P. H., Clark, M. E., Hand, S. C., Bowlus, R. D., and Somero, G. N. (1982) Living with water stress: evolution of osmolyte systems, *Science 217*, 1214-1222.

[13] Bolen, D. W. (2001) Protein stabilization by naturally occurring osmolytes, In *Protein structure, stability, and folding*, pp 17-36, Springer.

[14] Larsen, P., Sydnes, L., Landfald, B., and Strøm, A. (1987) Osmoregulation in *Escherichia coli* by accumulation of organic osmolytes: betaines, glutamic acid, and trehalose, *Arch. Microbiol. 147*, 1-7.

[15] Falkenberg, P., and Strøm, A. R. (1990) Purification and characterization of osmoregulatory betaine aldehyde dehydrogenase of *Escherichia coli*, *Biochim. Biophys. Acta. 1034*, 253-259.

[16] Sévin, D. C., and Sauer, U. (2014) Ubiquinone accumulation improves osmotic-stress tolerance in *Escherichia coli*, *Nat. Chem. Biol. 10*, 266.

[17] Giaever, H., Styrvold, O. B., Kaasen, I., and Strøm, A. (1988) Biochemical and genetic characterization of osmoregulatory trehalose synthesis in *Escherichia coli*, *J. Bacteriol. 170*, 2841-2849.

[18] Cayley, S., Lewis, B., and Record, M. (1992) Origins of the osmoprotective properties of betaine and proline in *Escherichia coli* K-12, *J. Bacteriol. 174*, 1586-1595.
[19] Khan, S. H., Ahmad, N., Ahmad, F., and Kumar, R. (2010) Naturally occurring organic osmolytes: from cell physiology to disease prevention, *IUBMB life 62*, 891-895.
[20] Diamant, S., Eliahu, N., Rosenthal, D., and Goloubinoff, P. (2001) Chemical chaperones regulate molecular chaperones in vitro and in cells under combined salt and heat stresses, *J. Biol. Chem. 276*, 39586-39591.
[21] Weber, A., Kögl, S. A., and Jung, K. (2006) Time-dependent proteome alterations under osmotic stress during aerobic and anaerobic growth in *Escherichia coli*, *J. Bacteriol. 188*, 7165-7175.
[22] Grubbs, J., Rahmanian, S., DeLuca, A., Padmashali, C., Jackson, M., Duff Jr, M. R., and Howell, E. E. (2011) Thermodynamics and solvent effects on substrate and cofactor binding in *Escherichia coli* chromosomal dihydrofolate reductase, *Biochemistry 50*, 3673-3685.
[23] Chopra, S., Dooling, R. M., Horner, C. G., and Howell, E. E. (2008) A balancing act between net uptake of water during dihydrofolate binding and net release of water upon NADPH binding in R67 dihydrofolate reductase, *J. Biol. Chem. 283*, 4690-4698.
[24] Bhojane, P. P., Duff Jr, M. R., Patel, H. C., Vogt, M. E., and Howell, E. E. (2014) Investigation of osmolyte effects on FolM: comparison with other dihydrofolate reductases, *Biochemistry 53*, 1330-1341.
[25] Narayana, N., Matthews, D. A., Howell, E. E., and Xuong, N.-h. (1995) A plasmid-encoded dihydrofolate reductase from trimethoprim-resistant bacteria has a novel D 2-symmetric active site, *Nat. Struc. Biol. 2*, 1018.
[26] Bhojane, P. P., Duff Jr, M. R., Bafna, K., Rimmer, G. P., Agarwal, P. K., and Howell, E. E. (2016) Aspects of Weak Interactions between Folate and Glycine Betaine, *Biochemistry 55*, 6282-6294.
[27] Duff Jr, M. R., Grubbs, J., Serpersu, E., and Howell, E. E. (2012) Weak interactions between folate and osmolytes in solution, *Biochemistry 51*, 2309-2318.
[28] Poe, M. (1973) Proton Magnetic Resonance Studies of Folate, Dihydrofolate, and Methotrexate *J. Biol. Chem. 248*, 7025-7032.
[29] Diehl, R. C., Guinn, E. J., Capp, M. W., Tsodikov, O. V., and Record Jr, M. T. (2013) Quantifying additive interactions of the osmolyte proline with individual functional groups of proteins: comparisons with urea and glycine betaine, interpretation of m-values, *Biochemistry 52*, 5997-6010.
[30] Courtenay, E., Capp, M., Saecker, R., and Record Jr, M. (2000) Thermodynamic analysis of interactions between denaturants and protein surface exposed on unfolding: Interpretation of urea and guanidinium chloride m-values and their correlation with changes in accessible surface area (ASA) using preferential interaction coefficients and the local-bulk domain model, *Proteins: Struct, Funct, Bioinf. 41*, 72-85.
[31] Knowles, D., Shkel, I. A., Phan, N. M., Sternke, M., Lingeman, E., Cheng, X., Cheng, L., O'Connor, K., and Record, M. T. (2015) Chemical interactions of polyethylene glycols (PEGs) and glycerol with protein functional groups: applications to effects of PEG and glycerol on protein processes, *Biochemistry 54*, 3528-3542.

[32] Courtenay, E., Capp, M., Anderson, C., and Record, M. (2000) Vapor pressure osmometry studies of osmolyte− protein interactions: implications for the action of osmoprotectants in vivo and for the interpretation of “osmotic stress” experiments in vitro, *Biochemistry 39*, 4455-4471.
[33] Tsodikov, O. V., Record Jr, M. T., and Sergeev, Y. V. (2002) Novel computer program for fast exact calculation of accessible and molecular surface areas and average surface curvature, *J. Comput. Chem. 23*, 600-609.
[34] Winther, L. R., Qvist, J., and Halle, B. (2012) Hydration and mobility of trehalose in aqueous solution, *J. Phys. Chem. B 116*, 9196-9207.
[35] Teramoto, N., Sachinvala, N., and Shibata, M. (2008) Trehalose and trehalose-based polymers for environmentally benign, biocompatible and bioactive materials, *Molecules 13*, 1773-1816.
[36] Lin, T. Y., and Timasheff, S. N. (1996) On the role of surface tension in the stabilization of globular proteins, *Prot. Sci. 5*, 372-381.
[37] Auton, M., Rösgen, J., Sinev, M., Holthauzen, L. M. F., and Bolen, D. W. (2011) Osmolyte effects on protein stability and solubility: a balancing act between backbone and side-chains, *Biophys. Chem. 159*, 90-99.
[38] Sapir, L., and Harries, D. (2010) Linking trehalose self-association with binary aqueous solution equation of state, *J. Phys. Chem. B 115*, 624-634.
[39] Babaoglu, K., Qi, J., Lee, R. E., and White, S. W. (2004) Crystal structure of 7, 8-dihydropteroate synthase from *Bacillus anthracis*: mechanism and novel inhibitor design, *Structure 12*, 1705-1717.
[40] Chotpatiwetchkul, W., Boonyarattanakalin, K., Gleeson, D., and Gleeson, M. P. (2017) Exploring the catalytic mechanism of dihydropteroate synthase: elucidating the differences between the substrate and inhibitor, *Org. Biomol. Chem. 15*, 5593-5601.
[41] Yun, M.-K., Wu, Y., Li, Z., Zhao, Y., Waddell, M. B., Ferreira, A. M., Lee, R. E., Bashford, D., and White, S. W. (2012) Catalysis and sulfa drug resistance in dihydropteroate synthase, *Science 335*, 1110-1114.
[42] Levy, C., Minnis, D., and Derrick, J. P. (2008) Dihydropteroate synthase from *Streptococcus pneumoniae*: structure, ligand recognition and mechanism of sulfonamide resistance, *Biochem. J. 412*, 379-388.
[43] Achari, A., Champness, J. N., Bryant, P. K., Rosemond, J., and Stammers, D. K. (1997) Crystal structure of the anti-bacterial sulfonamide drug target dihydropteroate synthase, *Nat. Struc. Mol. Biol. 4*, 490.
[44] Morgan, R. E., Batot, G. O., Dement, J. M., Rao, V. A., Eadsforth, T. C., and Hunter, W. N. (2011) Crystal structures of *Burkholderia cenocepacia* dihydropteroate synthase in the apo-form and complexed with the product 7, 8-dihydropteroate, *BMC Struct. Biol. 11*, 21.
[45] Hampele, I. C., D’Arcy, A., Dale, G. E., Kostrewa, D., Nielsen, J., Oefner, C., Page, M. G., Schönfeld, H.-J., Stüber, D., and Then, R. L. (1997) Structure and function of the dihydropteroate synthase from *Staphylococcus aureus*, Elsevier.
[46] Kasekarn, W., Sirawaraporn, R., Chahomchuen, T., Cowman, A. F., and Sirawaraporn, W. (2004) Molecular characterization of bifunctional hydroxymethyldihydropterin pyrophosphokinase-dihydropteroate synthase from *Plasmodium falciparum*, *Mol. Biochem. Parasitol. 137*, 43-53.

[47] Pemble IV, C. W., Mehta, P. K., Mehra, S., Li, Z., Nourse, A., Lee, R. E., and White, S. W. (2010) Crystal structure of the 6-hydroxymethyl-7, 8-dihydropterin pyrophosphokinase• dihydropteroate synthase bifunctional enzyme from *Francisella tularensis*, *PloS one 5*, e14165.
[48] Yogavel, M., Nettleship, J. E., Sharma, A., Harlos, K., Jamwal, A., Chaturvedi, R., Sharma, M., Jain, V., Chhibber-Goel, J., and Sharma, A. (2018) Structure of 6-hydroxymethyl-7, 8-dihydropterin pyrophosphokinase–dihydropteroate synthase from Plasmodium vivax sheds light on drug resistance, *J. Biol. Chem. 293*, 14962-14972.
[49] Lawrence, M. C., Iliades, P., Fernley, R. T., Berglez, J., Pilling, P. A., and Macreadie, I. G. (2005) The three-dimensional structure of the bifunctional 6-hydroxymethyl-7, 8-dihydropterin pyrophosphokinase/dihydropteroate synthase of *Saccharomyces cerevisiae*, *J. Mol. Biol. 348*, 655-670.
[50] Greenfield, R. A., and Bronze, M. S. (2003) Prevention and treatment of bacterial diseases caused by bacterial bioterrorism threat agents, *Drug Discov. Today 8*, 881-888.
[51] Patel, O. G., Mberu, E. K., Nzila, A. M., and Macreadie, I. G. (2004) Sulfa drugs strike more than once, *Trends Parasitol. 20*, 1-3.
[52] Djapa, L. Y., Zelikson, R., Delahodde, A., Bolotin-Fukuhara, M., and Mazabraud, A. (2006) *Plasmodium vivax* dihydrofolate reductase as a target of sulpha drugs, *FEMS Microbiol. Lett. 256*, 105-111.
[53] Hammoudeh, D. I., Zhao, Y., White, S. W., and Lee, R. E. (2013) Replacing sulfa drugs with novel DHPS inhibitors, *Future Med. Chem. 5*, 1331-1340.
[54] Stone, S. R., and Morrison, J. F. (1986) Mechanism of inhibition of dihydrofolate reductases from bacterial and vertebrate sources by various classes of folate analogues, *Biochim. Biophys. Acta. 869*, 275-285.
[55] Amyes, S., and Smith, J. (1974) R-factor trimethoprim resistance mechanism: an insusceptible target site, *Biochem. Biophys. Res. Commun. 58*, 412-418.
[56] Stinnett, L. G., Smiley, R. D., Hicks, S. N., and Howell, E. E. (2004) “Catch 222,” the Effects of Symmetry on Ligand Binding and Catalysis in R67 Dihydrofolate Reductase as Determined by Mutations at Tyr-69, *J. Biol. Chem. 279*, 47003-47009.
[57] Neuenschwander, M., Butz, M., Heintz, C., Kast, P., and Hilvert, D. (2007) A simple selection strategy for evolving highly efficient enzymes, *Nat. Biotech. 25*, 1145.
[58] Bertram, R., and Hillen, W. (2008) The application of Tet repressor in prokaryotic gene regulation and expression, *Microb. Biotechnol. 1*, 2-16.
[59] Lutz, R., and Bujard, H. (1997) Independent and tight regulation of transcriptional units in *Escherichia coli* via the LacR/O, the TetR/O and AraC/I1-I2 regulatory elements, *Nucleic acids Res. 25*, 1203-1210.
[60] Butz, M., Neuenschwander, M., Kast, P., and Hilvert, D. (2011) An N-terminal protein degradation tag enables robust selection of highly active enzymes, *Biochemistry 50*, 8594-8602.
[61] Howell, E. E. (2005) Searching sequence space: two different approaches to dihydrofolate reductase catalysis, *ChemBioChem 6*, 590-600.

[62] Krahn, J. M., Jackson, M. R., DeRose, E. F., Howell, E. E., and London, R. E. (2007) Crystal structure of a type II dihydrofolate reductase catalytic ternary complex, *Biochemistry 46*, 14878-14888.
[63] Howell, E. E., Shukla, U., Hicks, S. N., Smiley, R. D., Kuhn, L. A., and Zavodszky, M. I. (2001) One site fits both: a model for the ternary complex of folate+ NADPH in R67 dihydrofolate reductase, a D 2 symmetric enzyme, *J. Comput. Aided Mol. Des. 15*, 1035-1052.
[64] Bennett, B. D., Yuan, J., Kimball, E. H., and Rabinowitz, J. D. (2008) Absolute quantitation of intracellular metabolite concentrations by an isotope ratio-based approach, *Nat. Protoc. 3*, 1299.
[65] Feng, J., Grubbs, J., Dave, A., Goswami, S., Horner, C. G., and Howell, E. E. (2010) Radical redesign of a tandem array of four R67 dihydrofolate reductase genes yields a functional, folded protein possessing 45 substitutions, *Biochemistry 49*, 7384-7392.
[66] Guenther, B. D., Sheppard, C. A., Tran, P., Rozen, R., Matthews, R. G., and Ludwig, M. L. (1999) The structure and properties of methylenetetrahydrofolate reductase from *Escherichia coli* suggest how folate ameliorates human hyperhomocysteinemia, *Nat. Struc. Mol. Biol. 6*, 359.
[67] Sheppard, C. A., Trimmer, E. E., and Matthews, R. G. (1999) Purification and Properties of NADH-Dependent 5, 10-Methylenetetrahydrofolate Reductase (MetF) from *Escherichia coli*, *J. Bacteriol. 181*, 718-725.
[68] Trimmer, E. E., Ballou, D. P., and Matthews, R. G. (2001) Methylenetetrahydrofolate reductase from *Escherichia coli*: elucidation of the kinetic mechanism by steady-state and rapid-reaction studies, *Biochemistry 40*, 6205-6215.
[69] Kwon, Y. K., Lu, W., Melamud, E., Khanam, N., Bognar, A., and Rabinowitz, J. D. (2008) A domino effect in antifolate drug action in *Escherichia coli*, *Nat. Chem. Biol. 4*, 602.
[70] Matthews, R. G., and Baugh, C. M. (1980) Interactions of pig liver methylenetetrahydrofolate reductase with methylenetetrahydropteroylpolyglutamate substrates and with dihydropteroylpolyglutamate inhibitors, *Biochemistry 19*, 2040-2045.
[71] Landgraf, J., Levinthal, M., and Danchin, A. (1994) The role of H-NS in one carbon metabolism, *Biochimie 76*, 1063-1070.
[72] Ogawa, H., Gomi, T., and Fujioka, M. (2000) Serine hydroxymethyltransferase and threonine aldolase: are they identical?, *Int. J. Biochem. Cell Biol. 32*, 289-301.
[73] Scarsdale, J. N., Radaev, S., Kazanina, G., Schirch, V., and Wright, H. (2000) Crystal structure at 2.4 Å resolution of *E. coli* serine hydroxymethyltransferase in complex with glycine substrate and 5-formyl tetrahydrofolate1, *J. Mol. Biol. 296*, 155-168.
[74] Schirch, V., Hopkins, S., Villar, E., and Angelaccio, S. (1985) Serine hydroxymethyltransferase from *Escherichia coli*: purification and properties, *J. Bacteriol. 163*, 1-7.
[75] Andrews, P., Cain, E., Rizzardo, E., and Smith, G. (1977) Rearrangement of chorismate to prephenate: Use of chorismate mutase inhibitors to define the transition state structure, *Biochemistry 16*, 4848-4852.
[76] Haslam, E. (1993) *Shikimic acid: metabolism and metabolites*, John Wiley & Sons Inc.

[77] Kast, P., Asif-Ullah, M., Jiang, N., and Hilvert, D. (1996) Exploring the active site of chorismate mutase by combinatorial mutagenesis and selection: the importance of electrostatic catalysis, *Proc. Natl. Acad. Sci. 93*, 5043-5048.

2 EXPLORATION OF WEAK INTERACTIONS BETWEEN TREHALOSE AND FOLATE

2.1 Introduction

Water has a relatively high heat capacity, a high dielectric constant and can hydrogen bond to form ordered structures. For this reason water is proposed to enslave the macromolecules of the cell [1]. Hydration and viscosity of the solvent influences the reactions, dynamics and activity of these macromolecules [2]. To understand cellular chemistry, it is important to study the role of water in those reactions. One of the greatest challenges in understanding the function of the cell is due to the lack of knowledge about non-covalent interactions, attractive and repulsive forces that exist in water [3]. One way to explore the role of water in these systems is to add small molecule osmolytes that will perturb water activity by reducing the concentration of water in the solution. Osmolytes are small molecules that occupy volume in a system and have different chemical properties. Osmolytes are present in most living cells and function as osmoregulators.

Our lab has used biophysics to understand the role of water in the binding of folates to the enzyme, dihydrofolate reductase (DHFR) [4-6]. Isothermal titration calorimetry studies have found that osmolytes tighten the binding of cofactor NADPH to DHFR. Tighter binding was attributed to a decreased solvation shell around the cofactor in the presence of osmolytes. The exclusion of osmolytes from the surface of NADPH reduced the desolvation penalty associated with enzyme-cofactor complex formation. Fewer waters solvate the cofactor in osmolyte-contain solutions, therefore less energy is needed to remove the waters from NADPH, increasing the overall binding affinity. However, osmolytes had an opposite effect on substrate, dihydrofolate (DHF), binding to the enzyme. Weaker DHF binding to the enzyme was attributed to preferential interaction of osmolytes with different functional groups on DHF. This interaction of the ligand with the osmolyte made binding less favorable as osmolytes, as well as water, had to be removed from the solvation shell around the binding interface. Our lab has wn similar osmolyte effects on DHF binding to enzymes (EcDHFR, R67 DHFR and FolM) performing DHFR activity. NMR and VPO studies have further indicated that the osmolyte, glycine betaine, preferentially interacts with the aromatic groups in the pABA ring, as well as amide and cationic nitrogens [7, 8]. Thus osmolytes participate in weak interactions with different functional groups on folate, and most likely will interact with other cellular components with similar functional groups.

One of the predominant cellular osmolytes is the saccharide, trehalose. Steady state kinetics on R67 DHFR performed in the presence of trehalose yielded a decrease in the K_m of DHF, while there was no effect on k_{cat} [5]. Further, we explored if these weak interactions were relevant *in vivo* by developing a cell-based assay where enzyme activity was lowered relative to basal cellular levels, and then exposing the cells to osmotic stress. *E. coli*, under high osmotic stress, produce osmolytes to regulate the osmotic pressure inside the cell. The lower enzyme activity led to less product formation, and ultimately reduced cell growth, with increasing osmotic stress [9]. The studies were performed under nutrient limiting conditions where trehalose is proposed to be the predominant osmolyte [10]. Under osmotic stress, trehalose weakly interacted with folate cycle metabolites, decreasing their binding to their respective enzymes [9]. Both osmolytes and water molecules would have to be released from the substrate solvent shell, which lowered

enzyme-ligand association and product formation. It is therefore intriguing to understand the molecular interactions between trehalose and functional groups on folates.

A vapor pressure osmometry (VPO) technique was developed by the Record lab to monitor weak interactions between osmolytes and other molecules [11,12]. Preferential interaction coefficients measure the change in the chemical potential of a compound upon addition of an osmolyte. Interaction or exclusion of the osmolyte with the atom types present on a compound can occur. Such favorable or unfavorable interactions of osmolytes with several model test compounds were explored in these experiments. The model test compounds used displayed different functional groups and were used to study the interaction of an osmolyte with several atom types. The preferential interaction value (μ_{23}/RT) is indicative of the preference of a test compound to either interact with the osmolyte or water in a three-component system (water, test compound and osmolyte). A negative μ_{23}/RT value is indicative of preferential interaction of the test compound with the osmolyte, a positive μ_{23}/RT value is indicative of preferential interaction of the test compound with water. A value of zero is indicative of equal preference for water and osmolyte.

The μ_{23}/RT value is the sum of the contributions of the favorable and unfavorable interactions of an osmolyte with the different functional groups present on the test compound. Thus, the information on the area occupied by the solvent accessible functional groups along with the μ_{23}/RT values can be dissected to obtain the contributions arising from each atom type on the test compound. The values from each atom type is called the atomistic interaction coefficient (α values), which indicates the preference of the interaction/exclusion of the functional group with the osmolyte.

In a study done by Hong et al [19], freezing point depression osmometry was employed to obtain the preferential interactions coefficients for trehalose. The test compounds used were mainly amino acids, salts and aromatic compounds. It was reported that trehalose preferentially interacted with phosphate, carboxylate and amide oxygens, and preferentially excluded aliphatic carbons and cationic nitrogen. There were dual values reported for aromatic carbons (positive or negative values depending on the test compound used for α value analysis). No information on the behavior of trehalose with aromatic nitrogens was reported. Folate is made up of a pterin and a *p*-aminobenzoate ring, and hence we wanted to delve into understanding how trehalose interacted with aromatic carbons and nitrogens. In this chapter we have focused on extending the osmometry studies of trehalose using vapor pressure osmometer with test compounds that better mimic the functional groups of folates.

2.2 Materials and methods

2.2.1 Vapor Pressure Osmometry (VPO)

VPO experiments were performed according to the protocol by the Record group [12]. Samples were measured on a Wescor Vapro 5520 osmometer. In cases of osmolality

readings above 1.000 Osm, a calibration curve was made using 1.000, 1.500 and 2.000 osmol standards to correct sample readings. VPO was used to measure the preferential interaction coefficients of trehalose with 50 model test compounds. The model test compounds can be broadly classified as salts, carboxylates, polyols, amino acids and amides, heterocyclic and non-heterocyclic aromatic compounds. Stock solutions of the test compounds and trehalose were prepared gravimetrically. Sapir and Harries have reported that trehalose deviates from ideal behavior at concentrations above 0.5 molal due to self-association [13]. It can hydrogen bond using its hydroxyl groups, and these interactions increase with increasing concentrations of trehalose. Thus, the experiments were performed such that the final molal concentrations of trehalose were kept between 0.1-0.5 molal. Three component solutions contained a series of trehalose (0.1-0.5 m) and test compound (between 0.1-0.8 m) concentrations were prepared by aliquoting from stock solutions and mixing with water to achieve the desired final molality. The same molalities of trehalose and test compound were each used as the two-component series. These solutions were equilibrated at room temperature for 15 minutes prior to measuring the osmolality in triplicate.

The difference between the osmolalities of the three component solutions and the trehalose and test compound two component solutions (∆Osm) were plotted against the product of the molalities of trehalose and test compound (Eq. 1):

$$\Delta Osm = Osm(m_2, m_3) - Osm(m_2, 0) - Osm(0, m_2) \qquad \text{Eq. 2.1 [12]}$$

where m_2 and m_3 are the molal concentrations of the test compound and trehalose, respectively. These data were fit linearly. The intercept should be set to zero as under ideal conditions when there is no self-association of the test compound or trehalose, as in the absence of either the test compound or trehalose, the value of ∆Osm is zero. The slope of the line is the preferential interaction coefficient (μ_{23}/RT) and this coefficient is independent of m_2 and m_3 (Eq. 2.2):

$$\Delta Osm \cong \left(\frac{\mu_{23}}{RT}\right) m_2 m_3 \qquad \text{Eq. 2.2}$$

In case of heterocyclic, non-heterocyclic aromatic compounds and folate, the pH of the solutions was adjusted to 7.0 to increase their solubility.

2.2.2 Calculation of *α*-values

Trehalose interacts differently with all types of functional groups or atom types. The degree of interaction is dependent upon how much area of the functional group/atom is exposed. Thus, the μ_{23}/RT can be broken up into components based on the surface area

of the atom types and is dependent upon the interaction of trehalose with a type of atom and its solvent accessible surface area. The summation of the favorable or unfavorable interactions of trehalose with the different atom types on the test compound gives the preferential interaction coefficient for that test compound.

The structures of the test compounds were obtained from BMRB, PDB or from Bhojane et al [7]. The solvent accessible areas of each functional group was determined using the program Surface racer.[14] A 1.4 Å water molecule radius was used to probe the surface of the molecule and determine the areas of each atom types exposed to the solvent. This information can be used to deconvolute the μ_{23}/RT values into atomistic interaction coefficient (α values) using the equation 2.3 [12]:

$$\frac{\mu_{23}}{RT} = \sum_i \left(\frac{\mu_{23}}{RTASA}\right)_i (ASA)_i + \sum_j \beta_j \sigma_j \qquad \text{Eq. 2.3}$$

Where $\mu_{23}/RTASA$ is the α value, the measure of the interaction of trehalose with each atom type per solvent exposed surface area of the atom, ASA is the solvent exposed surface area of atom type i, β is preferential interaction of trehalose with K^+, Na^+ or Cl^- ions and σ is the number of ions j. The data were fit for aliphatic carbons; aromatic carbons and nitrogens; amide, amine and cationic nitrogen; hydroxyl, carboxylate and phosphate oxygen atom types. Matlab 2018a was used for this with the code provided in Bhojane et al.[7] The α values for trehalose, along with the accessible surface area of any compound (for example folate), can be used to obtain the predicted preferential interaction coefficient of that compound.

2.2.3 Calculation of predicted μ_{23}/RT for protein unfolding in presence of trehalose

Atomistic interaction coefficients can be used to calculate the interactions of trehalose with proteins. In order to do this, we used literature data for the thermal stability of proteins (free energy of unfolding) in the presence of trehalose [11, 15-17]. The free energy of unfolding was then used to calculate the change in the chemical potential ($\Delta\mu_{23}$) of the proteins with trehalose using Eq 2.4:

$$\frac{\Delta G_{unf}}{m_3} = \Delta\mu_{23} \qquad \text{Eq. 2.4}$$

Where ΔG_{unf} is the free energy of unfolding. The preferential interaction coefficient can be determined by dividing $\Delta\mu_{23}$ by the gas constant and the temperature at which ΔG was measured. The predicted μ_{23}/RT values for the proteins were calculated from the α values and the solvent accessible surface area of the atoms on the folded protein. Structures for the proteins were obtained from the Protein Data Bank and the surface areas calculated using Surface racer [14]. The unfolded proteins were prepared in Pymol [18] as linear structures with random phi and psi angels. Unfolding of a protein is the equilibrium between the denatured and native states, and the free energy of unfolding is the difference in the free energy of the unfolded state minus the free energy of the folded

state. Therefore, the predicted preferential interaction coefficient for the protein was determined as the difference in the μ_{23}/RTs of the unfolded protein and the folded protein.

2.2.4 Calculation of μ_{23}/RT predicted values ligand binding

The change in predicted preferential interaction coefficients ($\Delta\mu_{23}$/RT) were calculated for ligand binding to proteins by determining the μ_{23}/RTs of the bound complex, as well as the apo-protein and free ligand. The surfaces areas of the structures were calculated in Surface racer [14], and were multiplied by the α values for the corresponding atom types. The $\Delta\mu_{23}$/RT was then determined by subtracting the μ_{23}/RT values for the ligand and apo-protein from the preferential interaction coefficient of the ligand-protein complex.

2.3 Results

In vitro biophysical and *in vivo* microbiological assay results indicate that trehalose interacts with folates [5, 9]. To explore which functional groups on folate were responsible for interaction/exclusion with trehalose, osmometry was performed on 50 model compounds. The compounds were chosen based on the structure of folate, and can be grouped into amino acids, carboxylates, polyols, salts and non-heterocyclic and heterocyclic aromatic compounds.

2.3.1 Aromatic compounds

Folate contains both aromatic carbons and nitrogens in its rings (see Figure 2.1), and previous studies indicated that betaine preferentially interacted with amine nitrogen off the aromatic rings and preferentially excluded the aromatic nitrogens [7]. It is of utmost importance for us to look at the contributions arising from the interactions of trehalose with these atom types. We wanted to segregate atom types as amine nitrogen off the aromatic ring (*m*-aminobenzoate) and aromatic nitrogens (i.e., nicotinic acid). We used heterocyclic aromatic compounds containing nitrogen in the ring and aromatic compounds to determine this distinction.

2.3.2 Non heterocyclic aromatic compounds

We tested benzoate variants with hydroxyl and amino groups at the ortho, meta and para positions in the ring. We also included toluic acid in our studies, which has a methyl group at the para position (Figure 2.1) All the compounds in this series exhibited positive preferential interaction coefficient (Figure 2.2). The μ_{23}/RT for toluic acid was the most positive in this series. Hydroxybenzoates in general exhibited higher μ_{23}/RT than

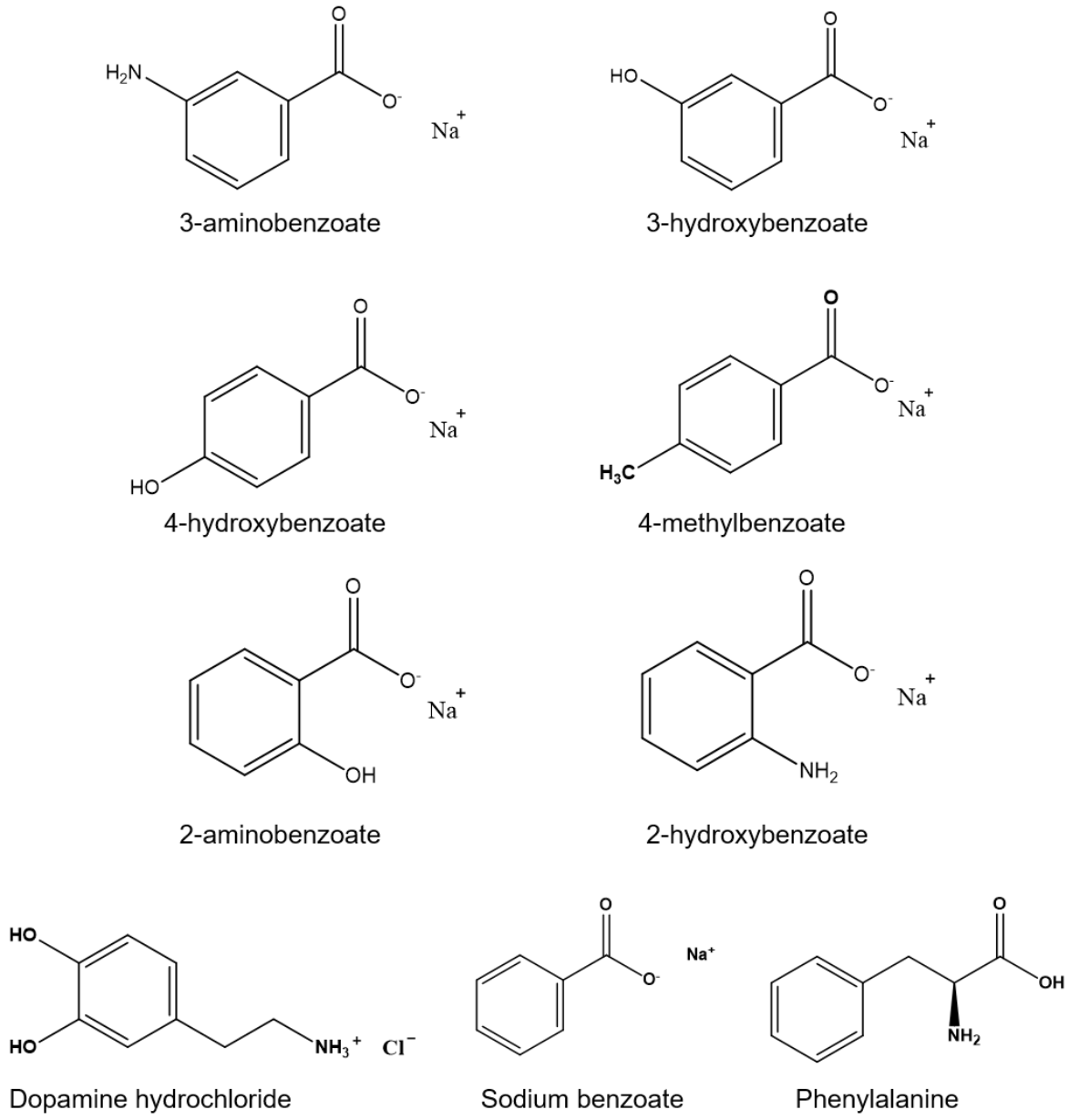

Figure 2.1: Aromatic compounds used in this study

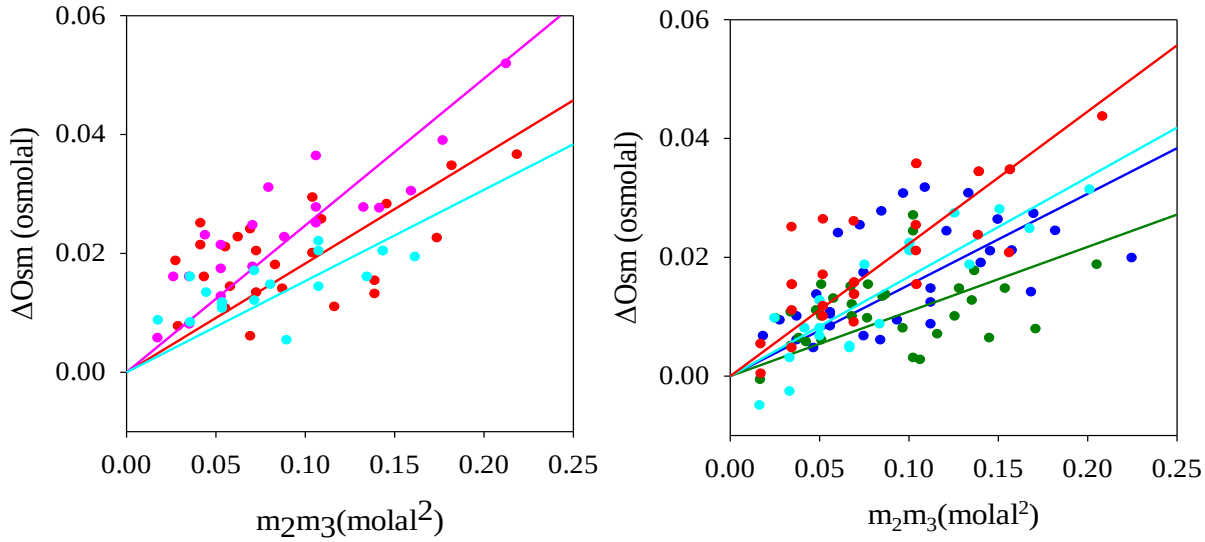

Figure 2.2: Determination of the preferential interaction coefficients (μ_{23}/RT) of trehalose with aromatic compounds

The ΔOsm is plotted against the product of trehalose and test compound molalities (m_2m_3) and the slope of the line is the μ_{23}/RT value for the compound. A: Data are shown for the aromatic compounds in panel A are amino and methyl substitutions at different positions in the benzene ring (●) 3-aminobenzoic acid, (●) 2-aminobenzoic acid, (●) 4-methylbenzoic acid. B: the variants of hydroxyl substitutions in the benzene ring (●) 3-hydroxybenzoic acid, (●) 4-hydroxybenzoic acid, (●) 2-hydroxybenzoic acid and (●) dopamine HCl

aminobenzoates. Hong et al used sodium benzoate to obtain the preferential interaction of trehalose with aromatic carbons. The value reported was -0.004 ± 0.038 m^{-1}. This value is within error of zero. None of the benzoate derivatives used in our study had μ_{23}/RT values near zero.

2.3.3 Heterocyclic aromatic compounds with nitrogen in the ring

The pH of all the compounds in the heterocyclic aromatic molecules was adjusted to 7 except for nicotinamide and pyrimidone. The structures are shown in Figure 2.3. The preferential interaction coefficients for this series were all positive (Figure 2.4A). Nicotinamide and pyrimidone exhibited the lowest positive μ_{23}/RT value in this series. The μ_{23}/RT values for quinaldic acid and nicotinic acid are similar, even though quinaldic acid has an extra 6-membered aromatic ring as compared to nicotinic acid. Interestingly, nicotinic acid has slightly higher μ_{23}/RT than nictonamide, which might be due to the pH of nicotinic acid being adjusted using NaOH. There could be contributions arising from sodium ions on the μ_{23}/RT value. Pyrrole-2 carboxylate and indole acetate exhibited the highest μ_{23}/RT values in this series.

The nucleotide monophosphates 5-membered nitrogen containing heterocyclic ring compounds TMP and UMP exhibited highest μ_{23}/RT values (Figure 2.4B). TMP had slightly higher μ_{23}/RT value than UMP. AMP and GMP exhibited lower μ_{23}/RT value than TMP and UMP.

2.3.4 Amino acids

The interaction of trehalose with amino acids was also explored (Figure 2.5). The μ_{23}/RT values for all amino acids were found to be positive (Figure 2.6). The μ_{23}/RT value is higher for Na-glutamate as compared to K-glutamate, which is indicative of sodium ions contributing more positive value to the μ_{23}/RT coefficient than the potassium ions. On comparison of polar amino acids serine and threonine, the latter exhibited a higher μ_{23}/RT. This is similar to the trend observed by Hong et al. The μ_{23}/RT value obtained for serine was -0.014 ± 0.015 m^{-1} and for threonine was 0.128 ± 0.019 m^{-1} [19]. The values obtained from our study were 0.11 ± 0.1 m^{-1} and 0.27 ± 0.02 m^{-1} for serine and threonine, respectively. The μ_{23}/RT value increased with longer and complex R group present on the amino acid. Glycine had the μ_{23}/RT closest to zero in this series, and the values increased with increasing number of methyl carbons in the R group. Isoleucine exhibited the highest μ_{23}/RT value in this series.

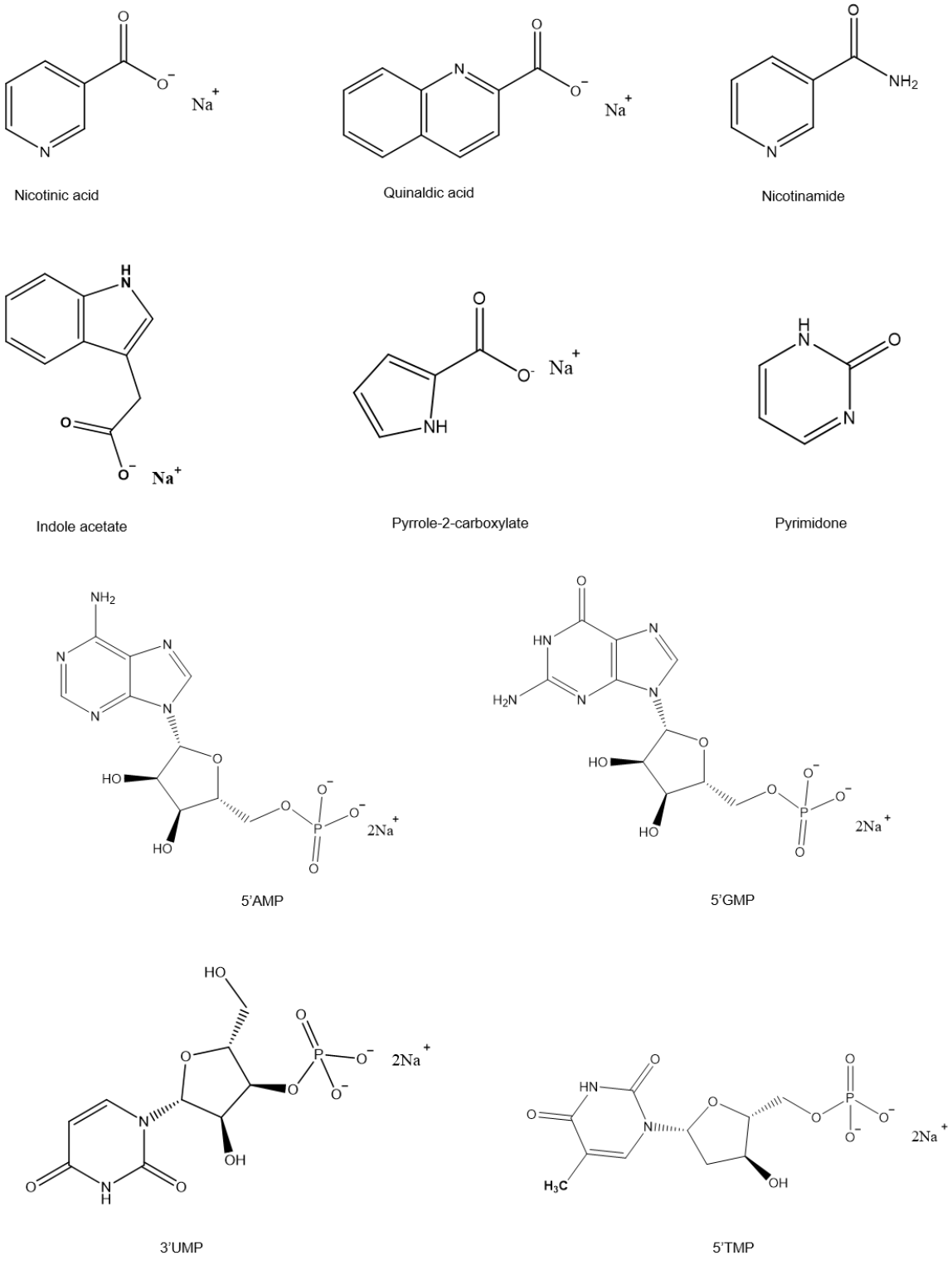

Figure 2.3: Structures of the non-heterocyclic aromatic compounds used in this study

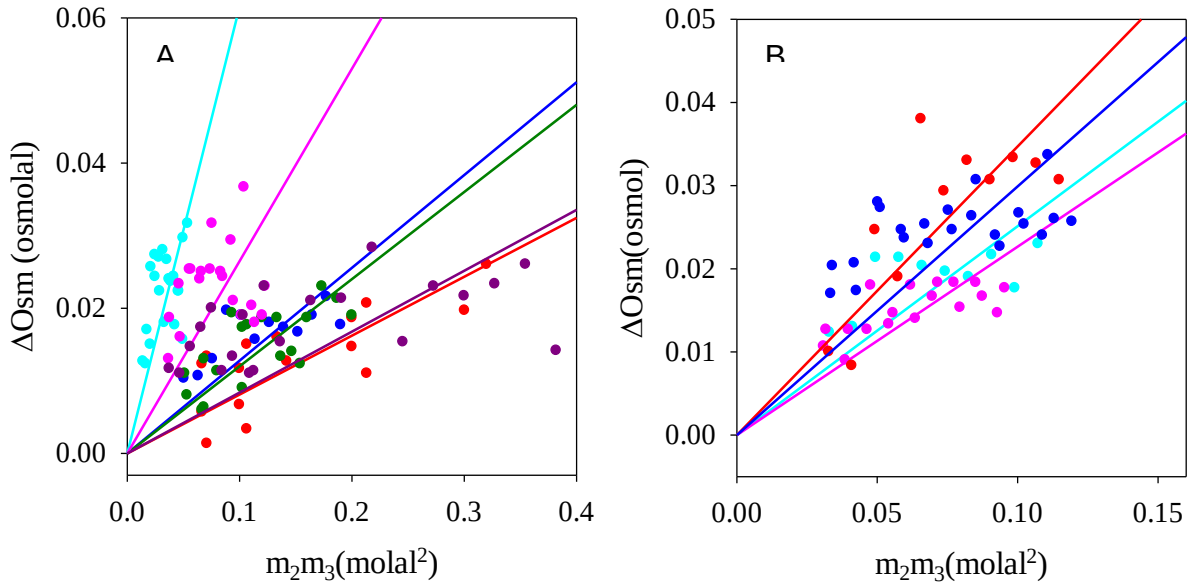

Figure 2.4: VPO studies for heterocyclic compounds

A: The data points are represented as (●) nicotinamide, (●) nicotinic acid, (●) quinaldic acid, (●) indole acetate, (●) pyrrole 2-carboxylic acid, (●) pyrimidone B: Nucleotide mono phosphate data are represented as (●) AMP, (●) GMP, (●) TMP and (●) UMP.

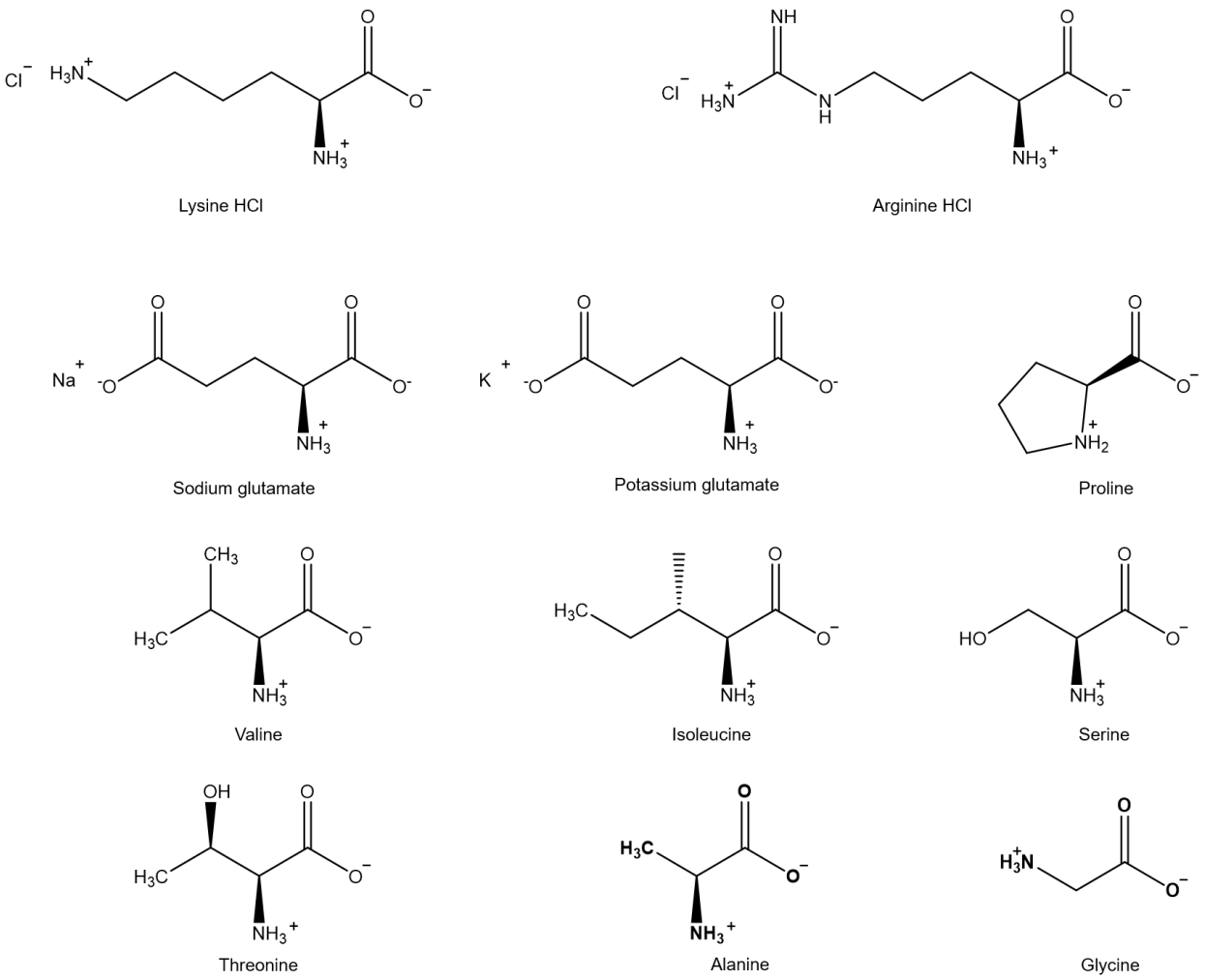

Figure 2.5: Structures of the amino acids used in the VPO study

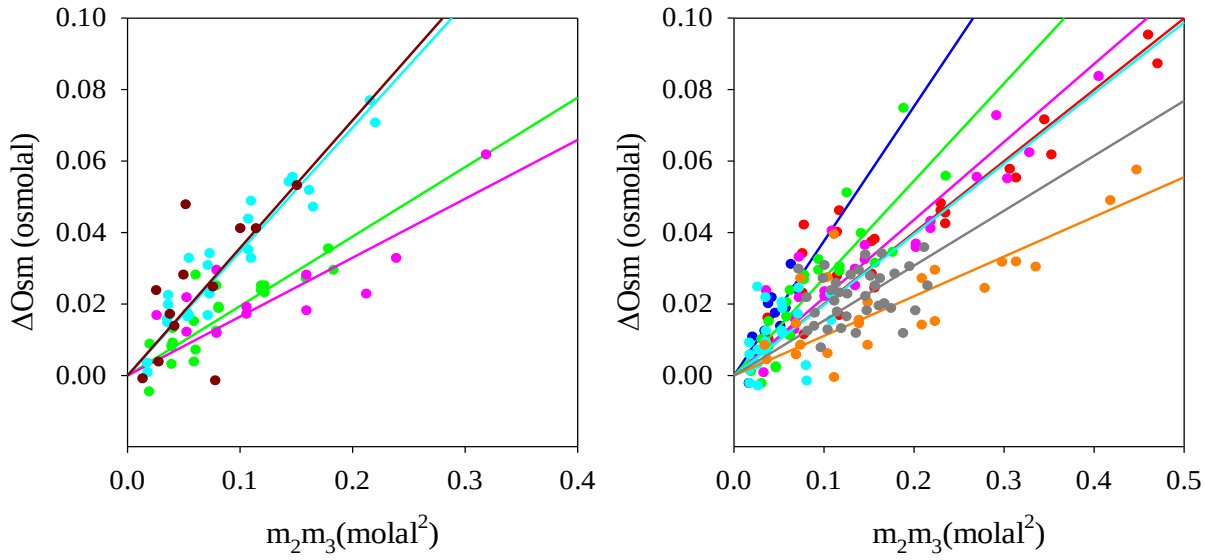

Figure 2.6: Plots of ΔOsm vs m_2m_3 for amino acids

The slopes in the graph are representative of the μ_{23}/RT value of the compound. A: Charged amino acids are as (●) lysine HCl, (●) K-glutamate, (●) Na-glutamate, (●) arginine HCl. B: Other types of amino acids are represented as (●) alanine, (●) isoleucine, (●) proline, (●) threonine, (●) valine, (●) glycine, (●) serine.

2.3.5 Amides and modified amino acids

Several compounds containing amides were also studied (Figure 2.7). All the amide and modified amino acid compounds, except urea had positive μ_{23}/RT values (Figure 2.8). Urea was reported to have a μ_{23}/RT value of -0.139 ± 0.009 m^{-1} in studies done by Hong et al [19]. The value obtained from our study was -0.07 ± 0.01 m^{-1}. The μ_{23}/RT value increased with triglycine > diglycine > glycine (Table 2.1). This trend was seen in the data obtained by Hong et al [19]. Dimethylglycine had lower μ_{23}/RT value than trimethylglycine (betaine). The μ_{23}/RT value for betaine in our study was 0.30 ± 0.01 m^{-1}. The value reported in the Hong et al study was 0.203 ± 0.009 m^{-1} [19]. Acetylalanine methylamide had the most positive μ_{23}/RT value in this series. Urea is the only compound in this series that exhibited negative preferential interaction coefficient with trehalose.

2.3.6 Carboxylate and carboxylic acids

Carboxylates are protonated at low pH and the atom type contributions arising from carboxylate versus protonated carboxylic acid oxygens differ. There is a difference in the interaction of TEG and interior groups of PEG400 with carboxylate oxygens and carboxylic acid oxygens [20]. The osmolytes interacted favorably with carboxylic acid oxygen but unfavorably with carboxylate oxygen. Hence, we decided to split these compounds in our study into carboxylates and carboxylic acids as well (Figure 2.9). Malic acid had a lower positive μ_{23}/RT value than citric acid (Figure 2.10). Comparison of citric acid with sodium citrate and potassium citrate indicated that the μ_{23}/RT was highest for sodium citrate, followed by potassium citrate and citric acid. Sodium propionate had a lower μ_{23}/RT value than sodium oxamate, though both were still positive.

2.3.7 Polyols

Since trehalose self-interacts, we also tested its interactions with other polyols (Figure 2.11). All the compounds exhibited highly positive μ_{23}/RT value (Table 2.1 and Figure 2.12). Hong et al have reported μ_{23}/RT value of 0.258 ± 0.013 m^{-1} for mannitol [19] and we have obtained a value of 0.27 ± 0.01 m^{-1}.

2.3.8 Salts

Many of the model compounds used in this study are sodium, potassium or chloride salts, so to determine the contribution of the counter ions, interaction of trehalose with salts were studied (Figure 2.13). The slopes from this plot were used to calculate β values (Eq. 2.3) for the ions such as sodium, potassium and chloride. β value is the preferential interaction of trehalose with sodium, potassium and chloride ions. Sodium pyrophosphate

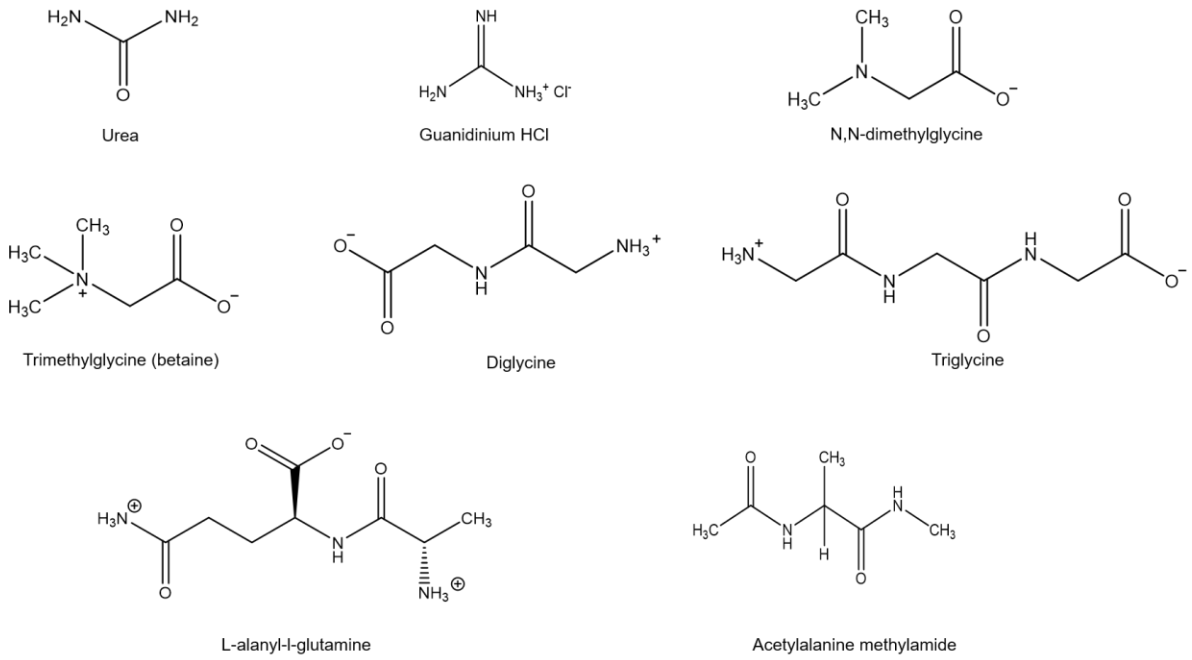

Figure 2.7: Structures of the amides and modified amino acids used in the VPO study

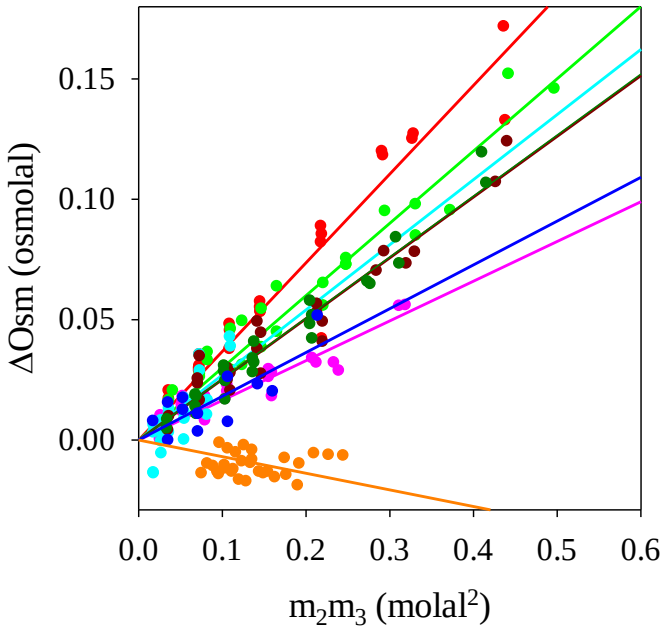

Figure 2.8: The representation of the μ_{23}/RT value for amides and modified amino acids

The data points are represented for (●) L-alanyl-Lglutamine, (●) acetylalanine methylamide, (●) guanidinium HCl, (●) diglycine, (●) triglycine, (●) urea, (●) betaine, (●) N,N-dimethylglycine.

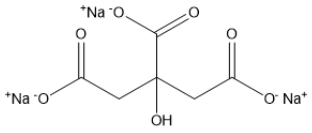

Trisodium citrate

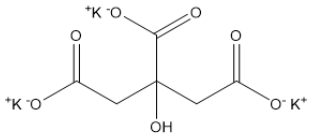

Tripotassium citrate

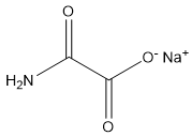

Sodium Oxamate

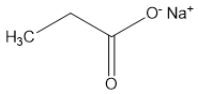

Sodium propionate

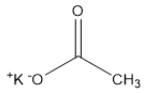

Potassium acetate

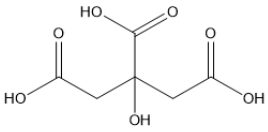

Citric acid

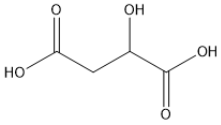

Malic acid

Figure 2.9: The structures of the carboxylates and carboxylic acids used in the study

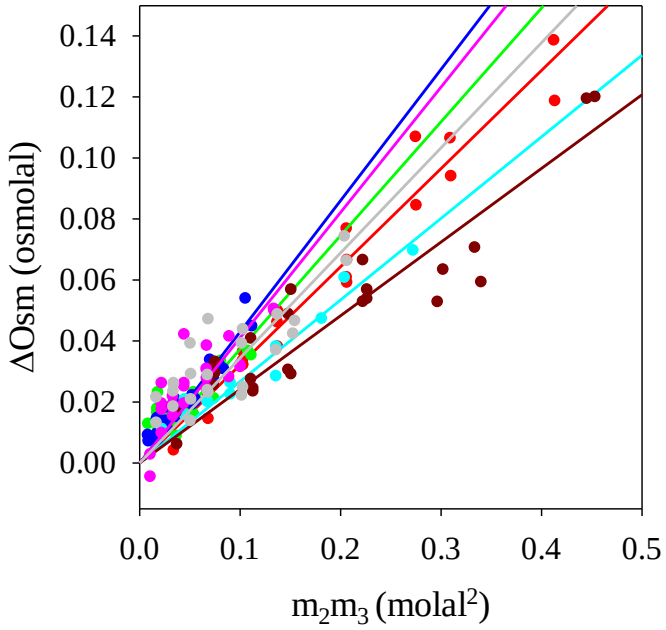

Figure 2.10: Interaction of trehalose with carboxylates and carboxylic acid

The data points are shown for (●) malic acid, (●) citric acid, (●) tripotassium citrate, (●) trisodium citrate, (●) potassium acetate, (●) sodium oxamate, (●) sodium propionate.

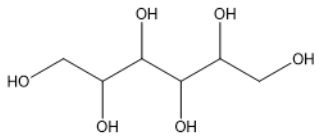

Sorbitol

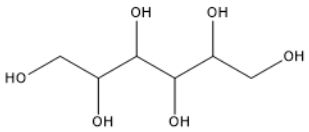

Mannitol

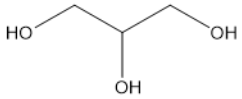

Glycerol

Figure 2.11: Structures of the polyols used in the VPO study

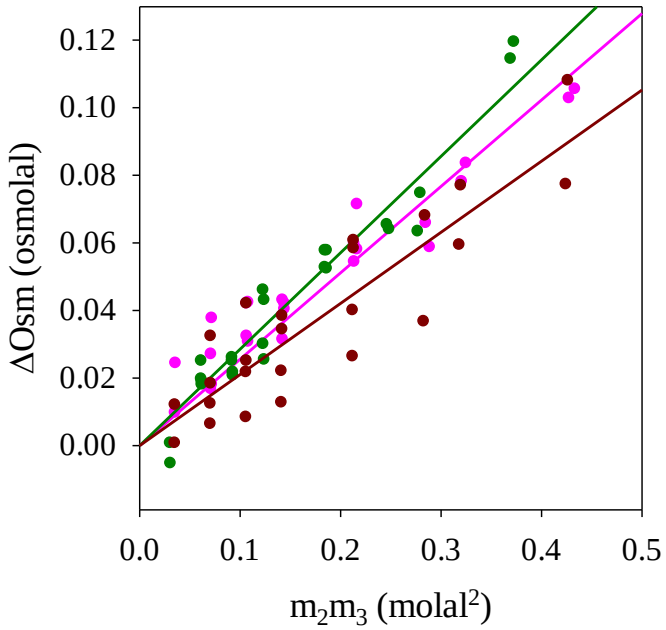

Figure 2.12: Determination of the μ_{23}/RT value from the plot of ΔOsm vs product of molalities of trehalose and test compound

Interaction of trehalose with the polyols (●) sorbitol, (●) glycerol and (●) mannitol.

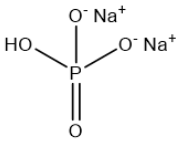

Sodium phosphate dibasic

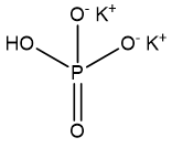

Potassium phosphate dibasic

$Na^+ Cl^-$

Sodium chloride

$K^+ Cl^-$

Potassium chloride

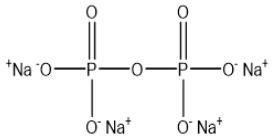

Sodium pyrophosphate tetrabasic

Figure 2.13: The structures of the salts used in the study

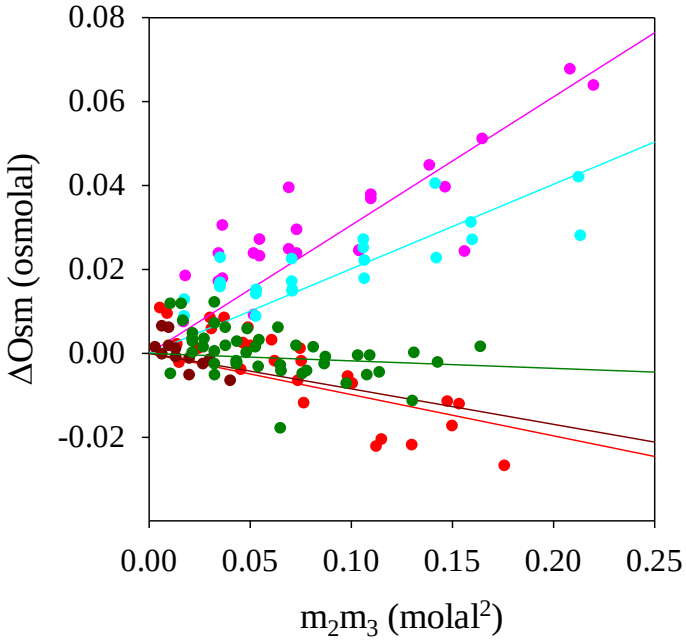

Figure 2.14: Interaction of trehalose with salts

Compounds with phosphate groups showed near zero to negative μ23/RT value. The compounds are represented as (●) sodium pyrophosphate tetrabasic, (●) potassium phosphate dibasic, (●) sodium phosphate dibasic, (●) potassium chloride, (●) sodium chloride.

Table 2.1: The compounds used in our study with the experimental μ_{23}/RT values. The predicted μ_{23}/RT values were obtained from the α values.

Non heterocyclic aromatic compound	Experimental μ_{23}/RT	Predicted μ_{23}/RT	Difference
3-aminobenzoate	0.18 ± 0.02	0.17 ± 0.05	0.01
3-hydroxybenzoate	0.15 ± 0.01	0.21 ± 0.04	0.07
4-hydroxybenzoate	0.11 ± 0.01	0.21 ± 0.04	0.10
4-methylbenzoate	0.25 ± 0.01	0.29 ± 0.04	0.04
2-aminobenzoate	0.16 ± 0.01	0.17 ± 0.04	0.01
2-hydroxybenzoate	0.17 ± 0.01	0.20 ± 0.04	0.03
Dopamine hydrochloride	0.22 ± 0.01	0.29 ± 0.03	0.07
Monosodium benzoate	0.26 ± 0.02	0.21 ± 0.04	0.05
Phenylalanine	0.27 ± 0.07	0.17 ± 0.03	0.10

Heterocyclic aromatic compounds	Experimental μ_{23}/RT	Predicted μ_{23}/RT	Difference
Nicotinic acid	0.13 ± 0.01	0.23 ± 0.04	0.10
Quinaldic acid	0.12 ± 0.01	0.23 ± 0.01	0.11
Nicotinamide	0.08 ± 0.01	0.08 ± 0.03	0.00
Indole acetate	0.26 ± 0.02	0.27 ± 0.05	0.01
Pyrrole-2-carboxylate	0.61 ± 0.04	0.25 ± 0.04	0.36
Pyrimidone	0.09 ± 0.01	0.15 ± 0.03	0.06
Adenosine Mono Phosphate	0.25 ± 0.02	0.19 ± 0.09	0.06
Guanosine Mono Phosphate	0.21 ± 0.02	0.25 ± 0.10	0.04
Thymidine Mono Phosphate	0.35 ± 0.02	0.28 ± 0.09	0.07
Uridine Mono Phosphate	0.29 ± 0.02	0.30 ± 0.09	0.01

Table 2.1 continued

Amino acids	Experimental μ_{23}/RT	Predicted μ_{23}/RT	Difference
Glycine	0.11 ± 0.01	0.10 ± 0.02	0.01
Alanine	0.19 ± 0.01	0.18 ± 0.02	0.01
Threonine	0.27 ± 0.02	0.19 ± 0.02	0.08
Serine	0.11 ± 0.01	0.16 ± 0.02	0.05
Proline	0.22 ± 0.01	0.26 ± 0.02	0.04
Isoleucine	0.38 ± 0.03	0.29 ± 0.03	0.09
Valine	0.19 ± 0.03	0.27 ± 0.02	0.08
Lysine monohydrochloride	0.35 ± 0.01	0.35 ± 0.05	0.00
Monosodium glutamate	0.42 ± 0.04	0.29 ± 0.05	0.13
Potassium glutamate	0.15 ± 0.02	0.25 ± 0.05	0.10
Arginine hydrochloride	0.19 ± 0.01	0.26 ± 0.05	0.07

Amides and modified amino acids	Experimental μ_{23}/RT	Predicted μ_{23}/RT	Difference
Urea	-0.07 ± 0.01	-0.30 ± 0.02	0.23
Guanidine hydrochloride	0.18 ± 0.02	0.09 ± 0.04	0.09
N,N-dimethylglycine	0.25 ± 0.01	0.30 ± 0.02	0.05
Betaine (trimethylglycine)	0.30 ± 0.01	0.35 ± 0.02	0.05
Diglycine	0.16 ± 0.01	0.17 ± 0.03	0.01
Triglycine	0.27 ± 0.03	0.27 ± 0.04	0.00
L-alanyl-L-glutamine	0.25 ± 0.01	0.33 ± 0.01	0.08
Acetyl alanine methylamide	0.36 ± 0.01	0.35 ± 0.03	0.01

Table 2.1 continued

Carboxylates and carboxlic acids	Experimental μ_{23}/RT	Predicted μ_{23}/RT	Difference
Citric acid	0.31 ± 0.01	0.32 ± 0.08	0.01
Trisodium citrate	0.41 ± 0.01	0.51 ± 0.08	0.10
Potassium citrate	0.39 ± 0.03	0.37 ± 0.08	0.02
Malic acid	0.28 ± 0.02	0.26 ± 0.01	0.02
Sodium Oxamate	0.42 ± 0.03	0.26 ± 0.04	0.16
Sodium propionate	0.34 ± 0.02	0.31 ± 0.03	0.03
Potassium acetate	0.27 ± 0.01	0.25 ± 0.03	0.02

Polyols	Experimental μ_{23}/RT	Predicted μ_{23}/RT	Difference
Sorbitol	0.19 ± 0.01	0.19 ± 0.01	0.00
Glycerol	0.27 ± 0.01	0.21 ± 0.01	0.06
Mannitol	0.27 ± 0.01	0.25 ± 0.01	0.02

Salts	Experimental μ_{23}/RT	Predicted μ_{23}/RT	Difference
Sodium phosphate dibasic	-0.04 ± 0.02	-0.03 ± 0.06	0.01
Potassium phosphate dibasic	-0.10 ± 0.02	-0.11 ± 0.06	0.01
Sodium Chloride	0.31 ± 0.02	0.25 ± 0.02	0.06
Potassium Chloride	0.20 ± 0.01	0.20 ± 0.02	0.00
Sodium pyrophosphate tetrabasic	-0.08 ± 0.05	-0.03 ± 0.10	0.05

tetrabasic had a negative μ_{23}/RT, indicating its preferential interaction with trehalose (Figure 2.14 and Table 2.1). We tested sodium phosphate dibasic and potassium phosphate dibasic as additional salts containing phosphate groups. Sodium phosphate dibasic had an interaction coefficient near zero, whereas potassium phosphate dibasic was negative. This indicated that sodium and potassium ions are excluded from trehalose. In the study done by Hong et al, sodium phosphate dibasic had the most negative μ_{23}/RT value of -0.785 ± 0.071 m^{-1} [19]. We were unable to obtain such low values with sodium phosphate dibasic with VPO or freezing point depression osmometer. The μ_{23}/RT values for NaCl and KCl were highly positive which also indicated that sodium, potassium and chloride ions were excluded from interacting with trehalose.

The μ_{23}/RT values for the compounds are listed at the end of the results for each category in Table 2.1.

2.3.9 α-value calculation

If a compound has a positive μ_{23}/RT value, it does not necessarily mean that all the atom types on the compound exclude trehalose. The μ_{23}/RT value is the additive contribution of the interaction of trehalose with different functional groups or atom types. There can be functional groups that interact with trehalose, but the contribution to the μ_{23}/RT value from the functional groups that exclude may be much higher. To understand the contribution from each functional group on the overall μ_{23}/RT value, α-values were calculated by fitting the data from each test compound to equation 2.3 using matrices/multiple linear regression [12]. The contribution of each functional group to the overall μ_{23}/RT can be used to understand the interaction between trehalose and various compounds. Table 2.2 enlists the α-values calculated for different functional groups from values obtained from our study. Amide and cationic nitrogens, amines off of aromatic carbons and phosphate oxygen are the only groups that have negative values, while all the other atom types have positive α values.

2.3.10 VPO studies with folate

Previous *in vitro* and *in vivo* studies have indicated trehalose interacts with folate. The weak interactions between trehalose and folate prevent the folate binding to the enzyme dihydrofolate reductase and decrease its activity [5, 9]. VPO studies were therefore conducted to understand the preferential interaction of trehalose with folate. VPO studies were conducted using 0.063 *m* of folate at pH 7 with 0.11-0.5 *m* trehalose. Folate is soluble from 0.02-0.3 *m* in water at pH 7, but has a K_d of dimerization of 0.08 *m* [8]. Folate concentrations below 0.05 *m* yield data that are noisy and have high error. While a 0.63 *m* concentration of folate would have significant populations of both monomer and dimer, it also gives VPO signals that yield accurate values. A μ_{23}/RT value of 0.46 ± 0.06 m^{-1} was obtained (Figure 2.15 and Table 2.3). This is indicative of preferential exclusion of trehalose from folate at the concentration tested.

Table 2.2: Atomistic interaction coefficients (α values) for trehalose with the different surface types

Functional groups	α values (x10^4 m^{-1} Å^{-2})	
	From Hong et al[a]	From this current work
Aliphatic C	22.4 ± 0.8	14.8 ± 0.6
Aromatic C	5.9 ± 1.5 or -8.9 ± 1.6	3.0 ± 0.8
Hydroxyl O	-0.8 ± 0.7	2.0 ± 0.5
Amide O	-19.6 ± 5.4	11.7 ± 1.8
Amide N	-4.7 ± 2.2	-7.6 ± 1.2
Carboxylate O	-28.2 ± 2.1	6.1 ± 1.5
Carboxylic acid O	ND[b]	9.5 ± 0.5
Cationic N	12.9 ± 2.1	-3.5 ± 1.4
Phosphate O	-59.2 ± 5.1	-14.5 ± 2.0
Amine N	ND[b]	-3.9 ± 2.1
Aromatic N	ND[b]	8.1 ± 2.3

Ions	β values (x10^2 m^{-1})[a]	β values (x10^2 m^{-1})[b]
Na^+	9 ± 3	8.9 ± 1.3
K^+	ND[c]	4.6 ± 1.5
Cl^-	0 ± 3	16 ± 1

[a]Data from reference [*19*]. [b]Not determined.

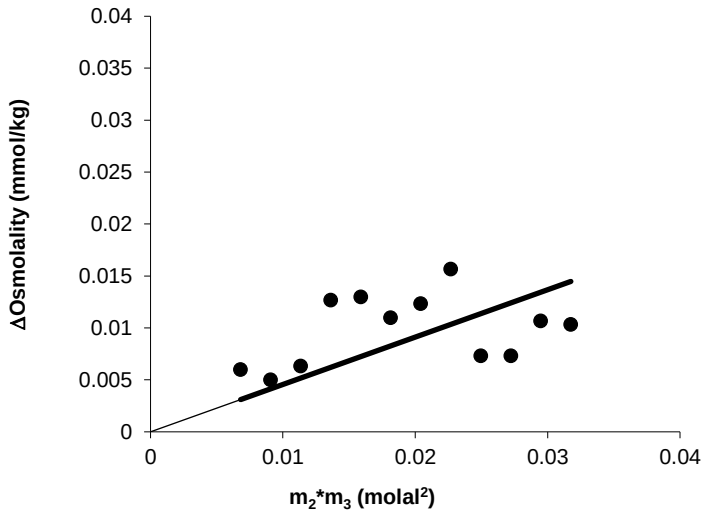

Figure 2.15: Plot of ΔOsm vs m_2m_3 to determine the preferential interaction coefficient of folate with trehalose

The μ_{23}/RT value was 0.46 ± 0.06 m^{-1}. Trehalose is excluded from the solvation shell of folate. The concentration used for the experiment was 0.063 *m*.

Table 2.3: Comparison of the preferential interaction coefficient values obtained in Hong et al studies vs this study

Compounds	μ_{23}/RT (m^{-1})	
	From Hong et al[a]	From the current study
Glycine	-0.027 ± 0.008	0.11 ± 0.01
Proline	0.17 ± 0.01	0.22 ± 0.01
Alanine	0.102 ± 0.013	0.019 ± 0.01
Glycine betaine	0.203 ± 0.009	0.30 ± 0.01
Mannitol	0.258 ± 0.013	0.27 ± 0.01
Serine	-0.014 ± 0.015	0.11 ± 0.01
Threonine	0.128 ± 0.019	0.27 ± 0.02
Diglycine	0.012 ± 0.014	0.16 ± 0.01
Phenylalanine	0.035 ± 0.027	0.27 ± 0.01
Na benzoate	-0.004 ± 0.038	0.26 ± 0.02
Urea	-0.139 ± 0.009	-0.07 ± 0.01
Lysine HCl	0.225 ± 0.025	0.35 ± 0.01
NaCl	0.105 ± 0.016	0.31 ± 0.02
Na_2HPO_4	-0.785 ± 0.071	-0.04 ± 0.02

[a]Data from reference [*19*] . [b]Data from this current work.

2.4 Discussion

Trehalose is an osmolyte of interest due to its dominance in most living forms as an important osmoprotectant during stress conditions. Previous *in vitro* and *in vivo* studies in the lab have identified that trehalose interacts with reduced folates, weakening their association to their respective enzyme [5, 9]. VPO studies, using 50 model test compounds, were thus performed to shed additional light on the atomistic interactions between trehalose and folate. The predicted preferential interaction coefficiencts, along with experimental VPO studies on the interaction of trehalose with folate, have helped us gain a better understanding of the extent of these weak interactions. In the discussion below we have contrasted our results with an existing data set from Hong et al [19]. Our studies contain an additional 25 compounds that represent the atom types in folates: aromatic carbons, aromatic nitrogens, cationic and amide nitrogens. Lastly, we have used literature data on the interaction of trehalose with different proteins and ligands to compare the ability of our data to predict interactions versus the Hong et al data [19].

2.4.1 Osmometry studies with trehalose

Hong et al used freezing point depression osmometry to determine the interaction coefficients of trehalose with different functional groups [19]. However, they did not fit their ΔOsm vs m_2m_3 data with a line that had an intercept of zero. As mentioned in the methods section, an intercept of zero is expected if there are no self-interactions between molecules of test compound or trehalose. While trehalose does self-associate at concentrations above 0.5 M [13], both our study and the Hong et al study [19] used trehalose concentrations below 0.5 M. Therefore, there trehalose self-interactions should not interfere in our respective osmometry studies. The compounds that were fit with a line that did not have an intercept of zero included: sodium benzoate, sodium chloride, mannitol, threonine, serine, proline, lysine hydrochloride, glutamine, urea and diglycine. These test compounds have been used in this study, and were fit with a line that had an intercept set to zero. More positive interaction potentials have been reported in our studies. Table 2.3 shows a comparison of the values reported in Hong et al [19] vs the VPO studies performed in the Howell lab.

We were primarily interested in understanding the interaction of trehalose with aromatic nitrogens and carbons, atom types that are present in folates. There was a discrepancy on the effect of trehalose with aromatic groups reported by Hong et al. The compounds used for the calculation of atomistic interaction coefficients for these atom types were histidine, 4-benzylalcohol, phenylalanine and sodium benzoate. A positive α value was reported when phenylalanine was used for the fitting, while a negative α value when histidine was used for the fitting. There are several concerns about how they determined the α value for aromatic atoms. First, phenylalanine has low solubility in water, so the molality range used was narrow. Second, in the case of histidine, there was favorable interaction with a negative μ_{23}/RT. Histidine is a heterocyclic aromatic compound with nitrogens and carbons in the ring. Hong et al [19] did not delineate these different atom

types in their study. Additionally, imidazole rings are known to dimerize [21], which would need to be taken into account when calculating the surface area of the atoms of histidine. The surface areas of the atoms in histidine will change depending upon which atoms are exposed to the solvent in the monomer compared to the dimer. If multiple concentrations of histidine were used in their studies, then the ratio of monomeric to dimeric histidines would change with the concentration of the amino acid. Also, if trehalose preferential interacts with either the monomer or dimer of histidine more than the other, then this will also shift the equilibrium. We have previously shown that betaine shifts the monomer-dimer equilibrium of folate [7, 8]. Changes in the monomer to dimer ratio with solution condition makes predicting preferential interactions of trehalose with histidine difficult. Hence the self-association of the imidazole ring makes histidine a non-ideal candidate for osmometry studies. Our α value of 3.0 ± 0.8 and 8.1 ± 2.3 x 10^{-4} m^{-1} Å^2 for aromatic carbons and nitrogens, respectively, indicates that their positive value for aromatic atoms (5.9 m^{-1} Å^2) is more likely to the accurate value.

Comparing the α values from our study to Hong et al, our data contained more positive α values (Table 2.2). Amide oxygens and carboxylate oxygens were predicted to preferentially interact with trehalose according to Hong et al [19], but the prediction is opposite in our data. Trehalose is predicted to stay away from the protein backbone. So preferential exclusion of trehalose from amide oxygens can be one of the ways in which trehalose is excluded from the protein surface and helping solvated proteins. The values for trehalose interaction with sodium and chloride ions is predicted to be close to zero and no data is available for interaction of trehalose with potassium ions. We predict preferential exclusion of trehalose from sodium, potassium and chloride ions. It is also observed that sodium, potassium and chloride salts of the compounds have higher positive preferential interaction coefficients because of the exclusion of trehalose from the ions.

2.4.2 Comparison of trehalose with other osmolytes

Comparing the atomistic interaction coefficients for several osmolytes (see Table 3.4 in Chapter 3), it is noted that trehalose and glycerol have similar interaction coefficients for most of the atom types except for aromatic carbons. Glycerol and trehalose are predicted to participate in weak interactions via hydrogen bonding. On the other hand, the interactions of the surface atoms with trehalose and with betaine and proline were different. Trehalose preferentially interacted with phosphate oxygens and preferentially excluded aromatic carbons. Betaine and proline on the other hand, preferentially interacted with aromatic carbons and preferentially excluded phosphate oxygens. The interaction of trehalose, betaine and proline were similar for other groups. That is, there was preferential interaction with amide nitrogens, but preferential exclusion from amide and carboxylate oxygens. This is one of the reasons why these osmolytes stay away from the peptide backbone and hence do not interact with proteins, thus stabilizing them. Trehalose has similar preferential interactions as TEG and PEG400 with most atom types except for aliphatic carbons. Trehalose preferentially excludes aliphatic carbons whereas TEG and PEG400 prefers to interact with them.

2.4.3 Predicted preferential interaction coefficients for folate

We have used 50 model test compounds and segregated them as the aromatic groups, carboxylates and carboxylic acids, polyols, amino acids and amides and salts. The deconvolution of the preferential interaction coefficients into α values has allowed us to understand the interaction of trehalose with surface atom types. Depending on the solvent accessible surface area of the atoms types on folate, preferential interaction coefficient of trehalose with folate can be calculated.

Using the α-values obtained for the different atom types, the preferential interaction coefficients for folate and folate precursor molecules were calculated. A μ_{23}/RT value of 0.54 m^{-1} was predicted using the α-values from our studies, which predicts folate would preferentially exclude trehalose. This is similar to the μ_{23}/RT value from our experiments, which was 0.46 m^{-1}. We predicted the μ_{23}/RT value for folate using the α-values from Hong et al and obtained a predicted value of -0.16 m^{-1} (Table 2.4), which is significantly lower than our experimental value. This indicates that using atomistic interaction coefficients for aromatic nitrogens, and improved values for aromatic carbons, leads to more accurately predicted μ_{23}/RT values.

The preferential interaction coefficients can be predicted for other reduced folates. We were specifically interested in enzymes of the folate pathway that use ligands containing aromatic carbons and phosphate oxygens. Dihydropteroate synthase (DHPS) was one such enzyme that condenses dihydropteridine pyrophosphate and para-aminobenzoate (pABA) to form dihydropteroate. Using our values, pterin pyrophosphate (an analog of dihydropterin pyrophosphate) was predicted to exhibit equal preference to interact with trehalose and water. On the other hand, trehalose will preferentially exclude pABA. When the αvalues from Hong et al studies were used, trehalose was predicted to preferentially interact with pterin pyrophosphate, while pABA exhibited equal preference to trehalose and water (Table 2.4). These variations in the results were checked by determining the binding of the ligands to the enzyme DHPS in presence of trehalose using isothermal titration calorimetry and are explained in detail in Chapter 3. ITC studies of pterin pyrophosphate binding to DHPS in presence of 0.5 M and 1 M trehalose had negligible effects on binding. pABA binding was tightened to DHPS in presence of 0.5 M and 1 M trehalose. If there was equal preference of pteridine pyrophosphate to interact with trehalose and water, then the presence of trehalose would not alter the binding affinity of the ligand to the enzyme. This is what was reflected in our ITC results of pteridine pyrophosphate binding to DHPS enzyme. On the other hand, if pABA preferentially excluded trehalose, there is lower desolvation penalty that is associated with binding of pABA to the enzyme in presence of trehalose. This is reflected as the tightened binding of pABA to DHPS in presence of trehalose. Thus, our predicted preferential interaction coefficients for folates seem to correlate with the experimental ITC data. We do acknowledge that the addition of trehalose changes other solvent properties like viscosity, dielectric constants and these have been discussed in more detail in Chapter 3.

Table 2.4: The predicted and experimental preferential interaction coefficients for folate

Molecule	Experimental μ_{23}/RT (m^{-1})[a]	Predicted μ_{23}/RT (m^{-1})	
		From Hong et al[b]	From this current work
Folate	0.46 ± 0.06	0.16	0.54 ± 0.08
Pterin pyrophosphate	ND[c]	0.875	-0.05 ± 0.07
pABA	ND[c]	0.096	0.11 ± 0.03

[a]Data from this current work. [b]α values from reference [*19*] [c]ND: not determined.

2.4.4 Effect of trehalose on thermal protein unfolding

Atomistic interaction coefficients obtained from this study can also be used to calculate the interactions of trehalose with proteins, or how it impacts the stability of proteins. The experimentally obtained free energy of unfolding was compared to the difference in predicted preferential interaction coefficient for the unfolded and folded variants of the proteins in presence of trehalose (Table 2.5). The predictions of the interaction of trehalose with proteins concur with the predicted free energy of unfolding. The free energy of unfolding of five proteins RNAse, BSA, lysozyme, α-chymotrypsin and adenylate kinase was obtained from literature [11, 15-17]. The unfolding energies were close to the predicted $\Delta\mu_{23}$/RT values. Our values were closer than Hong et al exept for BSA. This highlights the importance of VPO technique and the use of α values to predict the behavior of macromolecules in the presence of osmolytes.

While the predicted values are close to the experimental μ_{23}/RT values, they are not the same. The most likely reason for the difference is that, under experimental conditions, there are populations of molecules with different conformations. The predicted values are typically obtained from just one static structure for the native protein, and one denatured structure. The degree to which osmolytes interact will depend upon the protein's conformation, and which atom types are solvent exposed. Indeed, the μ_{23}/RT values for a molecule will vary with its conformation. For 100 conformations of folate obtained from molecular dynamic simulations varied from -0.18 to 0.09 m^{-1} depending upon the extent to which the folate conformation was extend versus bent [7]. More accurate predicted μ_{23}/RT values may be obtained by using a set of structures for both the native and denatured states of the proteins, and calculating an average preferential interaction for each state.

2.4.5 Effect of trehalose on R67 DHFR enzyme kinetics

The experimental data for the effect of trehalose on R67 dihydrofolate reductase (R67 DHFR) reduction of dihydrofolate (DHF) [5] were not predicted well using either our α values, or the values from Hong et al [19] (Table 2.5). There are several reasons for the poor predictions. The predicted values are dependent upon the structures used calculate the μ_{23}/RTs. Only one structure was used to predict the $\Delta\mu_{23}$/RT values, while under experimental conditions, proteins and ligands are in many different conformations. The dependence of osmolyte interaction on the conformation of the protein, or particularly the ligand, could account for some of the differences between the predicted and experimental $\Delta\mu_{23}$/RT values, especially if there is a particular ligand conformation that is more likely to bind to the protein. How much an osmolyte interacts with a favored binding conformation would impact osmolyte effects on ligand binding more than its interaction with other conformations of the ligand. Additionally, if the single, static conformation used in predicting the $\Delta\mu_{23}$/RT is not the predominant conformation adopted by the protein in solution, then the predicted value will not be representative of what occurs in solution.

Table 2.5: Comparison of the alpha values with the data in literature

	$\Delta\mu_{23}$/RT (m^{-1})		
	Experimental	Predicted Hong[a]	Predicted[b]
RNAse A[c]	7.3±0.2[d]	5.9±0.02	6.0±0.01
Bovine serum albumin[e]	21±2[d]	21.6±0.1	27.7±0.1
RNAse A, pH 2.5[cf]	4.96±0.15[g]	6.13±0.01	6.92±0.01
Lysozyme, pH 2.5[f,h]	4.32±0.29[g]	8.29±0.01	6.06±0.01
α-chymotrypsin, pH 8.2[if,i]	15.0±0.9[j]	20.8±0.1	19.1±0.1
Adenylate kinasef,[k]	9.3±0.7[l]	7.2±0.1	9.9±0.1
DHF kinetics with R67 DHFR (k_{cat}/K_m)[m]	0.91±0.21[n]	-0.05±0.02	-0.48±0.01
PtPP binding to BaDHPS[o]	0.17±0.02[p]	1.4±0.1	0.06±0.01
pABA binding to BaDHPS[q]	-0.50±0.05[p]	0.17±0.03	-0.19±0.01
STZ binding to BaDHPS[r]	-0.39±0.04[p]	0.09±0.01	-0.13±0.01

[a]α values from reference [*19*]. [b]From the current study. [c]Bovine RNase A (PDB ID 3DH5) was used [*22*]. [d]Trehalose interaction with folded RNAse A and BSA are taken from reference [*11*]. [e]PDB 1D 3V03 used for the structure of bovine serum albumin [*23*]. [f]Unfolded structures for RNase A and lysozyme were prepared in Pymol as extended peptides. [g]Reversible DSC unfolding data in the presence of trehalose were taken from reference [*16*]. [h]PDB ID 1JJ3 was used from lysozyme [*24*]. [i]PDB ID 1T7C was used for the structure of bovine α-chymotrypsin [*25*]. [j]DSC unfolding free energies were taken from reference [*17*]. [k]PDB ID 1AKE was used for the structure of adenylate kinase [*26*]. [l]Thermal unfolding data were taken from reference [*15*]. [m]R67 DHFR-NADPH and R67 DHFR-NADPH-DHF structures taken from reference [*27*]. [n]Kinetics data were taken from reference [*5*]. [o]The apoDHPS (PDB ID 1TWS) and DHPS-PtPP (PDB ID 1TWW) structures were used [*28*]. [p]From Table 3 in Chapter 3. [q]DHPS-PtPP-pABA structures was produced by replacing dihydropterin from PDB ID 3TYB with PtPP [*29*]. [r]Dihydropterin in the PDB structure (3TYE) was replaced with PtPP to prepare the DHPS-PtPP-STZ file [*29*].

Model structures that do not approximate what occurs in solution will not yield accurate predictions of the preferential interactions of osmolytes.

2.4.6 Effect of trehalose on enzyme ligand binding

As mentioned in section 2.4.2, the α values were used to predict the influence of trehalose on the binding of pterin pyrophosphate and pABA to the enzyme DHPS. The predicted $\Delta\mu_{23}$/RT values of ligand binding correlated well with the experimental ITC results obtained for pABA and STZ binding to DHPS in the presence of trehalose. Any differences in between the predicted and experimental values most likely occurs due to the single structures used in the predictions. Particularly since two loops that form the pABA and STZ binding binding pocket are fairly dynamic [28, 29]. Our prediction for PtPP binding to apo-DHPS also concurred with the experimental value. Using the data from Hong et al [19], it would be predicted that PtPP binding should decrease more in the presence of trehalose than it actually does.

Overall, despite very different atomistic interaction coefficients from the Hong et al [19] study from this current work, the predicted $\Delta\mu_{23}$/RT values are very similar. There are, however, two experimental data sets where our atomistic interaction coefficients yielded more accurate predictions of the data. The first is pABA binding to the DHPS-PtPP binary complex. Our data predicted a value of -0.19 m^{-1} was the same sign as the experimentally determined $\Delta\mu_{23}$/RT of -0.50 m^{-1}, while the value predicted from the Hong et al values, was positive (0.17 m^{-1}). The second data set, which had the largest difference between the two predictions, was for PtPP binding to apo-DHPS (Table 2.5). The $\Delta\mu_{23}$/RT calculated using data from Hong et al [19], was 1.4 m^{-1}, much higher than the experimentally determined 0.17 m^{-1}. The predicted value using our data was 0.06 m^{-1}. These results may indicate that the Hong et al data overestimated the interaction of trehalose with phosphate groups. Though, there is not enough literature data to determine which data set accurately predicts trehalose interactions with phosphates. There is experimental data for the effect of trehalose on the ATP K_m with H^+-ATPase from *Kluyveromyces lactis* [30]. Unfortunately, the structural data for the apo and ATP-, or ATP-analog, bound forms of H^+-ATPase for *K. lactis* are not available, so the predicted values cannot be calculated. More experimental data sets are need, especially for structures that contain phosphate groups, to distinguish our α values from those of Hong et al [19].

2.5 Conclusion

From our VPO studies, we find that trehalose is highly excluded from most atom types. Phosphate oxygens, amines off of aromatic rings and amide, cationic nitrogens interact with trehalose. Our α values are significantly different that those previously determined by Hong et al [19]. To determine which data set is correct, we compared experimentally determined $\Delta\mu_{23}$/RT values with those predicted by the two sets of α values. Most of the

predicted values for both sets of α values were close to the experimental values, suggesting that both our and Hong et al's [19] data sets accurately predict trehalose interactions. Predicted $\Delta\mu_{23}$/RT values for pterin pyrophosphate binding to dihydropteroate synthase had the largest difference between the two sets of α values, with our data set more accurately predicted the experimental values. This suggests that our data more accurately predicts trehalose interactions with phosphates, though more experimental data is needed to distinguish the two sets of α values.

2.6 References

[1] Khodadadi, S., Roh, J., Kisliuk, A., Mamontov, E., Tyagi, M., Woodson, S., Briber, R., and Sokolov, A. (2010) Dynamics of biological macromolecules: Not a simple slaving by hydration water, *Biophys. J. 98*, 1321-1326.

[2] Frauenfelder, H., Fenimore, P., and McMahon, B. (2002) Hydration, slaving and protein function, *Biophys. Chem. 98*, 35-48.

[3] Whitesides, G. M., and Krishnamurthy, V. M. (2005) Designing ligands to bind proteins, *Q. Rev. Biophys. 38*, 385-395.

[4] Chopra, S., Dooling, R. M., Horner, C. G., and Howell, E. E. (2008) A balancing act between net uptake of water during dihydrofolate binding and net release of water upon NADPH binding in R67 dihydrofolate reductase, *J. Biol. Chem. 283*, 4690-4698.

[5] Chopra, S., Lynch, R., Kim, S.-H., Jackson, M., and Howell, E. E. (2006) Effects of temperature and viscosity on R67 dihydrofolate reductase catalysis, *Biochemistry 45*, 6596-6605.

[6] Grubbs, J., Rahmanian, S., DeLuca, A., Padmashali, C., Jackson, M., Duff Jr, M. R., and Howell, E. E. (2011) Thermodynamics and solvent effects on substrate and cofactor binding in *Escherichia coli* chromosomal dihydrofolate reductase, *Biochemistry 50*, 3673-3685.

[7] Bhojane, P. P., Duff Jr, M. R., Bafna, K., Rimmer, G. P., Agarwal, P. K., and Howell, E. E. (2016) Aspects of weak interactions between folate and glycine betaine, *Biochemistry 55*, 6282-6294.

[8] Duff Jr, M. R., Grubbs, J., Serpersu, E., and Howell, E. E. (2012) Weak interactions between folate and osmolytes in solution, *Biochemistry 51*, 2309-2318.

[9] Nambiar, D., Berhane, T.-K., Shew, R., Schwarz, B., Duff, M. R., and Howell, E. E. (2018) In vivo titration of folate pathway enzymes, *Appl. Environ. Microbiol. 84*, e01139-01118.

[10] Cayley, S., and Record, M. T. (2003) Roles of cytoplasmic osmolytes, water, and crowding in the response of *Escherichia coli* to osmotic stress: Biophysical basis of osmoprotection by glycine betaine, *Biochemistry 42*, 12596-12609.

[11] Courtenay, E., Capp, M., Anderson, C., and Record, M. (2000) Vapor pressure osmometry studies of osmolyte− protein interactions: Implications for the action of osmoprotectants in vivo and for the interpretation of “osmotic stress” experiments in vitro, *Biochemistry 39*, 4455-4471.

[12] Capp, M. W., Pegram, L. M., Saecker, R. M., Kratz, M., Riccardi, D., Wendorff, T., Cannon, J. G., and Record Jr, M. T. (2009) Interactions of the osmolyte glycine betaine with molecular surfaces in water: Thermodynamics, structural interpretation, and prediction of m-values, *Biochemistry 48*, 10372-10379.

[13] Sapir, L., and Harries, D. (2010) Linking trehalose self-association with binary aqueous solution equation of state, *J. Phys. Chem. B 115*, 624-634.

[14] Tsodikov, O. V., Record Jr, M. T., and Sergeev, Y. V. (2002) Novel computer program for fast exact calculation of accessible and molecular surface areas and average surface curvature, *J. Comput. Chem. 23*, 600-609.

[15] Auton, M., Rösgen, J., Sinev, M., Holthauzen, L. M. F., and Bolen, D. W. (2011) Osmolyte effects on protein stability and solubility: A balancing act between backbone and side-chains, *Biophys. Chem. 159*, 90-99.
[16] Kaushik, J. K., and Bhat, R. (2003) Why is trehalose an exceptional protein stabilizer? An analysis of the thermal stability of proteins in the presence of the compatible osmolyte trehalose, *J. Biol. Chem. 278*, 26458-26465.
[17] Kumar, A., Attri, P., and Venkatesu, P. (2010) Trehalose protects urea-induced unfolding of α-chymotrypsin, *Int. J. Biol. Macromol. 47*, 540-545.
[18] The PyMOL molecular graphics system, *Version 2.3.2 Schrodinger, LLC*.
[19] Hong, J., Gierasch, L. M., and Liu, Z. (2015) Its preferential interactions with biopolymers account for diverse observed effects of trehalose, *Biophys. J. 109*, 144-153.
[20] Knowles, D., Shkel, I. A., Phan, N. M., Sternke, M., Lingeman, E., Cheng, X., Cheng, L., O'Connor, K., and Record, M. T. (2015) Chemical interactions of polyethylene glycols (PEGs) and glycerol with protein functional groups: Applications to effects of PEG and glycerol on protein processes, *Biochemistry 54*, 3528-3542.
[21] Peral, F., and Gallego, E. (1997) Self-association of imidazole and its methyl derivatives in aqueous solution. A study by ultraviolet spectroscopy, *J. Mol. Struct. 415*, 187-196.
[22] Kurpiewska, K., Font, J., Ribó, M., Vilanova, M., and Lewiński, K. (2009) X-ray crystallographic studies of RNase A variants engineered at the most destabilizing positions of the main hydrophobic core: Further insight into protein stability, *Proteins: Struct., Funct., Bioinf. 77*, 658-669.
[23] Majorek, K. A., Porebski, P. J., Dayal, A., Zimmerman, M. D., Jablonska, K., Stewart, A. J., Chruszcz, M., and Minor, W. (2012) Structural and immunologic characterization of bovine, horse, and rabbit serum albumins, *Mol. Immunol. 52*, 174-182.
[24] Datta, S., Biswal, B., and Vijayan, M. (2001) The effect of stabilizing additives on the structure and hydration of proteins: A study involving tetragonal lysozyme, *Acta Crystallogr. D 57*, 1614-1620.
[25] Czapinska, H., Helland, R., Smalås, A. O., and Otlewski, J. (2004) Crystal structures of five bovine chymotrypsin complexes with P1 BPTI variants, *J. Mol. Biol. 344*, 1005-1020.
[26] Müller, C. W., and Schulz, G. E. (1992) Structure of the complex between adenylate kinase from *Escherichia coli* and the inhibitor Ap5A refined at 1.9 Å resolution: A model for a catalytic transition state, *J. Mol. Biol. 224*, 159-177.
[27] Kamath, G., Howell, E. E., and Agarwal, P. K. (2010) The tail wagging the dog: insights into catalysis in R67 dihydrofolate reductase, *Biochemistry 49*, 9078-9088.
[28] Babaoglu, K., Qi, J., Lee, R. E., and White, S. W. (2004) Crystal structure of 7, 8-dihydropteroate synthase from *Bacillus anthracis*: Mechanism and novel inhibitor design, *Structure 12*, 1705-1717.
[29] Yun, M.-K., Wu, Y., Li, Z., Zhao, Y., Waddell, M. B., Ferreira, A. M., Lee, R. E., Bashford, D., and White, S. W. (2012) Catalysis and sulfa drug resistance in dihydropteroate synthase, *Science 335*, 1110-1114.

[30] Sampedro, J. G., Munoz-Clares, R. A., and Uribe, S. (2002) Trehalose-mediated inhibition of the plasma membrane H^+-ATPase from *Kluyveromyces lactis*: Dependence on viscosity and temperature, *J. Bacteriol. 184*, 4384-4391.

3 THE EFFECTS OF OSMOLYTES ON BINDING OF LIGANDS AND SULFATHIAZOLE TO DIHYDROPTEROATE SYNTHASE FROM *BACILLUS ANTHRACIS*

3.1 Introduction

Osmolytes are produced by cells in response to heat, dehydration, and high salt concentrations, helping proteins to fold and properly function [1]. Typical osmolytes used to protect cells during stress conditions include amino acids and polyols, such as glycine betaine and trehalose, respectively [2]. These osmoprotectants are proposed to be excluded from the protein surface [3-5], while denaturants, such as urea, can interact with the protein [6]. While most studies of osmolytes focus on their interaction with macromolecular surfaces and how they affect protein stability and function [7-10], we have recently found that ligands such as folate and dihydrofolate also weakly interact with osmolytes [11-14]. These weak contacts add a complicating layer to the effects of osmolytes and are known as quinary interactions [15].

Our initial osmolyte studies were done with three structurally unrelated dihydrofolate reductases (DHFRs), *E. coli* chromosomal DHFR [12], the plasmid-encoded antibiotic resistant enzyme R67 DHFR [11] and the pterin reductase-like enzyme, FolM [13]. Cofactor, NADPH, binding became tighter in the presence of osmolytes, consistent with dehydration of the protein-ligand interface and a smaller desolvation penalty [11]. In contrast, substrate, dihydrofolate (DHF), binding was weakened upon osmolyte addition and is sensitive to osmolyte identity; similar effects were previously noted on the K_m of DHF in the presence of trehalose and sucrose [16]. DHF and NADPH bind to symmetry related residues in the active site [17], which indicates that the effects on DHF are not due to osmolytes interacting with the active site pore. If osmolytes did interact with the protein surface, then similar effects would be noted for both ligands. The NADPH data indicate that the osmolytes affect binding by a “preferential exclusion” mechanism, where water prefers to interact with the protein and ligand, while the osmolytes are excluded. Elimination of osmolyte interactions with R67 DHFR altering DHF binding indicated that the osmolyte effects were on free DHF. This observation indicates that osmolytes interact with the free DHF in solution, which weakens binding of the ligand to the enzyme. If osmolytes are more difficult to remove than water, then ligand binding is disfavored and impedes binding to DHFR, which shifts the equilibrium towards the unbound species. In the cases of EcDHFR and FolM [12, 13], there were further complicating effects on ligand binding due to osmolytes interacting with the proteins in addition to DHF.

Other studies have provided chemical guidance for understanding the interactions between osmolytes and ligands. For example, Record and coworkers have monitored the preferential interaction coefficients (μ_{23}/RT) for different osmolytes (betaine,[18] glutamate [19], proline [20], urea [6] and PEGs [21]) with numerous small molecules using vapor pressure osmometry to determine how they interact with water as compared to the osmolyte. These μ_{23}/RT values for up to 30-50 different compounds were then deconvoluted into chemical interaction coefficients (α-values), which describe the interaction of the osmolyte with atoms/groups (e.g. aliphatic carbons, aromatic carbons, cationic nitrogens and amide nitrogens, phosphate oxygens, carboxylate oxygens, hydroxyls, and carbonyls). More recently, we have studied the interaction of betaine with folate and other small aromatic compounds [22]. In a similar manner, Hong et al. have studied the preferential interaction of trehalose with many small molecules [23]. Preferential interactions can be used to understand osmolytes effects on ligand binding.

We have already found that osmolytes interact with the ligands of DHFR [11, 12, 22], we want to test whether osmolytes also interact with other ligands in the folate synthesis pathway. In the present work, we focused on dihydropteroate synthase from *Bacillus anthracis* (BaDHPS). DHPS is a dimeric $\alpha_8\beta_8$ TIM barrel protein (62 kDa) that catalyzes the condensation of 6-hydroxymethyl-7, 8-dihydropterin pyrophosphate (H_2PtPP) and *p*-aminobenzoic acid (pABA) to form dihydropteroate and Mg^{2+}-pyrophosphate (Figure 3.1). H_2PtPP binds first to the active site with the pyrophosphate coordinating with the Mg^{2+} ion, which leads to a rearrangement of two conserved loops that create a previously unformed binding pocket for pABA. Also of interest, sulfa drugs are competitive inhibitors of DHPS and can react with H_2PtPP to form sulfa-dihydropterin conjugates [24, 25]. Sulfa drugs have been used as antibacterial drugs since 1930's [26] and are used to treat bacterial and protozoal infections. There has been an alarming increase in sulfa drug resistance, but the drugs are still used in combination with trimethoprim to treat several infections [27]. We have used the α-values for several osmolytes to predict how the DHPS ligands may interact with various osmolytes and have evaluated the effects of the osmolytes on substrate and drug binding to BaDHPS.

3.2 Materials and methods

3.2.1 Protein expression and purification

E.coli BL21 (DE3)-RIL cells with the dihydropteroate synthase gene from *Bacillus anthracis* in a pET28a vector were a generous gift from Richard Lee from St. Jude Children's Research Hospital (Memphis, TN). BaDHPS was expressed according to a literature protocol [28], but without using size exclusion chromatography. The protein fractions were dialyzed four times against 40 mM HEPES, 4 mM $MgCl_2$, pH 7.6 buffer. Aliquots of the protein were flash-frozen in liquid N_2 and stored at -80 °C. The protein concentration and extinction coefficients were determined using the bicinchoninic acid (BCA) assay (Pierce).

3.2.2 Isothermal titration calorimetry (ITC)

Pterin pyrophosphate, PtPP (Schircks Laboratories, Switzerland), an oxidized and stable analog of the substrate H_2PtPP, was used to prevent catalysis. Ligand binding was monitored in 40 mM HEPES, 4 mM $MgCl_2$, pH 7.6 in the presence or absence of cosolutes (osmolytes) using a VP-ITC from MicroCal. The PtPP concentration was determined by measuring the absorbance at 253 nm (ε_{253} = 23,500 M^{-1} cm^{-1}) in 0.1 N NaOH [29]**.** Typically PtPP (300-1200 µM) was titrated into 25-50 µM BaDHPS monomer. The cosolutes used for the experiments were trehalose, glycine betaine, proline, sucrose, glycerol, tetraethylene glycol (TEG) and PEG400. At least two replicate titrations for each condition were performed. Data were integrated using NITPIC software [30] and the replicates were globally fit using a one-site binding model in SEDPHAT [31] to obtain the affinities,

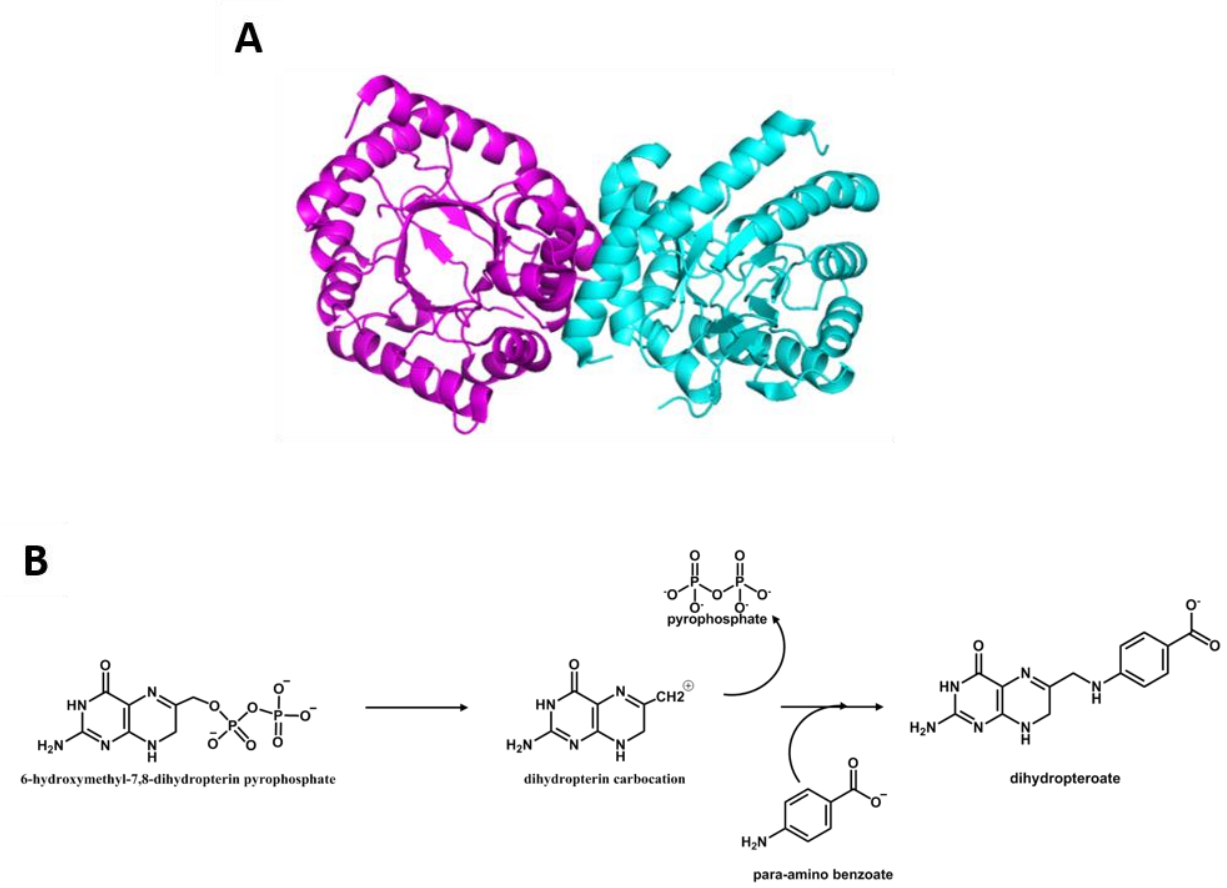

Figure 3.1: Structure and reaction mechanism of DHPS

A: DHPS is homodimeric $(\alpha\beta)_8$ TIM barrel with each monomer represented in pink and cyan (PDB ID: 1TWW) [25]. B: DHPS catalyzes the formation of dihydropteroate through condensation of pABA with dihydropterin pyrophosphate. The reaction proceeds in an ordered manner with dihydropterin pyrophosphate occupying the center of the barrel. The pyrophosphate moiety is cleaved leading to the formation of DHP^+ carbocation intermediate. Loops 1 and 2 undergo conformational change to allow pABA to access the binding pocket and form the product, dihydropteroate [25, 28].

stoichiometries and ΔH values. For titrations with a particular cosolute, buffer containing that osmolyte was used in the reference cell. The "c value" (=[P_{total}]/K_d) for binding was from 2-45, within the suggested range of 1-1000 [32]. The osmolalities of the solutions were measured on a Wescor Vapro 5520 osmometer. The binding of 0.8-1.6 mM pABA (MP Biomedicals) to BaDHPS (25-50 µM of monomer) saturated with 0.2 mM PtPP (~200 times the K_d) was studied in 40 mM HEPES, 4 mM $MgCl_2$, pH 7.6 in the absence or presence of cosolutes. The concentration of pABA was calculated by measuring the absorbance at 267 nm using an extinction coefficient of 15,000 M^{-1} cm^{-1} [33].

The effects of osmolytes on the binding of sulfathiazole (STZ, Tokyo Chemical Industry) to BaDHPS were also monitored using ITC. The concentration of sulfathiazole was obtained by measuring the absorbance at 254 nm (ε_{254} = 18,019 M^{-1} cm^{-1}) in 0.1 M sodium acetate buffer, pH 5 [34]. Sulfathiazole (800-1000 µM) was titrated into 19-25 µM BaDHPS monomer saturated with 0.2 mM PtPP.

3.2.3 Viscosity measurements

The kinematic viscosities (η/ρ in mm^2/s) of the buffers with osmolytes were measured using a Cannon-Feske viscometer at 25 °C [11]. The densities (ρ in g/ml) were measured using an Anton Paar DMA35 densitometer. The viscosity (η) of the buffers was calculated by multiplying the density of the solution by the kinematic viscosity. Relative viscosities (η/η_0) were calculated using buffer without osmolyte as the reference.

3.2.4 Differential Scanning Calorimetry (DSC)

The stability of DHPS (6-18 µM monomer) in 40 mM HEPES buffer, pH 7.6, was monitored between 15 and 95 °C at a scan rate of 1 °C/min using a Microcal VP DSC in the presence of osmolytes [13]. $MgCl_2$ was not added as it resulted in precipitation of the protein during the scan. Experiments were performed at least twice. The Origin software supplied with the DSC was used for data analysis.

3.2.5 Circular Dichroism

The effects of osmolytes on the secondary structure of BaDHPS were monitored using an AVIV model 202 CD spectrometer. BaDHPS (5-7 µM of monomer) was prepared in different osmolyte solutions and the spectra were obtained at 25 °C in a 1 mm cuvette. Blanks of buffer with each osmolyte were measured and used to subtract from the CD spectra of the enzyme in the osmolyte solution.

3.2.6 Computer Simulations

The BaDHPS-PtPP structure (PDB ID 1TWW) is missing loops 1 and 2, so to build back the loops, the monomer in the apo-BaDHPS structure (PDB ID 1TWS) that possess loops 1 and 2 was aligned with the binary structure in PyMol [35]. The PtPP ligands were then copied into the aligned apo-BaDHPS structure, and this structure was used for the simulations. Since Mg^{2+} was present in our ITC binding studies, a Mg^{2+} ion from the *Y. pestis* DHPS structure (PDB ID 3TYZ), was also added to the binary complex structure. PtPP, trehalose and zwitterionic proline were parameterized and the BaDHPS-PtPP structure was prepared using the Amber simulation package [36]. Previously prepared parameterization files were used for betaine [22]. A total of 171 osmolytes were added, for a concentration of 0.65 M, to the solvation box (63 Å x 63 Å x 113 Å) using the program PackMol [37]. Simulations of the binary complex in water, or in the presence of osmolytes, were performed using a previously described protocol [38]. The ff14SB force field was used, and the proteins were solvated using the TIP3P model in a 2 Å solvation shell, as well as the lrcm_cm parameter set for Mg^{2+} [39]. The systems were neutralized with Na^+. Duplicate production runs of 100 nanoseconds were performed under NVE conditions using 2 fs timesteps. The simulations were performed using NVIDIA graphics cards and AMBER's pmemd.cuda MD simulation engine [40, 41].

3.2.7 Prediction of preferential interactions of ligands with osmolytes

Preferential interaction coefficients (μ_{23}/RT) measure the extent to which molecules interact with osmolytes, or are solvated by water [6, 18, 20-23]. Preferential interaction coefficients can be predicted for molecules like PtPP, pABA and sulfathiazole using experimentally determined chemical interaction coefficients (α values) for a set of atom types (aromatic or aliphatic carbons, hydroxyl, amide, carboxylate or phosphate oxygens, and amide or cationic nitrogens) with individual osmolytes (betaine, trehalose, etc.) [6, 18, 20-23]. Values of μ_{23}/RT greater than 0 indicate that the molecules are solvated by water, while molecules that preferentially interact with osmolytes more than water have negative μ_{23}/RT values. A μ_{23}/RT value of 0, indicates it has equal preference for water and osmolytes. The predicted μ_{23}/RT values were calculated using (Eq. 3.1) [18]:

$$\frac{\mu_{23}}{RT} = \sum_i \alpha_i SASA_i + \sum_k \beta_k n_k \qquad \text{Eq. 3.1}$$

where *i* is an atom in the molecule, SASA is the solvent accessible surface area of the atom, *k* is each type of ion (Na^+, K^+ or Cl^-), β is the chemical interaction coefficient for the osmolyte with each ion, and n is the number of ions associated with the molecule (3 Na^+ for PtPP and 1 Na^+ for pABA). The surface areas of the ligands were calculated from structures obtained from the RCSB database using the program SurfaceRacer [42] and a water probe radius of 1.4 Å. For PEG400, it was assumed that there are nine interior ethylene glycol ethers when calculating the preferential interaction coefficient [21].

3.2.8 Predicted preferential interactions for protein-ligand complexes

Values of $\Delta\mu_{23}$/RT were predicted for the formation of ligand-protein complexes by calculating the μ_{23}/RT values for the individual components, and then subtracting the μ_{23}/RT of the complex (binary or ternary) from the values for the protein (apo or binary) and the free ligand. To add back loops 1 and 2 that are missing [28], the BaDHPS-PtPP, BaDHPS-PtPP-pABA and BaDHPS-PtPP-STZ complexes were prepared by aligning the PDB structures of the complexes with the apo-BaDHPS dimer in PyMol. The PDB coordinates of the ligands where then copied into the apo-BaDHPS coordinates. The μ_{23}/RT values for the protein (apo or binary complex) and the bound structure (binary or ternary complexes) were calculated as described above. The predicted $\Delta\mu_{23}$/RT values can be compared with those experimentally determined by ITC. The experimental $\Delta\mu_{23}$/RTs for PtPP, pABA and STZ binding to BaDHPS were calculated using equation 3.2 [6]:

$$-\frac{\ln(K_a)}{m_3} = \frac{\Delta\mu_{23}}{RT} \qquad \text{Eq. 3.2}$$

where K_a is the association constant, m_3 is the molality of the osmolyte, R is the gas constant and T is the temperature.

3.3 Results

3.3.1 Binding of ligands to *Bacillus anthracis* Dihydropteroate Synthase (BaDHPS)

The binding of ligands to BaDHPS in buffer alone was studied prior to measuring the effects of osmolytes. Ligand binding to BaDHPS occurs in an ordered fashion, with dihydropterin pyrophosphate binding followed by conformational changes that allow the second substrate, pABA, to bind [25]. Upon binding of dihydropterin pyrophosphate to DHPS, the pyrophosphate dissociates from the substrate, which forms a carbocation [25].

To avoid additional effects from the dissociation of the substrate, the stable analog, PtPP was used in ITC binding studies (Table 3.1). Binding of PtPP was enthalpy driven (Figure 3.2). Our observed K_d of 1.01 ± 0.20 µM, with a stoichiometry of 1.09 ± 0.01, is similar to the BaDHPS K_m of 3.2 µM for dihydropterin pyrophosphate [25]. While K_m values can contain additional rate information [43], we also note the substrate and its analog are in different oxidation states, which can also account for some of the differences in the affinities of the pterins. For example, the K_ds of DHF and its oxidize form, folate, binding to apo *E. coli* chromosomal DHFR are 1.8 and 4.7 µM, respectively [12].

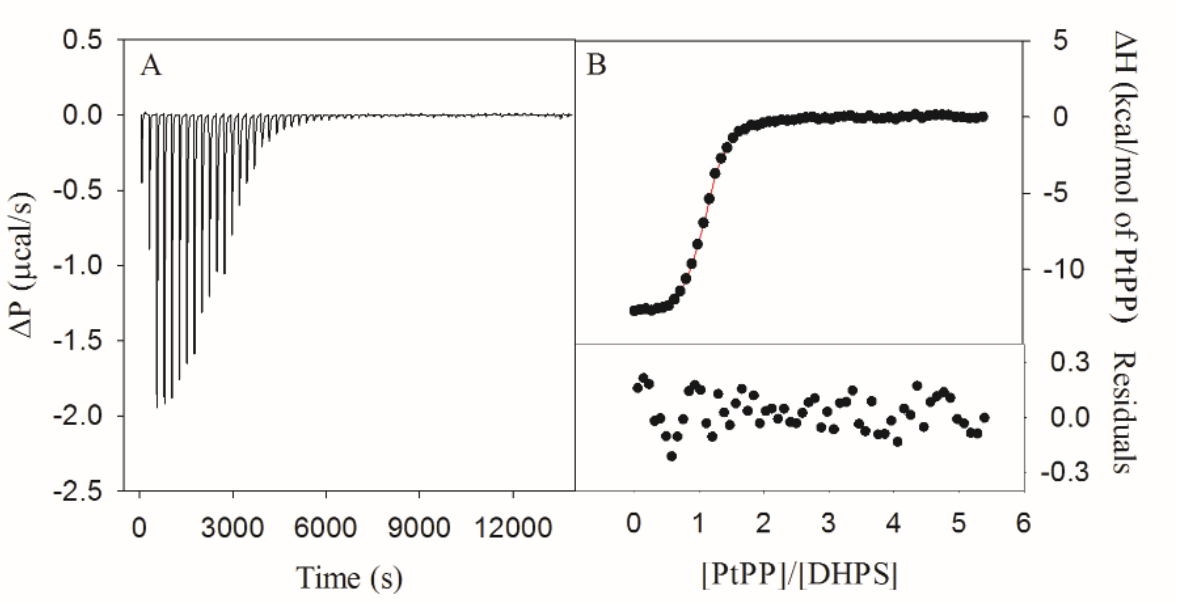

Figure 3.2: ITC data for the binding of PtPP to BaDHPS

A: The raw ITC data for addition of 1 mM PtPP to 40 μM apo-BaDHPS. B: The integrated thermogram was fitted to a one-site binding model (red line). The thermodynamic parameters are given in Table 3.1.

Table 3.1: Thermodynamic parameters of ligand binding measured by ITC in 40 mM HEPES, 4 mM $MgCl_2$ buffer with pH 7.6, at 25 °C

Protein/Protein ligand complex	Ligand	K_d (µM)	ΔG (kcal/ mol)	ΔH_{obs} (kcal/mol)	$T\Delta S$ (kcal/ mol)	n
BaDHPS	PtPP	1.01 ± 0.20	-8.1	-14.7 ± 0.2	-6.5	1.09 ± 0.01
BaDHPS-PtPP	pABA	10.7 ± 0.5	-6.8	-20.9 ± 0.3	-14.2	0.88 ± 0.01
BaDHPS-PtPP	STZ	2.57 ± 0.30	-7.6	-22.3 ± 0.5	-14.7	0.80 ± 0.01

There was no heat released when pABA was titrated into apo-BaDHPS, which indicates the pterin moiety needs to be present for pABA to bind. These data are consistent with ordered binding. Formation of a ternary complex involved binding of pABA to PtPP-saturated BaDHPS (Figure 3.3), which yields a K_d of 10.7 ± 0.5 µM (Table 3.1) and a stoichiometry of 0.88 ± 0.01 per DHPS monomer. The K_d is higher than the K_m for pABA binding to dihydropterin pyrophosphate-BaDHPS, 1.8 µM [25]. The K_d is also slightly higher the 3.1 µM K_d reported for pABA binding to pyrophosphate saturated *Staphylococcus aureus* DHPS [44].

Sulfathiazole (STZ) is a competitive inhibitor of DHPS that replaces pABA in the active site, and can react with dihydropterin pyrophosphate to form a covalent dihydropterin-STZ product [23]. ITC studies on BaDHPS by titrating STZ into the BaDHPS-PtPP binary complex yielded a K_d of 2.57 ± 0.30 µM and stoichiometry of 0.80 ± 0.01 (Table 3.1). The results indicated STZ bound 4-fold tighter to BaDHPS than pABA. The K_m of STZ as a substrate for BaDHPS is 0.33 µM [24]. The K_ds for both pABA and STZ are 10-fold weaker than their K_ms, which indicates that K_d and K_m are not measuring the same value, and that the K_ms most likely have contributions from other steps in the kinetics mechanism.

3.3.2 Calculation of preferential interaction coefficients of various osmolytes with the ligands of BaDHPS

To understand if osmolytes weakly interact with BaDHPS ligands and can perturb the binding process, we predicted the preferential interaction coefficients (μ_{23}/RT) for PtPP, pABA and STZ with several osmolytes (Table 3.2). Cosolutes (osmolytes) with different chemical nature and size were chosen, such as trehalose, betaine, proline, glycerol, tetraethylene glycol (TEG) and PEG400. The α-values and atom types and surface areas used in the calculations are listed in the supplement (Tables 1.1 and 3.3).

The μ_{23}/RT values predict different interactions of the osmolytes with PtPP, which can affect binding of the ligand to BaDHPS. The phosphates on PtPP are predicted to interact with water (which yields positive μ_{23}/RT values) and exclude most of the osmolytes. However, trehalose is predicted to have a stronger preference to interact with phosphate groups compared to water (negative μ_{23}/RT values) [23]. Other contributors to the net μ_{23}/RT values include a preference for most of the osmolytes to interact more with aromatic carbons compared to trehalose.

While there are differences between μ_{23}/RT values for pABA and sulfathiazole with the different cosolutes, they are not as pronounced. These calculated μ_{23}/RT values were most affected by the presence of nitrogens in the aromatic rings of sulfathiazole. These aromatic nitrogens are similar to amide nitrogens, and osmolytes that interact with amide nitrogens will interact with sulfathiazole more than pABA.

We also note that PEG400 is different from the other osmolytes because it is a polymer with nine interior ethylene glycol ethers that interact with amide nitrogens and aromatic carbons. As there are nine of these ethylene glycol units, its contribution gets multiplied

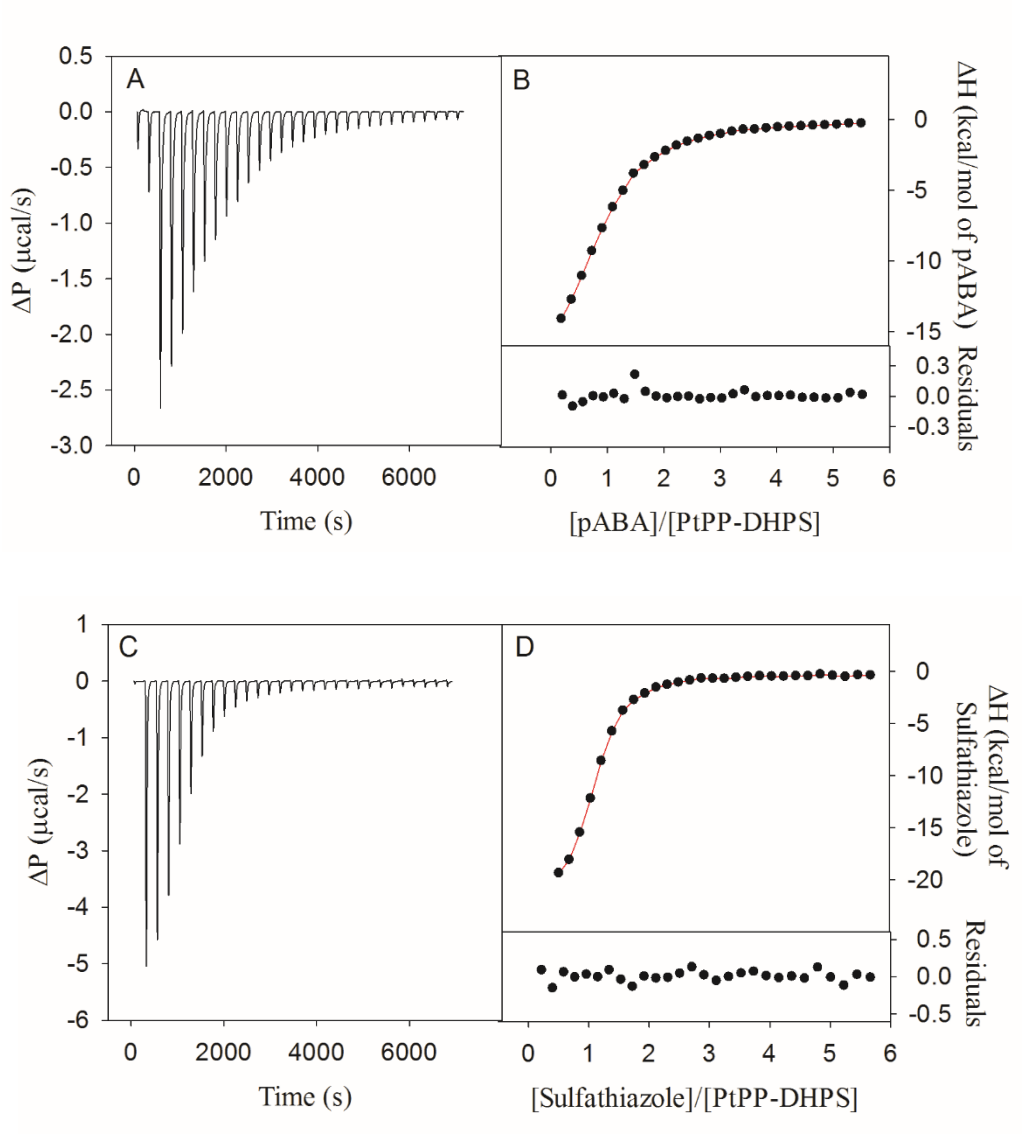

Figure 3.3: Ternary complex formation in BaDHPS as monitored by ITC

A: The raw ITC data for titration of pABA (800 μM) to into the BaDHPS (30 μM) saturated with PtPP (200 μM). B: Thermogram and the fit of the pABA titration. Residuals of the fit are shown in the lower panel. C: The ITC data for titration of sulfathiazole (780 μM) into DHPS (30 μM) saturated with 200 μM PtPP. D: The integrated areas and best fits for the titration. The thermodynamic parameters are given in Table 3.1.

Table 3.2: Predicted preferential interaction coefficients of osmolytes with PtPP, pABA and STZ

Osmolyte	Predicted μ_{23}/RT (m^{-1})[a]		
	PtPP	pABA	STZ
Trehalose[a]	-0.930	-0.096	-0.027
Betaine[b]	0.852	-0.469	-0.763
Proline[c]	0.084	-0.079	-0.246
Glycerol[d]	0.265	-0.032	-0.165
TEG[d]	0.936	-0.070	-1.04
PEG400[d]	6.09	-0.221	-2.86

[a]Calculated using the values from *23*. [b]For the values in *22*. [c]From ref *20*. [d]From ref *21*.

Table 3.3: Atom type and surface areas calculated from SurfaceRacer [42] for the ligands of DHPS

PtPP		
Atom name[a]	Atom type	SASA (Å^2)
N1	aromatic nitrogen	23.9
C2	aromatic carbon	4.7
NA2	amine off of an aromatic ring	61.7
N3	aromatic nitrogen	24.4
C4	aromatic carbon	7.6
O4	amide oxygen	37.5
C4A	aromatic carbon	5.4
N5	aromatic nitrogen	8.2
C6	aromatic carbon	2.8
C7	aromatic carbon	30.4
N8	aromatic nitrogen	29.0
C8A	aromatic carbon	5.0
C9	aliphatic carbon	35.6
O10	phosphate oxygen	13.6
P11	phosphate phosphorus	0
O12	phosphate oxygen	31.0
O13	phosphate oxygen	25.8
O14	phosphate oxygen	12.7
P15	phosphate phosphorus	0
O16	phosphate oxygen	41.2
O17	phosphate oxygen	27.3
O18	phosphate oxygen	46.1
pABA		
Atom name[a]	Atom type	SASA (Å^2)
N10	amine off of an aromatic ring	63.4
C11	aromatic carbon	5.2
C12	aromatic carbon	30.4
C13	aromatic carbon	25.6
C14	aromatic carbon	5.5
C15	aromatic carbon	25.7
C16	aromatic carbon	30.4
C	aliphatic carbon	10.5
O	carboxyl oxygen	44.8
O2	carboxyl oxygen	44.8

Table 3.3 continued

sulfathiazole		
Atom name[a]	Atom type	SASA (Å^2)
N10	amine off of an aromatic ring	53.7
C11	aromatic carbon	3.6
C12	aromatic carbon	27.5
C13	aromatic carbon	37.4
C14	aromatic carbon	9.4
C15	aromatic carbon	15.0
C16	aromatic carbon	35.8
S	aliphatic carbon	0
O	amide oxygen	31.9
O2	amide oxygen	37.4
N	nitrogen off an aromatic ring	19.2
C17	aromatic carbon	12.3
S18	aromatic nitrogen	5.7
C19	aromatic carbon	55.9
C20	aromatic carbon	50.6
N21	aromatic nitrogen	21.7

[a]The atom names are based on the folate atom naming scheme.

Structures:
PtPP

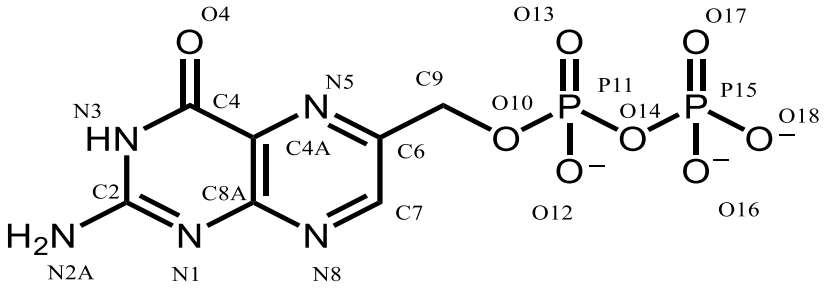

pABA

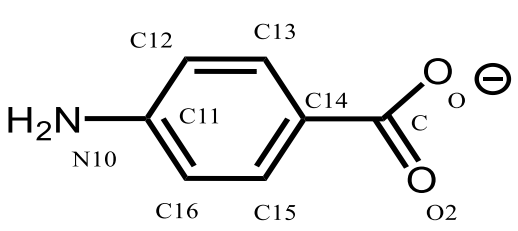

STZ

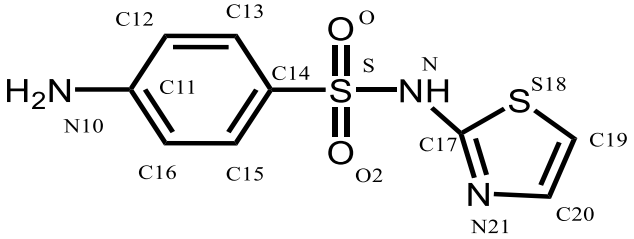

Ligand binding studies in the presence of osmolytes

3.3.2.1 Pterin pyrophosphate binding to BaDHPS

To assess our predictions of the effects of osmolytes on PtPP binding to DHPS, we added various cosolutes to the ITC titrations (Figure 3.4A). Within error, neither trehalose nor sucrose (another polyol osmolyte) weakens binding. However, addition of either 2 M betaine or 20% TEG tightens binding, 5- and 8-fold, respectively (Table 3.4). Osmolytes tighten binding in the following order: PEG400 > betaine/TEG > proline/glycerol. While the K_d values for PtPP binding in the presence of 10% PEG400 are in the range of the 10% TEG values, the osmolalities of the PEG400 solutions are lower, thus they have a stronger effect, as seen by the slope in the plot. Except for the predicted interaction of the PtPP phosphates with trehalose, which should weaken PtPP binding, in general, the osmotic stress effects follow the predicted μ_{23}/RT values, suggesting they are useful if there are no additional layers involved (i.e., conformational changes upon ligand binding, or osmolytes interacting with the protein/binding site). We additionally tried using larger cosolutes in our studies (PEG3350, PEG8000 and 40 kDa dextran); however, this resulted in precipitation of BaDHPS (data not shown).

3.3.2.2 pABA binding to DHPS-PtPP

Next, we added cosolutes to the titrations of pABA into BaDHPS saturated with PtPP (Figure 3.4B). Different patterns were observed in comparison to PtPP. While PtPP binding was unaffected to slightly weaker in the presence of trehalose, and tightened binding in the presence of betaine, the opposite trends were noted for pABA. Binding of pABA became tighter in the presence of trehalose, but weaker when betaine was the cosolute. While our more negative μ_{23}/RT values (Table 3.2) predicted pABA binding in the presence of betaine and PEG400 to be the weakest, we observed the biggest effect experimentally (~3 fold weaker binding) in the presence of proline. Osmolyte effects that weaken binding followed the order: proline > betaine > glycerol. K_d values for pABA in the presence of PEG400 were within error of those in buffer. Tighter pABA binding (up to 1.6-fold) was observed in the presence of TEG, trehalose and sucrose. As none of the osmolytes had positive μ_{23}/RT values above 0.002 (the value for glycerol) that would predict much tighter binding (Table 3.5), these results mostly seem reasonable.

3.3.2.3 *Binding of Sulfathiazole to BaDHPS*

The effects of cosolutes on the sulfa drug, STZ, binding to PtPP saturated BaDHPS were also measured (Figure 3.4C). PEG400/proline/betaine/TEG all weakened STZ binding to similar extents, with 2 M betaine increasing the K_d up to 5-fold (Table 3.6). Sulfathiazole

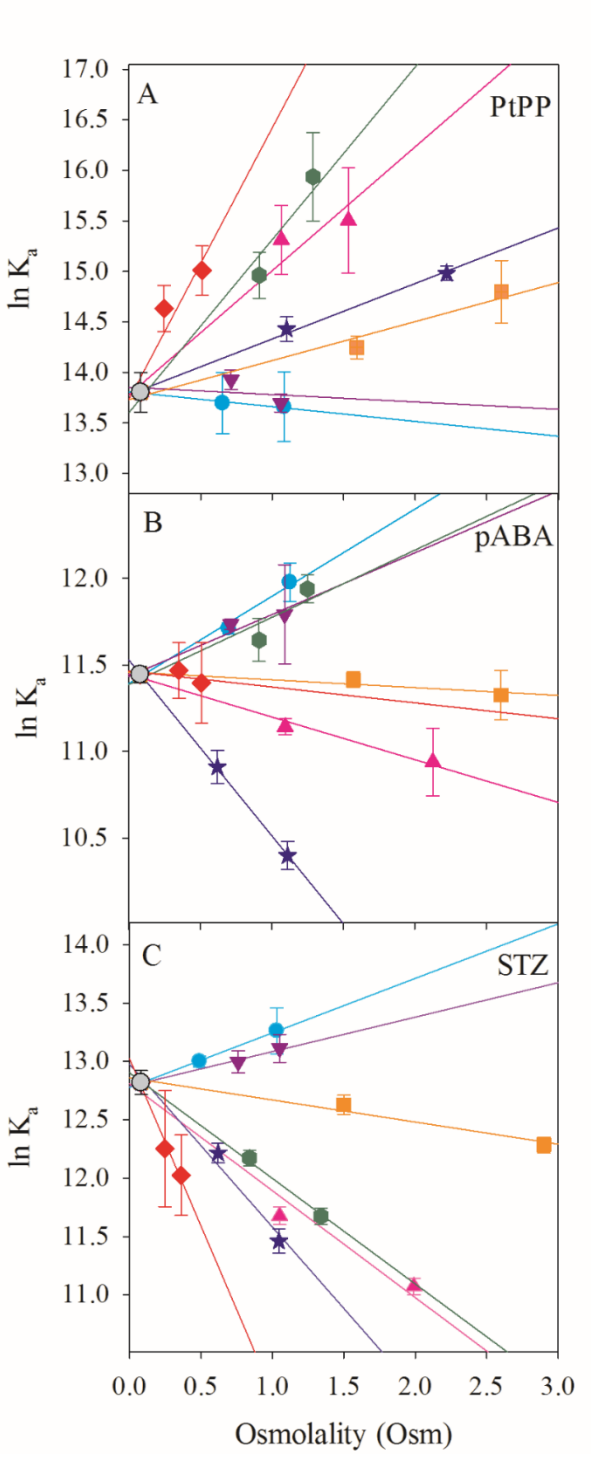

Figure 3.4: The effects of various osmolytes on the binding of ligands to BaDHPS for A: PtPP, B: pABA, and C: STZ

The ln(K_a) values are plotted versus osmolality for buffer (●), trehalose (●), betaine (▲), proline (★), sucrose (▼), glycerol (■), TEG (⬢), and PEG400 (♦).

Table 3.4: Thermodynamic parameters for the effects of osmolytes on PtPP binding to BaDHPS

Osmolyte	Osmolality (Osm)	K_d (μM)	ΔG (kcal/mol)	ΔH_{obs} (kcal/mol)	$T\Delta S$ (kcal/mol)	n
No osmolyte	0.08	1.01 ± 0.20	-8.1	-14.7 ± 0.2	-6.5	1.09 ± 0.01
0.5 M trehalose	0.66	1.10 ± 0.30	-8.1	-13.5 ± 0.2	-5.3	1.10 ± 0.01
1 M trehalose	1.08	1.20 ± 0.30	-8.1	-11.9 ± 0.3	-3.9	1.07 ± 0.01
1 M betaine	1.06	0.22 ± 0.06	-9.1	-17.2 ± 0.3	-8.1	1.09 ± 0.02
2 M betaine	1.53	0.19 ± 0.08	-9.2	-15.8 ± 0.3	-6.6	0.87 ± 0.01
1 M proline	1.10	0.54 ± 0.07	-8.6	-17.7 ± 0.1	-9.1	0.76 ± 0.01
2 M Proline	2.22	0.31 ± 0.02	-8.9	-16.4 ± 0.1	-7.5	0.60 ± 0.01
0.5 M sucrose	0.71	0.89 ± 0.08	-8.2	-13.4 ± 0.2	-5.2	0.80 ± 0.01
1 M sucrose	1.06	1.13 ± 0.09	-8.1	-13.2 ± 0.2	-5.1	0.78 ± 0.01
10% glycerol	1.59	0.65 ± 0.07	-8.4	-14.1 ± 0.3	-5.7	0.88 ± 0.01
20% glycerol	2.60	0.38 ± 0.11	-8.8	-14.8 ± 0.3	-5.9	0.83 ± 0.01
10% TEG	0.91	0.32 ± 0.07	-8.9	-19.4 ± 0.3	-10.6	0.63 ± 0.01
20% TEG	1.29	0.12 ± 0.05	-9.5	-16.8 ± 0.3	-7.3	0.92 ± 0.01
5% PEG400	0.25	0.44 ± 0.09	-8.7	-14.5 ± 0.2	-5.8	0.91 ± 0.01
10% PEG400	0.51	0.30 ± 0.07	-8.9	-16.9 ± 0.2	-8.1	0.66 ± 0.01

Table 3.5: Thermodynamic parameters for the effect of osmolytes on pABA binding to PtPP-BaDHPS by ITC

Osmolyte	Osmolality (Osm)	K_d (μM)	ΔG (kcal/mol)	ΔH_{obs} (kcal/mol)	$T\Delta S$ (kcal/mol)	n
No osmolyte	0.08	10.7 ± 0.5	-6.8	-20.9 ± 0.3	-14.2	0.88 ± 0.01
0.5 M trehalose	0.69	8.2 ± 0.1	-6.9	-21.9 ± 0.7	-15.7	0.81 ± 0.01
1 M trehalose	1.13	6.3 ± 0.7	-7.1	-20.5 ± 0.8	-13.4	0.83 ± 0.01
1 M betaine	1.09	14.5 ± 0.7	-6.6	-18.3 ± 0.5	-11.7	0.93 ± 0.03
2 M betaine	2.13	17.8 ± 3.2	-6.5	-20.7 ± 2.8	-14.3	0.78 ± 0.07
0.5 M proline	0.62	18.3 ± 1.7	-6.5	-23.3 ± 2.4	-16.8	0.69 ± 0.05
1 M proline	1.11	30.5 ± 2.3	-6.2	-20.9 ± 1.4	-14.8	0.79 ± 0.04
0.5 M sucrose	0.71	8.1 ± 0.3	-6.9	-21.9 ± 0.5	-14.9	0.65 ± 0.01
1 M sucrose	1.09	7.5 ± 1.8	-6.9	-21.1 ± 3.1	-14.1	0.55 ± 0.06
10% glycerol	1.57	11.1 ± 0.5	-6.8	-20.3 ± 0.7	-13.5	0.74 ± 0.02
20% glycerol	2.60	12.1 ± 1.6	-6.7	-18.8 ± 1.7	-12.1	0.85 ± 0.06
10% TEG	0.91	8.8 ± 1.0	-6.9	-22.1 ± 1.4	-15.2	0.60 ± 0.02
20% TEG	1.25	6.5 ± 0.5	-7.1	-22.4 ± 0.7	-15.4	0.82 ± 0.01
7.5% PEG400	0.35	10.5 ± 1.6	-6.8	-24.1 ± 3.3	-17.2	0.77 ± 0.09
10% PEG400	0.51	11.3 ± 2.3	-6.8	-24.1 ± 2.2	-17.3	0.71 ± 0.08

Table 3.6: ITC thermodynamic parameters for osmolytes effects on sulfathiazole binding to PtPP-BaDHPS

Osmolyte	Osmolality (Osm)	K_d (μM)	ΔG (kcal/mol)	ΔH_{obs} (kcal/mol)	$T\Delta S$ (kcal/mol)	n
No osmolyte	0.08	2.6 ± 0.3	-7.6	-22.3 ± 0.5	-14.7	0.80 ± 0.01
0.5 M trehalose	0.49	2.3 ± 0.1	-7.7	-23.5 ± 0.3	-15.8	0.79 ± 0.01
1 M trehalose	1.03	1.8 ± 0.3	-7.9	-23.1 ± 1.0	-15.2	0.80 ± 0.01
1 M betaine	1.05	8.5 ± 0.6	-6.9	-22.2 ± 0.9	-15.3	0.80 ± 0.01
2 M betaine	1.99	15.5 ± 1.0	-6.6	-21.9 ± 1.2	-15.4	0.87 ± 0.01
0.5 M proline	0.62	4.9 ± 0.4	-7.2	-24.2 ± 0.7	-16.9	0.77 ± 0.01
1 M proline	1.05	10.5 ± 1.0	-6.8	-24.4 ± 1.4	-17.6	0.77 ± 0.03
0.5 M sucrose	0.76	2.3 ± 0.2	-7.7	-24.6 ± 0.6	-16.9	0.78 ± 0.01
1 M sucrose	1.05	2.0 ± 0.2	-7.8	-24.9 ± 0.7	-17.1	0.70 ± 0.01
10% glycerol	1.50	3.3 ± 0.3	-7.4	-26.4 ± 0.5	-18.9	0.79 ± 0.01
20% glycerol	2.90	4.6 ± 0.3	-7.3	-26.3 ± 0.6	-18.9	0.77 ± 0.01
10% TEG	0.84	5.2 ± 0.3	-7.2	-24.6 ± 0.6	-17.3	0.83 ± 0.01
20% TEG	1.34	8.5 ± 0.6	-6.9	-27.7 ± 0.9	-20.8	0.67 ± 0.03
5% PEG400	0.25	4.8 ± 1.9	-7.3	-26.9 ± 3.7	-19.6	0.76 ± 0.03
7.5% PEG400	0.36	6.0 ± 1.8	-7.1	-26.1 ± 3.7	-18.9	0.80 ± 0.07

binding was approximately 1.7 times weaker in the presence of glycerol, while trehalose/sucrose marginally tightened binding up to 1.5-fold. Again, these results mostly seem reasonable based on the predicted μ_{23}/RT values provided in Table 3.2.

3.4 Effects of Viscosity, Dielectric Constant and Volume Exclusion on Ligand Binding to BaDHPS

While preferential interaction coefficients likely play a large role in modulating binding, other solvent properties, such as viscosity, dielectric constants and/or volume exclusion effects, could also be involved. For the osmolytes used in this study, there were no observable trends in the ln(K_a) versus viscosity of the solutions for PtPP, pABA or STZ (Figure 3.5). For example, the TEG solutions have higher viscosities than those of trehalose, yet the two osmolytes have opposite effects on the binding of the three ligands. Additionally, 0.5 M trehalose and 2 M betaine have similar viscosities, yet the trehalose weakened PtPP binding, while binding of PtPP was tighter in the presence of betaine. Further, at viscosities that weakened PtPP binding to BaDHPS, the binding of pABA became tighter. If viscosity were the reason for the differences in binding, its effects would be consistent with all ligands. These results together indicate that viscosity is not a contributing factor to how the osmolytes alter ligand binding to BaDHPS.

The solution dielectric constant can affect binding upon cosolute addition. Dielectric constants of the cosolutes used in the study were obtained from literature [45-47]. Betaine addition increased the dielectric constant of the solution but imposed opposite effects on PtPP and pABA binding to BaDHPS (Figure 3.6). Again, if alterations in dielectric properties affected ligand binding, the effects would be consistent for both ligands. Moreover, 1 M trehalose and 20% glycerol have similar dielectric constants but had opposite effects on PtPP and pABA binding to BaDHPS. These various results suggest that the observed changes in ligand binding in the presence of cosolutes were not due to alterations in the dielectric properties.

Further, volume exclusion effects were explored as contributing factors for differences in binding in the presence of osmolytes (Figure 3.7). It is predicted that if excluded volume effects deter binding, the trend in altered binding would be consistent with the change in the molecular volume of the added cosolute [48, 49]. However, there were no such correlations between the molecular volumes of the cosolutes and their effects on binding of the ligands to BaDHPS. Therefore, volume exclusion most likely does not play a role in the changes associated with ligand binding in presence of cosolutes.

3.5 Stability of DHPS in the presence of osmolytes

Osmolytes can additionally interact with proteins, thus we performed CD and DSC to evaluate any of these effects. CD spectra in the presence of betaine and proline could

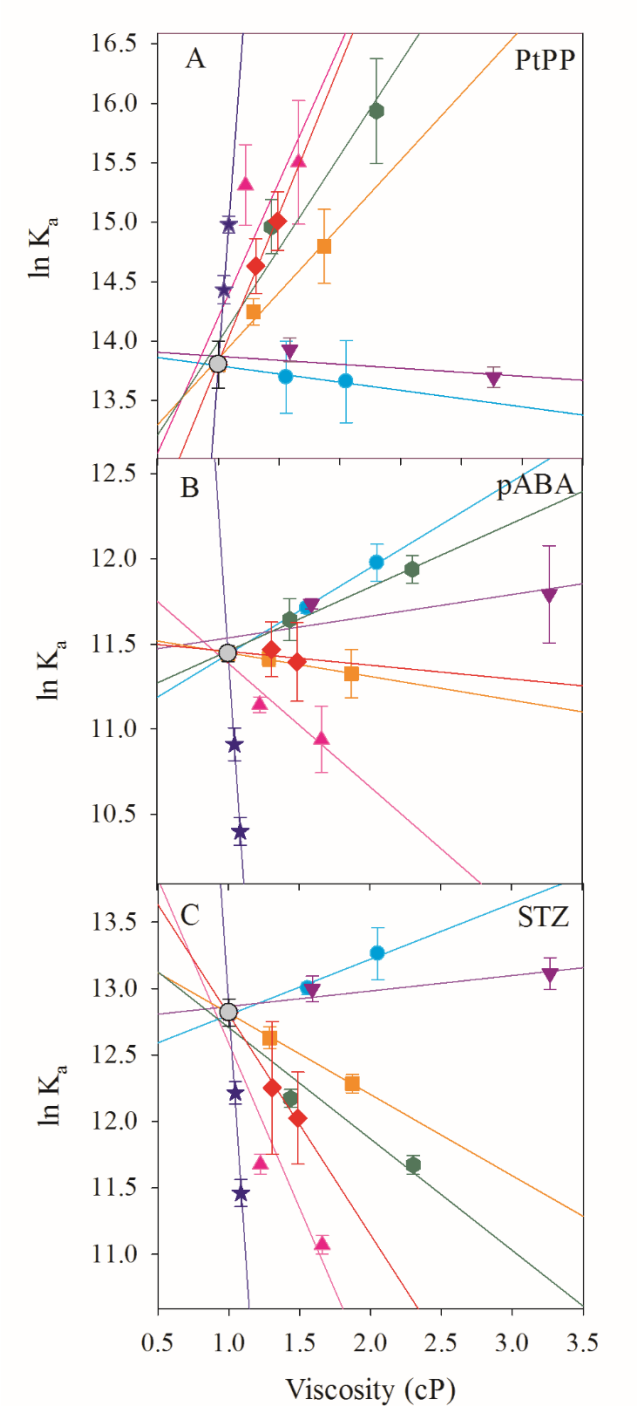

Figure 3.5: Plots for effect on viscosity on ligand binding

ln K_a versus relative viscosity was plotted for A: PtPP B: pABA and C: STZ. The data points are represented buffer (●), trehalose (●), betaine (▲), proline (★), sucrose (▼), glycerol (■), TEG (⬢), and PEG400 (♦).

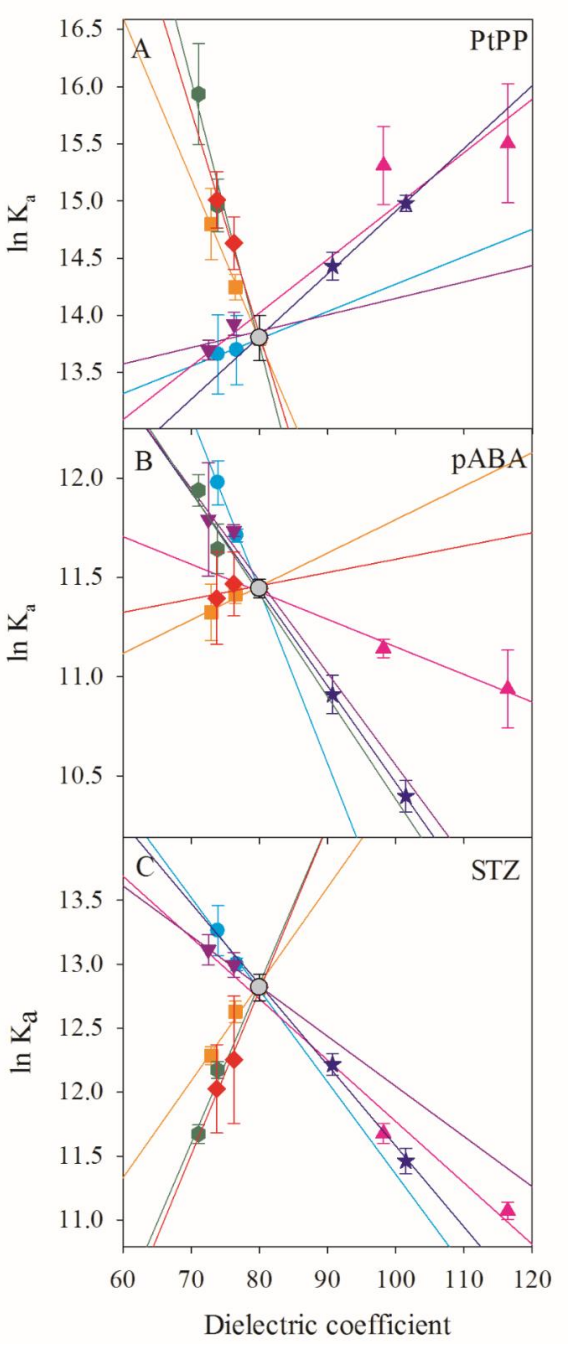

Figure 3.6: The change in ligand binding as a function of dielectric constant

The ln(K_a) versus the dielectric constant of the solution was plotted for A: PtPP, B: pABA and C: STZ. The data points are represented as (●) for buffer, (●) for trehalose, (▲) for betaine, (★) for proline, (▼) for sucrose, (■) for glycerol, (⬢) for TEG, and (♦) for PEG400.

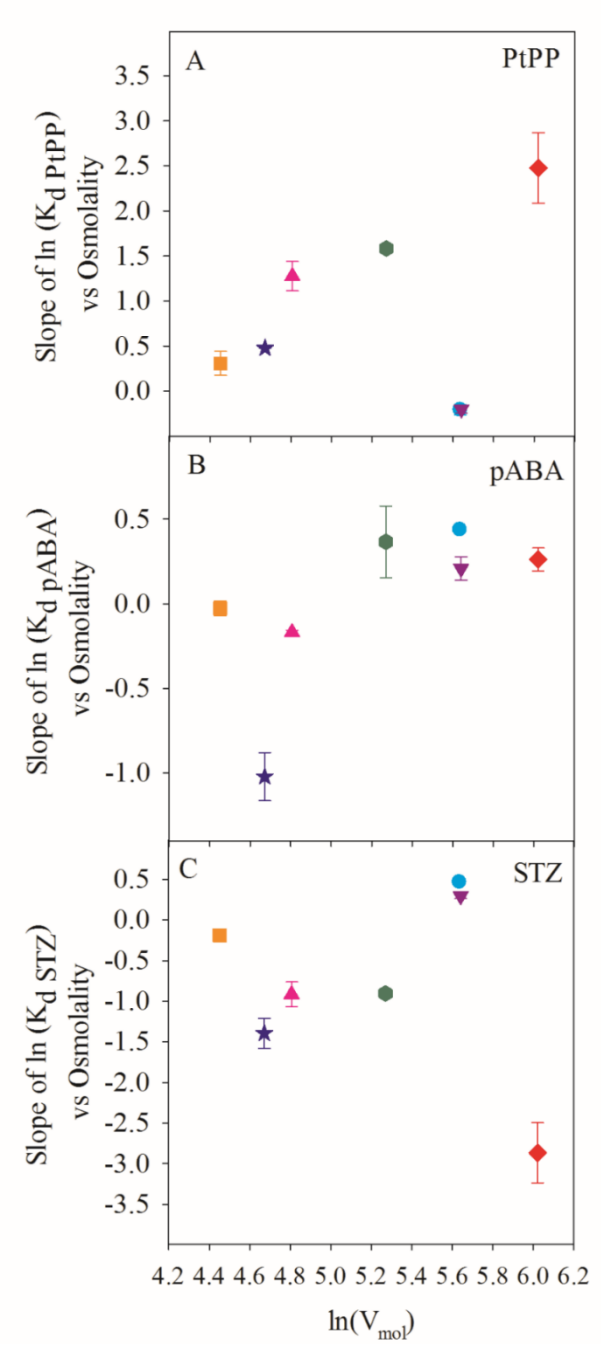

Figure 3.7: Slope of lines from the data in Figure 3.4 vs ln molar volume for all three ligands, A: PtPP, B: pABA and C: STZ

The data points colored as trehalose (●), betaine (▲), proline (★), sucrose (▼), glycerol (■), TEG (⬢), and PEG400 (♦). No correlation was found between the volume occupied by the osmolyte and its effect on binding of the ligand to DHPS.

not be measured due to the high absorbance of the osmolytes below 240 nm. The secondary structure of BaDHPS in buffer and most of the osmolytes showed minima at 210 and 220 nm. However in presence of PEG and higher concentrations of TEG, the minimum was around 210 nm and none was seen at 220 nm (Figure 3.8). This indicated that PEG may induce changes in the secondary structure of BaDHPS. Previous studies have found addition of osmolytes/crowders can induce changes in active site volume, perhaps due to compression associated with the osmotic stress [7, 10].

DSC thermograms of BaDHPS in buffer had a single unfolding transition with a T_m of 45.3 ± 0.7 °C (Figure 3.9). The unfolding of BaDHPS with increasing temperature was irreversible, so all thermodynamic parameters obtained from fits of the data are apparent (Table 3.7). The T_m of 45.3 °C is similar those reported for two different wild type variants from *Staphylococcus aureus* DHPS, with T_ms of either 38.6 °C or 42.4 °C [44].

Addition of 1 M trehalose to BaDHPS increased the T_m to 56.4 ± 0.3 °C, while addition of 2 M betaine increased the T_m to 58.1 ± 0.1 °C (Figure 3.10). Both osmolytes have stabilizing effects on the protein. Betaine and trehalose have both been indicated to stabilize proteins by a preferential exclusion mechanism [6, 50-52]. The betaine or trehalose DSC results are consistent with this model as addition of either cosolute increased the BaDHPS T_m (Table 3.8). Even in the presence of osmolytes the unfolding of the protein was irreversible, therefore enthalpy of unfolding is reported as an apparent (ΔH_{app}). The addition of trehalose, betaine and proline did not change ΔH_{app}. The presence of TEG and PEG400 both destabilized DHPS, decreasing the ΔH_{app} 2 to 3-fold, while the T_m was mostly unaffected. The thermal destabilization of DHPS by TEG and PEG400 indicates that they may interact with the protein.

3.6 Computer Simulations

To determine if the osmolytes accumulate near the active site short, 100 ns, simulations were performed in the presence of 0.65 M betaine, proline or trehalose, as these small molecule osmolytes had the biggest effect on ligand binding to BaDHPS. Trehalose would form clusters during the simulation. Clustering of trehalose has been noted previously, even at concentrations as low as 0.22 M [53]. One of the hydroxyls of at least one molecule of trehalose was within 5 Å of the phosphates of PtPP in one of the active sites of simulation 1 and both the active site PtPP molecules in simulation two 80% of the time (Figure 3.11). This indicates that trehalose is most likely interacting with the phosphates of the bound PtPP as well. Since the ligand is partially solvent exposed, there is access for the osmolytes to enter the active site and interact with the phosphate oxygens. These data concur with phosphate oxygens preferentially interacting with trehalose over water [23]. However, trehalose was found within 5 Å of the other active site's PtPP phosphates only 35% of the time. The discrepancy in trehalose proximity to this PtPP and the other PtPPs in the simulation could occur if the active site is slightly less solvent exposed for the PtPP that interacts with a trehalose only 35% of the time. Additionally, the clusters of trehalose near the active site may make it harder for single osmolyte molecules to enter

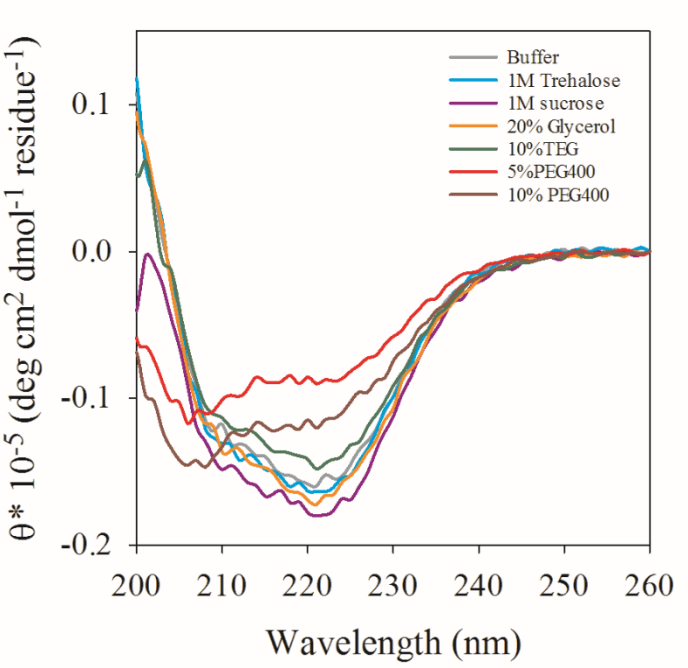

Figure 3.8: The secondary structure of BaDHPS is unaffected by most of the osmolytes, except PEG400

CD spectra were performed in buffer (light grey line), 1 M trehalose (cyan line), 1 M sucrose (purple line), 20% glycerol (orange line), 10% TEG (dark green line), 5% PEG400 (red line) and 10% PEG400 (brown line).

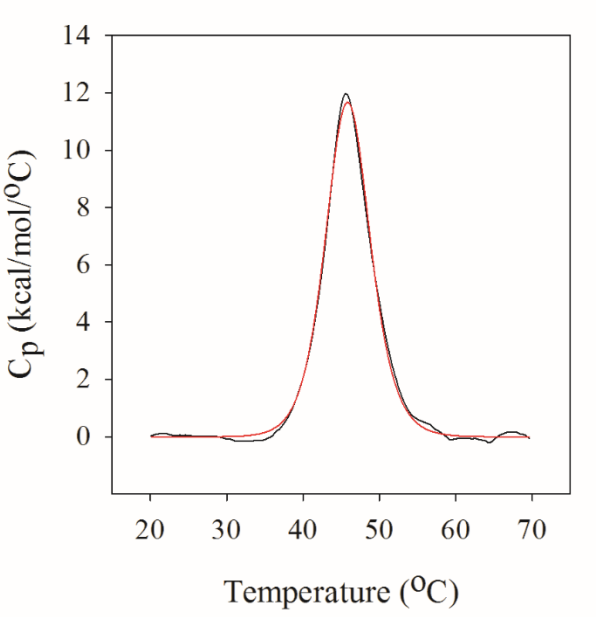

Figure 3.9: DSC data for 19.3 µM of DHPS monomer in 40 mM HEPES, pH 7.6 at a scan rate of 1 ^{0}C/min

The solid black line represents the thermogram and the red line represents the fit to a single transition in a two-state unfolding model (folded to unfolded). Fit of the data yields a T_m of 45.3 ± 0.7 ^{o}C.

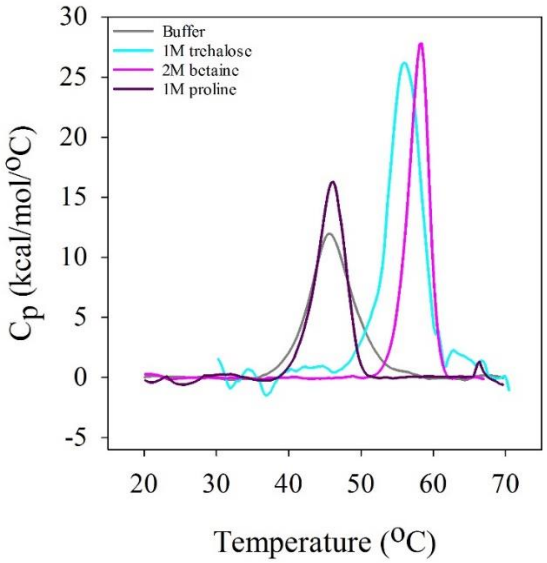

Figure 3.10: DSC scans of BaDHPS in solutions containing varying concentrations of osmolytes

Addition of the osmolytes increased the melting temperature of the enzyme with respect to the buffer. Increased concentration of the osmolyte resulted in a further increase in the melting temperature. The addition of betaine and trehalose increased the thermal stability of BaDHPS.

Table 3.7: Melting temperatures (T_m) of BaDHPS in 40 mM HEPES pH 7.6 in the absence and presence of osmolytes using DSC

Protein with osmolyte	T_m (°C)	ΔH_{app} (kcal/mol)[a]
Buffer	45.3 ± 0.7	80 ± 16
0.5 M trehalose	47.6 ± 0.3	55 ± 8
1 M trehalose	56.4 ± 0.3	114 ± 39
1 M betaine	51.3 ± 0.1	88 ± 4
2 M betaine	58.1 ± 0.1	98 ± 5
0.5 M proline	45.9 ± 0.1	99 ± 1
1 M proline	45.9 ± 0.1	82 ± 1
10% TEG	45.2 ± 0.1	48 ± 4
20% TEG	44.2 ± 0.1	55 ± 3
5% PEG400	47.7 ± 0.1	28 ± 1

[a]The unfolding of BaDHPS was irreversible under these conditions, therefore the enthalpy of unfolding is reported as an apparent value (ΔH_{app}).

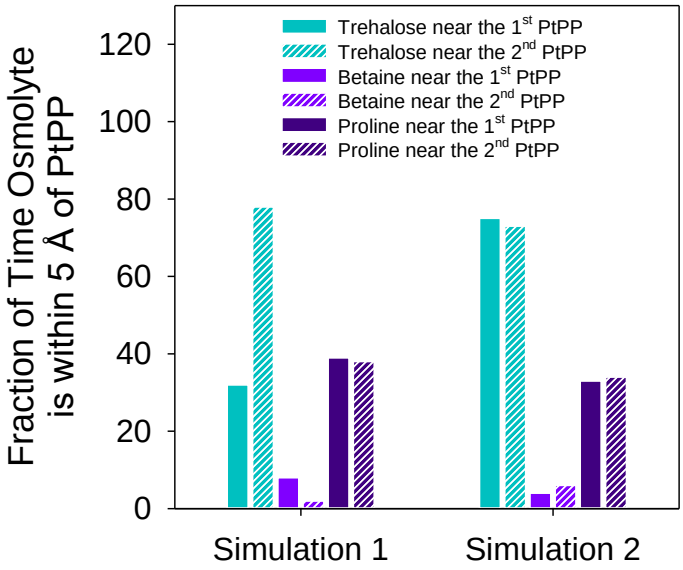

Figure 3.11: The fraction of the time that an osmolyte is near the phosphate group of PtPP during the 100 ns computer simulations

Simulations contained 0.65 M osmolyte. Data are shown for the duplicate simulations, as well as each of the two PtPP molecules in the complex.

the active site to interact with the phosphates. Overall, though, the simulation data suggest that trehalose interacts with PtPP bound in the BaDHPS active site.

Betaine and proline are both excluded from phosphate oxygens [18, 20, 22], which are preferentially solvated by water molecules. Therefore, it was predicted that the two osmolytes would not be found near the bound PtPP during the simulations. For the betaine and proline simulations, the distances between the cationic nitrogens of the osmolytes and the phosphate oxygens on PtPP were calculated. Betaine was mostly absent from the active site, with an osmolyte residing near the phosphate oxygens of PtPP less than 10% of the time during the simulation (Figure 3.11). This is not surprising as betaine tends to be excluded from the surface of phosphate groups [18, 22]. Proline is also predicted to be highly excluded from phosphate oxygens [20]; however, there was at least one osmolyte molecule within 5 Å of the phosphate oxygens at least 35% of the time during the simulations. If proline is not interacting with the phosphates of PtPP, then this indicates that the cyclic amino acid may be interacting with some of the residues in the active site. Further analysis will need to be performed to explore these potential interactions. Overall, these simulation data indicate that trehalose and proline are likely to associate with the active site of BaDHPS. Though, this is only a preliminary analysis of the simulation results. Further analysis still needs to be performed. The types of interactions formed between the osmolytes and the PtPP ligand, as well as interactions of the osmolytes with protein residues are still being measured.

3.7 Discussion

3.7.1 Effects of cosolutes on ligand binding to BaDHPS

Addition of PtPP to apo-BaDHPS in the presence of osmolytes shows variable effects that are mostly consistent with the μ_{23}/RT predictions provided in Table 3.2. One consideration is how the phosphates of PtPP are interacting with the active site, a SN1 reaction can slowly result in loss of the pyrophosphate moiety [25]. Pyrophosphate likely remains trapped in the anion binding pocket where it is proposed to help position several loops to accommodate the incoming pABA [25].

Addition of pABA, as well as STZ, to PtPP-BaDHPS in the presence of osmolytes shows variable effects that are mostly consistent with the μ_{23}/RT predictions provided in Table 3.2. Additional interactions that could be involved include effects of osmolytes the on two flexible loops that help establish the pABA/STZ site. Using both the BaDHPS and *Yersinia pestis* DHPS (YpDHPS) structures, Yun et al. note the pABA site only forms in the ternary complex [25]. They also provide crystal structures of dihydropterin pyrophosphate-STZ structures showing that that STZ can replace pABA as the second substrate, allowing formation of sulfonamide-pterin adduct as an alternate product.

The effect of osmolytes on STZ is less pronounced than on pABA. This could be seen as the fold effect of the osmolytes on each of the ligand. Possibly the effects are less on STZ because it binds tighter to the enzyme. In one example, PEG400 and TEG had

opposite effects for pABA and STZ binding, weakening the binding of the sulfadrug, but having no affect to slightly tightening pABA binding. STZ has an extra thiazole group which has the sulfate oxygens, amide nitrogen and the aromatic nitrogens. Record and coworkers have reported that aromatic nitrogens can be treated as amide nitrogens. Looking at the α values, TEG and PEG400 are predicted to interact with the amide nitrogens, thus decreasing the association of STZ to the enzyme. Comparing this to pABA, which does not have amide/aromatic nitrogens, the predicted μ_{23}/RT is less positive and hence the effects on association are not weakened. Additionally, there are mutations in DHPS that are present beyond the substrate envelope and these cause a decrease in binding of STZ but does not affect binding of pABA [25, 44]. Perhaps the osmolytes interact, or change the structure, of the residues/loops that interact with STZ, but not pABA.

We initially had tried large molecular weight cosolutes (crowders) in our studies. However, ligand stoichiometries for high molecular weight PEGs and dextrans (data not shown) tended to be lower than for other osmolyte conditions (Tables 3.5-3.7), perhaps these crowders can change the size or shape of the active site. This notion could fit with the YpDHPS [25] crystal structure data that once H_2PtPP is bound to the enzyme, and the SN1 reaction occurs, the subsequent interaction of Mg^{2+} with loops 1 and 2 allows the formation of the pABA site from conserved residues F33, P69, K220, and F189. Loop 1 was also proposed to form a lid over the active site.

Further, detailed temperature jump studies by the Callender and coworkers on ligand binding and loop movement in lactate dehydrogenase [54] and triose phosphate isomerase [55] found osmolyte effects can shift the enzyme to prefer substrate binding competent or incompetent species. In general, they conclude “osmolyte-induced changes in the energy landscape of the protein complexes can shift the conformational nature of functional sub-states within the protein ensemble.” The crowders may cause BaDHPS to favor conformations that are less likely to bind ligands, resulting in lower stoichiometries of binding. More recent studies find potential roles for changes in protein dynamics [56] and trapped waters [57], which can vary depending on osmolyte identity as well as altered water structure in a crowded environment [58].

3.7.2 The role of cosolvent properties in their effects on binding

Viscosity affects the diffusion of reacting species as well as changes the enzyme motions, which leads to alterations in enzyme kinetics. A direct correlation has been reported between the decrease in velocity of enzyme and increasing viscosity of the solvent [59]. In our system, the added viscogens affected the K_d of all the ligands. The increase in the viscosity, however, was not responsible for this alteration in ligand binding (Figure 3.5).

Addition of cosolutes can alter the polarity of the solvent, particularly the dielectric constant. No trend was observed in our experiments when the ligand binding to DHPS was plotted as a function of the dielectric constant. It has been previously suggested that the addition of organic solvents and dielectric changes in the medium affect enzyme

substrate complexes where hydrophobic interactions dominate binding as compared to electrostatic interactions [60].

Exclusion for a certain volume due to occupancy by other molecules gives rise to volume exclusion effects. Increased crowding/volume exclusion leads to favoring of the bound state in the reaction equilibrium [48]. In our study there is no trend seen with increase in molar volume occupied by the cosolute and tight binding. Similarly, there were no volume effects on cyclic AMP receptor protein binding to its target DNA when cosolutes had molecular volumes less than 6 mL/mol [61]. Only when larger crowders were used did volume exclusion effects become more apparent. Our data indicate that viscosity, dielectric and volume exclusion effects are not playing a role in how osmolytes alter the binding of ligands to BaDHPS. This leaves preferential interaction as the main conduit of the osmolyte effects.

3.7.3 Preferential interaction of osmolytes with the ligands of DHPS

Osmotic stress effects can be complicated and layered [62]. The simplest case is preferential exclusion, where the osmolytes do not interact with the protein surface. This typically results in all osmolytes showing the same effect and tightening ligand binding. Examples of this behavior include NADPH binding to R67 DHFR [11], and binding of *E. coli* lactose repressor to its regulatory site in the *lac* promoter and its transfer from the O1 site to nonspecific DNA [63]. Osmolytes can also weakly interact with the protein surface. This results in variable effects on ligand binding, from tighter to weaker binding [11-13]. In addition, preferential interaction studies have raised the possibility of osmolytes interacting with small molecules, such as substrates, cofactors, drugs, sugars, amino acids, etc [14]. While weak, if they are more difficult to remove than water, the binding equilibrium will be shifted towards the free species, loosening binding. Here, we discuss these various possibilities for BaDHPS.

One way for osmolytes to affect ligand binding is by interacting with the protein/binding site. The CD spectra suggest the interaction of osmolytes with apo BaDHPS might be minimal except in the presence of PEG400 and higher concentrations of TEG (Figure 3.8). DSC provides additional support for exclusion of osmolytes from BaDHPS (Figure 3.10). Here the BaDHPS T_m values increased in the presence of betaine or trehalose, consistent with the contention that osmolytes typically stabilize proteins by increasing hydration [64]. Indeed, in our previous studies with FolM, we found addition of 10-20% DMSO destabilized the protein while addition of 10-20% betaine increased the T_m [13]. These results suggested interaction of DMSO with the protein, while betaine was excluded.

3.7.4 Comparing predicted $\Delta\mu_{23}$/RT values with ITC

The μ_{23}/RT of the free ligand only describes part of the binding equation. Osmolytes can still interact with any functional groups on the ligand that are still exposed to solvent in the bound complex [22]. Therefore, we calculated the predicted $\Delta\mu_{23}$/RTs for each osmolyte and determined the experimental $\Delta\mu_{23}$/RTs from the ITC data using equation 3.2 (Table 3.8) [6]. The slopes of the $\ln(K_a)$ versus osmolality in Figure 3.4 correspond to the difference in preferential interaction of the osmolytes with the complex versus the free ligand and protein. PtPP predicted values were matched the experimentally determined $\Delta\mu_{23}$/RT for most of the osmolytes.

The exception was trehalose, where the binding affinity was predicted to decrease 10-fold more than it did experimentally. One possible reason for the difference in predicted and experimental $\Delta\mu_{23}$/RT values could be that there are aromatic nitrogens in PtPP. In the predicted values, these nitrogens were treated as amides. Perhaps trehalose is excluded more from aromatic nitrogens than it is from amide nitrogens. A second reason could be that the phosphates of PtPP may coordinate Mg^{2+}, which would be similar to ADP coordinating Mg^{2+} in solution [65]. Trehalose preferentially interacts with phosphate groups, but may be more excluded from Mg^{2+}-coordinated phosphates. This would decrease the overall effect of trehalose on PtPP binding, as less trehalose would be interacting with free PtPP. Since the other osmolytes are excluded from the phosphate groups, they may not be affected by, or be similarly excluded from, potential coordination of Mg^{2+} by PtPP. A third reason might be that trehalose can may still be able to interact with the bound PtPP. Trehalose was present in the active site in as much as 85% of the time in the computer simulation. The phosphates of bound PtPP are partially exposed to the solvent and can still interact with trehalose. Not all the trehalose molecules may be removed from the pyrophosphate moiety upon PtPP binding. We have previously shown that exclusion of betaine from ligand functional groups that do not form contacts in the bound complex do not affect binding of the ligand [22]. Therefore, if trehalose can still interact with PtPP even when it is bound, then the effect of the osmolyte on ligand binding would be less than is predicted from the preferential interaction coefficients.

For pABA and STZ, the predicted $\Delta\mu_{23}$/RTs correspond to the experimentally determined values for most of the osmolytes, including trehalose (Table 3.8). Proline is the exception, where the osmolyte weakened the binding of both ligands to a greater extent than was predicted. As proline is a cyclic molecule with carboxylate and amine moieties, it can reasonably fit into the active site in place of pABA. Indeed, 35% of the time in the computer simulations a proline was near the phosphate groups of PtPP. Proline is cyclic, with a carboxylate and amine group, which is structurally similar to pABA and sulfa drugs, therefore it can be reasonably hypothesized that proline may bind in the BaDHPS active site. Binding of proline may indicate why there are larger effects of the osmolyte on pABA and STZ binding than would be predicted from the μ_{23}/RTs alone. At 1-2 M concentrations, proline will not only interact with free pABA or STZ, but also decrease the apparent binding affinity by blocking access of the ligands to the active site. This suggests that proline may also be able to bind to the active site, where it would compete with pABA and STZ, decreasing the K_ds for the two ligands. Thus, proline's effects on

Table 3.8: Predicted $\Delta\mu_{23}$/RT values for ligands binding to BaDHPS compared to the $\Delta\mu_{23}$/RT values obtained from ITC

Osmolyte	PtPP		pABA		STZ	
	Predicted	ITC	Predicted	ITC	Predicted	ITC
Trehalose	1.4±0.1	0.17±0.02	0.17±0.03	-0.50±0.05	0.09±0.01	-0.39±0.04
Betaine	-1.5±0.1	-1.2±0.3	0.51±0.01	0.25±0.03	1.1±0.1	0.93±0.17
Proline	-0.34±0.01	-0.55±0.03	-0.06±0.02	1.0±0.1	0.49±0.01	1.4±0.2
Glycerol	-0.41±0.01	-0.38±0.07	-0.019±0.001	0.047±0.016	0.19±0.01	0.20+±0.02
TEG	-3.8±0.1	-1.7±0.3	-0.39±0.01	-0.39±0.15	1.3±0.1	0.94±0.02
PEG400	-11±1	-2.7±0.9	-0.25±0.1	-0.11±0.14	2.0±0.1	3.0±0.4

pABA and STZ binding are probably two-fold, due both to preferential interactions and competitive binding. Overall, though, the preferential interaction model was able to accurately predict the effects of the other osmolytes on ligand binding to BaDHPS.

The preferential interaction model predicts that osmolytes can be either excluded from, or interact with, other molecules in solution [6, 18, 20-22]. What effects the osmolyte have on ligand binding will depend upon whether the osmolyte interact with the free ligand, or are excluded from it (Figure 3.12). Osmolytes that are excluded by the ligand (i.e., the ligand prefers to be solvated by water) will bind tighter in the presence of osmolyte. However, when there is preferential interaction between the osmolytes and free ligand, then binding of the ligand to its target protein will be weaker in the presence of osmolytes. The ligand will prefer to be solvated by cosolutes over water, so the cosolutes will need to be removed upon ligand binding. The energy required to remove the solvating osmolytes will shift the binding equilibrium from the bound state to the free state.

3.7.5 Expansion to the Folate Pathway

Our previous *in vitro* studies on three DHFRs find osmolytes weakly interact with folate and DHF and affect catalytic efficiency, primarily through weak interactions with the substrate, which shifts the equilibrium towards the free species though there are often effects on the protein as well [11-13]. As the functional groups found on osmolytes are also found on macromolecular surfaces (e.g., carboxylates, amides, carbonyls, aliphatic and aromatic groups, etc), we recently studied how larger molecular weight crowders alter the function of two DHFRs and find larger decreases in $k_{cat}/K_{m\,(DHF)}$ [66]. In a recent *in vivo* foray into *E. coli* genetics, we found osmotic stress could block growth of bacteria where expression levels of several folate pathway enzymes were less than that encoded by the chromosome [67]. The protein activities that could be titrated by osmotic stress included DHFR, serine hydroxymethyltransferase and methylenetetrahydrofolate reductase. A short version of the folate synthesis pathway is shown in Figure 3.13 and both these *in vitro* and *in vivo* effects are highlighted. In Table 3.9, we provide predicted μ_{23}/RT values for unstudied folate pathway enzyme substrates and speculate that the activities of the corresponding enzymes will be modulated by osmolytes as well as the crowded environment of the cell.

Of interest are the observations that drugs are affected by these weak interactions as well. In this study, we find variable effects of osmolytes on binding of STZ to BaDHPS. We previously found weaker binding of the antifolate drug, methotrexate, to FolM upon osmolyte addition [13], and that crowders weakened binding of methotrexate to *E. coli* chromosomal DHFR [66]. Previous μ_{23}/RT calculations predicted the experimental result of ~4 fold weaker binding of warfarin to bovine serum albumin in the presence of proline or betaine [14]. These various results support the hypothesis of weak interactions between ligands and osmolytes and/or crowders can readily impact drug binding, particularly in a crowded or gel-like environment. Use of μ_{23}/RT values can help predict these ligand-osmolyte effects, although effects of the osmolyte on the protein will be more difficult to forecast.

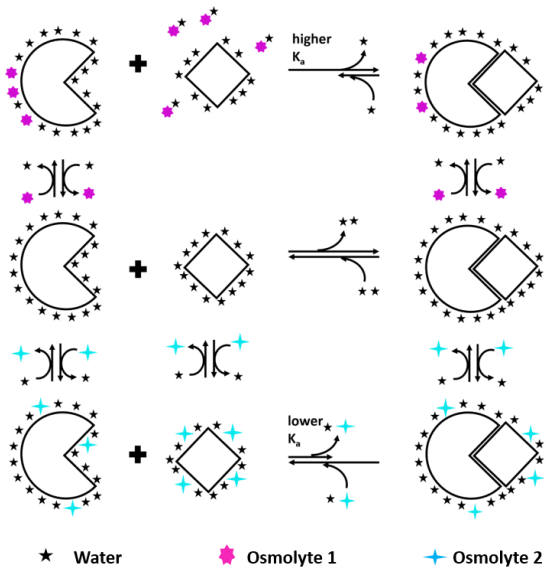

Figure 3.12: Model for the effects of osmolytes on ligand binding due to preferential interaction and exclusion

Top: Preferential exclusion of osmolytes (✸) from the ligand leads to tighter association due to desolvation. Middle: Binding of the ligands to the enzyme in the absence of osmolytes. Bottom: In the presence of osmolytes (✦) that interact with the ligand, there is lower association of the ligand to the enzyme in comparison to the absence of osmolytes (middle panel).

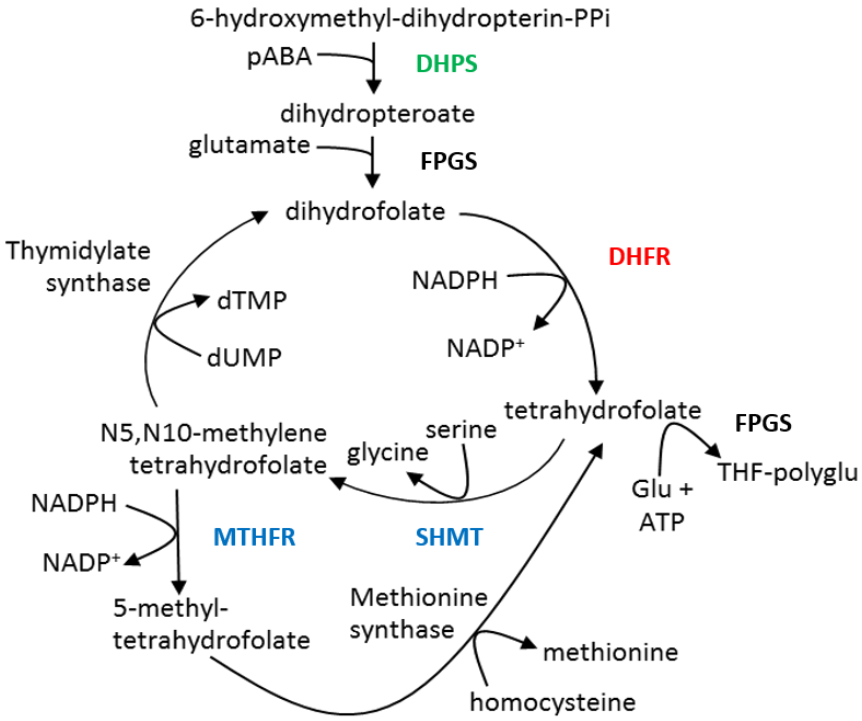

Figure 3.13: Simplified folate mediated one carbon cycle

Osmolyte effects on enzyme DHFR (highlighted in red) has been studied *in vitro* as well as *in vivo*. The enzymes highlighted in blue (MTHFR and SHMT) have been used to study osmotic stress effects *in vivo*. *In vitro* osmolyte effects has been studied on DHPS (highlighted in green).

Table 3.9: Predicted μ_{23}/RT values for metabolites used in the folate cycle pathway

Folate cycle enzyme	metabolite	Predicted μ_{23}/RT						
		Trehalose[a]	Betaine[b]	Proline[c]	Glutamate[d]	Glycerol[e]	TEG[e]	PEG 400[e]
HPPK[f]	ATP	-1.48	0.85	0.30	-0.23	0.31	1.1	9.0
	6-hydroxymethyl-7,8-dihydropterin	0.10	-0.30	-0.08	0.22	-0.06	-0.36	-0.95
Methionine Synthase	5-methylTHF	-0.18	-0.14	0.22	0.51	0.04	0.22	0.70
	Homocysteine	0.04	0.19	0.14	0.07	0.06	0.47	1.4
Thymidylate synthase	2-dUMP[g]	-0.75	0.96	0.35	0.06	0.25	0.74	3.9
	5,10-methyleneTHF	-0.18	-0.07	0.23	0.50	0.05	0.27	0.84
AICART[h]	AICAR[i]	-0.80	0.48	0.20	0.01	0.10	0.34	3.0
	10-formylTHF	-0.32	0.16	0.58	0.47	0.10	0.59	1.7
FPGS[j]	Dihydropteroate	-0.09	-0.49	-0.04	0.28	-0.08	-0.45	-1.2
	Glutamate	-0.24	0.40	0.28	0.12	0.13	0.93	2.7
	ATP	-1.48	0.85	0.30	-0.23	0.31	1.1	9.0
GART[k]	GAR[l]	-0.58	0.80	0.31	-0.13	0.19	0.73	4.0
	10-formyl-THF	-0.32	0.16	0.25	0.47	0.10	0.59	1.7

[a]From Hong, et al.[23] [b]From Bhojane, et al.[22] [c]From Diehl, et al.[20] [d]From Cheng, et al.[19] [e]From Knowles, et al.[21] [f]6-hydroxymethyldihydropterin pyrophosphate kinase. [g]2'-deoxyuridine-5'-monophosphate. [h]aminoimidazole carboxamide ribonucleotide transformylase. [i]aminoimidazole carboxamide ribonucleotide. [j]folylpolyglutamate synthase. [k]glycinamide ribonucleotide transformylase. [l]glycinamide ribonucleotide.

3.8 Conclusions

The effects of osmolytes on the binding of PtPP, pABA and STZ to BaDHPS are specific for a particular ligand and osmolyte pair. Changes in the viscosity and dielectric constants were not responsible for the changes in ligand binding, but the preferential interaction of the osmolytes with the free ligand plays a large role in increasing/decreasing the binding affinity. Indeed, for the most part, predicted preferential interaction coefficients for the ligands with the osmolytes were in agreement with the ITC results. This indicates that the predicted preferential interaction of osmolyte with the components of the binding equilibrium accurately portrays what occurs experimentally. Even the using just the μ_{23}/RT values for the free ligands insight can be gained into what effects the osmolytes might play on binding. Additionally, osmolytes were found to weaken sulfathiazole binding to BaDHPS, which indicates that preferential interactions can affect drugs binding to their targets. With the high concentrations of metabolites and macromolecules in the cell that possess similar functional groups as osmolytes, these preferential interactions may be prevalent *in vivo*.

3.9 References

[1] Yancey, P. H., Clark, M. E., Hand, S. C., Bowlus, R. D., and Somero, G. N. (1982) Living with water stress: Evolution of osmolyte systems, *Science 217*, 1214-1222.

[2] Bolen, D. W. (2001) Protein stabilization by naturally occurring osmolytes, *Methods Mol. Biol. 168*, 17-36.

[3] Courtenay, E. S., Capp, M. W., Anderson, C. F., and Record, M. T., Jr. (2000) Vapor pressure osmometry studies of osmolyte-protein interactions: Implications for the action of osmoprotectants in vivo and for the interpretation of "osmotic stress" experiments *in vitro*, *Biochemistry 39*, 4455-4471.

[4] Record, M. T., Jr., Courtenay, E. S., Cayley, D. S., and Guttman, H. J. (1998) Responses of *E. coli* to osmotic stress: Large changes in amounts of cytoplasmic solutes and water, *Trends Biochem. Sci. 23*, 143-148.

[5] Record, M. T., Jr., Courtenay, E. S., Cayley, S., and Guttman, H. J. (1998) Biophysical compensation mechanisms buffering *E. coli* protein-nucleic acid interactions against changing environments, *Trends Biochem. Sci. 23*, 190-194.

[6] Guinn, E. J., Pegram, L. M., Capp, M. W., Pollock, M. N., and Record, M. T., Jr. (2011) Quantifying why urea is a protein denaturant, whereas glycine betaine is a protein stabilizer, *Proc. Natl. Acad. Sci. U.S.A. 108*, 16932-16937.

[7] Parsegian, V. A., Rand, R. P., and Rau, D. C. (1995) Macromolecules and water: Probing with osmotic stress, *Methods Enzymol. 259*, 43-94.

[8] Parsegian, V. A., Rand, R. P., and Rau, D. C. (2000) Osmotic stress, crowding, preferential hydration, and binding: A comparison of perspectives, *Proc. Natl. Acad. Sci. U.S.A. 97*, 3987-3992.

[9] Baskakov, I. V., Kumar, R., Srinivasan, G., Ji, Y. S., Bolen, D. W., and Thompson, E. B. (1999) Trimethylamine N-oxide-induced cooperative folding of an intrinsically unfolded transcription-activating fragment of human glucocorticoid receptor, *J. Biol. Chem. 274*, 10693-10696.

[10] Stanley, C., Krueger, S., Parsegian, V. A., and Rau, D. C. (2008) Protein structure and hydration probed by SANS and osmotic stress, *Biophys. J. 94*, 2777-2789.

[11] Chopra, S., Dooling, R., Horner, C. G., and Howell, E. E. (2008) A balancing act: Net uptake of water during dihydrofolate binding and net release of water upon NADPH binding in R67 dihydrofolate reductase, *J. Biol. Chem. 283*, 4690-4698.

[12] Grubbs, J., Rahmanian, S., Deluca, A., Padmashali, C., Jackson, M., Duff, M. R., and Howell, E. E. (2011) Thermodynamics and solvent effects on substrate and cofactor binding in *Escherichia coli* chromosomal dihydrofolate reductase, *Biochemistry 50*, 3673-3685.

[13] Bhojane, P., Duff Jr., M. R., Patel, H. C., Vogt, M. E., and Howell, E. E. (2014) Investigation of osmolyte effects on FolM: Comparison with other dihydrofolate reductases, *Biochemistry 53*, 1330-1341.

[14] Duff, M. R., Jr., and Howell, E. E. (2015) Thermodynamics and solvent linkage of macromolecule-ligand interactions, *Methods 76*, 51–60.

[15] Cohen, R. D., and Pielak, G. J. (2017) A cell is more than the sum of its (dilute) parts: A brief history of quinary structure, *Protein Sci. 26*, 403-413.

[16] Chopra, S., Lynch, R., Kim, S.-H., Jackson, M., and Howell, E. E. (2006) Effects of temperature and viscosity on R67 dihydrofolate reductase catalysis, *Biochemistry 45*, 6596-6605.
[17] Krahn, J., Jackson, M., DeRose, E. F., Howell, E. E., and London, R. E. (2007) Structure of a type II dihydrofolate reductase ternary complex: Use of identical binding sites for unrelated ligands, *Biochemistry 46*, 14878-14888.
[18] Capp, M. W., Pegram, L. M., Saecker, R. M., Kratz, M., Riccardi, D., Wendorff, T., Cannon, J. G., and Record, J., M.T. (2009) Interactions of the osmolyte glycine betaine with molecular surfaces in water: Thermodynamics, structural interpretation, and prediction of m-values, *Biochemistry 48*, 10372–10379.
[19] Cheng, X., Guinn, E. J., Buechel, E., Wong, R., Sengupta, R., Shkel, I. A., and Record, M. T., Jr. (2016) Basis of protein stabilization by K glutamate: Unfavorable interactions with carbon, oxygen groups, *Biophys. J. 111*, 1854-1865.
[20] Diehl, R. C., Guinn, E. J., Capp, M., Tsodikov, O. V., and Record Jr., M. T. (2013) Quantifying additive interactions of the osmolyte proline with individual functional groups of proteins: Comparisons with urea and glycine betaine, interpretation of m-values, *Biochemistry 52*, 5997–6010.
[21] Knowles, D. B., Shkel, I. A., Phan, N. M., Sternke, M., Lingeman, E., Cheng, X., Cheng, L., O'Connor, K., and Record, M. T. (2015) Chemical interactions of polyethylene glycols (PEGs) and glycerol with protein functional groups: Applications to effects of PEG and glycerol on protein processes, *Biochemistry 54*, 3528-3542.
[22] Bhojane, P. P., Duff, M. R., Jr., Bafna, K., Rimmer, G. P., Agarwal, P. K., and Howell, E. E. (2016) Aspects of weak interactions between folate and glycine betaine, *Biochemistry 55*, 6282-6294.
[23] Hong, J., Gierasch, L. M., and Liu, Z. (2015) Its preferential interactions with biopolymers account for diverse observed effects of trehalose, *Biophys. J. 109*, 144-153.
[24] Valderas, M. W., Andi, B., Barrow, W. W., and Cook, P. F. (2008) Examination of intrinsic sulfonamide resistance in *Bacillus anthracis*: A novel assay for dihydropteroate synthase, *Biochim. Biophys. Acta 1780*, 848-853.
[25] Yun, M. K., Wu, Y., Li, Z., Zhao, Y., Waddell, M. B., Ferreira, A. M., Lee, R. E., Bashford, D., and White, S. W. (2012) Catalysis and sulfa drug resistance in dihydropteroate synthase, *Science 335*, 1110-1114.
[26] Jayachandran, S., Lleras-Muney, A., and Smith, K. V. J. A. E. J. A. E. (2010) Modern medicine and the twentieth century decline in mortality: Evidence on the impact of sulfa drugs, *2*, 118-146.
[27] Capasso, C., Supuran, C. T., and chemistry, m. (2014) Sulfa and trimethoprim-like drugs–antimetabolites acting as carbonic anhydrase, dihydropteroate synthase and dihydrofolate reductase inhibitors, *J. Enzyme Inhib. Med. Chem. 29*, 379-387.
[28] Babaoglu, K., Qi, J., Lee, R. E., and White, S. W. (2004) Crystal structure of 7,8-dihydropteroate synthase from *Bacillus anthracis*: Mechanism and novel inhibitor design, *Structure 12*, 1705-1717.
[29] Hampele, I. C., D'Arcy, A., Dale, G. E., Kostrewa, D., Nielsen, J., Oefner, C., Page, M. G., Schonfeld, H. J., Stuber, D., and Then, R. L. (1997) Structure and function

of the dihydropteroate synthase from *Staphylococcus aureus*, *J. Mol. Biol. 268*, 21-30.
[30] Keller, S., Vargas, C., Zhao, H., Piszczek, G., Brautigam, C. A., and Schuck, P. (2012) High-precision isothermal titration calorimetry with automated peak-shape analysis, *Anal. Chem. 84*, 5066-5073.
[31] Zhao, H., Piszczek, G., and Schuck, P. (2015) SEDPHAT--a platform for global ITC analysis and global multi-method analysis of molecular interactions, *Methods 76*, 137-148.
[32] Plotnikov, V. V., Brandts, J. M., Lin, L. N., and Brandts, J. F. (1997) A new ultrasensitive scanning calorimeter, *Anal. Biochem. 250*, 237-244.
[33] Quinlivan, E. P., Roje, S., Basset, G., Shachar-Hill, Y., Gregory, J. F., and Hanson, A. D. (2003) The folate precursor p-aminobenzoate is reversibly converted to its glucose ester in the plant cytosol, *J. Biol. Chem. 278*, 20731-20737.
[34] Batchu, S. R., Panditi, V. R., and Gardinali, P. R. (2014) Photodegradation of sulfonamide antibiotics in simulated and natural sunlight: Implications for their environmental fate, *J. Environ. Sci. Health B 49*, 200-211.
[35] The PyMOL molecular graphics system *Version 2.3.2 Schrodinger, LLC*.
[36] Case, D. A., Cheatham III, T. E., Darden, T., Gohlke, H., Luo, R., Merz Jr, K. M., Onufriev, A., Simmerling, C., Wang, B., and Woods, R. J. (2005) The Amber biomolecular simulation programs, *J. Comput. Chem. 26*, 1668-1688.
[37] Martínez, L., Andrade, R., Birgin, E. G., and Martínez, J. M. (2009) PACKMOL: A package for building initial configurations for molecular dynamics simulations, *J. Comput. Chem. 30*, 2157-2164.
[38] Ramanathan, A., and Agarwal, P. K. (2009) Computational identification of slow conformational fluctuations in proteins, *J. Phys. Chem. B 113*, 16669-16680.
[39] Li, P., Roberts, B. P., Chakravorty, D. K., and Merz Jr, K. M. (2013) Rational design of particle mesh Ewald compatible Lennard-Jones parameters for+ 2 metal cations in explicit solvent, *J. Chem. Theory Comput. 9*, 2733-2748.
[40] Le Grand, S., Götz, A. W., and Walker, R. C. (2013) SPFP: Speed without compromise—A mixed precision model for GPU accelerated molecular dynamics simulations, *Comput. Phys. Commun. 184*, 374-380.
[41] Salomon-Ferrer, R., Götz, A. W., Poole, D., Le Grand, S., and Walker, R. C. (2013) Routine microsecond molecular dynamics simulations with AMBER on GPUs. 2. Explicit solvent particle mesh Ewald, *J. Chem. Theory Comput. 9*, 3878-3888.
[42] Tsodikov, O. V., Record Jr, M. T., and Sergeev, Y. V. (2002) Novel computer program for fast exact calculation of accessible and molecular surface areas and average surface curvature, *J. Comput. Chem. 23*, 600-609.
[43] Segel, I. H. (1975) *Enzyme Kinetics: Behavior and Analysis of Rapid Equilibrium and Steady-State Enzyme Systems*, John Wiley and Sons, New York.
[44] Griffith, E. C., Wallace, M. J., Wu, Y., Kumar, G., Gajewski, S., Jackson, P., Phelps, G. A., Zheng, Z., Rock, C. O., Lee, R. E., and White, S. W. (2018) The structural and functional basis for recurring sulfa drug resistance mutations in *Staphylococcus aureus* dihydropteroate synthase, *Front. Microbiol. 9*, 1369.
[45] Edsall, J. (1943) Dielectric constants and dipole moments of dipolar ions, In *Proteins, Amino Acids and Peptides as Ions and Dipolar Ions* (Cohn, E., and Edsall, J., Eds.), pp 140-154, Reinhold, New York.

[46] Sengwa, R., and Sankhla, S. (2007) Characterization of heterogeneous interaction in binary mixtures of ethylene glycol oligomer with water, ethyl alcohol and dioxane by dielectric analysis, *J. Mol. Liq. 130*, 119-131.
[47] Matsuoka, T., Okada, T., Murai, K., Koda, S., and Nomura, H. (2002) Dynamics and hydration of trehalose and maltose in concentrated solutions, *J. Mol. Liq. 98*, 319-329.
[48] Gomez, D., and Klumpp, S. (2015) Biochemical reactions in crowded environments: Revisiting the effects of volume exclusion with simulations, *Front. Phys. 3*, 45.
[49] Zimmerman, S. B., and Minton, A. P. (1993) Macromolecular crowding: Biochemical, biophysical, and physiological consequences, *Annu. Rev. Biophys. Biomol. Struct. 22*, 27-65.
[50] Kaushik, J. K., and Bhat, R. (2003) Why is trehalose an exceptional protein stabilizer? An analysis of the thermal stability of proteins in the presence of the compatible osmolyte trehalose, *J Bio. Chem. 278*, 26458-26465.
[51] Olsson, C., Jansson, H. n., and Swenson, J. (2016) The role of trehalose for the stabilization of proteins, *J. Phys. Chem. B 120*, 4723-4731.
[52] Liao, Y.-T., Manson, A. C., DeLyser, M. R., Noid, W. G., and Cremer, P. S. (2017) Trimethylamine N-oxide stabilizes proteins via a distinct mechanism compared with betaine and glycine, *Proc. Natl. Acad. Sci. U.S.A. 114*, 2479-2484.
[53] Sapir, L., and Harries, D. (2011) Linking trehalose self-association with binary aqueous solution equation of state, *J. Phys. Chem. B 115*, 624-634.
[54] Zhadin, N., and Callender, R. (2011) Effect of osmolytes on protein dynamics in the lactate dehydrogenase-catalyzed reaction, *Biochemistry 50*, 1582-1589.
[55] Gulotta, M., Qiu, L., Desamero, R., Rosgen, J., Bolen, D. W., and Callender, R. (2007) Effects of cell volume regulating osmolytes on glycerol 3-phosphate binding to triosephosphate isomerase, *Biochemistry 46*, 10055-10062.
[56] Kossowska, D., Kwak, K., and Cho, M. (2018) Do osmolytes impact the structure and dynamics of myoglobin?, *Molecules 23*, 1.
[57] Serratos, I. N., Millan-Pacheco, C., Garza-Ramos, G., Perez-Hernandez, G., and Zubillaga, R. A. (2018) Exploring interfacial water trapping in protein-ligand complexes with multithermal titration calorimetry, *Biochim. Biophys. Acta 1866*, 488-495.
[58] Feig, M., Yu, I., Wang, P. H., Nawrocki, G., and Sugita, Y. (2017) Crowding in cellular environments at an atomistic level from computer simulations, *J. Phys. Chem. B 121*, 8009-8025.
[59] Uribe, S., and Sampedro, J. G. (2003) Measuring solution viscosity and its effect on enzyme activity, *Biol. Proced. 5*, 108.
[60] Maurel, P. (1978) Relevance of dielectric constant and solvent hydrophobicity to the organic solvent effect in enzymology, *J. Biol. Chem. 253*, 1677-1683.
[61] Vossen, K. M., Wolz, R., Daugherty, M. A., and Fried, M. G. (1997) Role of macromolecular hydration in the binding of the *Escherichia coli* cyclic AMP receptor to DNA, *Biochemistry 36*, 11640-11647.
[62] Rani, A., and Venkatesu, P. (2018) Changing relations between proteins and osmolytes: A choice of nature, *Phys. Chem. Chem. Phys. 20*, 20315-20333.

[63] Fried, M. G., Stickle, D. F., Smirnakis, K. V., Adams, C., MacDonald, D., and Lu, P. (2002) Role of hydration in the binding of lac repressor to DNA, *J. Biol. Chem. 277*, 50676-50682.
[64] Santoro, M. M., Liu, Y., Khan, S. M., Hou, L. X., and Bolen, D. W. (1992) Increased thermal stability of proteins in the presence of naturally occurring osmolytes, *Biochemistry 31*, 5278-5283.
[65] Tran-Dinh, S., and Neumann, J. (1977) A 31P-NMR study of the interaction of Mg2+ ions with nucleoside diphosphates, *Nucleic Acids Res. 4*, 397-403.
[66] Duff, M. R., Jr., Desai, N., Craig, M. A., Agarwal, P. K., and Howell, E. E. (2019) Crowders steal dihydrofolate reductase ligands through quinary interactions, *Biochemistry 58*, 1198-1213.
[67] Nambiar, D., Berhane, T. K., Shew, R., Schwarz, B., Duff, M. R., Jr., and Howell, E. E. (2018) In vivo titration of folate pathway enzymes, *Appl. Environ. Microbiol. 84*, e01139-01118.

4 *IN VIVO* TITRATION OF FOLATE PATHWAY ENZYMES

This part is a slightly revised version of a manuscript with the same title published in the journal, Applied and Environmental Microbiology

(DOI: 10.1128/AEM.01139-18)

Address correspondence to Elizabeth E. Howell, lzh@utk.edu

4.1 Abstract

How enzymes behave in cells is likely different from how they behave in the test tube. Previous *in vitro* studies find that osmolytes interact weakly with folate. Removal of the osmolyte from the solvation shell of folate is more difficult than removal of water, which weakens binding of folate to its enzyme partners. To examine if this phenomenon occurs in vivo, osmotic stress titrations were performed in Escherichia coli.

Two strategies were employed: resistance to an antibacterial drug or complementation of a knockout strain by the appropriate gene cloned in a plasmid that allows tight control of expression levels as well as labeling by a degradation tag. The abilities of the knockout and complemented strains to grow under osmotic stress were compared. Typically, the knockout strain could grow to high osmolalities on supplemented media while the complemented strain stopped growing at lower osmolalities on minimal media. This pattern was observed for an R67 dihydrofolate reductase clone rescuing a Δ*folA* strain, for a methylenetetrahydrofolate reductase clone rescuing a Δ*metF* strain and for a serine hydroxymethyltransferase clone rescuing a Δ*glyA* strain. Additionally, an R67 dihydrofolate reductase clone allowed *E. coli* DH5α to grow in the presence of trimethoprim until ~0.81 Osm while cells in a control titration lacking antibiotic could grow until 1.90 Osm.

4.2 Importance

E. coli can survive in drought and flooding conditions and can tolerate large changes in osmolality. However, the cell processes that limit bacterial growth under high osmotic stress conditions are not known. This study decreases the dose of four different enzymes in *E. coli* by using deletion strains complemented by the gene carried in a tunable plasmid. Under conditions of limiting enzyme concentration (lower than that achieved by chromosomal gene expression), cell growth can be blocked by osmotic stress conditions that are normally tolerated. These observations indicate *E. coli* have evolved to deal with variations in their osmotic environment and that normal protein levels are sufficient to buffer the cell from environmental changes. Additional factors involved in the osmotic

pressure response may include altered protein concentration/activity levels, weak solute interactions with ligands which can make it more difficult for proteins to bind their substrates/inhibitors/cofactors *in vivo* and/or viscosity effects.

4.3 Introduction

Osmolytes are small molecules produced by cells in response to harsh conditions such as heat, dehydration, and high salt concentration [1]. Three classes of osmolytes are amino acids (e.g. proline, taurine and glutamate); polyols (glycerol, sucrose and trehalose); and methylamines (trimethylamine oxide and glycine betaine) [2]. When *Escherichia coli* are perturbed by osmotic stress, they use trehalose, K^+ and glutamate as osmoprotectants [3-6]. For cells grown in media containing exogenous glycine betaine, it is the predominant osmoprotectant [7]. As the osmolality increases, the cell becomes more crowded due to loss of water. An upper limit of osmolality occurs (~1.9 Osm) where free water no longer exists and E. coli growth stops [7].

Previous studies have found that the in vitro addition of osmolytes to three different protein scaffolds that catalyze the dihydrofolate reductase (DHFR) reaction results in tighter binding of cofactor, NADPH [8-10]. Addition of osmolytes lowers the water activity of a solution; dehydration typically leads to tighter ligand binding as less solvent needs to be removed to form a complex. In contrast, binding of DHF "breaks the rules" as weaker binding upon osmolyte addition is observed in these three different proteins [8-10]. To model this behavior, we proposed that osmolytes weakly associate with DHF. If the osmolyte-DHF interactions are more difficult to break than the water-DHF interactions, this shifts the equilibrium towards the unbound species and impedes binding to DHFR. This model, depicted in Figure 4.1, is supported by small molecule NMR data [11] as well as high hydrostatic pressure experiments [12] and osmometry studies [13].

Additional studies provide chemical guidance in understanding these weak interactions. For example, the Record group has also monitored the preferential interaction of betaine, glutamate, proline and PEGs with numerous small molecules to determine which groups/atoms (e.g. aliphatic carbons, aromatic carbons, cationic nitrogens and amide nitrogens, phosphate oxygens, carboxylate oxygens, hydroxyls, and carbonyls) prefer to interact with water as compared to several osmolytes (betaine, glutamate, PEGs) [14-17]. In a similar manner, Hong et al. have studied the preferential interaction of trehalose with many small molecules [18]. In a recent study, we have studied the interaction of betaine with folate and other small aromatic compounds [13]. We find that folate interacts almost equally well with betaine and water. Specifically, the glutamate tail prefers to interact with water, while the aromatic rings prefer betaine. As other redox states of folate such as dihydrofolate, 5-methyl-tetrahydrofolate, 5-10-methylene-tetrahydrofolate also contain these groups/atoms, these folates may also weakly associate with osmolytes and negatively impact protein function. Also, as the groups (hydroxyls, amides, cationic amines, etc.) found in osmolytes are also displayed on protein surfaces, DHF may also weakly associate with proteins.

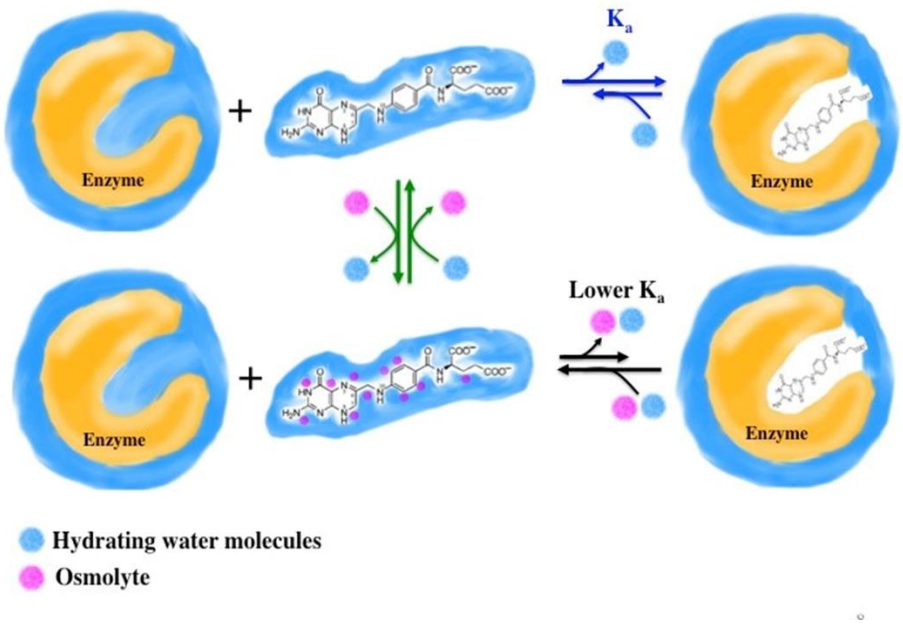

Figure 4.1: Model of osmolyte interaction with DHF that results in weaker binding to DHFR.

For enzyme assays in buffer, DHF binds tightly to DHFR (target enzyme) and water (blue) is released. Added osmolytes (magenta spheres) interact weakly with DHF. For DHF to bind to DHFR, both osmolytes and water need to be released. While these interactions are weak, if the osmolyte-DHF interaction is stronger than the water-DHF interaction, then binding to DHFR is weakened. (Note: Osmolytes may additionally bind to sites on the enzyme (not shown) and affect activity). We have used high hydrostatic pressure as an orthogonal technique to examine the top row of the model (blue equilibrium arrows) [12]. We have also used NMR and vapor pressure osmometry to monitor interactions between folate and osmolytes (middle column, green equilibrium arrows) [11, 13]. All data sets are consistent with this model.

In a recent review, Wood indicated that the cell processes that limit bacterial growth under osmotic stress conditions are not known [19]. Here we ask whether these "soft interactions" [20] or "quinary" behavior [21-24] between folate metabolites and osmolytes/crowders might occur *in vivo* and play a role in osmotic stress by helping to titrate enzyme activity. In other words, a high osmolyte concentration might sequester substrate and lower the concentration of available, free substrate in the cell. This, in turn, could limit cell growth.

The enzyme concentrations/activities in *E. coli* are usually sufficient to overcome these weak folate-osmolyte interactions, even in the gel-like environment of the cell under high osmotic stress conditions [25, 26]. Here we ask what happens when the target enzyme concentration in the cell is less than that achieved by expression from the chromosomal gene? To achieve this condition, we cloned the gene of interest behind a tunable P_{tet} promoter in the pKTS plasmid [27]. To achieve very low protein expression levels, the pKTS plasmid adds an SsrA tag to the C-terminus of the protein, which targets the protein to be degraded by the ClpX protease. This plasmid is then transformed into a knockout strain of *E. coli*. The low protein dose lets us target the role of one specific protein in osmotic stress.

4.4 Materials and Methods

4.4.1 Bacterial strains

The strains used in this work are listed in Table 4.1. The *thyA* Δ*folA::kan* strain (named LH18) was constructed in 1988 [28]. The Keio deletion strains [29] for *metF* and g*lyA* were procured from the Coli Genetic Stock Center (CGSC; http://cgsc2.biology.yale.edu/). The deletion strains were unable to grow on Bonner-Vogel (BV) minimal media containing 40 µg/ml guanine, 50 µg/ml of tyrosine, histidine and tryptophan as well as 1 mM thiamine [30]. The Δ*folA::kan* strain required addition of 200 µg/ml thymidine, 30 µg/ml adenine, 10µg/ml pantothenate and 50 µg/ml glycine and methionine for growth [31]. The Δ*metF::kan* strain required addition of methionine (50 µg/ml) while the Δ*glyA::kan* strain needed glycine and serine (50 µg/ml each) for growth. Kanamycin (50 µg/ml) was added to select for the deletion strain. Bonner-Vogel media for the chorismate mutase *aroQ* deletion strain included 20 µg/ml phenylalanine, 20 µg/ml tyrosine and 20 µg/ml chloramphenicol [32].

4.4.2 Plasmids

Table 4.1 also lists the plasmids used. The pKTS plasmid was obtained from Donald Hilvert and Peter Kast (ETH Zurich) [27]. This plasmid enables control of gene expression via the P_{tet} promoter. Addition of a C-terminal SsrA degradation tag targets the expressed protein to the ClpX protease, decreasing the gene product concentration *in vivo*. The protein expression level can be less than that associated with expression of the gene from the *E. coli* chromosome. The plasmid also confers ampicillin resistance.

Table 4.1: Strains and plasmids used in this study

Strain	**Source**	**Genotype**
DH5α	Invitrogen	*F - Φ80lacZΔM15(lacZYA-argF) U169 recA1 endA1 hsdR17 (rK–, mK+) phoA supE44 λ– thi-1 gyrA96 relA1*
NM522	Howell [a]	*F' Δlac-pro supE hsdRS lac(lq-ZAM15)+ pro'*
NM522 *thyA*	Howell [a]	*F' Δlac-pro supE hsdRS lac(lq-ZAM15)+ pro' thyA*
LH18	Howell [a]	NM522 *thyA ΔfolA::kan*
BW25113	CGSC	*F - Δ(araD-araB)567 ΔlacZ4787*(::rrnB-3) *λ- rph-1 Δ(rhaD-rhaB)568 hsdR514*
JW2535-1	CGSC	BW25113 *ΔglyA725::kan*
JW3913-1	CGSC	BW25113 *ΔmetF728::kan*
KA12/pKIMP-UAUC	Colquhoun [b]	*Δ(srlR-recA)306::Tn10, Δ(pheA-tyrA-aroF), thi-1, endA-1, hsdRl7, Δ(argF-lac) U169, supE44.* The strain is complemented by the pKIMP plasmid (= pACYC184, which confers chloramphenicol resistance and carries the *pheC* and *tyrA* genes) which restores Phe and Tyr biosynthetic pathways.
Plasmid	**Source**	**Antibiotic Resistance and other information**
CM-pKTS	Kast and Hilvert [c]	Ampicillin, P_{tet} promoter control of CM expression, SsrA tag added
R67 DHFR-pKTS	This study	Ampicillin, P_{tet} promoter control of R67 DHFR expression, SsrA tag added, trimethoprim resistance when protein expressed
Quad4-pKTS	This study	Ampicillin, P_{tet} promoter control of Quad4 expression, SsrA tag added, trimethoprim resistance when protein expressed
MTHFR-pKTS	This study	Ampicillin, P_{tet} promoter control of MTHFR expression, SsrA tag added
SHMT-pKTS	This study	Ampicillin, P_{tet} promoter control of SHMT expression, SsrA tag added

[a] From reference [28]

[b] From references [32, 33]

[c] From reference [27]

4.4.3 Complementation

Each deletion strain was transformed with several pKTS constructs. The pKTS constructs were made by introducing the gene using the primers listed in Table 4.2. The deletion strain was complemented with the pKTS vector containing the corresponding gene; these are the complemented or rescued strains. The complemented strains could grow on minimal media containing tetracycline, indicating the plasmid restored prototrophy to the bacteria. For example, the Δ*metF* strain was complemented by transformation with the MTHFR-pKTS clone. Vector controls consisted of deletion strains transformed with the pKTS vector containing genes encoding other folate pathway enzymes. For example, transformation of the Δ*metF* strain by the SHMT-pKTS or R67 DHFR-pKTS plasmids did not rescue cells from methionine auxotrophy.

4.4.4 Tetracyline titrations

The complemented strains were grown overnight in Luria-Bertani broth with 50 µg/ml kanamycin and 100 µg/ml ampicillin. The cells were centrifuged and the pellet washed with 1X Bonner-Vogel (BV) salts [30]. These steps were repeated and the cell pellet resuspended in 1X BV salts to a turbidity of 1.0 at 600 nm; 10 µl of solution was then streaked on solid media. The plates contained 50 µg/ml kanamycin, 100 µg/ml ampicillin and varying tetracycline concentrations (0, 10, 25, 50, 75, 100, 200 or 500 ng/ml). The plates were incubated at 37°C for up to 5 days. Good growth was defined as confluent growth without an overlay of single (suppressor) colonies. Table 4.3 lists the tetracycline concentrations used for each construct.

4.4.5 Osmotic stress titrations

Once the appropriate tetracycline concentration was determined, osmotic stress titrations were performed. As described above, cells were streaked on BV minimal media containing different concentrations of sorbitol or NaCl and growth was monitored for up to 5 days at 37°C. The plates were incubated in the dark. To determine if the results of our osmotic stress titrations were affected by the identity of the major osmolyte present in the cell, BV media containing 1mM betaine was used as indicated in the text.

The water activity of the solid media was measured at room temperature using an AquaLab dew point water activity meter 4TE (Decagon Devices, Inc., Pullman, WA). Then, the osmolality was calculated using equation (1):

$$\text{Osmolality} = \frac{\ln A_{H2O}}{-0.018} \qquad (1)$$

where AH2O is the water activity.

Table 4.2: List of PCR primer sequences used to introduce Nde1 and Xho1 restriction enzyme sites

Enzyme (plasmid)	**Primer sequences with the introduced restriction enzyme sequence underlined**
MTHFR (pCAS30)	5'TATTTACATATGAGCTTTTTTCACGCCAGC 3' (NdeI)
	5'AAGGGGTTATGCTAGTTATTGCTCA 3' (reverse primer)
SHMT (pBSGlyA)	5'GGGAGGAGGCATATGTTAAAGCGTGAAATGAACATTGCCGATTATGATGCC 3' (NdeI)
	5'GAGAGAGAGCTCGAGTGCGTAAACCGGGTAACGTGC 3' (XhoI) (reverse primer)

Table 4.3: Antibiotic concentrations and supplements used for each strain

Strains	Antibiotics			Supplement(s) for growth in minimal media
	Kanamycin	Ampicillin	Tetracycline	
***E. coli* DH5α**	N/A	N/A	N/A	N/A
***E. coli* DH5α + R67 DHFR-pKTS**	N/A (20 µg trimethoprim /ml)	100 µg/ml	100 ng/ml	N/A
***E. coli* DH5α + Quad4-pKTS**	N/A (20 µg trimethoprim /ml)	100 µg/ml	100 ng/ml	N/A
NM522	N/A	N/A	N/A	N/A
NM522 *thyA8*	N/A	N/A	N/A	200 µg/ml thymidine
LH18 (Δ*folA*)	50 µg/ml	N/A	N/A	200 µg/ml thymidine, 50 µg/ml methionine and glycine, 30 µg/ml adenine, 10 µg/ml pantothenate
LH18 (Δ*folA*) + R67 DHFR-pKTS	50 µg/ml	100 µg/ml	200 ng/ml for agar plates (100 for liquid media)[a]	N/A
LH18 (Δ*folA*) + Quad4-pKTS	50 µg/ml	100 µg/ml	200 ng/ml for agar plates (100 ng/ml for liquid media)	N/A
***E. coli* BW25113**	N/A	N/A	N/A	N/A

Table 4.3 Continued

Strains	Antibiotics			Supplement(s) for growth in minimal media
	Kanamycin	Ampicillin	Tetracycline	
JW3913-1 (Δ*metF*)	50 µg/ml	N/A	N/A	50 µg/ml methionine
JW3913-1 (Δ*metF*) + MTHFR-pKTS	50 µg/ml	100 µg/ml	100 ng/ml for agar plates (75 ng/ml for liquid media)	N/A
JW2535-1 (Δ*glyA*)	50 µg/ml	N/A	N/A	50 µg/ml glycine and serine
JW2535-1 (Δ*glyA*) + SHMT-pKTS	50 µg/ml	100 µg/ml	75 ng/ml for agar plates (50 ng/ml for liquid media)	N/A
KA12/pKIMP-UAUC	N/A (50 µg/ml chloramphenicol)	N/A	N/A	50 µg/ml phenylalanine and tyrosine
KA12/pKIMP-UAUC + CM-pKTS	N/A (50 µg/ml chloramphenicol)	100 µg/ml	200 ng/ml	N/A

We used 200 ng/ml of tetracycline for the LH18:: Δ*folA* + R67 DHFR-pKTS titration as compared to 100 ng/ml for DH5α+ R67 DHFR-pKTS to avoid overgrowing colonies at lower osmotic stress.

A positive control is the growth of the cells on BV supplemented media containing increasing concentrations of sorbitol or NaCl. This allows discrimination between the lack of cell growth due to loss of free water in the cell [7] from the effect of osmolytes on enzyme activity. Each experiment was done at least in duplicate.

4.4.6 Osmotic stress titrations of trimethoprim resistance

The activity of chromosomal *E. coli* DHFR is inhibited by trimethoprim, but R67 DHFR provides resistance to this drug. The *E. coli* strain DH5α was transformed with R67 DHFR-pKTS or Quad4-pKTS vectors. The ability of these clones to confer TMP resistance was assessed by the ability of the transformed cells to grow on BV minimal media containing 20 µg/ml TMP, 100 µg/ml ampicillin, 100 ng/ml tetracycline and various concentrations of sorbitol (0 to 1.50 M). The plates were incubated at 37 ^{0}C and cell growth observed for 5 days. As a control to evaluate the concentration of sorbitol that blocked DH5α growth, cells were grown on BV minimal media with increasing sorbitol concentrations, but without antibiotics.

4.4.7 Isolation and characterization of suppressors

Overgrowing colonies were frequently observed on plates with low tetracycline concentrations and/or high osmotic stress conditions. Plasmids were isolated from these colonies and re-transformed into the appropriate deletion cells. Plasmid DNA from those transformants that were still able to grow on media containing 1 M sorbitol were sequenced to identify the mutation(s).

4.4.8 Measurement of growth in liquid media and doubling time calculations

Cell growth was monitored on an automated 96 well plate reader (BioTek Cytation 5) in liquid BV minimal media with shaking at 37 ^{0}C. Turbidities at 600 nm of triplicate samples were observed every 20 mins for 36 hours. A gas permeable sealing membrane (Breathe Easy, Diversified Biotech) for microtiter plates (Costar 3370) reduced evaporation. Osmotic stress was applied using either sorbitol or NaCl. The osmolality of liquid media was measured with a vapor pressure osmometer (Wescor Vapro 5520). Natural log values of absorbance were plotted against time to obtain the slope, which was used to calculate the doubling time (Dt) as per equation (2):

$$Dt = \ln(2)/\text{slope} \qquad (2)$$

The solution osmolality increased ~ 5% over 24 hours. At longer times (36 hrs.), the osmolality increased by ~ 11%.

The water activity meter is typically used to measure dry, solid foods while the VPO measures solutions. This difference in sample type led us to standardize and compare

the Aqualab dew point water activity meter with the Vapro Pressure Instrument. The osmolalities of standard solutions with increasing sorbitol (0-1.5 M) or NaCl (0-0.7 M) were determined using both instruments. A graph of the osmolalities from these two different instruments was used to correct the AquaLab values.

4.5 Results

To determine which enzymes to use in our *in vivo* osmotic stress experiments, we considered whether the folate pathway enzyme is selectable by either antibiotic resistance or by restoration of prototrophy to an auxotrophic strain. We also considered whether modifications to the C-terminus would affect enzyme activity, which is the case for thymidylate synthase [34]. Another factor considered was the oligomerization state of the enzyme as additional SsrA degradation tags might help lower the protein concentration in the cell. Table 4.4 lists some pertinent parameters associated with the folate mediated 1C metabolism enzymes we examined, and Figure 4.2 shows where they occur in the pathway. The enzymes are serine hydroxymethyl transferase (SHMT encoded by the *glyA* gene), methylene tetrahydrofolate reductase (MTHFR, *metF*) and the type II R67 DHFR. The latter is unrelated to chromosomal DHFR (*folA* gene) and possesses a homotetrameric structure with a single active site pore [50]. A tandem array of 4 fused R67 DHFR genes produces a protein with four times the mass of the normal R67 DHFR monomer. This protein, named Quad4, was also used in our studies [40]. We additionally studied osmotic stress effects on chorismate mutase (CM).

4.5.1 Osmotic stress titration of trimethoprim resistance associated with R67 DHFR

The target of trimethoprim is chromosomal *E. coli* DHFR (TMP, K_i = 20 pM) [51], however R67 DHFR provides resistance to this antibacterial drug as its K_i is 7.5 million fold higher (K_i =0.15 mM) [52]. We previously monitored the growth of *E. coli* DH5α expressing various R67 DHFR clones carried in pUC8 [9]. Since wildtype (wt) R67 DHFR was overproduced and possessed sufficient activity, no selection by osmotic pressure was observed in the presence of TMP. The K32M R67 DHFR mutant clone in pUC8 had insufficient activity to allow growth in the presence of TMP, so again, no selection was observed. However, using osmotic pressure, we could titrate the ability of DH5α carrying a Y69L R67 DHFR clone to confer resistance to TMP. The Y69L mutant enzyme has intermediate levels of activity between the R67 DHFR and the K32M mutant [9, 53]. This pattern of behavior indicates a window of enzyme activity that allows cell growth and selection by osmotic stress. Too low an activity does not enable growth, while too high an activity does not allow titration [54, 55]. This situation is depicted in Figure 1.14.

As mentioned above, R67 DHFR is a homotetramer with a single active site pore 39. Another construct is Quad4, which has four R67 DHFR genes linked in frame [40]. The Quad4 protein is almost fully active as a monomer. In addition, its oligomerization state

Table 4.4: Enzyme parameters

Enzyme	k_{cat} (s^{-1})	K_M (μM)	*In vivo* substrate concentration [a]	Rate determining step	Oligomeric state
R67 Dihydro-folate reductase	1.3 [b]	NADPH: 3.0 DHF: 5.8 [b]	NADPH: 120 μM Various polyglutamylated DHF species: ~45 μM	Hydride transfer [c]	Tetramer [d]
Quad4 Dihydrofolate reductase	1.8 [f]	NADPH: 2.6 DHF: 5.6 [f]	NADPH: 120 μM Various polyglutamylated DHF species: ~45 μM	nd [g]	Dimer K_d of ~1 μM; both monomer and dimer active [f]
E. coli Methylene tetrahydrofolate reductase (*metF*)	10.4 [h]	NADH: 20 5,10-CH_2-THF: 0.5 [h]	NADH: 83 μM Various polyglutamylated CH_2-THF species: ~12 μM	Re-oxidation of the reduced flavin by CH_2-THF [h]	Tetramer; active dimer at low [protein] [i]
E. coli Serine hydroxy-methyl transferase (*glyA*)	10.6 [j]	Serine: 800 [j] THF: 80	Serine: 68 μM Various polyglutamylated THF species: ~6 μM	nd [k]	Dimer [l]
Mutant hexameric chorismate mutase domain from *E. coli* bifunctional CM-prephenate dehydratase [m] (*aroQ*)	0.16 (100 fold lower than *E. coli* CM domain) [m]	Chorismate: 600 [m]	na	na, but rate for the CM domain not limited by diffusion [n]	Hexamer [m]

[a] From references [35, 36]

[b] From reference [37]

[c] From reference [38]

[d] From reference [39]

[e] From reference [9]

[f] From reference [40]

[g] Not determined, but presumably the same as R67 DHFR as the enzyme rates and binding constants are similar.

[h] From reference [41]

[i] From references [42, 43]

[j] Main reaction catalyzed [44]. Other reactions listed in text.

[k] From reference [45]

[l] From reference [46]

[m] From reference [47]. Also of interest, CM uses the diaxial form of its substrate; 44% glycerol and 33% sucrose shift the conformational equilibrium slightly (1.5 & 3.5%) towards the pseudo-diequatorial form. [48] Additionally no effect of 44% glycerol on either k_{cat} or K_m was observed while an ~2 fold tighter K_m for substrate was monitored in 33% sucrose [48].

[n] From reference [49]

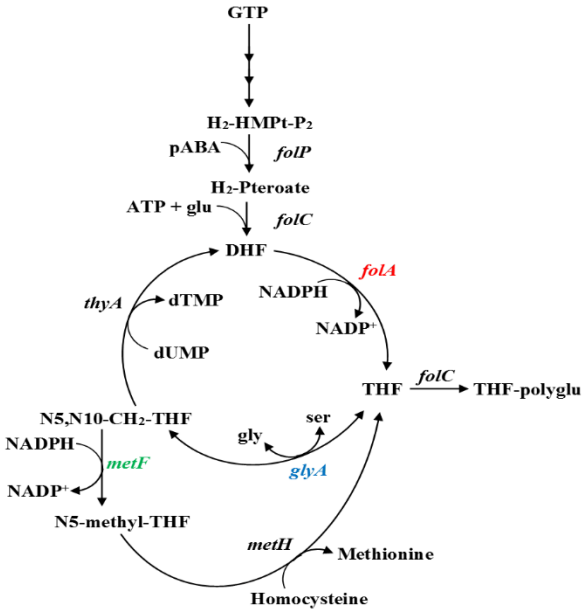

Figure 4.2: Selected folate cycle enzymes

The *folP* gene encodes dihydropteroate synthase or DHPS; this protein forms 7,8-dihydropteroate from 6-hydroxymethyl-dihydropterin diphosphate and ***p*-amino benzoate**. The *folC* gene encodes folylpolyglutamate synthase, which adds L-glutamate to dihydropteroate to form 7,8-dihydrofolate (DHF). The *folA* gene encodes dihydrofolate reductase or DHFR which catalyzes the NADPH-dependent reduction of DHF to 5,6,7,8-tetrahydrofolate (THF). The *glyA* gene encodes serine hydroxymethyl transferase or SHMT, which interconverts L-serine and glycine using THF and 5,10-methylene-THF and pyridoxal phosphate as a cofactor. The *metF* gene encodes methylene-tetrahydrofolate reductase or MTHFR, which reduces 5, 10 methylene-THF to 5-methyl-THF using NADPH as a cofactor. The *thyA* gene encodes thymidylate synthase or TS; this enzyme catalyzes the reductive methylation of 2'-deoxyuridine-5'-monophosphate (dUMP) using 5, 10 methylene-THF to produce thymidine-5'-monophosphate (dTMP) and DHF. The *metH* gene encodes methionine synthase, which forms methionine and THF from 5-methy-THF and homocysteine. The *in vivo* activities of the colored enzymes were examined by our osmotic stress approach.

depends on the protein concentration. Our *in vitro* ultracentrifugation studies find a Quad4 dimerization K_d of ~1 µM [40]. Since use of the pKTS vector leads to low expression levels, our *in vivo* studies likely describe monomeric Quad4.

To examine whether the wt R67 DHFR and Quad4 activities could be titrated by osmotic αstress *in vivo*, their genes cloned in the pKTS plasmid [27] were transformed into DH5α and the tetracycline concentration that allowed confluent growth on M9 minimal media was determined. Use of the P_{tet} promoter results in cell growth that is proportional to the amount of tetracycline added to the medium. Figure 4.3 identifies tetracycline concentrations of 50-200 ng/ml that allowed DH5 carrying the R67 DHFR-pKTS clone to grow in the presence of 20 µg/ml TMP. DH5α carrying the Quad4-pKTS clone showed confluent growth in plates containing 10-200 ng/ml tetracycline.

Our next step used osmotic stress to determine if growth of DH5α carrying an R67 DHFR-pKTS clone could be titrated using resistance to trimethoprim as our selection. As shown in Figure 4.4, a control titration of DH5α on media lacking TMP showed confluent growth until 1.9 Osm. The upper growth limit has been proposed by the Record lab to correspond to loss of free water in the cell [7]. In contrast, the R67 DHFR-pKTS clone allowed confluent growth of host *E. coli* in media containing 20 µg/ml TMP to 0.50 to 0.81 Osm. Sparse growth was observed until 1.28 Osm. The Quad4-pKTS clone allowed growth until <1.93 Osm. As R67 DHFR and Quad4 have the same active site, Quad4 serves as an internal control. Monomeric Quad4 possesses a single SsrA tag in contrast to homotetrameric R67 DHFR, which displays 4 degradation tags. This difference in SsrA tag number likely leads to faster turnover of R67 DHFR compared to Quad4. This proposed difference in enzyme concentration could provide higher DHFR activities for the Quad4 protein, which could more readily rescue the DH5α cells. Also, the fact that Quad4-pKTS continued to provide TMP resistance at high osmolalities (past where R67 DHFR-pKTS does) suggested that any osmotic pressure effects on the tet repressor were not playing a large role in alteration of protein expression levels.

4.5.2 Osmotic stress titration of R67 DHFR enzyme activity using a deletion strain

While TMP is a competitive inhibitor of DHFR, antibiotics can also involve effects on uptake and efflux mechanisms as well as secondary targets [57]. Thus, we also employed a more direct assay of DHFR activity using a deletion strain. The *folA* gene in E. coli strain NM522 was previously deleted (Δ*folA*::kan) [28]. These cells also carry an uncharacterized mutation in the thymidylate synthase (thyA) gene and thymidine is required for cell growth. This strain, named LH18, grows on media supplemented with folate pathway end products (thymidine, adenine, pantothenate, glycine, methionine) [28]. Transformation of LH18 by R67 DHFR-pKTS or Quad4-pKTS rescues the cells from folate end product auxotrophy and allows growth of cells in Bonner-Vogel (BV) minimal media 30 plus thymidine.

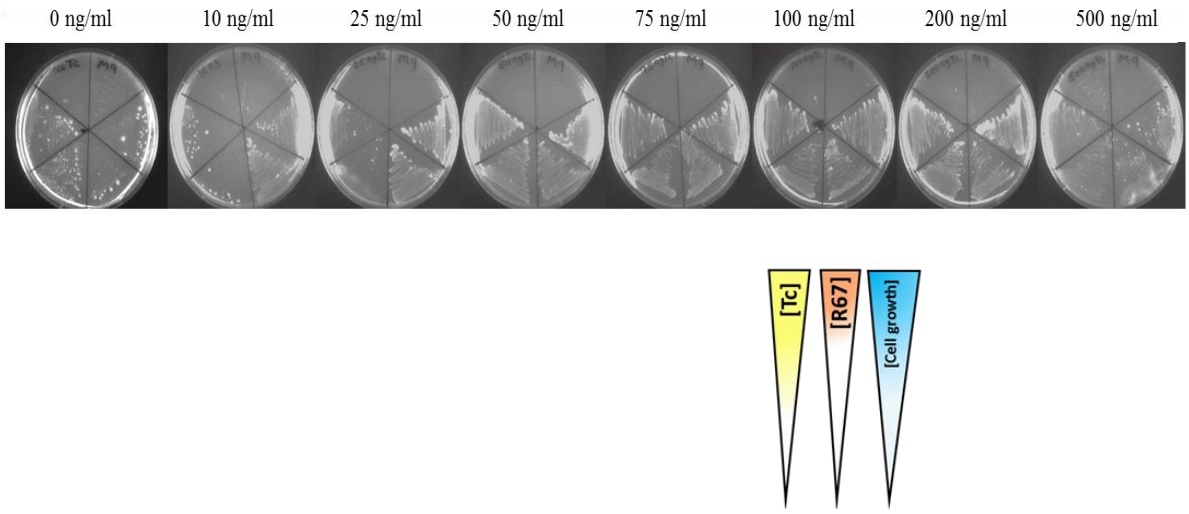

Figure 4.3: Shows a series of plates with DH5α cells carrying either no plasmid or R67 DHFR-pKTS or Quad4-pKTS in increasing tetracycline concentration

DH5α cells carrying either no plasmid or R67 DHFR-pKTS or Quad4-pKTS were streaked on minimal M9 media containing 20 µg/ml TMP. Two colonies per plasmid transformant are shown. The tetracycline concentration is indicated above the plates. The tetracycline concentration required to produce sufficient DHFR activity for confluent cell growth was 50-200 ng/ml tetracycline for R67 DHFR-pKTS and 10-200 ng/ml for Quad4-pKTS. R67 DHFR is a homotetramer and will be tagged with four SsrA sequences as compared to Quad4 DHFR which will be a monomer with one SsrA tag. This will lead to increased degradation of R67 DHFR, thus more tetracycline is needed for the growth of these cells. The cartoon below shows how the constructs are streaked on the plates. The colored arrows indicate that with increasing tetracycline concentration (yellow), protein expression (red) is increased. This results in better cell growth (blue) until tetracycline begins acting as an antibiotic [56].

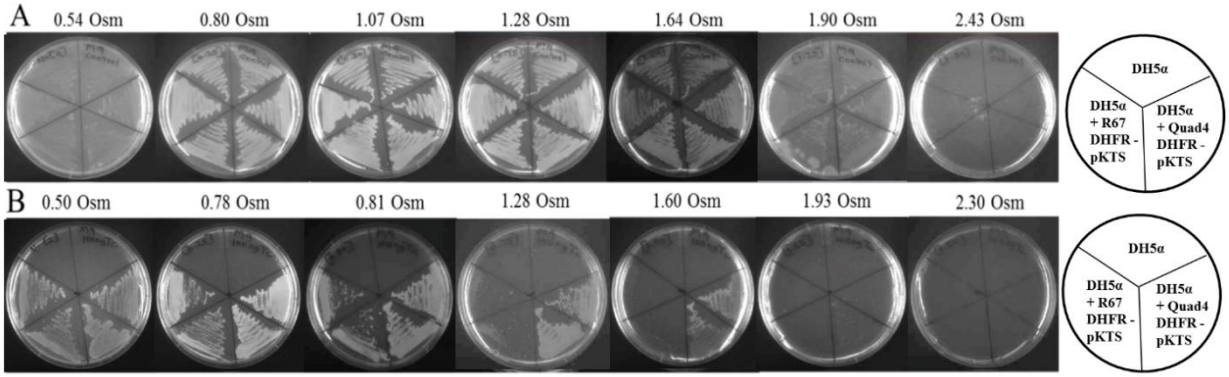

Figure 4.4: The effect of osmolality on the ability of R67 and Quad4 DHFR to rescue *E. coli* DH5α from trimethoprim

Panel A shows the effect of sorbitol on cell growth in M9 minimal media lacking TMP. Cells can grow up to 1.90 Osm, although growth is slow and sparse. Panel B shows the effect of sorbitol on growth in media containing 20 µg/ml TMP, 100 µg/ml ampicillin and 100 ng/ml tetracycline. Cells carrying the R67 DHFR-pKTS clone can only grow until $0.81 < x < 1.28$ Osm while cells carrying the Quad4-pKTS clone can grow until $1.60 < x < 1.93$ Osm. Table 4.5 lists the growth patterns as a function of osmolality. The cartoons at right show how various cultures were streaked on the plates. Two independent colonies were streaked per transformant.

Next, the tetracycline concentration was varied, and the cell growth pattern monitored on minimal media (as shown in Figure 4.5). For LH18 + R67 DHFR-pKTS, no growth was observed for the first 2 days at low tetracycline levels (0-25 ng/ml). This result indicates the pKTS plasmid can restrict protein expression so that DHFR activity is lower than that encoded by the chromosome. This type of result has previously been reported for chorismate mutase [27]. Confluent growth of the rescued cells was achieved at 100ng/ml tetracycline. Growth for 5 days resulted in isolated colonies at low tetracycline concentrations, consistent with occurrence of suppressing mutations. In contrast, LH18 carrying the Quad4-pKTS plasmid grew in the absence of tetracycline, consistent with some leakiness of the promoter as well as Quad4 possessing fewer degradation tags and sufficient activity to rescue the cell.

To monitor osmotic stress effects, the deletion and complemented strains were plated on BV minimal and supplemented plates containing increasing concentrations of sorbitol (Figure 4.6). On the plates supplemented with thymidine, adenine, pantothenate, glycine, methionine, all strains grew to $1.24 < x < 1.52$ Osm (Table 4.5 for a list of osmolality growth limits). In minimal plates containing 200ng/ml tetracycline, complemented strains of LH18 + R67 DHFR-pKTS grew until 0.57 Osm. At this concentration and above, isolated colonies were observed after several days. These isolated colonies persisted until $0.88 < x < 1.15$ Osm, however no growth was observed at higher osmolalities.

In contrast to the R67 DHFR case, Quad4-pKTS readily rescues LH18 as cells grew in BV minimal media until $1.15 < x < 1.81$ Osm. To determine if the activity of Quad4 DHFR could be titrated by osmotic stress, we redid the sorbitol titrations using 0 and 50 ng/ml tetracycline. Under both these conditions, Quad4-pKTS still allowed LH18 to grow until ~1.6 Osm, which was very close to the osmolality limit of the deletion strain grown on supplemented media. Thus, the activity of Quad4 DHFR could not be titrated by osmotic stress. In contrast, LH18 complemented by R67 DHFR-pKTS did not grow on plates without tetracycline and grew only as isolated colonies when 50 ng/ml tetracycline was added. These observations are consistent with moving up and down the titration axis when considering Figure 1.14. Conditions that favor low protein expression (e.g. R67 DHFR-pKTS with a low tetracycline concentration) and/or high degradation rates (higher number of SsrA tags) are not sufficient to rescue the cell from auxotrophy, while conditions that provide high enzyme activity do not allow titration.

4.5.3 Liquid cultures show similar effects as agar plates

The growth of LH18 as well as its parent strains and complemented strains were additionally monitored in liquid media by plots of turbidity vs. time. Figure 4.8 compares the growth rates in a bar graph while Table 4.6 lists the doubling times. LH18 and LH18 carrying Quad4-pKTS showed comparable growth even though LH18 was grown in BV media supplemented with thymidine, adenine, pantothenate, glycine, and methionine while the complemented strain was grown in BV minimal media plus 100 ng/ml tetracycline. The deletion strain carrying R67 DHFR-pKTS grew more slowly in minimal media with 100 ng/ml tetracycline.

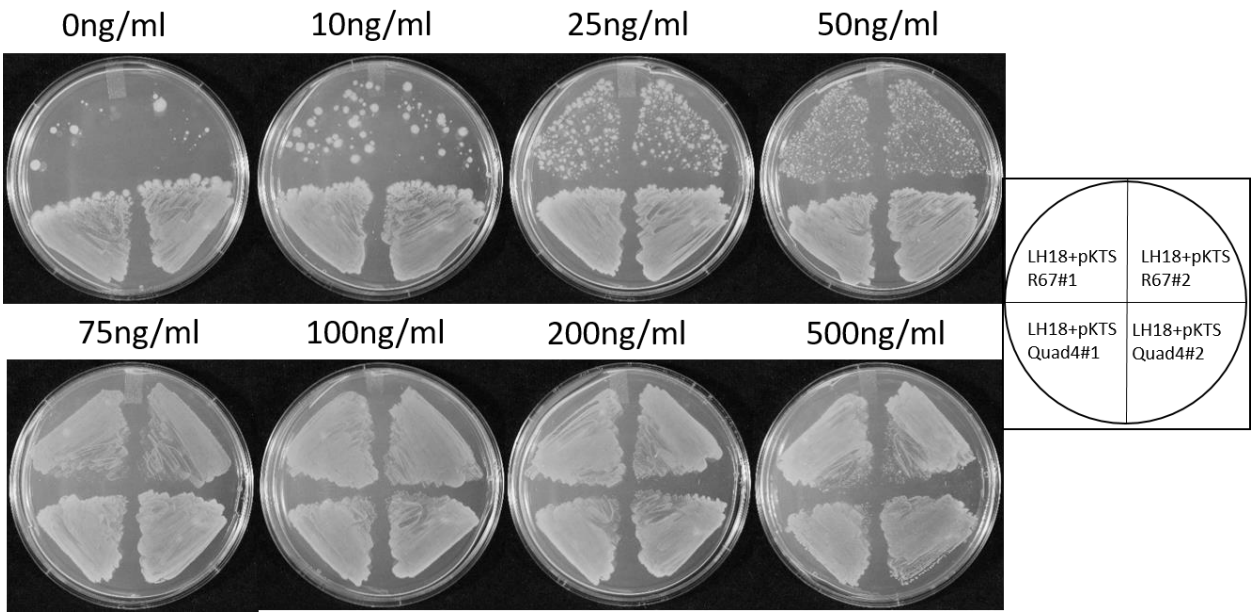

Figure 4.5: Growth of the LH18 Δ*folA* strains complemented by the R67 DHFR-pKTS or the Quad4-pKTS plasmids on minimal media in the presence of increasing concentrations of tetracycline after 5 days of incubation

The tetracycline concentration is indicated above the plates. Two clones of each complemented strain were streaked onto the plates. No growth at low tetracycline concentrations was seen for the first few days, with single colonies arising after ~2 days. Confluent growth was seen between 75-200ng/ml for R67 DHFR-pKTS, whereas good growth of Quad4-pKTS was seen on all concentrations of tetracycline.

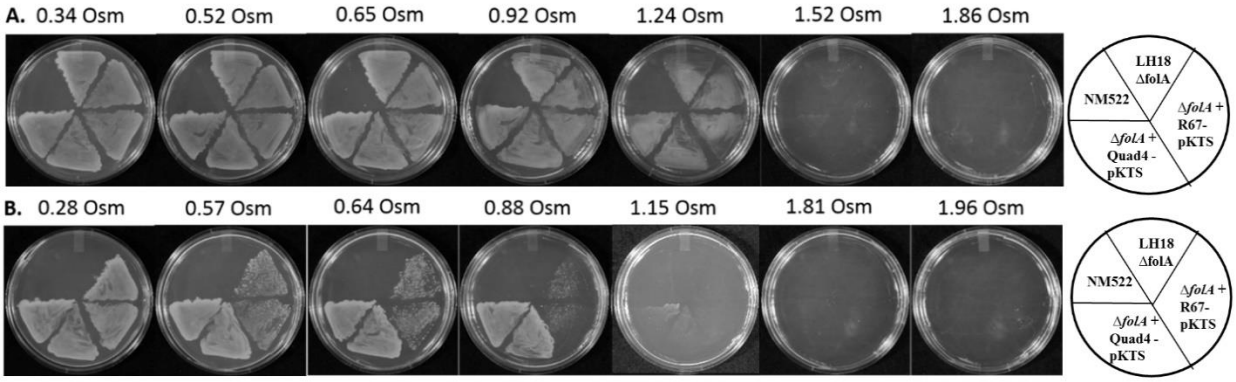

Figure 4.6: The effect of osmolality on R67 and Quad4 DHFR function in restoring the E. coli ΔfolA strain to prototrophy

Panel A shows the effect of sorbitol on cell growth in BV media supplemented with thymidine, adenine, pantothenate, glycine, methionine and containing kanamycin. Cells can grow up to $1.24 < x < 1.52$ Osm. Panel B shows the effect of sorbitol on growth in minimal BV media containing kanamycin, ampicillin and 200 ng/ml tetracycline. Cell growth is reliant on enzyme activity encoded by the DHFR genes cloned in the pKTS plasmid. Cells carrying the R67 DHFR-pKTS plasmid can only grow until $0.28 < x < 0.57$ Osm with isolated colonies appearing at higher osmolalities (until $0.88 < x < 1.15$ Osm). In contrast, cells carrying the Quad4-pKTS plasmid can grow confluently until 1.81 Osm. Table 4.5 lists the osmolalities where cells stop growing. The cartoons indicate the positioning of the various streaks on the plates. Two independent colonies were streaked per transformant. Figure 4.7 shows the titrations for NM522 and NM522 *thyA.*

Table 4.5: Osmolalities at which growth stops on solid media in various *E. coli* strains

Strain	**Media**	**Sorbitol (Osm)**	**NaCl (Osm)**
DH5α	M9 minimal	1.90 < x < 2.43	nd
DH5 α + R67 DHFR-pKTS	M9 minimal + 20 µg/ml TMP	0.81 < x < 1.28	nd
DH5 α + Quad4-pKTS	M9 minimal + 20 µg/ml TMP	1.60 < x < 1.93	nd
NM522	BV minimal	1.60 < x ≤ 2.02	1.6 < x < 1.8
NM522 *thyA*	BV minimal + thymidine	1.55 < x < 1.88	1.22 < x < 1.46
LH18 (Δ*folA*)	BV supplemented with thymidine, adenine, glycine, methionine, pantothenate	1.24 < x < 1.52	nd
LH18 + R67 DHFR-pKTS	BV minimal + thymidine	x ≤ 0.57 for mat growth; 0.57 < x ≤ 0.88 range for overgrowing colonies	nd
LH18 + Quad4-pKTS	BV minimal + thymidine	1.15 < x < 1.81	nd
LH18 (Δ*folA*)	BV supplemented with thymidine, adenine, glycine, methionine, pantothenate + 1 mM betaine	1.81 < x < 2.22	nd
LH18 + R67 DHFR-pKTS	BV minimal + thymidine + 1 mM betaine	x < 0.71 for mat growth; 1.40 < x < 1.67 range for overgrowing colonies	nd
LH18 + Quad4-pKTS	BV minimal + thymidine + 1 mM betaine	1.97 < x < 2.15	nd
BW25113	BV minimal	1.60 < x ≤ 2.02	1.6 < x < 1.8
Δ*metF*	BV minimal + methionine	1.64 < x < 2.21	1.35 < x ≤ 1.44
Δ*metF* + MTHFR-pKTS	BV minimal	x ≤ 1.20 for mat growth; 1.20 < x < 1.67 range for overgrowing colonies	x < 0.48 for mat growth; 0.48 < x ≤ 0.71 (overgrowing colonies)

Table 4.5: continued

Strain	Media	Sorbitol (Osm)	NaCl (Osm)
Δ*glyA*	BV minimal + glycine + serine	1.38 < x < 1.71	1.15 < x ≤ 1.33
Δ*glyA* + SHMT-pKTS	BV minimal	0.92 ≤ x for mat growth; 0.92 < x < 1.30 (overgrowing colonies)	x < 0.53 for mat growth; 0.53 < x ≤0.70 (overgrowing colonies)
KA12/pKIMP-UAUC	BV minimal + phenylalanine + tyrosine	1.35 < x < 1.82	nd
KA12/pKIMP-UAUC + CM-pKTS	BV minimal	0.65 ≤ x for mat growth; 0.65 < x < 1.40 (overgrowing colonies)	nd

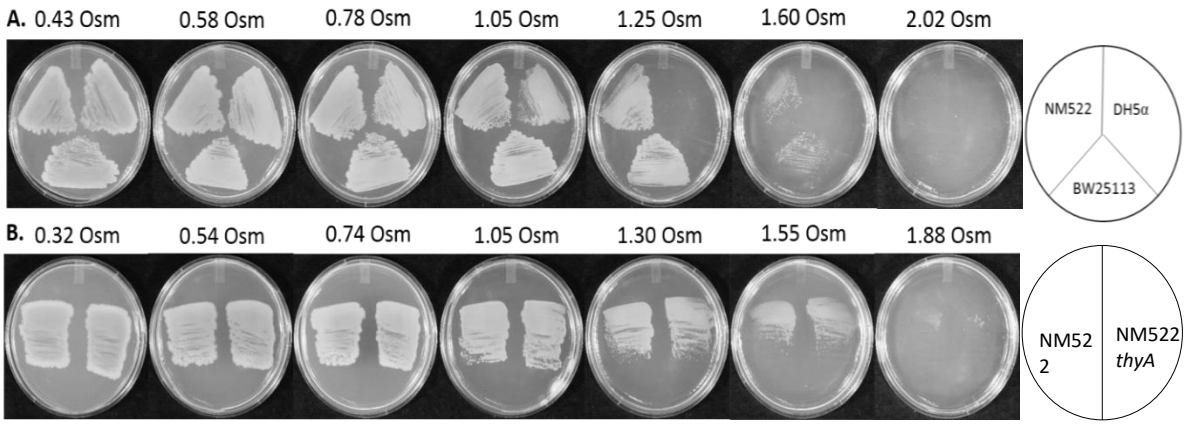

Figure 4.7: Shows how the parent E. coli strains are affected by osmotic stress when grown in Bonner Vogel minimal media with varying concentrations of sorbitol

NM522 and NM522 *thyA* are the parent strains for LH18 Δ*folA.* BW25113 is the parent strain for the Δ*metF* and Δ*glyA* Keio knockouts. Thymidine (200 µg/ml) was added to plates streaked by the NM522 *thyA* strain

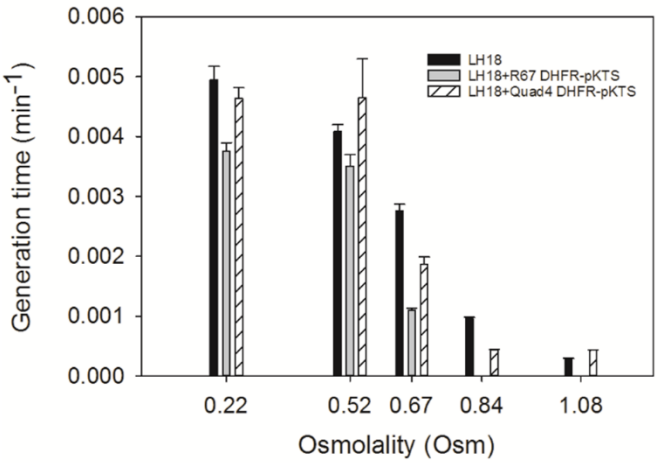

Figure 4.8: Growth rates of LH18 (ΔfolA) cells alone (black bar) or carrying the R67 DHFR-pKTS (gray bar) or Quad4-pKTS plasmid (bar with diagonal line) monitored in liquid culture

The growth rate is plotted as a function of media osmolality. The growth media and the doubling times are listed in Table 4.6.

Table 4.6: Doubling times for the various *E. coli* strains in minimal BV liquid media.

Mutant strains had the appropriate supplements added. Growth curves were performed in triplicate. Tetracycline concentrations used are listed in Table 4.3

Strain	**Osmolality of sorbitol containing media (Osm)**	**Doubling time in sorbitol containing media (mins)**	**Osmolality of NaCl containing media (Osm)**	**Doubling Time in NaCl containing media (mins)**
NM522	0.18	130 ± 10	0.18	210 ± 10
	0.44	160 ± 20	0.37	270 ± 10
	0.67	180 ± 20	0.51	950 ± 20
	0.93	340 ± 10	0.70	2100 ± 20
	1.07	1100 ± 30	0.88	3500 ± 90
	1.25	0	1.08	0
NM522 *thyA*	0.18	120 ± 10	0.18	170 ± 5
	0.44	100 ± 20	0.37	160 ± 5
	0.67	100 ± 20	0.51	350 ± 10
	0.93	470 ± 30	0.70	3500 ± 200
	1.07	1200 ± 50	0.88	6900 ± 300
	1.25	0	1.08	0
LH18=	0.22	200 ± 10	0.19	250 ± 10
NM522 *thyA*	0.52	240 ± 10	0.35	170 ± 10
Δ*folA::kan*	0.67	360 ± 20	0.55	490 ± 20
	0.84	1100 ± 20	0.60	900 ± 20
	1.08	3500 ± 70	0.81	1200 ± 60
	1.16	0	1.04	1700 ± 40
			1.12	1800 ± 100
			1.4	0
LH18Δ*folA*	0.22	260 ± 10	0.19	220 ± 10
+ R67 DHFR-	0.52	280 ± 20	0.35	520 ± 20
pKTS	0.67	900 ± 25	0.55	1500 ± 140
	0.84	0	0.60	0
LH18Δ*folA*	0.22	220 ± 10	0.19	280 ± 10
+ Quad4 DHFR-	0.52	220 ± 30	0.35	490 ± 20
pKTS	0.67	540 ± 40	0.55	1200 ± 80
	0.84	2400 ± 60	0.60	1700 ± 100
	1.08	2400 ± 30	0.81	1800 ± 40
	1.16	7200 ± 200	1.04	1900 ± 40
	1.42	0	1.12	2300 ± 50
			1.4	0

Table 4.6 Continued

Strain	Osmolality of sorbitol containing media (Osm)	Doubling time in sorbitol containing media (mins)	Osmolality of NaCl containing media (Osm)	Doubling Time in NaCl containing media (mins)
BW25113	0.21	110 ± 5	0.21	120 ± 5
	0.47	150 ± 5	0.35	140 ± 10
	0.67	230 ± 10	0.54	140 ± 10
	0.88	280 ± 10	0.65	170 ± 5
	1.08	360 ± 20	0.82	230 ± 20
	1.28	3500 ± 90	1.05	240 ± 10
	1.53	0	1.13	780 ± 20
Δ*metF*	0.18	130 ± 5	0.19	140 ± 5
	0.37	150 ± 5	0.33	130 ± 5
	0.6	160 ± 5	0.53	140 ± 5
	0.86	220 ± 20	0.73	190 ± 5
	1.07	380 ± 20	0.79	250 ± 10
	1.25	870 ± 70	0.98	460 ± 20
	1.47	0	1.18	2200 ± 70
			1.47	0
Δ*metF* + MTHFR-pKTS	0.18	290 ± 5	0.19	300 ± 10
	0.37	610 ± 20	0.33	530 ± 10
	0.6	1400 ± 20	0.53	860 ± 10
	0.86	2100 ± 40	0.73	950 ± 10
	1.07	2300 ± 40	0.79	1400 ± 20
	1.25	4600 ± 50	0.98	1700 ± 60
	1.47	0	1.18	2300 ± 60
			1.47	0
Δ*glyA*	0.18	150 ± 5	0.18	120 ± 5
	0.47	170 ± 5	0.39	120 ± 5
	0.67	170 ± 5	0.54	170 ± 5
	0.93	180 ± 5	0.66	170 ± 5
	1.11	350 ± 10	0.86	200 ± 5
	1.29	0	1.05	480 ± 50
			1.20	750 ± 50
			1.31	0
Δ*glyA* + SHMT-pKTS	0.18	390 ± 20	0.18	240 ± 10

Table 4.6 Continued

Strain	Osmolality of sorbitol containing media (Osm)	Doubling time in sorbitol containing media (mins)	Osmolality of NaCl containing media (Osm)	Doubling Time in NaCl containing media (mins)
Δ*glyA* + SHMT-pKTS	0.47	800 ± 40	0.39	500 ± 10
	0.67	990 ± 20	0.54	1000 ± 10
	0.93	1400 ± 20	0.66	2700 ± 50
	1.11	3100 ± 200	0.86	6900 ± 300
	1.29	0	1.05	0

As the osmolality of the media was increased, all cells grew more slowly. From Figure 4.8, the growth rate of LH18 cells carrying the R67 DHFR-pKTS clone was most impacted, with cell growth ceasing at 0.67 < x < 0.84 Osm. In contrast, the deletant LH18 cells and the complemented LH18 + Quad4-pKTS cells grew until 1.08 < x <1.16 Osm. These trends echo those seen in the agar plate titrations which are consistent with previous observations where immobilization of bacteria on agar plates or biofilms constrained growth compared to planktonic conditions and higher osmolalities could be required to inhibit growth [58, 59].

Lag times, in general, increased with increasing osmolality [60]. This is likely due to initial plasmolysis [61], however other factors such as the number of colony forming units added to initiate growth can play a role. The maximal turbidity of the cultures was also impacted, consistent with hyper-osmolality leading to cells devoting more resources to osmoprotection compared to metabolism [62].

The above growth curves were repeated using NaCl as the osmotic stressor. Doubling times are listed in Table 4.6. The deletant LH18 cells in media supplemented with thymidine, adenine, pantothenate, glycine, and methionine and the complemented Quad4-pKTS cells in minimal media could grow until 1.12 < x < 1.4 Osm. However, the LH18 strain, complemented by the R67 DHFR-pKTS clone, was affected more severely by NaCl stress and only grew until 0.55 < x < 0.60 Osm in minimal media. The trend is similar to that observed with sorbitol, however NaCl is a slightly better stressor. This difference may arise from sorbitol being used as an alternate carbon source [63, 64]. Alternatively, NaCl can have different effects than sorbitol, for example transcriptional responses [65], induction of different proteins [66, 67] and ionic effects [68], could alter the magnitude of the osmotic stress effect.

4.5.4 Growth under osmotic stress is dependent on the enzyme concentration in the cell

The DHFR concentration can be increased by addition of higher tetracycline concentrations, which drives expression of the P_{tet} promoter. To monitor growth rate as a function of varying amounts of sorbitol under different tetracycline concentrations, 3D plots were constructed with the culture turbidity at 600nm and the concentration of sorbitol as the axes. Figure 4.9 A depicts the growth of R67 DHFR-pKTS complemented LH18 cells in BV minimal media containing 0, 50, 100 and 200ng/ml tetracycline. Without tetracycline, there was no growth. Increased growth occurred with increasing tetracycline concentrations. Figure 4.9 B also shows the growth curves of the parent strains NM522 and NM522 *thyA*. Growth of the parent strains is faster than that of the pKTS complemented strains, consistent with the hypothesis that use of the pKTS plasmid allows lower levels of protein concentration/activity than provided by the chromosome [27].

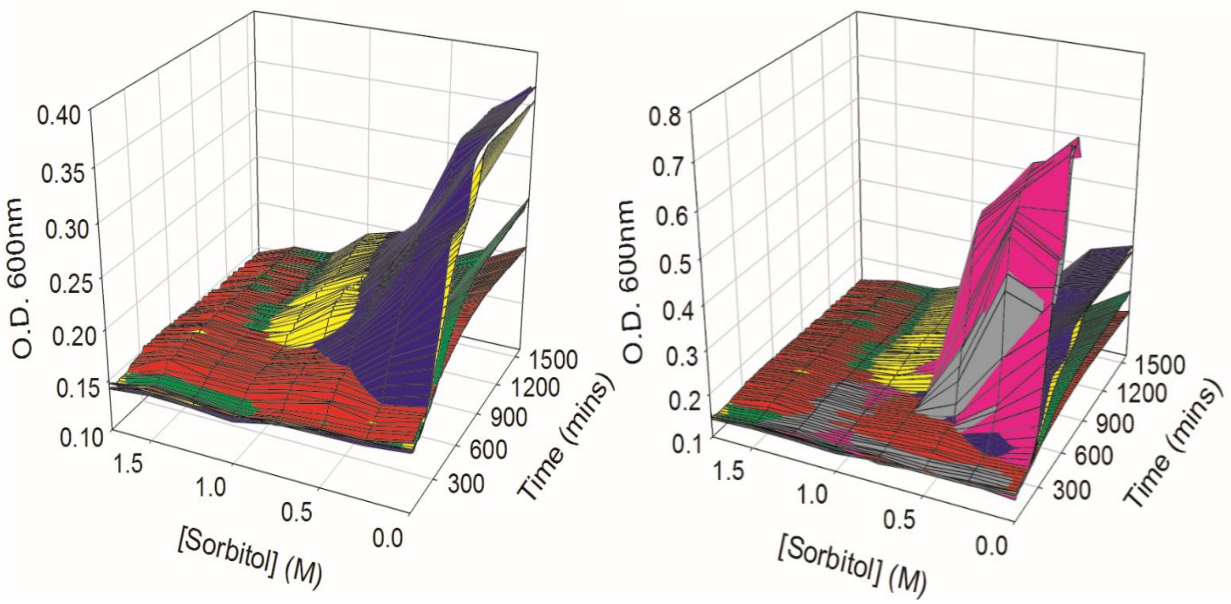

Figure 4.9: Provides 3D plots of cell growth

Left panel (A): growth in minimal media for the LH18 Δ*folA* strain complemented by the R67 DHFR-pKTS plasmid. Tetracycline concentrations are 0 ng/ml (red), 50 ng/ml (green), 100 ng/ml (yellow) and 200ng/ml (blue). Sorbitol concentrations are shown on the x-axis. Right panel, the same data with the growth curves from the parent strains NM522 (magenta) and NM522*thyA8* (gray) added. The faster growth of the parent strains is consistent with the Hilvert group's proposal that the pKTS plasmid results in protein concentrations/activity that are lower than those encoded by the chromosome [27]. Neuenschwander et al. supported their hypothesis by monitoring GFP expression in *E. coli* [27].

4.5.5 Addition of betaine to osmotic stress titrations enables growth to higher osmolalities

When glycine betaine is added to the growth media, it becomes the predominant osmolyte in the cell [7]. Betaine is an osmoprotectant that functions by preferential exclusion from protein surfaces [69], which results in it often being used to fold proteins [70-72]. To study the effect of added betaine, we redid our sorbitol titrations of LH18 carrying the R67 DHFR-pKTS plasmid with 1 mM betaine in the agar plates. The deletant and complemented cells grew until 1.81 Osm ≤ x ≤ 2.22 Osm in media supplemented by thymidine, adenine, pantothenate, glycine, and methionine (Figure 4.10). Addition of betaine increased the osmolality to which cells were able to grow [7]. When the complemented cells were plated on minimal media, they also tolerated much higher osmolalities when grown in the presence of 1 mM betaine. The R67 DHFR-pKTS complemented LH18 strain grew confluently at 0.71 Osm, however many overgrowing colonies were observed between 0.98-1.67 Osm. The Quad4-pKTS complemented LH18 cells grew until 1.97 Osm, however no growth was observed at 2.15 Osm. These results were similar to growth of the deletant LH18 strain in supplemented media. Liquid titrations of deletant and complemented strains were done using sorbitol as the osmotic stressor. Similar trends were observed as seen for the agar plates (Figure 4.10C). The ability of betaine to extend growth to higher osmolality conditions supports the hypothesis that water activity plays a role in our experiments.

4.5.6 Can osmotic stress titrations apply to other folate pathway enzymes?

To test whether the activity of other folate utilizing enzymes could be titrated by *in vivo* osmotic stress conditions, we used methylene tetrahydrofolate reductase (MTHFR encoded by the *metF* gene) and serine hydroxymethyl transferase (SHMT encoded by the *glyA* gene). Summaries of these 2 enzymes are provided in Table 4.4.

The metF and *glyA* genes from *E. coli* were cloned into the pKTS plasmid. Tetracycline titrations found 100ng/ml tetracycline allowed the Δ*metF* cells carrying the MTHFR-pKTS plasmid to grow in minimal media while 75ng/ml tetracycline allowed the Δ*glyA* cells carrying the SHMT-pKTS cells to grow confluently in minimal media (data not shown).

4.5.7 In vivo titrations of methylene tetrahydrofolate reductase activity

MTHFR is functional as a homotetramer and catalyzes the reduction of 5, 10-methylene-THF to 5-methyl THF using NADH and FAD as cofactors. The 5-methyl-THF product is used by methionine synthase to produce methionine from homocysteine.

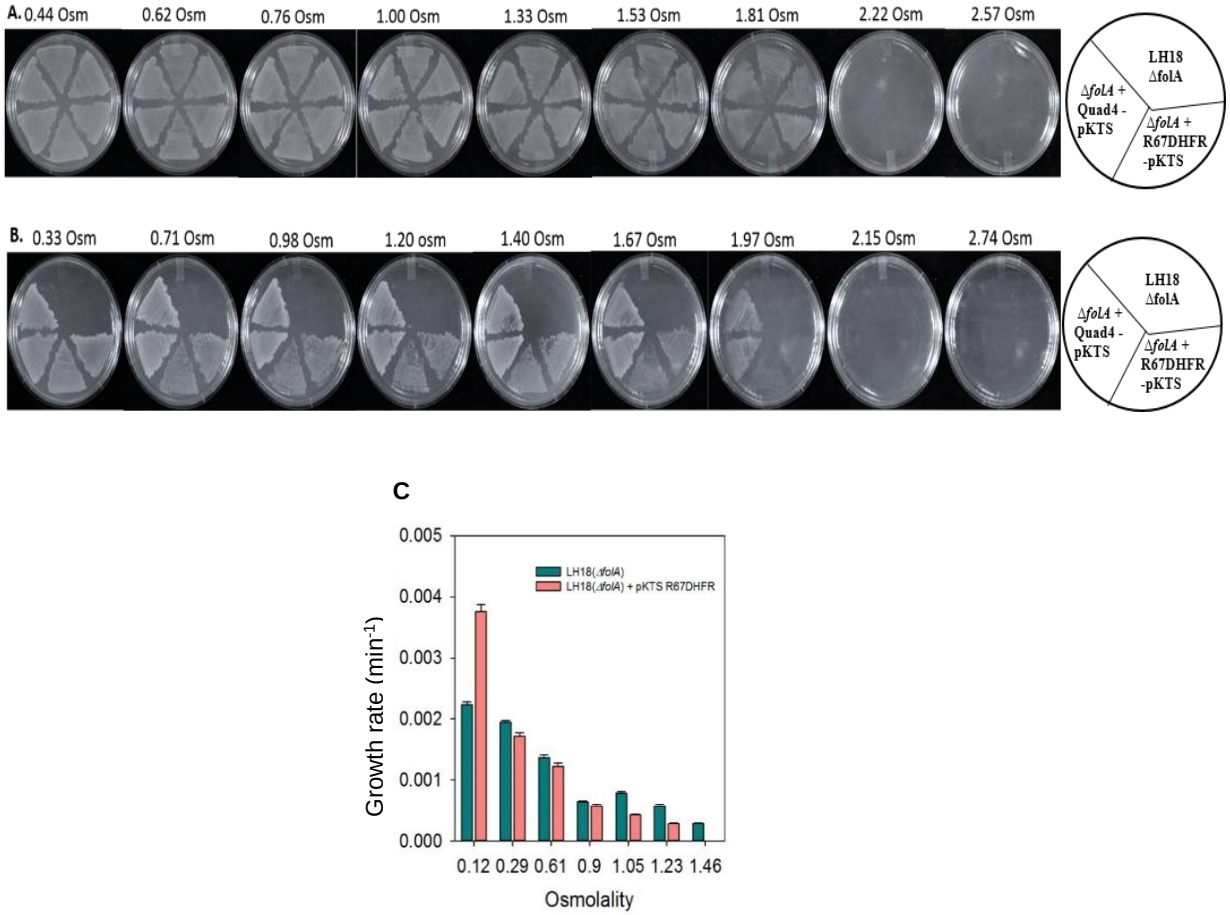

Figure 4.10: Growth of LH18 (ΔfolA) cells with and without R67 DHFR-pKTS and Quad4-pKTS plasmids in presence of betaine and sorbitol stress

Panel A shows the effect of sorbitol on LH18 (Δ*folA*) cells with and without R67 DHFR-pKTS and Quad4-pKTS plasmids grown on BV media supplemented with thymidine, adenine, pantothenate, glycine, methionine plus 1 mM betaine. Panel B shows how addition of 1mM betaine facilitates growth to higher osmolalities (vs. those seen in Figure 4 of the main text). Table 4.5 lists the osmolality range at which growth stops. In panel C, results from liquid cultures are provided. The bar graph compares the effect of 1 mM betaine on the growth rate of LH18 (green bar) vs. the cells rescued by the presence of the R67 DHFR-pKTS plasmid (red bar).

Addition of 100ng/ml tetracycline to the MTHFR-pKTS complemented Δ*metF* strain resulted in cell growth in minimal media lacking methionine. Figure 4.11 shows our in vivo sorbitol titrations. All strains grew confluently on media supplemented with methionine until 1.30 Osm. Sparse growth was observed at 1.64 Osm. In contrast, two different colonies of the complemented strain (ΔmetF + MTHFR-pKTS) showed confluent growth on minimal media until ~0.62 Osm, after which growth was dominated by isolated, overgrowing colonies. No growth was observed at osmolalities ≥1.17. Since the complemented strains did not grow in high osmolality conditions (1.17 Osm, minimal media), while the parent strain grew well at 1.30 Osm (media supplemented with methionine), we conclude that the MTHFR activity can be titrated by osmotic stress in vivo. Figure 4.7 shows the effect of osmotic stress on the parent E. coli strains when grown in BV minimal media with sorbitol.

Figure 4.12 shows titration of the ΔmetF strains using NaCl. Similar results were obtained as with sorbitol as all cells grew until 1.35 Osm on methionine supplemented media. However, the complemented cells showed confluent growth on minimal media until 0.22 Osm with suppressor colonies until 0.48 Osm and no growth after 0.71 Osm.

Doubling times of these strains in liquid media were also obtained and the values are listed in Table 4.6. With increasing sorbitol stress, the growth rate of all strains decreased (Figure 4.13A). As with the agar plates, the deletion cells could survive in higher osmolalities in media supplemented with methionine than the complemented cells in minimal media. A similar pattern was observed when NaCl was added to the media (Figure 4.13B).

4.5.8 In vivo titrations of serine hydroxymethyl transferase activity

SHMT is a homodimer that interconverts glycine and serine using 5,10-methylene-THF, THF and pyridoxal phosphate. It can also catalyze the conversion of 5,10-methenyl-THF to 5-formyl THF [73]. While this enzyme can also catalyze retroaldol cleavage, racemase, aminotransferase and decarboxylase reactions [74], Contestabile [75] suggests the SHMT reaction is its primary *in vivo* function. Both serine and glycine are required for growth of Δ*glyA* deletant cells. Transformation of the Δ*glyA* cells by SHMT- pKTS restored prototrophy to the strain in the presence of ≥75 ng/ml tetracycline. Sorbitol titrations of cell growth are shown in Figure 4.14**.** Control titrations find all cells grew in BV media supplemented with glycine and serine until 1.38 Osm. However, in minimal media, the deletant cells complemented by the SHMT-pKTS plasmid only grew confluently until 0.92 Osm; single colonies predominated from 1.23-1.3 Osm, while cell growth stopped at higher osmolalities.

The osmotic stress titrations were repeated using NaCl (Figure 4.15). Similar trends were observed as with sorbitol, although NaCl had a more pronounced effect.

Osmotic stress titrations were also performed in liquid media. Table 4.6 provides the doubling times while Figure 4.16 shows the growth rates. The behavior is similar to that observed in the agar plates, with the complemented cells not being able to survive in

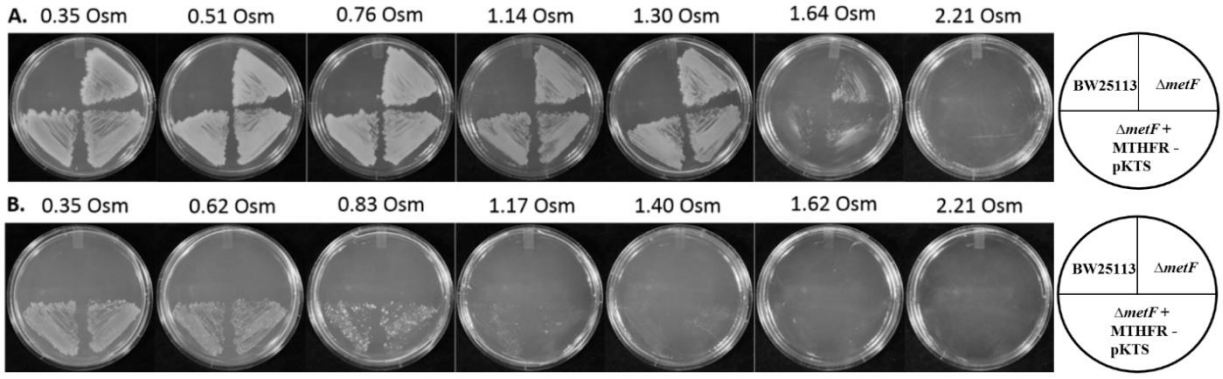

Figure 4.11: Osmotic stress severely impairs the growth of the metF complemented strains in minimal media

The top panel shows the growth of the *metF* deletant and complemented strains in minimal media supplemented with methionine and kanamycin. BW25113 does not grow due to the presence of kanamycin. Osmotic stress was induced by the addition of sorbitol to the media. The bottom panel shows growth of the deletion strain carrying the MTHFR-pKTS plasmid where protein production was induced by addition of 100 ng/ml tetracycline. Cells in panel A grow until $1.30 < x < 1.64$ Osm while cells in panel B grow to 0.62 Osm (confluent growth). Table 4.5 lists the osmolalities where cells stop growing. The cartoon shows how the cultures are streaked. Two independent colonies were streaked per transformant. Figure 4.8 shows how BW25113 is affected by increasing sorbitol concentrations.

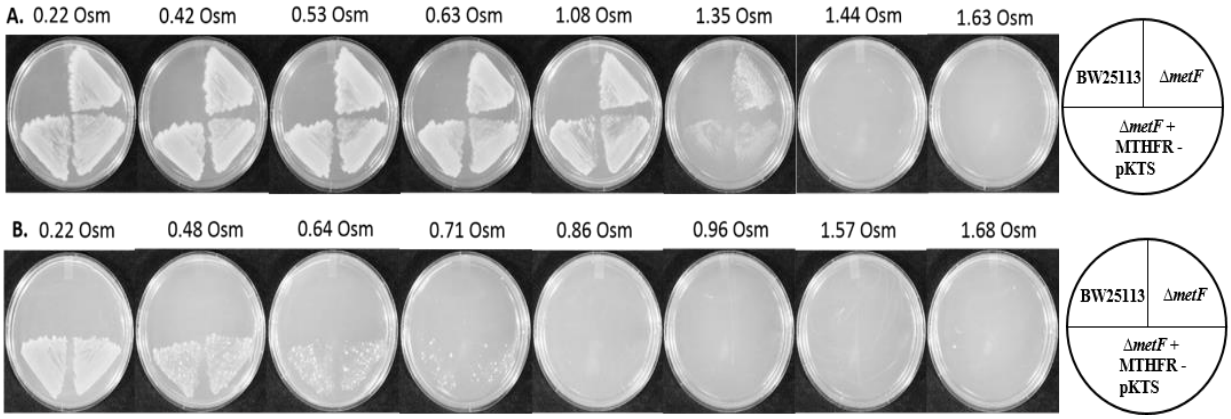

Figure 4.12: Osmotic stress titrations of ΔmetF strains using NaCl

Panel A (top) shows the growth of deletion and complemented strains in BV media supplemented with methionine and kanamycin. The cells grow until $1.35 < x < 1.44$ Osm. Panel B (bottom) shows the growth in BV minimal media with kanamycin, ampicillin and 100ng/ml tetracycline. Complemented cells carrying the MTHFR-pKTS plasmid grew confluently until 0.48 Osm. Isolated overgrowing colonies were observed until 0.71 Osm. The cartoons on the right provide a template for the positions of the different strains.

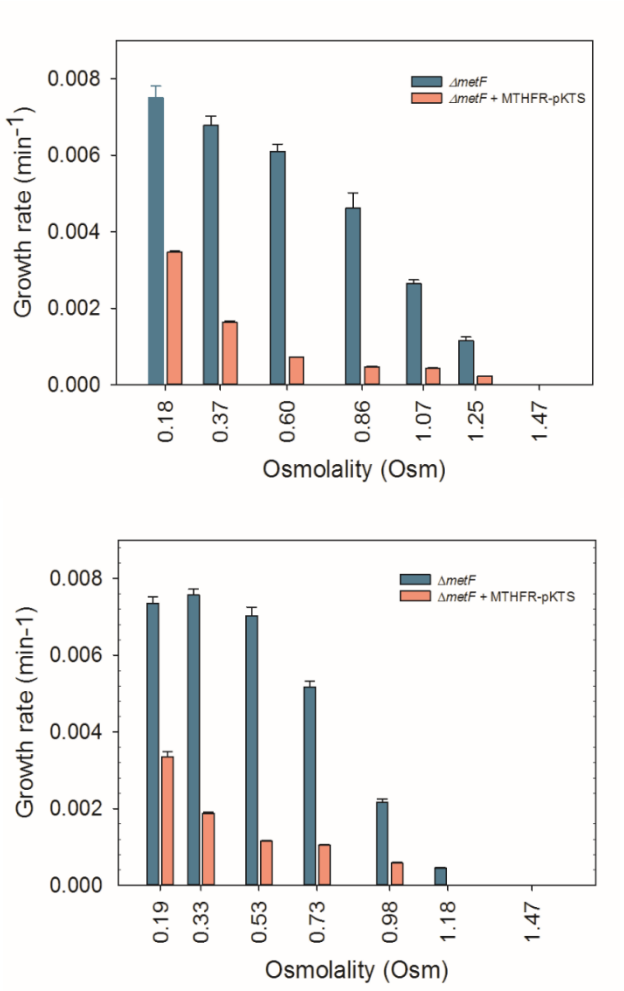

Figure 4.13: Plots of growth rates (min-1) vs. osmolality for the ΔmetF strain

Panel A (top) shows growth in the presence of sorbitol for the deletant strain (green bar) and the complemented strain (red bar). Panel B (bottom) shows growth in the presence of NaCl. With both osmotic stressors, the deletion strains were grown in BV media supplemented with methionine whereas the complemented strains (Δ*metF*+MTHFR-pKTS) were grown in minimal media with 75ng/ml tetracycline

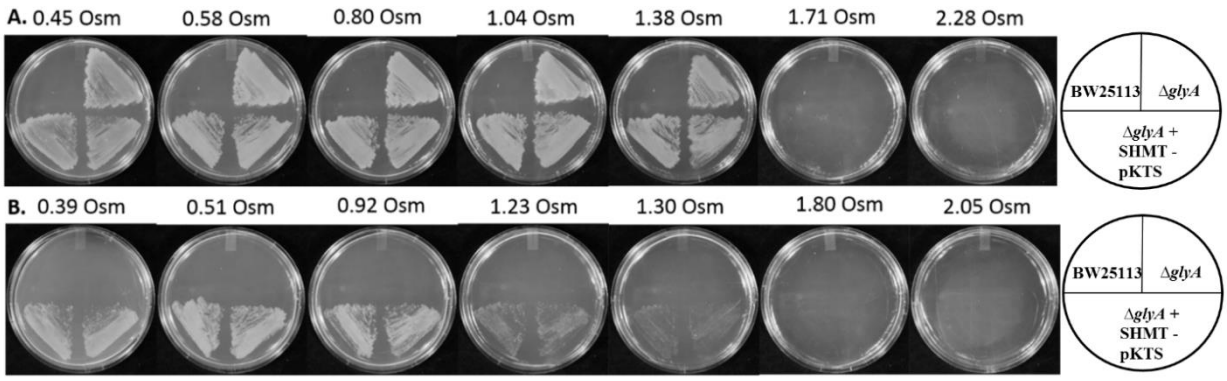

Figure 4.14: Addition of sorbitol to the growth media impacts the growth of the glyA complemented strains

The top panel shows the growth patterns in BV supplemented media containing serine and glycine. The bottom panel shows how the cells grow on minimal media plus 75 ng/ml tetracycline. Cells in the top panel (A) grow until $1.38 < x < 1.71$ Osm while cells in minimal media (panel B) grow until 0.92 Osm (mat growth). Table 4.5 lists the osmolalities where cells stop growing. The far-right drawing identifies how cultures were streaked on the plates. Two independent colonies were streaked per transformant. Figure 4.7 shows the titrations for BW25113.

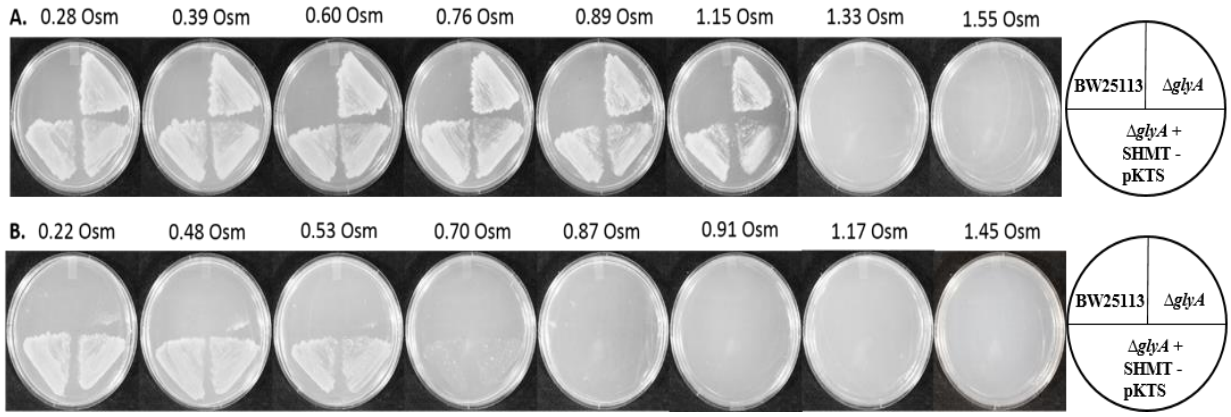

Figure 4.15: The growth of deletant and complemented cells of the ΔglyA strain using NaCl as the osmotic stressor

Panel A shows the growth of cells in BV media supplemented with glycine and serine as well as kanamycin. The cells show growth up to 1.15 Osm. Panel B shows the growth in BV minimal media with kanamycin, ampicillin and 75ng/ml tetracycline. The SHMT-pKTS clone allows cells to grow confluently until 0.48 Osm. Isolated overgrowing colonies appear until 0.70 Osm. The cartoons on the right provide a template for the position of the different strains.

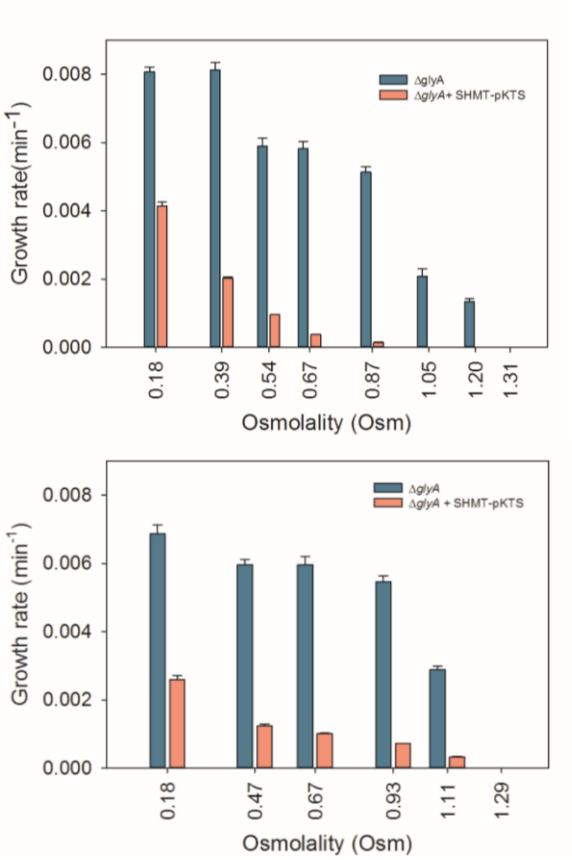

Figure 4.16: The activity of ΔglyA E. coli carrying the serine hydroxymethyl transferase gene cloned in the pKTS plasmid can be titrated with increasing in vivo osmotic stress

Panel A (top) plots the growth rate (min^{-1}) of the Δ*glyA* strain (green bar) vs. osmolality in sorbitol containing media while Panel B (bottom) shows the growth pattern in NaCl containing media. The deletion strain was grown in BV media supplemented with glycine and serine (green bar) whereas the Δ*glyA* + SHMT-pKTS complemented cells (red bar) were grown in minimal media with 50ngml tetracycline.

high osmolality conditions on minimal media, while the deletant cells could grow on media supplemented with glycine and serine.

4.5.9 Can the activity of chorismate mutase be titrated with osmotic stress?

To test whether another enzyme can undergo *in vivo* osmotic stress titrations of catalytic activity, we used a chorismate mutase gene (*aroQ*) that was initially cloned in the pKTS plasmid [27]. Chorismate sits at a metabolic branch point and this enzyme commits chorismate to phenylalanine and tyrosine production. A gene encoding a mutant chorismate mutase was used where insertion of five-amino-acids in the middle of a helix in the protein resulted in a hexamer with an approximately 600-fold decrease in activity [47]. This truncated, mutant gene cloned in pKTS was then transformed into a CM deficient strain (KA12/pKIMP-UAUC) to create a complemented strain [32, 33].

The chorismate mutase deficient strain grew in media supplemented with tyrosine and phenylalanine whereas prototrophy was restored in the CM-pKTS complemented cells by the addition of ≥ 200ng/ml tetracycline. As shown in Figure 4.17, osmotic stress experiments with increasing sorbitol concentrations allowed the CM deficient cells grown on media supplemented with tyrosine and phenylalanine to survive until 1.14 Osm with sparse growth seen at 1.35 Osm. The complemented cells showed confluent growth until 0.65 Osm on minimal media. An increasing number of overgrowing colonies dominated the growth from 1.04-1.17 Osm with no growth at 1.40 Osm. From these titrations, it appears that CM activity can be titrated by osmotic stress.

4.5.10 Suppressors in the SsrA tag

Streaks on agar plates allow us to discern where confluent growth diverges from single colony growth. We monitored agar plate growth daily and initially found confluent growth. After about two days, overgrowing colonies started to appear at lower tetracycline or higher sorbitol concentrations. Figure 4.18 shows a sample time course of colony growth as a function of time for the MTHFR-pKTS rescued ΔmetF cells.

Twenty overgrowing colonies from each of the ΔfolA, ΔglyA and ΔmetF knockout strains carrying their respective genes in the pKTS plasmid were sub-cultured in media containing 1M sorbitol. Plasmid DNA was extracted and retransformed into the appropriate parent strain. Typically, <10 colonies continued to grow on 1M sorbitol media, suggesting many original colonies had chromosomal mutations. DNA sequencing of the plasmids showed mutations in the SsrA tag or introduction of a stop codon near the end of the gene or in the SsrA tag sequence (Table 4.7).

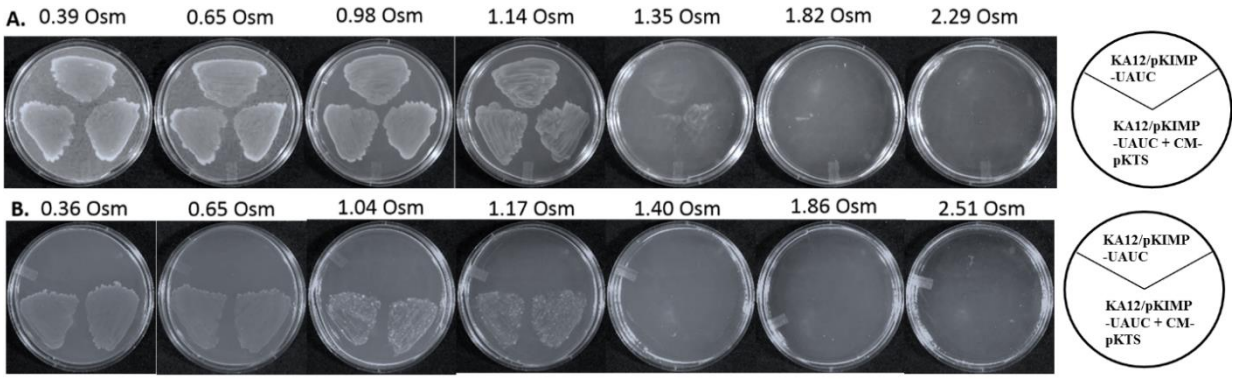

Figure 4.17: The effects of sorbitol on chorismate mutase function *in vivo*

The top panel shows the growth of the deletion and complemented cells in media supplemented with tyrosine and phenylalanine. The bottom panel depicts the growth pattern in minimal media plus 200 ng/ml tetracycline. Cells in supplemented media (Panel A) can grow until $1.35 < x < 1.82$ Osm while cells in minimal media (Panel B) can grow confluently until $0.65 < x < 1.04$ Osm. Table 4.5 lists the osmolalities where cells stop growing.

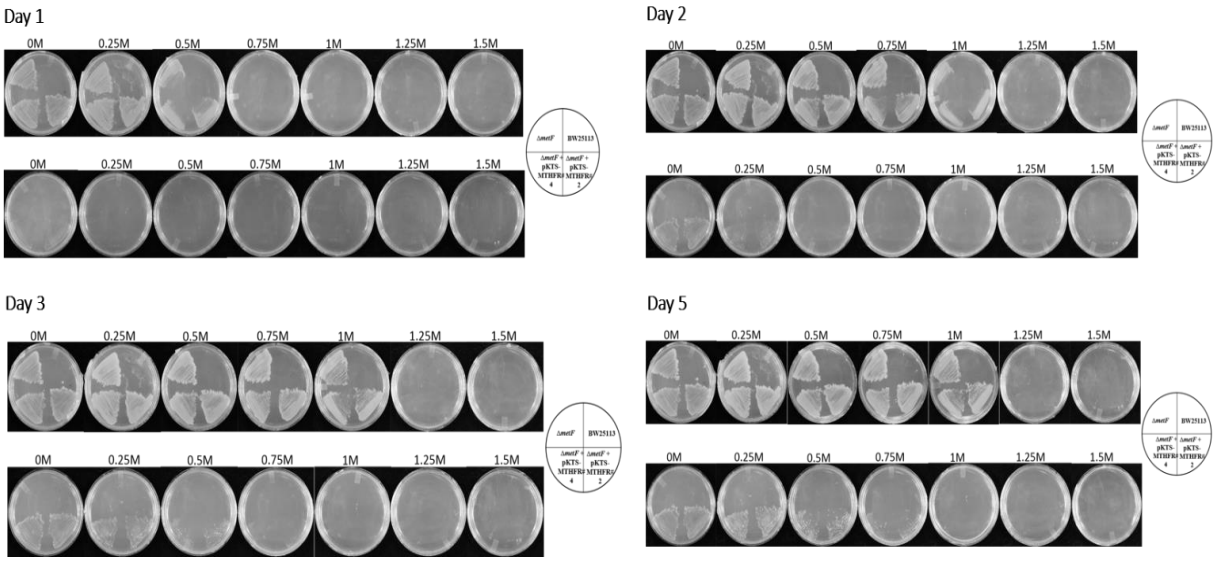

Figure 4.18: Time course of the growth of ΔmetF cells that are complemented by the MTHFR –pKTS plasmid

Cells were grown on BV media supplemented with methionine on the top panel and BV minimal media with 100ng/ml tetracycline on the bottom panel. The sorbitol concentrations used are listed on top of each plate. The plates were monitored every day for a span of five days. Cell growth on the minimal plates becomes confluent by 2-3 days and stays the same for 5 days. Isolated overgrowing colonies appeared around day 2-3.

Table 4.7: List of suppressors appearing at or near the SsrA tag

OverGrowerR67DHFR#7	Mutation in Xho1 site. SsrA tag not made
OverGrowerR67DHFR#9	Mutation in Xho1 site. SsrA tag not made. Different site than OG#7.
OverGrowerR67DHFR#11	Stop codon introduced in Xho1 Site.
OverGrowerR67DHFR#15	Stop codon introduced in Xho1 Site.
OverGrowerR67DHFR#19	Stop codon introduced in Xho1 Site.
OverGrowerR67DHFR#20	Stop codon introduced in Xho1 Site.
OverGrowerMTHFR#1	Stop codon in *metF* gene sequence, three amino acids before termination. No SsrA tag made.
OverGrowerMTHFR#2	Frameshift mutation in Xho1 restriction site. SsrA tag not made.
OverGrowerMTHFR#4	Base deletion in the *metF* gene sequence, 5 amino acids before termination. No SsrA tag made.
OverGrowerMTHFR#5	Bases introduced in SsrA tag leading to stop codon TGA where the 4th amino acid of SsrA tag would be. No tag made.
OverGrowerMTHFR#6	Stop codon in *metF* gene sequence in the last amino acid before termination. Thus, no SsrA tag made.
OverGrowerMTHFR#7	Stop codon TGA introduced in Xho1 restriction site. No SsrA tag made.
OverGrowerMTHFR#9	Bases introduced in SsrA tag leading to stop codon TGA in the 4th amino acid of SsrA tag. No tag made.
OverGrowerSHMT#2	Frameshift mutation in SsrAtag. The tag is not made.
OverGrowerSHMT#4	Stop codon introduced in SsrA tag.
OverGrowerSHMT#10	Stop codon introduced in SsrA tag.
OverGrowerSHMT#11	Stop codon introduced in SsrA tag.

That all these mutations alter or delete the SsrA tag suggests a common mechanism of suppression e.g. an increase in enzyme activity due to enhanced protein production. This points to the enzyme activity being limiting in the cell. This behavior has previously been observed by the Hilvert group in suppressors of chorismate mutase [27].

4.5.11 Are the observed effects bacteriostatic or bacteriocidal?

Colony forming units (CFUs) were measured for the R67 DHFR-pKTS rescued LH18 strain as well as the MTHFR-pKTS rescued Δ*metF* strain and the SHMT-pKTS rescued Δ*glyA* strain. Cells were incubated in several sorbitol concentrations ranging from 0 to 1.75M for up to 48 hrs. Complemented strains inoculated into BV minimal media plus the appropriate tetracycline concentration did not grow at higher osmolalities and dilutions of these cultures at 0, 24 and 48 hours showed similar CFUs (data not shown), indicating bacteriostatic effects [59, 76-78].

4.5.12 Mathematical modeling

A Matlab program was obtained from Drs. Nijhout and Reed (Duke) that describes the folate mediated one carbon metabolism cycle from bacteria (see Figure 4.19). This model is updated from that published in LeDuc et al. [79]. As genes for a flavin dependent thymidylate synthase (*thyX*)[79] and formyltetrahydrofolate synthetase (f*hs*)[80] do not occur in *E. coli*, those velocities were set equal to zero. Also we replaced the kinetic values for dihydropteridine reductase with those of FolM, a pteridine reductase that weakly catalyzes the DHFR reaction [8, 81]. Note the SHMT reaction is only modeled as occurring in the direction of glycine formation. A second reaction catalyzed by SHMT (i.e. methenyl-THF to 5-formyl-THF) is listed as SHMT2 [73]. A rate describing the non-enzymatic interconversion of THF to N5,N10-methylene-THF is additionally included as CH2. The mathematical model does not include any polyglutamylation effects, K_i values for inhibition or enzymes that degrade folate. No rates are entered for flux into the pathway (by dihydrofolate synthase (FolC) formation of DHF from dihydropteroate + p-aminobenzoate or by reduction of folate to DHF by DHFR) or flux out of the pathway (methionine formation via methionine synthase).

The effect of osmotic stress was analyzed on specific folate pathway enzymes in Matlab by either decreasing the V_{max} of the reaction to zero or by increasing the K_M value for the folate ligand to 1M. While the V_{max} for the deletion strain complemented by the pKTS plasmid should be smaller due to a lower dose of protein, we do not know what this level is. Thus, we maintained the original level in the model and elected to present the general trends observed. Figures 4.20-4.22 show the effects on SHMT, MTHFR and DHFR.

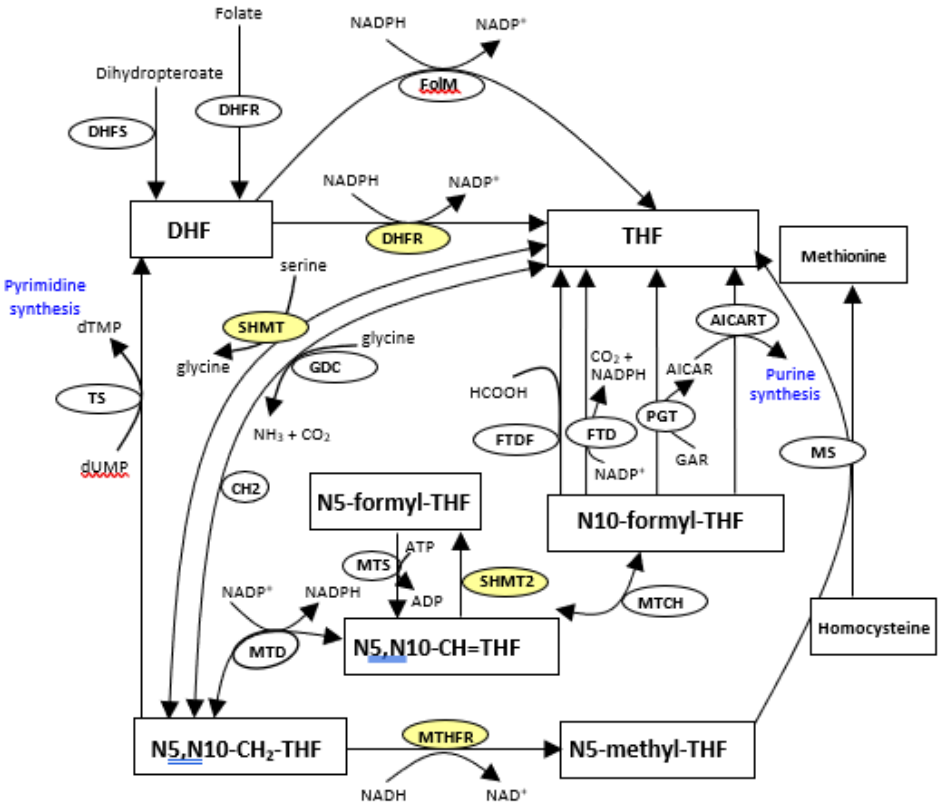

Figure 4.19: Simplified folate mediated one carbon reactions used in mathematical modelling

Substrates are shown in rectangles and enzymes in ellipses. The enzymes used in our osmotic stress titrations are highlighted in yellow ellipses. Substrate abbreviations are given below and the enzyme abbreviations and the values used in the mathematical model are provided in the following Table 4.8.

Substrate abbreviations:
AICAR, aminoimidazole carboxamide ribotide;
DHF, dihydrofolate;
GAR, glycinamide ribotide;
N5-formyl-THF, N5-formyltetrahydrofolate;
N10-formyl-THF, N10-formyltetrahydrofolate;
N5-methyl-THF,5-methyltetrahydrofolate;
N5,N10-CH_2-THF, N5,N10-methylenetetrahydrofolate;
N5,N10-CH=THF, N5,N10-methenyltetrahydrofolate;
THF, tetrahydrofolate;
dTMP, Deoxythymidine monophosphate;
dUMP, deoxyuridine monophosphate

Table 4.8: Abbreviations and values used in the mathematical model

Abbreviation	Enzyme	V_{max} (µM/hr)	K_{M1} (µM)	K_{M2} (µM)
AICART	Aminoimidazole carboxamide ribotide transformylase	562.5	dUMP: 6.3	N5,N10-CH_2-THF: 14
CH2	Non-enzymatic conversion of THF to N5,N10-methylene-THF	0.01	-	-
DHFR	Dihydrofolate reductase	225	DHF: 0.5	NADPH: 4.0
FolM	FolM	1.92	DHF: 4.3	NADPH: 4.0
FTD	10-Formyltetrahydrofolate dehydrogenase	1400	N10-formyl-THF: 20	-
FTDF	Formyltetrahydrofolate deformylase	2000	N10-formyl-THF: 49	-
GDC	Glycine decarboxylase	7500	THF: 50	Glycine: 3400
MTCH	5,10-Methylene-tetrahydrofolate cyclohydrolase	V_{max1}: 48000 V_{max2}: 2000	N5,N10-methenyl-THF: 250 N10-formyl-THF: 100	-
MTD	5,10-Methylenetetrahydrofolate dehydrogenase	V_{max1}: 20000 V_{max2}: 59400	N5,N10-methylene-THF: 2 N5,N10-methenyl-THF: 10	-
MTHFR	5,10-Methylene-tetrahydrofolate reductase	660	N5,N10-methylene-THF: 50	NADPH:16
MS	Methionine synthase	525	N5-methyl-THF: 25	Homocysteine: 0.1
MTS	Methenyltetrahydrofolate synthetase, also known as 5-formyl-THF cyclo-ligase	800	N5-formyltetrahydrofolate: 2	-

Table 4.8 Continued

Abbreviation	Enzyme	V_{max} (μM/hr)	K_{M1} (μM)	K_{M2} (μM)
PGT	Phosphoribosyl glycinamide detransformylase	9720	N10-formyltetrahydrofolate: 4.9	GAR: 520
SHMT	Serine hydroxymethyl-transferase	4000	THF: 50	Serine: 600
TS	Thymidylate synthase	562.5	N5,N10-methylenetetrahydrofolate: 14	dUMP: 6.3

Most come from the Brenda database (https://www.brenda-enzymes.org/). Additional values are from LeDuc et al. [79] The FolM V_{max} was scaled to the DHFR value based on their respective k_{cat} values (see Table 4.4).

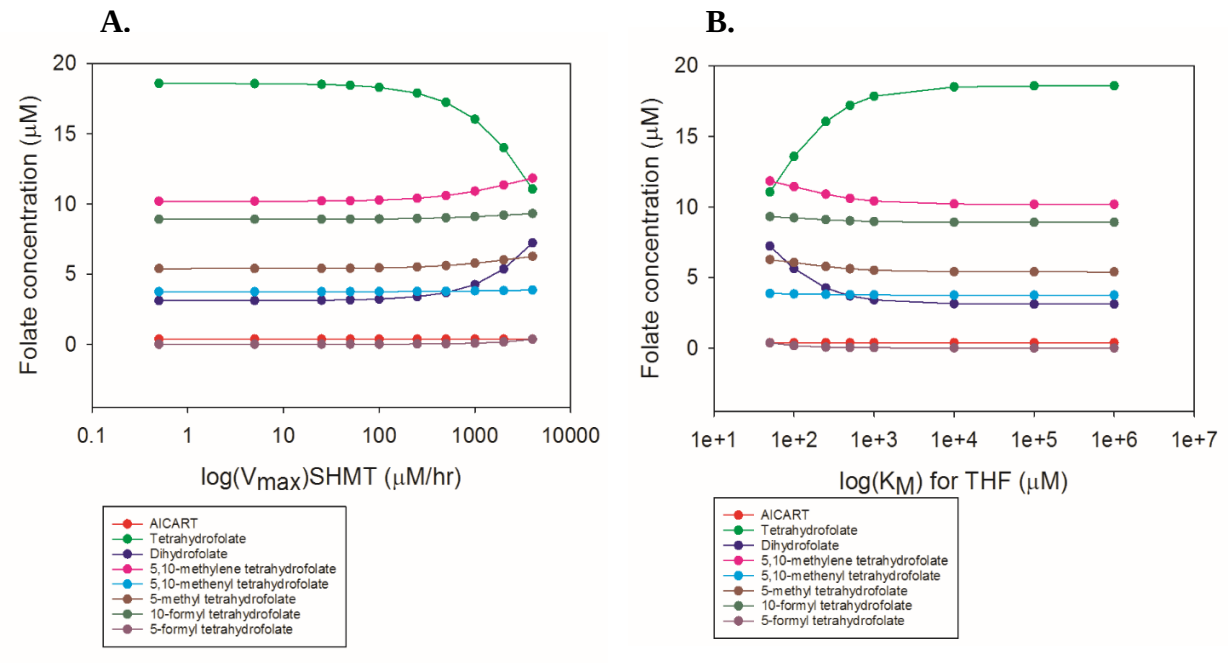

Figure 4.20: Mathematical modeling of SHMT activity impacted by osmotic stress

The reactions are described in Figure 4.19. Panels A and B show the effects of decreasing the V_{max} or increasing the K_M values for SHMT, respectively. As a second reaction catalyzed by SHMT is conversion of N5,N10-methenyl-THF to 5-formyl-THF, effects on this reaction were also entered in the mathematical model. For example, if a 10x effect was entered for the SHMT main reaction, a 10x effect was additionally entered for the SHMT2 reaction. The concentrations of various folate redox states are shown. Panel A should be read from right to left while panel B should be read from left to right

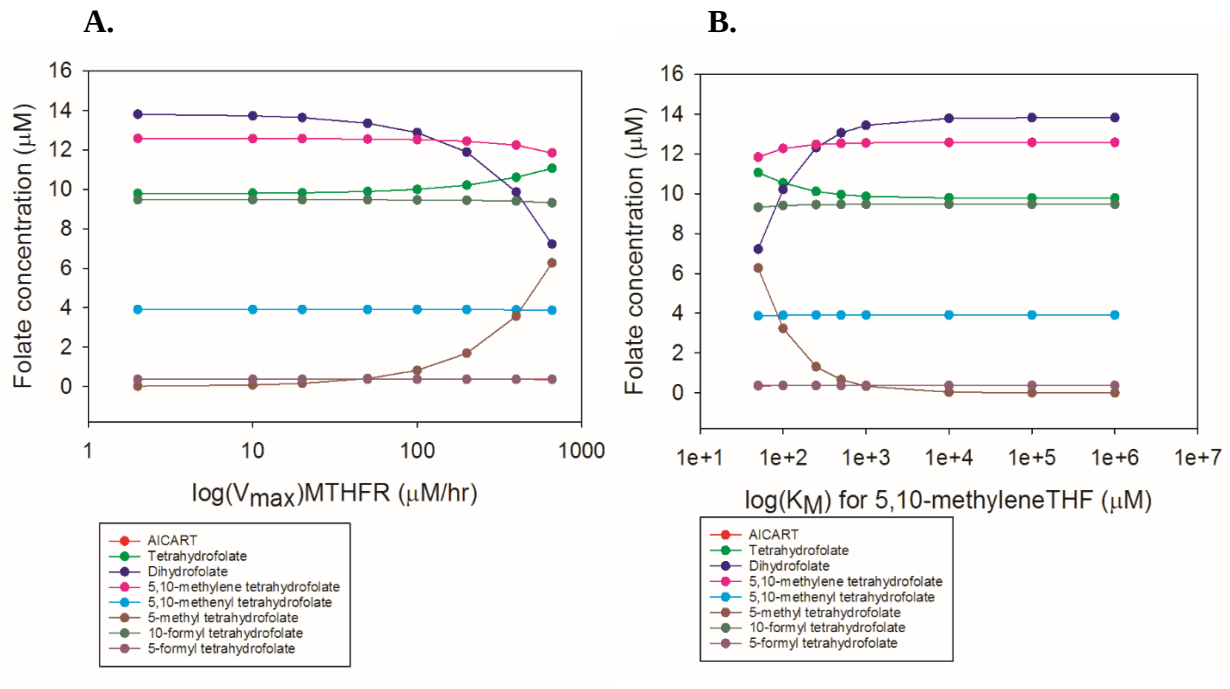

Figure 4.21: The impact of osmotic stress on MTHFR activity as fit to a mathematical model

The reactions are described in Figure 4.19. Panels A and B show the effects of decreasing the V_{max} or increasing the K_M values for MTHFR, respectively. The concentrations of various folate redox states are shown. Panel A should be read from right to left while panel B should be read from left to right. (AICART levels are hidden behind those of 5-formyl THF, i.e the values are similar).

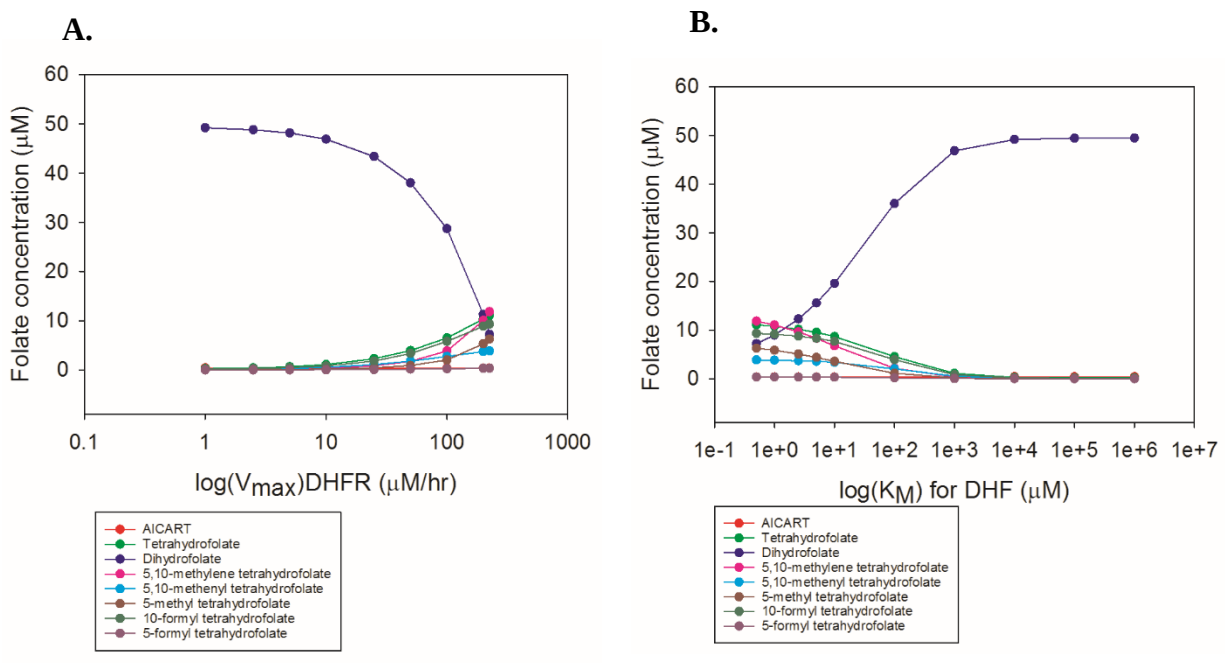

Figure 4.22: Osmotic stress titrations of DHFR activity as predicted by a mathematical model

The reactions are described in Figure 4.19. Panels A and B show the effects of decreasing the V_{max} or increasing the K_M values for DHFR, respectively. The concentrations of various folate redox states are shown. Panel A should be read from right to left while panel B should be read from left to right.

Not surprisingly, decreasing the V_{max} of SHMT leads to accumulation of its substrate, THF, and decreases in its product concentration (N5,N10-methylene-THF, see panel A of Figure 4.20). As glycine decarboxylase can also generate N5,N10- methylene-THF, the concentration of N5,N10-methylene-THF plateaus rather than being reduced to zero. There is also a depletion of 5-formyl-THF as a secondary reaction of SHMT is formation of 5-formyl-THF from methenyl-THF [73]. Surprisingly, the DHF concentration also decreases as the velocity of SHMT decreases. This situation arises as the thymidylate synthase velocity is sufficiently high (and the enzyme is not running at V_{max}) to form DHF, while the DHFR rate is almost at V_{max} and the FolM rate is small. These fluxes result in a build-up of DHF. Effects on the K_M of SHMT provide similar patterns (see panel B of Figure 4.20). In either case (lowered V_{max} or increased K_M), a decreased catalytic efficiency occurs.

Effects on MTHFR are similar to those predicted for SHMT, i.e. an increase in substrate concentration (N5, N10-methylene-THF) and loss of product concentration (5-methyl-THF, see Figure 4.21). As seen for the above loss of SHMT activity, the DHF levels increase due to the high flux through the thymidylate synthase reaction coupled with a low flux through DHFR and FolM. Changes in other folate redox state concentrations are minor. As there are no other reactions in the model that produce 5-methyl-THF, its concentration goes to zero. Since 5-methyl-THF leads into the methionine cycle, it is anticipated that this cycle will also be affected [82, 83].

Finally, use of the mathematical model to predict effects of osmotic pressure on DHFR activity *in vivo* finds that the DHF concentration rises and the THF concentration decreases (see Figure 4.22 panels A, B). Loss of DHFR function leads to depletion of [THF], which in turn leads to catastrophic loss of the other folate redox states. As a double knockout of DHFR and FolM is synthetic lethal [81] and as the catalytic efficiency of FolM is ~400 fold less efficient than EcDHFR (or 4 fold less than R67 DHFR) and as FolM is also affected by osmotic stress [8], we predicted what would happen if its activity were additionally titrated (in parallel to that of R67 DHFR). For this case, the concentrations of all folate species (except DHF) drop further (plots not shown).

For all the examples provided above, to the extent that other folate pathway enzymes are affected by osmotic stress, they can amplify the observed effects.

4.6 Discussion

4.6.1 The complexity and heterogeneity of the cell

The complexity of the cell provide many possible scenarios for how and why our osmotic stress titrations of enzyme activity may occur. Table 4.9 lists a few of the important variables which are protein concentration, the activity of the enzyme under cellular conditions, how the various solutes interact and the identity of the osmolytes in *E. coli*.

Table 4.9: Potential contributing factors associated with in vivo titrations

Variable	**Modulation by**
Protein concentration	Removed in knockout *E. coli* strains; re-added at tunable levels using the P_{tet} promoter and tetracycline in pKTS plasmid [a]
	Minimized via use of SsrA degradation tag in pKTS [a]
	Proteins can be stabilized or destabilized by interaction with osmolytes [b] and/or crowders [c]
	Enzyme activity can be modulated by interactions with neighboring macromolecules [d]
	Altered protein expression levels possible due to osmotic stress [e]
	May be affected by folding mechanism associated with oligomerization, e.g. if monomer can fold coming off the ribosome, it may be more stable than if an unfolded monomer needs another monomer to be synthesized to form a dimer
Enzyme activity	k_{on} and k_{off} rates as well as k_{cat}/K_m can be altered by interaction with crowders as well as increased viscosity upon addition of osmolytes and/or crowders. At high [substrate], if chemistry is rate determining, then viscosity will likely have minimal effects [f]
	Substrate capture (e.g. k_{cat}/K_m) can be rate determining at low [substrate]. [g]
	If enzyme activity is inhibited by osmotic stress, the [substrate] will rise
[Substrate] and [cofactor] in cell	Weak interaction of ligands with osmolytes for example, folate interaction with trehalose and betaine, can lower the concentration of **free** ligand [h]
	Weak interaction of ligands with macromolecular surfaces for example, folate interaction with lysozyme, BSA, and others can lower the concentration of **free** ligand [i]
	Gene knockout results in buildup of the [substrate] for the encoded enzyme
	No metabolomics information on folate redox state concentrations or NADPH in *E. coli* under osmotic stress [j]
	Exclusion of osmolytes from NADPH can tighten binding [k]
Domino effects	Buildup in [substrate] of inhibited enzymes can inhibit other enzymes in pathway. For example, inhibition of DHFR by trimethoprim results in buildup of [DHF] which in turn inhibits folyl-polyglutamate synthase [l]
	Inhibition of one enzyme will deplete the concentration of its product, which as the substrate of another enzyme, will reduce this rate as well. For example, a mathematical model of folate liver metabolism predicts >90% inhibition of DHFR is necessary to affect thymidylate synthase activity [m]

Table 4.9 Continued

Variable	Modulation by
Identity of osmolytes in *E. coli*	Normally trehalose is produced as an osmoprotectant against low water conditions. [n] Addition of betaine to the media results in its uptake and higher growth rates due to the preferential exclusion mechanism. Cells cannot grow when no free water remains (~1.9 Osm). [o]
	Addition of betaine switches *E. coli* to fermentative pathways at high [NaCl]. [p]

[a] From reference [27]
[b] From references [84, 85]
[c] From references [21, 86, 87]
[d] From reference [21, 90, 91]
[e] From references [66, 92-96].
[f] From references [49, 97-101]
[g] From references [102-104]
[h] From references [8-11, 13]
[i] From unpublished data and references [11, 105]
[j] From reference [106]
[k] From references [8-10]
[l] From reference [35]
[m] From reference [107]
[n] From reference [108]
[o] From reference [7]
[p] From reference [92]

A prime consideration is the protein concentration, which needs to be tightly controlled. Since *E. coli* are normally able to grow until ~1.9 Osm [7], the protein dose needs to be lower than that offered by chromosomal expression. The tunable plasmid, pKTS, provides a path to achieve low expression levels via use of the Ptet promoter and the SsrA degradation tag. Additionally, protein stability (and thus turnover) can be affected by the presence of osmolytes [84, 85], crowders [21, 86, 87] and/or volume exclusion [88, 89]. Both stabilization [84, 86] and destabilization [86, 87] have been observed.

A second important parameter is the available ligand concentration. For example, the glutamate tail of folate prefers to interact with water while the pterin and benzoyl groups prefer to interact with betaine [13]. If the weak folate•osmolyte or folate•crowder interactions are more difficult to break than the folate•water interaction, then binding to an enzyme partner is weakened (or restated, the binding equilibrium is shifted towards the free, unbound enzyme). This type of situation occurs with DHFR function in vitro [8-10]. It may also apply to ATP as an all atom molecular dynamics model of the Mycoplasma genitalium cytoplasm found ATP often associated with protein surfaces [86]. Most recently, ATP has been suggested to act as a biological hydrotrope, being able to decrease protein aggregation and liquid-liquid phase transitions [109]. In these examples, ligands weakly interact with macromolecular surfaces. If dissociation from these surfaces is slower than desolvation, then the concentration of free ligand available for binding to its specific enzyme partner is decreased. Additionally, Zotter et al. have recently studied TEM1-β-lactamase activity in Hela cells [105]. As the logP for the microinjected substrate is 4.5, they find slower diffusion rates than for a fused mCherry-lactamase construct. They modeled the reaction as having a soft interaction with macromolecule(s) X and proposed release of substrate from X as the slow step in the *in vivo* reaction.

Ligand concentration can also be altered by use of a deletion strain or an inhibitor or decreased enzyme expression levels. With low to no enzyme activity, the concentration of its substrate builds up. This can provide a domino effect if the increased substrate concentration inhibits another enzyme in the pathway. An example of this is inhibition of chromosomal E. coli DHFR by trimethoprim which results in an increased DHF concentration, which in turn inhibits folyl-polyglutamate synthase [35]. A related factor upon enzyme inhibition is loss of its product, which can limit the activity of downstream enzymes [110].

A third issue is how enzyme activity can be modulated by osmolytes and/or crowders. Enzyme activity can be either enhanced or decreased in vitro, depending on the identity of the enzyme, ligand and osmolyte or crowder added. Activities that are enhanced likely follow a preferential exclusion model where osmolytes are excluded from protein surfaces [111], while activities that are decreased likely follow a preferential interaction model where osmolytes act as a co-solvent and interact with the protein or ligand surface, albeit weakly. Acosta et al. summarize crowding effects for 32 different studies and conclude “a one-size-fits-all theory cannot fully reduce or explain the effects of crowding on enzyme kinetics” [101]. A related issue is altered viscosity, which can diminish enzyme activity by affecting either substrate binding, product release or altering any conformational changes in the enzyme [49, 97-100, 112]. Most enzymes listed in Table 4.4 have chemistry as their rate determining steps, suggesting viscosity effects might be minimal under saturating substrate conditions. Also, in Figure 4.6, Quad4-pKTS allows growth of the Δ*folA* cells at

1.06 Osm while R67 DHFR-pKTS allows growth to ≤ 0.87 Osm (a larger difference would exist if confluent lawns are considered vs. single colony growth). Here, Quad4 may serve as an internal control for R67 DHFR, as presumably the internal viscosity of the *E. coli* cells would be higher in the higher osmolality conditions. These various considerations suggest viscosity effects could play a role but likely do not dominate.

Another factor is the identity of the osmoprotectants produced by the organism in response to osmotic stress. *E. coli* produce trehalose, K^+ and glutamate in response to osmotic pressure [3-6]. *E. coli* take up betaine when it is added to the media; this typically allows cells to grow to higher osmolalities as betaine has been proposed to be the most excluded osmolyte from protein surfaces [7, 69]. The preferential interaction coefficient (μ_{23}/RT) measures whether a molecule prefers to be solvated by water or to interact with osmolytes present. Table 4.10 provides predicted μ_{23}/RT values for the substrates of the enzymes involved in this study with respect to trehalose and betaine. A positive value indicates a preference for solvation by water while a negative value supports interaction with the osmolyte. A value of zero indicates both osmolyte and water interact equally well. All the folates show negative to zero values, suggesting their likely interaction with trehalose, betaine and/or protein surfaces displaying these functional groups.

Even though the above discussion indicates many factors may be involved, the prime effect in our experiments appears to be a decreased enzyme activity, modulated by either the protein concentration and/or the availability of substrate. Another possibility is enzyme-osmolyte interactions that decrease k_{cat} or k_{cat}/K_m. This statement arises from the above discussion as well as the pKTS plasmid which lets us target the effect of a low protein dose for one specific protein in osmotic stress. Here we consider that all the strains are related and have sufficient protein doses to grow at high osmolalities except for the strain that under-expresses one protein. While the osmotic stress conditions could be affecting other proteins, their dose is sufficiently high to be able to tolerate these environmental changes. Rather it is the low dose enzyme that is sensitive to the altered milieu.

4.6.2 Which titrations worked and why?

The activities of wt R67 DHFR, SHMT, MTHFR, and CM are titratable *in vivo* by osmotic stress. One parameter associated with these enzymes is that they all have relatively low k_{cat} values (see Table 4.4). This likely enables titration of enzyme activity.

Another observation is that all these enzymes are oligomers, which allows presentation of multiple SsrA tags. Avidity effects due to multiple SsrA tags may aid proteolysis. Also folding pathways that involve unfolded monomeric intermediates could play a role.

While the folate pathway enzymes were predicted to be titratable based on their μ23/RT values (see Table 4.10), our results with chorismate mutase were a surprise. Why might the activity of CM be sensitive to osmotic stress *in vivo*? A first reason is if the hexameric mutant CM protein is unstable at low concentrations. Additionally, the presence of six SsrA tags should lead to rapid degradation. Another possibility is effects of the osmolytes on the enzyme.

Table 4.10: Predicted μ_{23}/RT values for various ligands associated with the enzymes studied

Enzyme	Ligand	Betaine μ_{23}/RT (m^{-1})[a]	Trehalose μ_{23}/RT (m^{-1}) [b]	Glutamate μ_{23}/RT (m^{-1}) [c]	LogP [d]
DHFR	NADPH	0.983	-0.408	0.781	-7.183
	DHF	-0.049	-0.110	0.650	-3.409
	$NADP^+$	1.051	-0.768	0.815	-7.417
	THF	-0.112	-0.122	0.547	-3.892
	Trimethoprim	-0.744	0.468	0.568	1.258
Serine-hydroxymethyl transferase	Serine	0.160	0.018	0.080	-3.661
	Glycine	0.156	-0.038	0.020	-3.022
	THF	-0.112	-0.122	0.547	-3.892
	5,10-methyleneTHF	-0.053	-0.105	0.712	-3.814
	Pyridoxal 5'-phosphate	0.820	-0.676	0.422	-1.550
Chorismate mutase	Chorismate	0.430	0.140	0.508	-2.758
	Prephenate	0.563	-0.006	0.451	-3.081
	Tyrosine	-0.200	0.007	0.136	-1.705
	Phenylalanine	-0.340	0.029	0.307	-1.411
Methylene tetrahydrofolate reductase	NADH	0.160	0.277	0.766	-4.967
	5,10-methyleneTHF	-0.053	-0.105	0.712	-3.814
	FAD	0.999	-0.651	1.159	-5.090
	5-methyl-THF	-0.089	-0.145	0.694	-3.550
	NAD^+	-0.169	0.112	0.793	-5.200

[a] Values calculated from reference [13] using equation 4.
[b] Values calculated from reference [18].
[c] Values calculated from reference [17].
[d] LogP values were calculated using MOE version 2015.1001

Substrates are listed in black; products are listed in blue; inhibitors are listed in red and pathway end products are listed in green

4.7 Conclusion

Mutations that provide some resistance to osmotic stress in bacteria identify differential expression of RNA polymerases, overproduction of osmolytes, increased transport of osmolytes, defective *N*-acetylglucosamine catabolism and mutations in the cell shape-regulating protein MreB [113-116]. In contrast, we took an under-expression approach and found that in the absence of external osmolyte, four different complemented strains can grow in minimal media at a low protein dosage. However, placing these cells in high osmolality conditions blocks growth. What is it about this combination of high osmolality and low enzyme activity that inhibits cell growth? Our *in vitro* studies suggest that water activity is critically important to catalytic efficiency and that weak folate-osmolyte interactions likely play a role, making it more difficult for proteins to find and bind their substrates/inhibitors/cofactors While other factors may also be important (Table 4.9), our study introduces the new possibility of osmolyte/crowder interactions with ligands influencing catalytic efficiency *in vivo*. This scenario could be an example of negative design, as these difficulties are not normally seen as protein expression levels are sufficient to allow cell growth at high osmolalities, indicating *E. coli* have evolved to deal with variations in their osmotic environment. Further study will let us know whether these titrations are restricted to folate metabolism or whether the activities of other enzymes can be titrated.

4.8 References

[1] Yancey, P. H., Clark, M. E., Hand, S. C., Bowlus, R. D., and Somero, G. N. (1982) Living with water stress: evolution of osmolyte systems, *Science 217*, 1214-1222.

[2] Bolen, D. W. (2001) Protein stabilization by naturally occurring osmolytes, *Methods Mol. Biol. 168*, 17-36.

[3] Larsen, P. I., Sydnes, L. K., Landfald, B., and Strom, A. R. (1987) Osmoregulation in *Escherichia coli* by accumulation of organic osmolytes: betaines, glutamic acid, and trehalose, *Arch. Microbiol. 147*, 1-7.

[4] Wood, J. M. (2011) Bacterial osmoregulation: a paradigm for the study of cellular homeostasis, *Annu. Rev. Microbiol. 65*, 215-238.

[5] Record, M. T., Jr., Courtenay, E. S., Cayley, D. S., and Guttman, H. J. (1998) Responses of *E. coli* to osmotic stress: large changes in amounts of cytoplasmic solutes and water, *Trends Biochem. Sci. 23*, 143-148.

[6] Record, M. T., Jr., Courtenay, E. S., Cayley, S., and Guttman, H. J. (1998) Biophysical compensation mechanisms buffering *E. coli* protein-nucleic acid interactions against changing environments, *Trends Biochem. Sci. 23*, 190-194.

[7] Cayley, S., and Record, M. T., Jr. (2003) Roles of cytoplasmic osmolytes, water, and crowding in the response of Escherichia coli to osmotic stress: biophysical basis of osmoprotection by glycine betaine, *Biochemistry 42*, 12596-12609.

[8] Bhojane, P., Duff Jr., M. R., Patel, H. C., Vogt, M. E., and Howell, E. E. (2014) Investigation of osmolyte effects on FolM: comparison with other dihydrofolate reductases, *Biochemistry 53*, 1330-1341.

[9] Chopra, S., Dooling, R., Horner, C. G., and Howell, E. E. (2008) A balancing act: Net uptake of water during dihydrofolate binding and net release of water upon NADPH binding in R67 dihydrofolate reductase, *J. Biol. Chem. 283*, 4690-4698.

[10] Grubbs, J., Rahmanian, S., Deluca, A., Padmashali, C., Jackson, M., Duff, M. R., and Howell, E. E. (2011) Thermodynamics and solvent effects on substrate and cofactor binding in *Escherichia coli* chromosomal dihydrofolate reductase, *Biochemistry 50*, 3673-3685.

[11] Duff, J., M.R. , Grubbs, J., Serpersu, E. H., and Howell, E. E. (2012) Weak interactions between folate and osmolytes in solution, *Biochemistry 51*, 2309−2318.

[12] Timson, M. J., Duff, J., M.R. , Dickey, G., Saxton, A. M., Reyes-De-Corcuera, J., and Howell, E. E. (2013) Further studies on the role of water in R67 dihydrofolate reductase, *Biochemistry 52*, 2118–2127.

[13] Bhojane, P. P., Duff, M. R., Jr., Bafna, K., Rimmer, G. P., Agarwal, P. K., and Howell, E. E. (2016) Aspects of weak interactions between folate and glycine betaine, *Biochemistry 55*, 6282-6294.

[14] Capp, M. W., Pegram, L. M., Saecker, R. M., Kratz, M., Riccardi, D., Wendorff, T., Cannon, J. G., and Record, J., M.T. (2009) Interactions of the osmolyte glycine betaine with molecular surfaces in water: thermodynamics, structural interpretation, and prediction of m-values, *Biochemistry 48*, 10372–10379.

[15] Guinn, E. J., Kontur, W. S., Tsodikov, O. V., Shkel, I., and Record, M. T., Jr. (2013) Probing the protein-folding mechanism using denaturant and temperature effects on rate constants, *Proc. Natl. Acad. Sci. U. S. A. 110*, 16784-16789.

[16] Knowles, D. B., Shkel, I. A., Phan, N. M., Sternke, M., Lingeman, E., Cheng, X., Cheng, L., O'Connor, K., and Record, M. T. (2015) Chemical interactions of polyethylene glycols (PEGs) and glycerol with protein functional groups: applications to effects of PEG and glycerol on protein processes, *Biochemistry 54*, 3528-3542.
[17] Cheng, X., Guinn, E. J., Buechel, E., Wong, R., Sengupta, R., Shkel, I. A., and Record, M. T., Jr. (2016) Basis of protein stabilization by K glutamate: unfavorable interactions with carbon, oxygen groups, *Biophys. J. 111*, 1854-1865.
[18] Hong, J., Gierasch, L. M., and Liu, Z. (2015) Its preferential interactions with biopolymers account for diverse observed effects of trehalose, *Biophys. J. 109*, 144-153.
[19] Wood, J. M. (2015) Bacterial responses to osmotic challenges, *J. Gen. Physiol. 145*, 381-388.
[20] Miklos, A. C., Li, C., Sharaf, N. G., and Pielak, G. J. (2010) Volume exclusion and soft interaction effects on protein stability under crowded conditions, *Biochemistry 49*, 6984-6991.
[21] Cohen, R. D., and Pielak, G. J. (2017) A cell is more than the sum of its (dilute) parts: a brief history of quinary structure, *Protein Sci. 26*, 403-413.
[22] Chien, P., and Gierasch, L. M. (2014) Challenges and dreams: physics of weak interactions essential to life, *Mol. Biol. Cell 25*, 3474-3477.
[23] Wang, Q., Zhuravleva, A., and Gierasch, L. M. (2011) Exploring weak, transient protein-protein interactions in crowded *in vivo* environments by in-cell nuclear magnetic resonance spectroscopy, *Biochemistry 50*, 9225-9236.
[24] Smith, A. E., Zhou, L. Z., Gorensek, A. H., Senske, M., and Pielak, G. J. (2016) In-cell thermodynamics and a new role for protein surfaces, *Proc. Natl. Acad. Sci. U. S. A. 113*, 1725-1730.
[25] Spitzer, J. (2011) From water and ions to crowded biomacromolecules: in vivo structuring of a prokaryotic cell, *Microbiol. Mol. Biol. Rev. 75*, 491-506.
[26] Spitzer, J., and Poolman, B. (2013) How crowded is the prokaryotic cytoplasm?, *FEBS Lett. 587*, 2094-2098.
[27] Neuenschwander, M., Butz, M., Heintz, C., Kast, P., and Hilvert, D. (2007) A simple selection strategy for evolving highly efficient enzymes, *Nat. Biotech. 25*, 1145-1147.
[28] Howell, E. E., Foster, P. G., and Foster, L. M. (1988) Construction of a dihydrofolate reductase-deficient mutant of *Escherichia coli* by gene replacement, *J. Bacteriol. 170*, 3040-3045.
[29] Baba, T., Ara, T., Hasegawa, M., Takai, Y., Okumura, Y., Baba, M., Datsenko, K. A., Tomita, M., Wanner, B. L., and Mori, H. (2006) Construction of *Escherichia coli* K-12 in-frame, single-gene knockout mutants: the Keio collection, *Mol. Systems Biol. 2*, 2006 0008.
[30] Vogel, H. J., and Bonner, D. M. (1956) Acetylornithinase of *Escherichia coli*: partial purification and some properties, *J. Biol. Chem. 218*, 97-106.
[31] Singer, S., Ferone, R., Walton, L., and Elwell, L. (1985) Isolation of a dihydrofolate reductase-deficient mutant of *Escherichia coli*, *J. Bacteriol. 164*, 470-472.

[32] Kast, P., Asif-Ullah, M., Jiang, N., and Hilvert, D. (1996) Exploring the active site of chorismate mutase by combinatorial mutagenesis and selection: the importance of electrostatic catalysis, *Proc. Natl. Acad. Sci. U. S. A. 93*, 5043-5048.
[33] Colquhoun, T. A., Schimmel, B. C. J., Kim, J. Y., Reinhardt, D., Cline, K., and Clark, D. G. (2010) A petunia chorismate mutase specialized for the production of floral volatiles, *Plant J. 61*, 145-155.
[34] Perry, K. M., Carreras, C. W., Chang, L. C., Santi, D. V., and Stroud, R. M. (1993) Structures of thymidylate synthase with a C-terminal deletion: role of the C-terminus in alignment of 2'-deoxyuridine 5'-monophosphate and 5,10-methylenetetrahydrofolate, *Biochemistry 32*, 7116-7125.
[35] Kwon, Y. K., Lu, W., Melamud, E., Khanam, N., Bognar, A., and Rabinowitz, J. D. (2008) A domino effect in antifolate drug action in *Escherichia coli*, *Nat. Chem. Biol. 4*, 602-608.
[36] Bennett, B. D., Kimball, E. H., Gao, M., Osterhout, R., Van Dien, S. J., and Rabinowitz, J. D. (2009) Absolute metabolite concentrations and implied enzyme active site occupancy in *Escherichia coli*, *Nat. Chem. Biol. 5*, 593-599.
[37] Reece, L. J., Nichols, R., Ogden, R. C., and Howell, E. E. (1991) Construction of a synthetic gene for an R-plasmid-encoded dihydrofolate reductase and studies on the role of the N-terminus in the protein, *Biochemistry 30*, 10895-10904.
[38] Park, H., Zhuang, P., Nichols, R., and Howell, E. E. (1997) Mechanistic studies of R67 dihydrofolate reductase. Effects of pH and an H62C mutation, *J. Biol. Chem. 272*, 2252-2258.
[39] Narayana, N., Matthews, D. A., Howell, E. E., and Nguyen-huu, X. (1995) A plasmid-encoded dihydrofolate reductase from trimethoprim-resistant bacteria has a novel D2-symmetric active site, *Nat. Struct. Biol. 2*, 1018-1025.
[40] Feng, J., Grubbs, J., Dave, A., Goswami, S., Horner, C. G., and Howell, E. E. (2010) Radical redesign of a tandem array of four R67 dihydrofolate reductase genes yields a functional, folded protein possessing 45 substitutions, *Biochemistry 49*, 7384-7392.
[41] Trimmer, E. E., Ballou, D. P., and Matthews, R. G. (2001) Methylenetetrahydrofolate reductase from Escherichia coli: elucidation of the kinetic mechanism by steady-state and rapid-reaction studies, *Biochemistry 40*, 6205-6215.
[42] Guenther, B. D., Sheppard, C. A., Tran, P., Rozen, R., Matthews, R. G., and Ludwig, M. L. (1999) The structure and properties of methylenetetrahydrofolate reductase from *Escherichia coli* suggest how folate ameliorates human hyperhomocysteinemia, *Nat. Struct. Biol. 6*, 359-365.
[43] Misra, S. K., and Bhakuni, V. (2003) Unique holoenzyme dimers of the tetrameric enzyme Escherichia coli methylenetetrahydrofolate reductase: characterization of structural features associated with modulation of the enzyme's function, *Biochemistry 42*, 3921-3928.
[44] Schirch, V., Hopkins, S., Villar, E., and Angelaccio, S. (1985) Serine hydroxymethyltransferase from Escherichia coli: purification and properties, *J. Bacteriol. 163*, 1–7.
[45] Schirch, D., Delle Fratte, S., Iurescia, S., Angelaccio, S., Contestabile, R., Bossa, F., and Schirch, V. (1993) Function of the active-site lysine in *Escherichia coli* serine hydroxymethyltransferase, *J. Biol. Chem. 268*, 23132-23138.

[46] Florio, R., Chiaraluce, R., Consalvi, V., Paiardini, A., Catacchio, B., Bossa, F., and Contestabile, R. (2009) The role of evolutionarily conserved hydrophobic contacts in the quaternary structure stability of *Escherichia coli* serine hydroxymethyltransferase, *FEBS J. 276*, 132-143.
[47] MacBeath, G., Kast, P., and Hilvert, D. (1998) Probing enzyme quaternary structure by combinatorial mutagenesis and selection, *Protein Sci. 7*, 1757-1767.
[48] Guilford, W. J., Copley, S. D., and Knowles, J. R. (1987) On the mechanism of the chorismate mutase reaction, *J. Am. Chem. Soc. 109*, 5013-5019.
[49] Mattei, P., Kast, P., and Hilvert, D. (1999) *Bacillus subtilis* chorismate mutase is partially diffusion-controlled, *Eur. J. Biochem. 261*, 25-32.
[50] Howell, E. E. (2005) Searching sequence space: two different approaches to dihydrofolate reductase catalysis, *ChemBioChem 6*, 590-600.
[51] Stone, S. R., and Morrison, J. F. (1986) Mechanism of inhibition of dihydrofolate reductases from bacterial and vertebrate sources by various classes of folate analogues, *Biochim. Biophys. Acta 869*, 275-285.
[52] Amyes, S. G., and Smith, J. T. (1976) The purification and properties of the trimethoprim-resistant dihydrofolate reductase mediated by the R-factor, R388, *Eur. J. Biochem. 61*, 597-603.
[53] Stinnett, L. G., Smiley, R. D., Hicks, S. N., and Howell, E. E. (2004) "Catch 222," the effects of symmetry on ligand binding and catalysis in R67 dihydrofolate reductase as determined by mutations at Tyr-69, *J. Biol. Chem. 279*, 47003-47009.
[54] Newton, M. S., Guo, X., Soderholm, A., Nasvall, J., Lundstrom, P., Andersson, D. I., Selmer, M., and Patrick, W. M. (2017) Structural and functional innovations in the real-time evolution of new (betaalpha)8 barrel enzymes, *Proc. Natl. Acad. Sci. U. S. A. 114*, 4727-4732.
[55] Butz, M., Neuenschwander, M., Kast, P., and Hilvert, D. (2011) An N-terminal protein degradation tag enables robust selection of highly active enzymes, *Biochemistry 50*, 8594-8602.
[56] Neuenschwander, M., Kleeb, A. B., Kast, P., and Hilvert, D. (2009) Equipping *in vivo* selection systems with tunable stringency, In *Protein Engineering Handbook* (Lutz, S., and Bornscheuer, U. T., Eds.), pp 537-561, Wiley-VCH, Weinheim.
[57] Nichols, R. J., Sen, S., Choo, Y. J., Beltrao, P., Zietek, M., Chaba, R., Lee, S., Kazmierczak, K. M., Lee, K. J., Wong, A., Shales, M., Lovett, S., Winkler, M. E., Krogan, N. J., Typas, A., and Gross, C. A. (2011) Phenotypic landscape of a bacterial cell, *Cell 144*, 143-156.
[58] Jeanson, S., Floury, J., Gagnaire, V., Lortal, S., and Thierry, A. (2015) Bacterial colonies in solid media and foods: a review on their growth and interactions with the micro-environment, *Front. Microbiol. 6*.
[59] Hachicho, N., Birnbaum, A., and Heipieper, H. J. (2017) Osmotic stress in colony and planktonic cells of *Pseudomonas putida* mt-2 revealed significant differences in adaptive response mechanisms, *AMB Express 7*, 62.
[60] Li, B., Qiu, Y., Shi, H., and Yin, H. (2016) The importance of lag time extension in determining bacterial resistance to antibiotics, *The Analyst 141*, 3059-3067.
[61] Konopka, M. C., Shkel, I. A., Cayley, S., Record, M. T., and Weisshaar, J. C. (2006) Crowding and confinement effects on protein diffusion in vivo, *J. Bacteriol. 188*, 6115-6123.

[62] Sevin, D. C., Stahlin, J. N., Pollak, G. R., Kuehne, A., and Sauer, U. (2016) Global metabolic responses to salt stress in fifteen species, *PloS one 11*, e0148888.
[63] Bren, A., Park, J. O., Towbin, B. D., Dekel, E., Rabinowitz, J. D., and Alon, U. (2016) Glucose becomes one of the worst carbon sources for *E.coli* on poor nitrogen sources due to suboptimal levels of cAMP, *Sci. Rep. 6*, 24834.
[64] Aidelberg, G., Towbin, B. D., Rothschild, D., Dekel, E., Bren, A., and Alon, U. (2014) Hierarchy of non-glucose sugars in *Escherichia coli*, *BMC Syst. Biol. 8*, 133.
[65] Hirasawa, T., Ashitani, K., Yoshikawa, K., Nagahisa, K., Furusawa, C., Katakura, Y., Shimizu, H., and Shioya, S. (2006) Comparison of transcriptional responses to osmotic stresses induced by NaCl and sorbitol additions in *Saccharomyces cerevisiae* using DNA microarray, *J. Biosci. Bioeng. 102*, 568-571.
[66] Weber, A., Kogl, S. A., and Jung, K. (2006) Time-dependent proteome alterations under osmotic stress during aerobic and anaerobic growth in *Escherichia coli*, *J. Bacteriol. 188*, 7165-7175.
[67] Ndimba, B. K., Chivasa, S., Simon, W. J., and Slabas, A. R. (2005) Identification of *Arabidopsis* salt and osmotic stress responsive proteins using two-dimensional difference gel electrophoresis and mass spectrometry, *Proteomics 5*, 4185-4196.
[68] Allakhverdiev, S. I., Sakamoto, A., Nishiyama, Y., Inaba, M., and Murata, N. (2000) Ionic and osmotic effects of NaCl-induced inactivation of photosystems I and II in *Synechococcus* sp, *Plant. Physiol. 123*, 1047-1056.
[69] Courtenay, E. S., Capp, M. W., Anderson, C. F., and Record, M. T., Jr. (2000) Vapor pressure osmometry studies of osmolyte-protein interactions: implications for the action of osmoprotectants in vivo and for the interpretation of "osmotic stress" experiments *in vitro*, *Biochemistry 39*, 4455-4471.
[70] Venkatesu, P., Lee, M. J., and Lin, H. M. (2009) Osmolyte counteracts urea-induced denaturation of alpha-chymotrypsin, *J. Phys. Chem. B 113*, 5327-5338.
[71] Belluzo, S., Boeris, V., Farruggia, B., and Pico, G. (2011) Influence of stabilizers cosolutes on catalase conformation, *Int. J. Biol. Macromol. 49*, 936-941.
[72] Bourot, S., Sire, O., Trautwetter, A., Touze, T., Wu, L. F., Blanco, C., and Bernard, T. (2000) Glycine betaine-assisted protein folding in a *lysA* mutant of *Escherichia coli*, *J. Biol. Chem. 275*, 1050-1056.
[73] Stover, P., and Schirch, V. (1990) Serine hydroxymethyltransferase catalyzes the hydrolysis of 5,10-methenyltetrahydrofolate to 5-formyltetrahydrofolate, *J. Biol. Chem. 265*, 14227-14233.
[74] Matthews, R. G., and Drummond, J. T. (1990) Providing one-carbon units for biological methylations: mechanistic studies on serine hydroxymethyltransferase, methylenetetrahydrofolate reductase, and methyltetrahydrofolate-homocysteine methyltransferase, *Chem. Rev. 90*, 1275-1290.
[75] Contestabile, R., Paiardini, A., Pascarella, S., di Salvo, M. L., D'Aguanno, S., and Bossa, F. (2001) l-Threonine aldolase, serine hydroxymethyltransferase and fungal alanine racemase. A subgroup of strictly related enzymes specialized for different functions, *Eur. J. Biochem. 268*, 6508-6525.
[76] Amyes, S. G., and Smith, J. T. (1974) Trimethoprim action and its analogy with thymine starvation, *Antimicrob. Agents Chemother. 5*, 169-178.
[77] Quinlivan, E. P., McPartlin, J., Weir, D. G., and Scott, J. (2000) Mechanism of the antimicrobial drug trimethoprim revisited, *FASEB J. 14*, 2519-2524.

[78] McMahon, M. A., Xu, J., Moore, J. E., Blair, I. S., and McDowell, D. A. (2007) Environmental stress and antibiotic resistance in food-related pathogens, *Appl. Environ. Microbiol. 73*, 211-217.
[79] Leduc, D., Escartin, F., Nijhout, H. F., Reed, M. C., Liebl, U., Skouloubris, S., and Myllykallio, H. (2007) Flavin-dependent thymidylate synthase ThyX activity: implications for the folate cycle in bacteria, *J. Bacteriol. 189*, 8537-8545.
[80] Sah, S., Aluri, S., Rex, K., and Varshney, U. (2015) One-carbon metabolic pathway rewiring in *Escherichia coli* reveals an evolutionary advantage of 10-formyltetrahydrofolate synthetase (Fhs) in survival under hypoxia, *J. Bacteriol. 197*, 717-726.
[81] Giladi, M., Altman-Price, N., Levin, I., Levy, L., and Mevarech, M. (2003) FolM, a new chromosomally encoded dihydrofolate reductase in *Escherichia coli*, *J. Bacteriol. 185*, 7015-7018.
[82] Reed, M. C., Nijhout, H. F., Neuhouser, M. L., Gregory III, J. F., Shane, B., James, S. J., Boynton, A., and Ulrich, C. M. (2006) A mathematical model gives insights into nutritional and genetics aspects of folate-mediated one-carbon metabolism, *J. Nutr. 136*, 2653-2661.
[83] Duncan, T. M., Reed, M. C., and Nijhout, H. F. (2013) The relationship between intracellular and plasma levels of folate and metabolites in the methionine cycle: a model, *Mol. Nutr. Food. Res. 57*, 628-636.
[84] Baskakov, I., and Bolen, D. W. (1998) Forcing thermodynamically unfolded proteins to fold, *J. Biol. Chem. 273*, 4831-4834.
[85] Parsegian, V. A., Rand, R. P., and Rau, D. C. (2000) Osmotic stress, crowding, preferential hydration, and binding: a comparison of perspectives, *Proc. Natl. Acad. Sci. U. S. A. 97*, 3987-3992.
[86] Yu, I., Mori, T., Ando, T., Harada, R., Jung, J., Sugita, Y., and Feig, M. (2016) Biomolecular interactions modulate macromolecular structure and dynamics in atomistic model of a bacterial cytoplasm, *Elife 5*.
[87] Stadmiller, S. S., Gorensek-Benitez, A. H., Guseman, A. J., and Pielak, G. J. (2017) Osmotic shock induced protein destabilization in living cells and its reversal by glycine betaine, *J. Mol. Biol. 429*, 1155-1161.
[88] Kuznetsova, I. M., Turoverov, K. K., and Uversky, V. N. (2014) What macromolecular crowding can do to a protein, *Int. J. Mol. Sci. 15*, 23090-23140.
[89] van den Berg, J., Boersma, A. J., and Poolman, B. (2017) Microorganisms maintain crowding homeostasis, *Nat. Rev. Microbiol. 15*, 309-318.
[90] Wu, F., and Minteer, S. (2015) Krebs cycle metabolon: structural evidence of substrate channeling revealed by cross-linking and mass spectrometry, *Angew. Chemie. 54*, 1851-1854.
[91] An, S. G., Kumar, R., Sheets, E. D., and Benkovic, S. J. (2008) Reversible compartmentalization of de novo purine biosynthetic complexes in living cells, *Science 320*, 103-106.
[92] Metris, A., George, S. M., Mulholland, F., Carter, A. T., and Baranyi, J. (2014) Metabolic shift of *Escherichia coli* under salt stress in the presence of glycine betaine, *Appl. Environ. Microbiol. 80*, 4745-4756.
[93] Huang, E. Y., Mohler, A. M., and Rohlman, C. E. (1997) Protein expression in response to folate stress in *Escherichia coli*, *J. Bacteriol. 179*, 5648-5653.

[94] Gunasekera, T. S., Csonka, L. N., and Paliy, O. (2008) Genome-wide transcriptional responses of *Escherichia coli* K-12 to continuous osmotic and heat stresses, *J. Bacteriol. 190*, 3712-3720.
[95] Schmidt, A., Kochanowski, K., Vedelaar, S., Ahrne, E., Volkmer, B., Callipo, L., Knoops, K., Bauer, M., Aebersold, R., and Heinemann, M. (2016) The quantitative and condition-dependent *Escherichia coli* proteome, *Nat. Biotechnol. 34*, 104-110.
[96] Kocharunchitt, C., King, T., Gobius, K., Bowman, J. P., and Ross, T. (2012) Integrated transcriptomic and proteomic analysis of the physiological response of *Escherichia coli* O157:H7 Sakai to steady-state conditions of cold and water activity stress, *Mol. Cell. Proteomics 11*, M111 009019.
[97] Snider, M. J., Gaunitz, S., Ridgway, C., Short, S. A., and Wolfenden, R. (2000) Temperature effects on the catalytic efficiency, rate enhancement, and transition state affinity of cytidine deaminase, and the thermodynamic consequences for catalysis of removing a substrate "anchor", *Biochemistry 39*, 9746-9753.
[98] Gulotta, M., Qiu, L., Desamero, R., Rosgen, J., Bolen, D. W., and Callender, R. (2007) Effects of cell volume regulating osmolytes on glycerol 3-phosphate binding to triosephosphate isomerase, *Biochemistry 46*, 10055-10062.
[99] Zhadin, N., and Callender, R. (2011) Effect of osmolytes on protein dynamics in the lactate dehydrogenase-catalyzed reaction, *Biochemistry 50*, 1582-1589.
[100] Phillip, Y., Harel, M., Khait, R., Qin, S., Zhou, H. X., and Schreiber, G. (2012) Contrasting factors on the kinetic path to protein complex formation diminish the effects of crowding agents, *Biophys. J. 103*, 1011-1019.
[101] Acosta, L. C., Perez Goncalves, G. M., Pielak, G. J., and Gorensek-Benitez, A. H. (2017) Large cosolutes, small cosolutes and dihydrofolate reductase activity, *Protein. Sci.*
[102] Fierke, C. A., Johnson, K. A., and Benkovic, S. J. (1987) Construction and evaluation of the kinetic scheme associated with dihydrofolate reductase from *Escherichia coli*, *Biochemistry 26*, 4085-4092.
[103] Walsh, C. T. (1979) *Enzymatic Reaction Mechanisms*, W.H. Freeman & Co., New York.
[104] Segel, I. H. (1975) *Enzyme Kinetics: Behavior and Analysis of Rapid Equilibrium and Steady-State Enzyme Systems*, John Wiley and Sons, New York.
[105] Zotter, A., Bauerle, F., Dey, D., Kiss, V., and Schreiber, G. (2017) Quantifying enzyme activity in living cells, *J. Biol. Chem. 292*, 15838-15848.
[106] Sevin, D. C., and Sauer, U. (2014) Ubiquinone accumulation improves osmotic-stress tolerance in *Escherichia coli*, *Nat. Chem. Biol. 10*, 266-272.
[107] Nijhout, H., Reed, M., Budu, P., and Ulrich, C. (2004) A mathematical model of the folate cycle: new insights into folate homeostasis, *J. Biol. Chem. 279*, 55008-55016.
[108] Giaever, H. M., Styrvold, O. B., Kaasen, I., and Strom, A. R. (1988) Biochemical and genetic characterization of osmoregulatory trehalose synthesis in *Escherichia coli*, *J. Bacteriol. 170*, 2841-2849.
[109] Patel, A., Malinovska, L., Saha, S., Wang, J., Alberti, S., Krishnan, Y., and Hyman, A. A. (2017) ATP as a biological hydrotrope, *Science 356*, 753-756.

[110] Kwon, Y. K., Higgins, M. B., and Rabinowitz, J. D. (2010) Antifolate-induced depletion of intracellular glycine and purines inhibits thymineless death in *E. coli*, *ACS Chem. Biol. 5*, 787-795.
[111] Parsegian, V. A., Rand, R. P., and Rau, D. C. (1995) Macromolecules and water: probing with osmotic stress, *Methods Enzymol. 259*, 43-94.
[112] Gadda, G., and Sobrado, P. (2018) Kinetic solvent viscosity effects as probes for studying the mechanisms of enzyme action, *Biochemistry 57*, 3445-3453.
[113] Jensen, S. I., Lennen, R. M., Herrgard, M. J., and Nielsen, A. T. (2015) Seven gene deletions in seven days: fast generation of *Escherichia coli* strains tolerant to acetate and osmotic stress, *Sci. Rep. 5*, 17874.
[114] Winkler, J. D., Garcia, C., Olson, M., Callaway, E., and Kao, K. C. (2014) Evolved osmotolerant *Escherichia coli* mutants frequently exhibit defective N-acetylglucosamine catabolism and point mutations in cell shape-regulating protein MreB, *Appl. Environ. Microbiol*. *80*, 3729-3740.
[115] Guo, Y., Winkler, J., and Kao, K. C. (2017) Insights on osmotic tolerance mechanisms in *Escherichia coli* gained from an rpoC mutation, *Bioengineering (Basel) 4*.
[116] Csonka, L. N. (1989) Physiological and genetic responses of bacteria to osmotic stress, *Microbiol. Rev. 53*, 121-147.

5. CONCLUSIONS AND FUTURE DIRECTIONS

Folate (Vitamin B9) serves as the donor in one carbon transfer reactions responsible for the synthesis of essential amino acids and nucleotide precursors. Folate is acquired through dietary intake, and the enzymes that process it are compartmentalized in humans and higher eukaryotes [1]. Malfunctioning of the enzymes of the folate pathway can lead to various diseases [2]. Bacteria on the other hand can synthesize their own folate and do not have to compartmentalize or sequester these enzymes. These enzymes, along with their reactants and products, are thus floating in a mixture of small molecules and macromolecules. One set of components in the cell are small molecule osmolytes. *E. coli* is known to synthesize small molecule osmolytes during times of osmotic stress to combat turgor pressure. These osmolytes can be amino acids, sugars and methylamines (Figure 1.4). Osmotic stress also leads to some water loss and increased crowding in the cell [3]. It is thus intriguing to think about how enzymes function in an extremely crowded cell under osmotic stress. How water affects enzymes of the folate pathway is also of interest. The folate pathway is found in most life forms and is essential for cell growth and survival. The enzymes of the folate pathway are major candidates for antibacterial and anticancer drug targets [2].

Previous work done in our lab has looked at the effect of small molecule osmolytes on the binding of dihydrofolate to dihydrofolate reductase (DHFR). Osmolytes weakly interacted with dihydrofolate preventing its association to DHFR, thus hindering its activity [4, 5]. Our lab has previously characterized the weak interactions of betaine with folate. Vapor pressure osmometry (VPO) and NMR studies were performed to understand the interactions of betaine with folate at the atomistic level [6, 7]. Nuclear Overhauser effect spectroscopy (NOESY) has identified that the bonds in folate rotate more slowly in presence of betaine, which suggests interactions of betaine with the aromatic carbons of folate, particularly the pABA ring [7]. This study was further extended using VPO studies, which indicated that betaine preferred to interact with the aromatic carbons, cationic and amide nitrogens. Betaine was predicted to associate with folate via cation-pi interactions [6]. Thus, these two techniques established that betaine prefers to interact with folate at certain functional atoms. The weak interactions between betaine and free folate shifts the binding equilibrium to the free species. This shift in equilibrium disrupts ligand binding and activity of dihydrofolate reductase.

The non-reducing sugar, trehalose, is another important cellular osmolyte, and is chemically different than betaine, a methylamine. Betaine is hypothesized to interact with folate through cation-pi stacking interactions [6]. Trehalose is known to interact with itself, and water molecules, with extensive hydrogen bonds [8]. It is thus predicted that if trehalose interacts with functional groups on folate, it will be via hydrogen bonding with its hydroxyl groups.

Previous osmometry studies done with trehalose and betaine have suggested that the two osmolytes interacted in an opposing manner with several functional groups [6, 9]. Betaine preferred to interact with aromatic carbons whereas trehalose preferred to stay away from them [6, 9]. Interactions with aromatic carbons are relevant to the studies in this thesis as this atom type is present in folates. Trehalose and betaine also have different effects on functional groups that are present on other metabolites of the folate pathway. For example, trehalose and betaine show opposing interactions with phosphate oxygens. Phosphate groups are present on dihydropterin pyrophosphate that is a substrate of *folP*

(DHPS) and the cofactors pyridoxal phosphate and nicotinamide adenine dinucleotide phosphate of the *glyA* (SHMT), *metF* (MTHFR) and *folA* (DHFR) enzymes, respectively. (see Figure 1.2 for the folate pathway). Thus, the weak interaction/repulsion imparted on the metabolites in the cell that possess functional groups with these atom types will differ in the presence of trehalose and betaine.

The bacterial cytoplasm is a crowded environment enriched with the potential for many weak interactions. We wondered if these weak interactions can be captured in *in vivo* experiments. Bacterial cells have evolved a clever way of synthesizing or transporting specific osmolytes depending on the environment. For example, betaine is the predominant osmolyte made during osmotic stress in nutrient rich conditions whereas trehalose gains dominance in a nutrient limited osmotic stress environment [10]. Depending on the dominance of certain osmolytes present in the cell, the weak interactions and behavior of macromolecules would change.

The research presented in this thesis addresses the effect of weak interaction on ligands and proteins of the folate pathway using *in vivo* and *in vitro* approaches. It is predicted that if osmolytes preferentially interact with functional groups present on the ligand/cofactors/proteins, they will affect the ligand/cofactor enzyme relationship. The interactions of osmolytes with biomolecules can be studied at the atomistic level using vapor pressure osmometry and at the molecular level using *in vitro* biophysical assays studying the effect of osmolyte interactions on ligand binding to and structure of the enzyme. These weak interactions can also be explored through *in vivo* microbiology assays by studying bacterial cells in osmotically stressed condition. From this work, we propose that the effects of osmolytes are specific to their chemical structure and that they form weak interactions *in vivo* at levels significant enough to affect cell growth under osmotic stress. The future direction of this research is to understand the functioning of macromolecules in a crowded environment and determine the effect of weak interactions on folate pathway enzymes under less stressed conditions.

5.1 Investigation of the weak interactions between trehalose and folate

One of the strategies to study the types of weak interactions that occur in the cell is to understand the effects osmolytes have on cellular macromolecules and their ligands. There are several biologically relevant osmolytes of varying chemical nature. Thus, the types of weak interactions they participate in depend on their chemical structure. These weak interactions have been shown to affect macromolecule function. Additionally, interactions between osmolytes and substrates of the folate pathway affect the binding of the folates to their respective enzyme [5, 6, 11, 12]. This hinders the activity of the enzymes in the cell. Osmolytes also affect the folding of proteins in the cell [13]. Since several of the osmolytes used in these studies are present in most living organisms, understanding the myriad of weak interactions in the cell is of utmost importance. If these interactions occur *in vitro*, then they will also occur *in vivo*, which could potentially affect cell behavior. Another term for these weak interactions between osmolytes and macromolecules is

preferential interaction. This is when the functional groups/atom types present on the surface of a macromolecule, or metabolite, prefer to interact with either osmolyte or water as compared to the other solute.

In Chapter 2, we used VPO to study the preferential interactions of osmolytes with model compounds that have the same functional groups as macromolecules and the metabolites of the folate cycle. We quantified these interactions as preferential interaction coefficients (μ_{23}/RT) of trehalose using more than 50 model test compounds. The functional groups explored in this study were: aliphatic and aromatic carbons; phosphate, hydroxyl and amide oxygens; and amide, cationic and aromatic nitrogens. A positive μ_{23}/RT indicates preferential interaction of test compound with water, and exclusion of trehalose from its solvation shell. A negative μ_{23}/RT indicates preferential interaction of test compound with trehalose rather than water, while a value of zero indicates equal preference for water and trehalose. The preferential interaction coefficients are the summation of the interaction potentials (α values) derived from solvent accessible atom types on the test compound. The preferential interaction coefficients were obtained for more than 50 model compounds, and these values were deconvulated to obtain atomistic interaction coefficients. Atomistic interaction coefficients represent the interaction potential of trehalose with solvent accessible atom types. Our results indicate that trehalose prefers to interact with phosphate oxygen, amide nitrogen and cationic nitrogen, but excludes aromatic carbon and nitrogen, aliphatic carbon, amide and hydroxyl oxygen.

5.1.1 How is trehalose different from other osmolytes?

Trehalose has similar favorable preferential interactions to glycerol except for aromatic carbons. Glycerol and trehalose are predicted to weakly interact via hydrogen bonding [14]. In the case of aromatic carbons, glycerol preferred to interact whereas trehalose was excluded from the surface of the aromatic rings. Polyols and small PEGs are also predicted to favorably interact with aromatic carbons [14]. Compared with betaine and proline, which are the other two predominant osmolytes that the cell accumulates under osmotic stress, trehalose favorably interacted with phosphate groups, while betaine and proline were excluded from the negatively charged oxygens. Likewise, trehalose had unfavorable interactions with aromatic carbons, while betaine and proline interacted favorably with aromatic carbons [6, 9, 15, 16]. Phosphates and aromatic carbon containing metabolites are widely present in the cell. Most of the secondary messengers and macromolecules of the cell have different levels of phosphorylation depending on the energy status of the cell. Hence the presence or dominance of one osmolyte over the other will influence the range of weak interactions in the cell.

5.1.2 Interaction of trehalose with folate and other techniques that can be used to explore this

The preferential interaction coefficients can be calculated for folate by multiplying the α values with the area occupied by the atom types on folate. Using the α values from Chapter 2, we predicted a preferential interaction coefficient for folate of 0.54 m^{-1}, which indicates preferential exclusion of trehalose from folate. Experimentally, the interaction of trehalose with folate gave a value of 0.46 m^{-1}, which is very close to our predicted value. A previous study done by Hong et al obtained different atomistic interaction coefficient values than the ones obtained in our study [9]. In the previous study, the technique of freezing depression osmometry, which relies on the change in the freezing point of water in solutions containing compound or osmolyte, was employed. The study was done with a set of 20 model compounds with less emphasis on compounds containing aromatic carbons and nitrogens. Additionally, the authors reported two atomistic interaction coefficients of trehalose with aromatic carbons depending on the test compound used in the study. Preferential interaction of trehalose with aromatic carbons was suggested when aromatic carbons in phenylalanine were used for data fitting whereas preferential exclusion was predicted when histidine and 4-benzylalcohol were used for the fitting [9]. The molality range for phenylalanine was extremely low due to its low solubility and this led to higher errors in the data set. Imidazole in histidine is known to dimerize at higher concentrations [17], and this makes the data analysis with histidine complicated, as the monomeric and dimeric histidine will interact with trehalose differently. In addition to the presents of histidine dimers, the aromatic carbons were not analyzed separately from aromatic nitrogens in the imidazole ring. Hence there was a need to obtain more refined values for preferential interaction of trehalose with aromatic nitrogens and carbons. Since folate has aromatic carbon and nitrogen, our study explored the effect of trehalose on these functional atom types in more detail. Using their α values, a preferential interaction coefficient of -0.403 was calculated for folate with trehalose. We propose other techniques must be used to understand the preferential interactions of trehalose with different atom types. This data can be used to support our VPO study, and hopefully resolve the differences seen between our and the Hong et al study.

NOESY NMR can be used to study the weak interactions of trehalose with folate at the atomistic level. NOESY measures the distances between two protons in close proximity. The phase and the tumbling intensity is dependent on the extent of the interactions. Faster tumbling rates give rise to positive NOE and slower tumbling will yield negative NOE [18]. NOESY experiments have been used to explore the weak interaction of betaine with folate. NOE between the protons on the pABA C3'/C5' carbons and the C9 protons of folate (see Figure 1.1 for folate numbering) were positive, while a negative NOE was obtained upon addition of deuterated betaine. This is indicative of slow tumbling of pABA ring of the folate in presence of betaine [7]. NOESY experiments can be performed with deuterated trehalose. Trehalose dihydrate has been previously reported to be partially deuterated at carbon positions 2, 3, 4, and 6 using a Raney nickel catalyst [19]. Our osmometry experiments indicated preferential exclusion of trehalose from aromatic carbons, as well as the glutamate oxygens, in folate and hence it is expected that the tumbling rate will not change in presence of trehalose. However, if there is preferential

interaction of trehalose with aromatic carbons, as one of the Hong α values suggests, and carboxylate oxygens, then a change in the NOE signs would be expected.

The effects of trehalose on folate dimerization can also be used to determine which α values for aromatic carbons is correct. Folate dimerization can be measured by NMR [7], and the K_d will change depending upon whether trehalose interacts with the folate monomer, or is excluded from it. Folate dimerizes with the pterin ring of one folate stacking over the pABA ring of the second folate molecule. Since our osmometry experiments predict preferential exclusion of trehalose from the atom types present in pterin and pABA ring, we would predict that the dimerization K_d will decrease in the presence of trehalose. Exclusion of trehalose from the aromatic rings indicates the desolvation penalty associated with dimer formation will be reduced. This should lead to association of folate molecules with each other at lower concentrations in the presence of trehalose. On the other hand, if the α values from Hong et al are accurate, then trehalose will interact with the aromatic carbons. Thus, trehalose will have to dissociate from the folate monomers first, before the dimer can form, increasing the K_d of folate dimerization.

The effects of trehalose on folate dimerization can also be used to determine which α values for aromatic carbons is correct. Folate dimerization can be measured by NMR [7], and the K_d will change depending upon whether trehalose interacts with the folate monomer, or is excluded from it. Folate dimerizes with the pterin ring of one folate stacking over the pABA ring of the second folate molecule. Since our osmometry experiments predict preferential exclusion of trehalose from the atom types present in pterin and pABA ring, we would predict that the dimerization K_d will decrease in the presence of trehalose. Exclusion of trehalose from the aromatic rings indicates the desolvation penalty associated with dimer formation will be reduced. This should lead to association of folate molecules with each other at lower concentrations in the presence of trehalose. On the other hand, if the α values from Hong et al are accurate, then trehalose will interact with the aromatic carbons. Thus, trehalose will have to dissociate from the folate monomers first, before the dimer can form, increasing the K_d of folate dimerization.

5.2 Different effects of osmolytes with ligands containing phosphate groups and aromatic carbons

Preferential interaction coefficients can yield information on how ligands and enzymes will behave in complex media. In order to test the effects, we predicted the preferential interaction coefficients of several reduced folate/ folate fragments and employed enzyme binding assays to understand how weak interactions perturbed these ligand-enzyme systems. Folate is made from the fusion of a pterin ring with a pABA ring to which a glutamate tail is later added (Figure 1.1). The enzyme dihydropteroate synthase (DHPS) is responsible for the cleavage of dihydropterin pyrophosphate and condensation of the pterin and pABA rings to form dihydropteroate [22]. In Chapter 3, the binding of the ligands pterin pyrophosphate and pABA was monitored using isothermal titration calorimetry

(ITC). The preferential interaction coefficients of osmolytes with these ligands were calculated. There was good agreement between the predicted preferential coefficients and the influence of the osmolytes on ligand binding. In the case where the ligands had negative μ_{23}/RT values for a particular osmolyte, weaker binding occurred. This was due to preferential interaction of the osmolytes with certain functional groups on the ligand that hindered the association of the ligand to the enzyme. Osmolyte interactions with the free ligand shift the binding equilibrium away from the bound complex, thus lowering the K_ds. The reverse also occurred wherein positive μ_{23}/RT values led to tighter binding of ligand to the enzyme. This was due to preferential exclusion of the osmolyte from the functional groups on the ligand and a reduction in the desolvation penalty associated with binding. Most of the osmolytes did not affect the secondary structure of DHPS, and increased the thermal stability of the enzyme. Increased solvation around the enzyme leads to increased thermal stability. Therefore, increased thermal stability is suggestive of exclusion of the osmolyte from the surface of the enzyme. The lack in change of the secondary structure of DHPS in the presence of osmolytes suggests there are no effective interactions of the osmolytes with the enzyme.

The effect of osmolytes on binding of the sulfa drug, sulfathiazole (STZ), was also explored. The predictions from the calculated preferential interaction coefficients concurred with the effects of osmolyte on the binding of STZ to DHPS. Thus, VPO studies serve as an effective tool to understand weak interactions, and can complement biophysical studies in evaluating the effects of osmolytes on ligand-enzyme binding. This can be extended to interactions between osmolytes and protein surfaces, which can help us predict the folding/unfolding of the protein in the presence of osmolytes. The weak interactions between osmolytes and ligands or enzymes can also affect catalysis. The functional groups addressed in our VPO studies are ubiquitously found on other macromolecule surfaces such as proteins, DNA, RNA. Hence these studies could also help us to predict the weak interactions between two different macromolecules or between macromolecules and small molecules of the cell.

5.2.1 Osmolyte effects on pteroate with DHPS

Trehalose preferentially interacted with phosphate groups and excluded aromatic carbons. The reverse is true for betaine where there is interaction of betaine with aromatic carbons and exclusion from phosphate groups [6, 9, 15]. Weakened binding of pterin pyrophosphate to DHPS was seen in presence of trehalose, while tightened binding in presence of betaine. When pABA was studied as a ligand, tighter binding was observed in the presence of trehalose whereas binding was weakened in the presence of betaine. The solvent exposed atoms on pteroate are predicted to preferentially interact with water instead of trehalose. These groups will, however, preferentially interact with betaine instead of water. So, it would be interesting to study the effect of trehalose and betaine on pteroate binding to DHPS, as well as the next enzyme in the folate pathway, dihydrofolate synthase.

Structures are available for product bound BaDHPS, where pteroate occupies the same position as the pterin and the pABA ring, participating in similar interactions as the substrates in the active site [23]. The calculated preferential interaction coefficient for pteroate is 0.323 for trehalose and -0.430 for betaine. If trehalose and betaine were to not affect the enzyme, then the binding of pteroate should follow the predicted preferential interaction coefficient values, with weaker binding in the presence of betaine, but tighter binding with trehalose.

Several pterin-sulfa conjugates that are analogs of pteroate are being explored as effective drugs against DHPS [24]. Understanding the preferential interactions of excipients like trehalose and betaine with the sulfa drug-pteroate analogs will help us understand the weak interactions of these excipients with the conjugate drug molecules. This will in turn help us resolve the stability and aggregation propensity of these drug molecule in the presence of excipients. It will also help with understanding the binding of the drug molecules in complicated heterogeneous cellular environments, where many of the molecules in the cell have similar functional groups as trehalose and betaine. We would predict that similar weak interactions would occur between the pteroate analogs and molecules of the cell that have the same functional groups as betaine and trehalose.

5.3 Can weak interactions predicted by *in vitro* experiments be seen in *in vivo* cellular environments?

Two strategies were employed for determining if weak interactions affect the enzymes of the folate pathway *in vivo*. The ability of an enzyme to rescue the cell from antibiotics, or to restore auxotrophy to a cell with its enzyme knocked, out was determined. R67 DHFR is resistant to the antibiotic trimethoprim (TMP), whereas chromosomal DHFR is sensitive to it. Addition of TMP can thus be used to knockdown the activity of chromosomal DHFR. The ability of R67 DHFR activity to allow the cells to grow in the presence of TMP and sorbitol stress was accessed. With increasing sorbitol stress, R67 DHFR activity dropped and the enzyme was unable to rescue the cells from TMP stress [12]. This is likely because of osmolyte interactions with dihydrofolate, preventing its association with R67 DHFR and thus inhibiting catalysis and product formation with increasing osmotic stress.

In another strategy, the ability of the enzyme to rescue knockout cells against prototrophy was studied. Cells with essential folate pathway enzyme genes knocked out were procured. Rescued cells were made by reintroducing the gene for the enzyme in a pKTS plasmid. The knockout cells were grown in minimal media with end products of the reaction. The rescued cells were grown in minimal media with concentrations of tetracycline needed for the induction of the enzyme. Three different folate pathway enzymes were tested: R67 DHFR, MTHFR and SHMT. Knockout and rescued cells for each enzyme were subjected to osmotic stress. For all the enzymes, the rescued cells tolerated lower osmolality than the knockout cells [12]. The rescued cells were dependent on the activity of the rescuing enzyme to grow on minimal media. With increasing osmotic stress, osmolytes in *E. coli* participate in weak interactions with the reduced folates and cofactors of the enzymes. There has to be removal of not only the osmolytes, but also

water, from the interface of the ligand or cofactor for the complex to form. This prevents enzyme-ligand/cofactor association, lowering the formation of the essential product(s). This was hypothesized to be one of the reasons for the decline of cell growth with increasing osmotic stress. Knockout cells grown in supplemented media grew until there was loss of water due to osmotic stress, and their growth was not dependent on a particular enzyme activity.

Sorbitol and NaCl were both used as osmotic stressors. The titration of enzyme activity was achieved with both the stressors, but NaCl stress was found to be more deleterious for cell growth. We also changed the predominant osmolyte to betaine by adding 1 mM betaine to our osmotic stress experiments [12]. Titration of enzyme activity was achieved, indicating that betaine and trehalose both interact with the ligands to prevent their association with the enzyme. This was seen in the *in vitro* ITC and steady state kinetic studies performed on R67 DHFR where trehalose and betaine increased the K_d and K_m of DHF [4, 11].

The preferential interaction coefficient of trehalose with chorismate is positive. It was predicted that chorismate would prefer to exclude trehalose. This would lead to reduction in the desolvation penalty association with binding, and hence the binding of chorismate would be tightened. The enzyme function should, therefore, not be affected in the presence of trehalose, and titration of the enzyme activity should not be observed with increasing osmotic stress. Chorismate mutase osmotic titration would thus serve as negative control for the study. However, titration of enzyme activity was observed with increasing osmotic stress [12]. The chorismate mutase used in these experiments was a hexameric mutant version, the rate determining catalysis step of which is not known. For the *in vivo* osmotic stress experiments to work, the rate determining step (rds) of the enzyme cannot be diffusion limited. If the rds is diffusion limited, then the K_m, as well as the k_{cat}, of the enzyme will be affected in the presence of osmolytes. We are trying to understand/capture the weak interactions that affect binding but do not want to affect the turnover rate of the enzyme. For an enzyme where the chemical step is the rds, the effect of weak interactions will be seen only on the K_m/K_d of the ligand. Therefore, another enzyme will be needed as a negative control for the *in vivo* titration of enzymatic activity by osmolytes.

5.3.1 Complexity of the cell

Our *in vivo* osmotic stress studies have allowed us to titrate enzyme activity in the cell with increasing osmotic stress. One reason that cell growth was titrated was the preferential interaction of osmolytes with the ligands. However, the cell is heterogeneous and complex in nature. The osmolytes produced in the cell can interact with the enzyme under study. Our *in vitro* experiments have shown that biologically relevant osmolytes, like trehalose and betaine, prefer to stay away from protein surface and stabilize them. But *in vivo* these interactions may differ under osmotic stress. There can be interactions between macromolecules, like other proteins and nucleic acids in the cell.

Cascading effects have been reported with folate pathway enzymes. Inhibition of DHFR by TMP leads to increase in DHF levels that can affect the glutamylation of folates [25]. Mathematical modeling has predicted that titration of DHFR activity will lead to a buildup of DHF and lower of the concentrations of other reduced folates in the cell, indicative of domino effects. However, these domino effects were not seen in mathematical models of MTHFR and SHMT [12]. This again points to the complexity of the pathway wherein alterations to the main enzyme of a cycle can cause cascading effects and affect several metabolites, but that may not be true for sub-pathways. These parameters need to be considered while studying and interpreting factors that affect enzymatic reactions of the cell.

One way to be sure of the effect of osmotic stress on enzyme activity would be to study the level of reduced folate metabolites in the cell. Since the cell is a complex environment enriched with weak interactions, many types of interactions are predicted (i.e., protein-ligand, protein-protein, ligand-ligand, protein-osmolyte and ligand/cofactor-osmolyte). All these interactions will feed into changing the activity of the enzymes in the cell. Metabolomics performed with knockout and rescued cells subjected to several different concentrations of sorbitol and NaCl stress would give us a quantitative value of the reduced folates present in the cell under these conditions. If our hypothesis of ligand/cofactor-osmolyte interactions is true within the cell, then the levels of reduced folate that are associated with the enzyme under study would be altered in rescued cells with respect to knockout cells. It can be predicted that the levels of the substrate would increase, and product would decrease. If the levels of other folates that follow the enzyme in the pathway increase or decrease in concentration in conjunction with the enzyme products, then it would suggest cascading effects. In the case where osmolytes interact with the enzymes, the metabolites levels should increase or decrease in both knockout and rescued cells. Metabolomics studies to quantitate the folate levels in the cell have been attempted before [25], yet these experiments are challenging due to the unstable nature of folate metabolites.

5.3.2 Where does this take us?

We were able to demonstrate the titration of enzyme activity with increasing osmotic stress. However, it is not clear yet whether the effects are universal to all enzymes of the cell or if any enzyme of the cell is immune to the titration with respect to osmotic stress. Thus, there is a need for a better negative control to understand our enzyme osmotic stress studies. In Chapter 4, osmotic stress titrations were noted for folate pathway enzymes and with chorismate mutase, which is indirectly associated into the folate pathway. Chorismate is at the branchpoint that is responsible for pABA and aromatic acid biosynthesis [26]. Chorismate mutase funnels products into the folate pathway, meaning a cascading effect could occur with other folate enzymes if less pABA is produced under osmotic stress. Less pABA availability along with the rds for this chorismate mutase mutant not being known, could be responsible for the osmotic effects on chorismate mutase. We would like the negative control enzyme to not be directly or indirectly associated with the folate pathway.

It was found in Chapters 3 and 4 that trehalose prefers to interact with phosphate groups whereas betaine is excluded by them. Thus, enzymes that process ligands that possess phosphate groups would serve as potential negative control candidates on which the osmotic titration studies can be conducted. Three candidates for the negative controls are dihydropteroate synthase, triose phosphate isomerase and guanylate cyclase.

The preferential interaction values in Chapter 3 predict that trehalose will interact with dihydropterin pyrophosphate (H_2PtPP), while betaine will be excluded by the substrate. When trehalose is the predominant osmolyte, we would expect that free H_2PtPP would interact with the osmolyte, decreasing the amount bound to DHPS. This would lead to lower growth of cells dependent upon DHPS for growth, as there will be lower enzyme activity due to less substrate being bound. Conversely, when betaine is the predominant osmolyte, H_2PtPP would bind tighter to DHPS, increasing enzyme activity. This would lead to DHPS-dependent cells surviving under higher osmolality stress conditions. Therefore, we would predict that when betaine is the predominant osmolyte, DHPS would act as a negative control. Thus, we performed our *in vivo* osmotic stress assay with DHPS. In order to ensure lower expression of DHPS, we pessimized the sequence of the *E.coli folP* gene, and complemented the knockout strains with the pessimized gene in the pKTS vector. This approach can be juxtaposed with using optimized sequences to increase protein expression levels. Construction of the pessimal *folP* sequence was done in collaboration with Dr. Mike Gilchrist (University of Tennessee – Knoxville). Groups of synonymous codons have different Ribosome Overhead Cost (ROC), which refers to the pausing time between codons. A program designed by the Gilchrist lab compares these groups of codons to find out which codons have the greatest or least pausing time. It then groups the codons by fitness and uses the least fit codons to generate a pessimized sequence (personal communication).

When performing the osmotic stress titration, the Δ*folP E. coli* knockout strain did not grow well in minimal media supplemented with the folate end products. We use several different knockout and rescued strains (C600, BL21 and MG1655), but none grew well in minimal media supplemented with folate end products. Knockout strains (*ΔfolP*) in a MG1655 background barely grew in BV supplemented plates. Under osmotic stress, there were a few colonies at 0.25 M sorbitol, and no growth was observed at higher sorbitol concentrations. From the titrations, we note that the *ΔfolP* cells are quite sick and are acutely sensitive to osmotic stress. Due to the poor growth of the knockout strain, we did not have a control for the osmotic stress experiments (Figure 5.1A). Since DHPS is at the top of the folate synthesis pathway, it may be that the cell lacks many folate species and many enzymes are affected (i.e., domino effects, also seen with our mathematical model for DHFR-see Chapter 4). Rescued strains in this background continued to grow until 1-1.25 M sorbitol in BV supplemented media. Interestingly, the pessimal *folP* gene apparently produces sufficient protein to rescue the cell even with no added tetracycline (Figure 5.1B top panel). With addition of 10 ng/ml tetracycline, the cells grew until 1.25 M sorbitol. If the pessimal sequence does result in low protein expression, this suggests that very low DHPS activity is sufficient to rescue the knockout strain. Since we did not have good controls and we were unable to lower DHPS levels in the cell, we decided to discontinue our studies with pessimized DHPS.

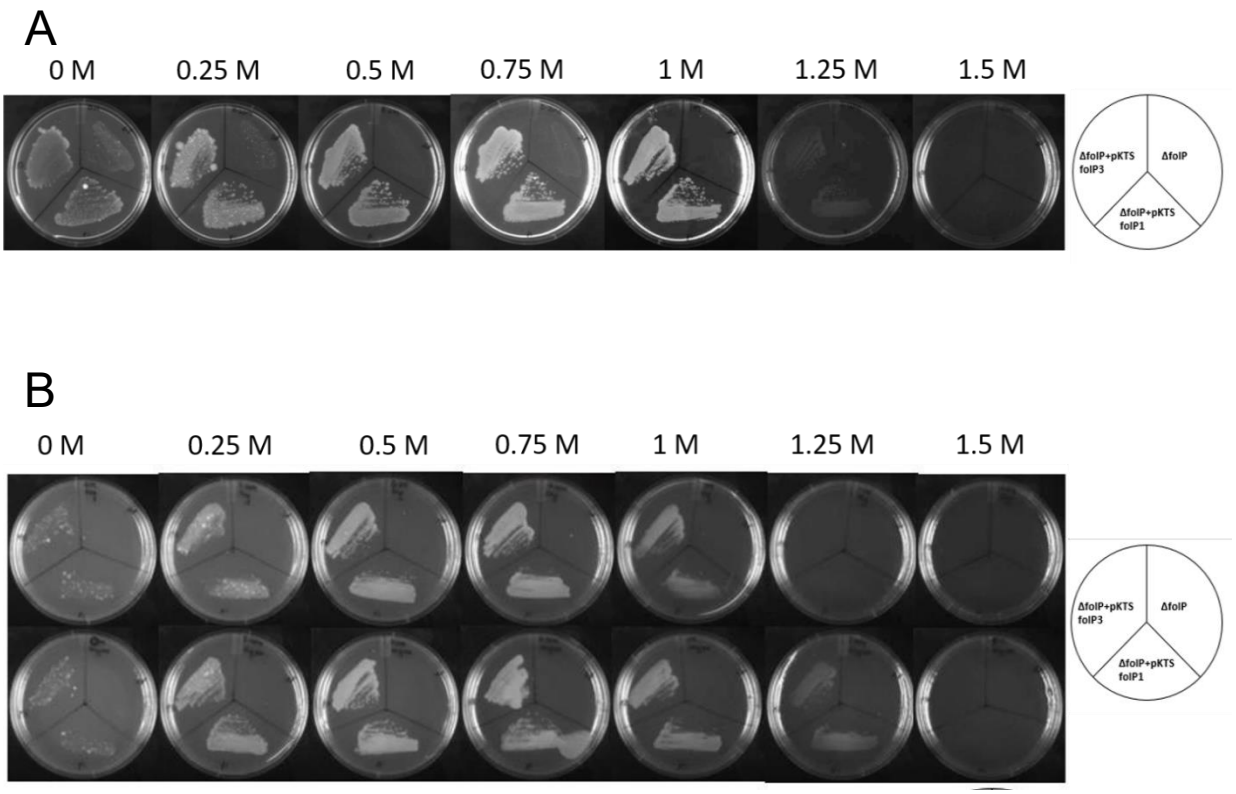

Figure 5.1: Sorbitol titration of dihydropteroate synthase

The concentrations of sorbitol are listed on top of the plates. A template depicting the position of the cells is shown to the right. The knockout cell is labelled as *ΔfolP*. Two clones of the rescued strain are labelled as *ΔfolP*+pKTS-folP1 & *ΔfolP*+pKTS folP3. To all the plates 50 µg/ml kanamycin was added, while 100 µg/ml ampicillin was added to plates in panel B. A: Growth of cells in BV minimal media plates supplemented with 50 µg/ml of thymidine, adenine, methionine, glycine and panthothenate. B: Growth of cells in BV minimal media with 0 ng/ml tetracycline (top) and 10 ng/ml tetracycline (bottom)

Triose phosphate isomerase (TPI) catalyzes the reversible isomerization of glyceraldehyde phosphate to dihydroxyacetone phosphate. The enzyme is classified as a perfect enzyme with every substrate-enzyme encounter being catalyzed into product. The rate determining step of the wild type enzyme is substrate diffusion. Since the enzyme is highly efficient, it would be better to work with a mutant enzyme which has a lower turnover number [27]. As mentioned in Chapter 4, the level of enzyme in the cell needs to be lower than the chromosomal level so that the enzyme activity can be maintained in a selectable range and osmotic stress can be scored for its effects on K_m of the enzyme (see Figure 1.14). The E165D/S96P mutant of TPI has about 10-fold difference in catalytic activity than the wild type [27]. This mutant induced from pKTS vector will ensure that the enzyme levels and activity are maintained in the selectable range. We predict that with increasing osmotic stress, trehalose will interact with the phosphate groups on the ligand and hinder its association with TPI thereby reducing its activity and inhibiting product formation. A minimal media with glycerol as the sole carbon source (M63) will need to be used so that knockout strains cannot grow without supplementation, and rescue of knockout strains with TPI activity will allow the cells to grow on glycerol as the carbon source. In the presence of osmotic stress, we predict that TPI activity will be titrated with osmotic stress in minimal media where trehalose is the predominant osmolyte. The same may not be true when the predominant osmolyte is betaine. Since betaine is preferentially excluded from phosphate groups, glyceraldehyde phosphate will bind tighter to the enzyme in the rescued strain. The rescued cells would be able to grow to similar osmolalities as the control strains. This would serve as a negative control for our osmotic stress experiments.

Another enzyme that can be explored for the same is diguanylate cyclase responsible for the biosynthesis of c-di-GMP using two GTP molecules [28]. We expect to see a similar pattern with this enzyme if osmolyte interaction/exclusion from the ligands affects its binding to the enzyme. The amount of c-di-GMP produced in the cells can be quantified by mass spectrometry [29]. The levels of c-di-GMP can be estimated under osmotic stress in cells grown in minimal media and minimal media with 1 mM betaine. Trehalose will be the predominant osmolyte in the first set of media whereas betaine will be the predominant one in the second. This will help us to understand the weak interaction of trehalose and betaine with GTP and its effect on the activity of diguanylate cyclase. c-di-GMP is an important secondary messenger in the cell that is involved with motility, virulence and biofilm formation [28]. The alteration of the levels of this metabolite in trehalose and betaine dominated environment in the cell will have interesting implications in understanding bacterial physiology.

5.3.3 Can pKTS vector and osmotic stress assay be used for understanding the mechanism and efficacy of antibiotics?

5.3.3.1 Sulfa drug titration

Sulfa drugs are competitive inhibitors of dihydropteroate synthase. The drugs competitively bind in the pABA binding pocket and results in the formation of a pterin-sulfa conjugate product. The conjugate feeds into the folate pathway and results in the formation of a dead-end folate products. Sulfathiazole binding to *Staphylococcus aureus* DHPS has been monitored in minimal media with a minimum inhibitory concentration (MIC) of 1.6 µg/ml sulfathiazole inhibiting growth by 80% [30]. Similar experiments were repeated with *E. coli* MG1655 and 1.6 µg/ml of STZ leads to inhibition of growth in M9 media. BaDHPS *folP* (DHPS gene) can be introduced in a pKTS vector and transformed into *E. coli* MG1655. Addition of tetracycline should be able to rescue the cells from the STZ. This would allow us to confirm that by increasing the enzyme concentration in the cell, increased DHPS activity is enough to allow the growth of the cells in 1.6 µg/ml STZ. Osmotic stress titrations can then be performed with *E. coli* MG1655 and *E. coli* MG1655-pKTS BaDHPS *folP*. With increasing osmotic stress, it is predicted that in the control *E. coli* MG1655, growth will be seen until 1.9 Osm, after which there is loss of cytoplasmic water and growth ceases [31]. When *E. coli* MG1655-pKTS BaDHPS *folP* are subjected to osmotic stress and 1.6 µg/ml STZ, it is predicted that the cells will stop growing at much lower osmolality. With increasing osmotic and STZ stress in these cells, it is predicted that the osmolytes will interact with dihydropterin pyrophosphate and pABA in the cell preventing them from binding to DHPS. Osmolytes will also interact with certain functional groups on STZ, but it binds more tightly to the BaDHPS compared to pABA (see Chapter 3). Thus, even though osmolytes will also weaken STZ binding, it will be able to outcompete pABA for the binding site. This would only be possible if STZ concentrations are high enough in the cell to lessen the effect of osmolyte interactions with STZ. Another condition for the experiment to work is that the levels of pABA must be lower than STZ. There are a lot of unknown variables in this experiment.

5.3.3.2 Metformin Effects

Biguanides (phenformin, metformin and buformin) competitively inhibit *E. coli* chromosomal DHFR with a K_i of 18 mM [32]. In another study, metformin was found to alter the folate pathway and methionine cycle in bacteria [33]. The folate pathway begins with dihydrofolate getting converted to tetrahydrofolate which goes through a series of one carbon reactions to make important nucleotide precursors and amino acids along with converting reduced folates in the cell. THF is converted to 10-formylTHF which can either be used to form purine precursors or converted to 5,10-methenylTHF. THF can also be converted to 5,10-methyleneTHF which can be converted to 5-methylTHF, which enters the methionine cycle. Addition of metformin led to build up of DHF concentrations and reduce the levels of THF in the bacterial cells. Reduction in the levels of 10-formylTHF

and 5,10-methenylTHF were also reported. It can be predicted that addition of metformin hampers the activity of DHFR leading to the reduction of the folate pool in the cell. On the other hand, levels of 5,10-methyleneTHF and 5-methylTHF were increased. Thus, it can be predicted that there is an increase of products from the methionine cycle. 5-methylTHF is used in the methionine cycle to produce methionine. An interesting mutant with increased resistance to metformin was discovered in these studies. The mutation was reported to be in the *glyA* (serinehydroxymethyl transferase gene), though it wasn't clear if the mutation led to a gain or loss of activity of SHMT. Exposure of these mutants to metformin had the same increase in methionine concentration, but the levels of DHF, THF and 10-formylTHF were unaffected [33]. Thus, the mutation of SHMT, and change in folate pools, led to this resistance. In order to test whether SHMT is inhibited by metformin, we conducted minimum inhibitory concentration assays using *E. coli* MG1655 (Figure 5.2).

Concentrations of 160 mM metformin inhibited the growth of *E. coli* MG1655. Addition of thymidine to the minimal media did not rescue the cells from metformin stress, and the cells did not grow at 160 mM of the drug. Thymidine is added to the cells to complement the activity of thymidylate synthase which is responsible for recycling DHF back into the folate cycle (see figure 1.2). Addition of glycine and serine rescued the cells from metformin stress and were capable of growth until 180 mM metformin. Glycine and serine are the reactants and products along with THF and 5,10-methyleneTHF for the SHMT reaction. Thus, addition of glycine and serine, which are produced by SHMT, rescued the cells from metformin stress. We extended these experiments to understand the effect of metformin in parent strain and *glyA* deleted cells (Figure 5.3). Parent strain MG1655 had a MIC of 160 mM, but the *glyA* knockout strain only grew to 120 mM metformin. Less and slow growth was observed in 140 mM metformin after 40 hours. This again indicates that metformin affected SHMT, as activity in the parent strains rescues the folate pool and leads to growth of the cells until 160 mM metformin. Lower levels of metformin were needed to inhibit growth of *glyA* deleted cells. In the future, glyA rescued strain can be used to study these effects in detail. We can understand the cell growth in metformin stress when different amounts of glyA are produced in the cell. With increasing SHMT levels we would hypothesize that the level of metformin tolerated by the cells would increase as compared to cells containing no SHMT. This can be done in rescued cells containing the glyA-pKTS vector. Also, metabolomics can be performed to understand the folate levels in the cell along with these experiments. Furthermore, osmotic stress assays can be done to modulate SHMT activity in the cell and understand the effects of metformin on the folate pathway.

5.4 Summary

This thesis has explored the effect of weak interactions of osmolytes with ligands and enzymes of the folate pathway. We have extrapolated our results to understand these weak interactions in the cell. Chapter 2 focuses on understanding the weak interactions of trehalose with different functional groups that are ubiquitously found in the cell. This has allowed us to predict weak interactions of trehalose with folate. We have used atomistic interaction coefficients to predict that several osmolytes will interact with

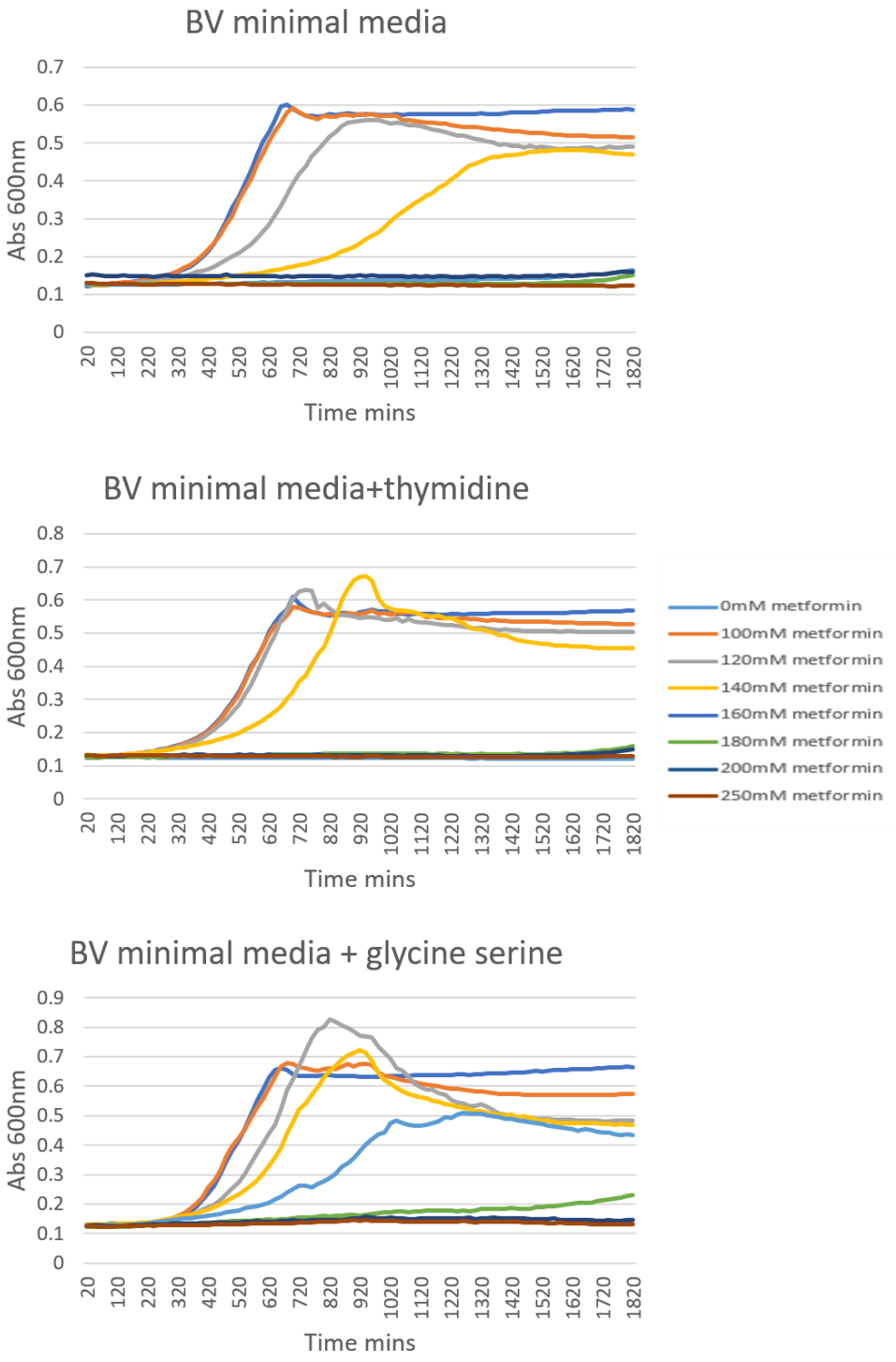

Figure 5.2: Effect of metformin on *E. coli* MG1655 grown in different medium supplements

E.coli MG1655 grew until 140mM in BV medium with no supplements. Additon of thymidine did not alter the concentration that inhibited growth of cells. Addition of glycine and serine allowed the cells to grow until 160mM.

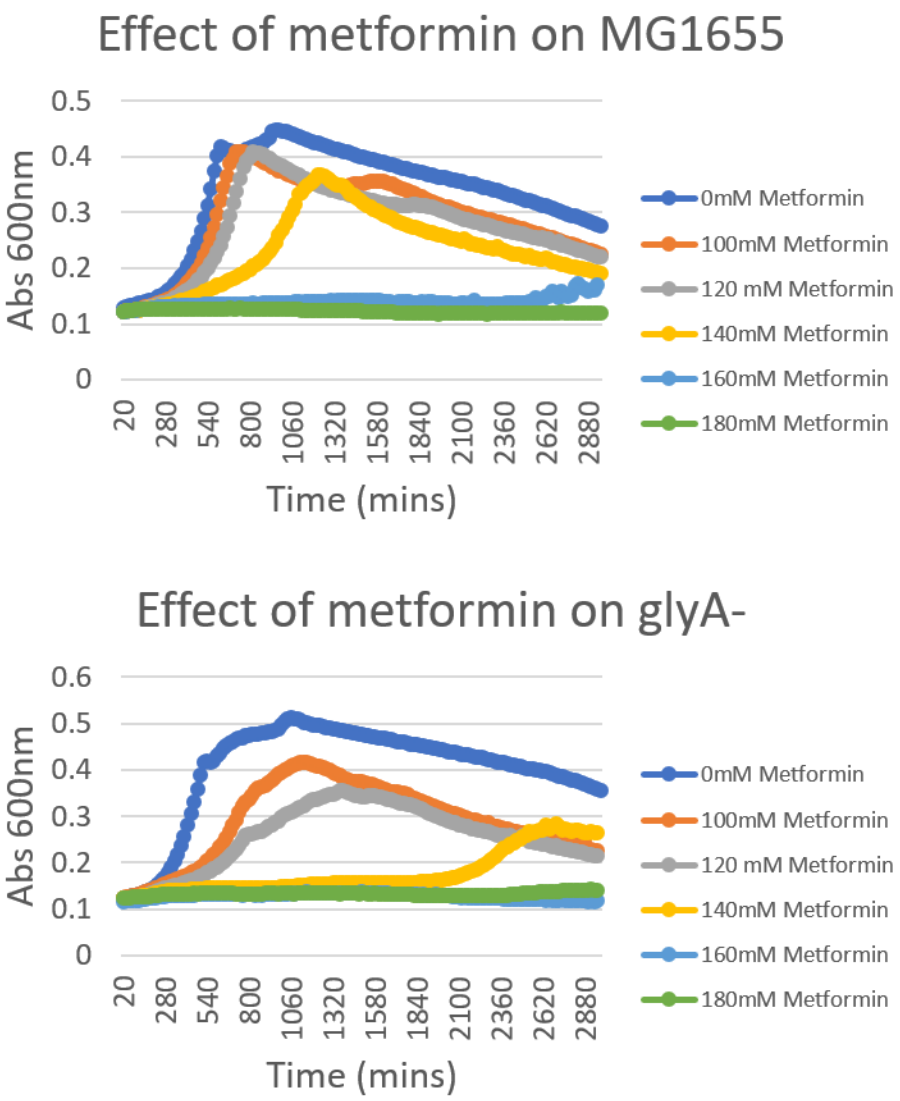

Figure 5.3: Growth on *E. coli* MG1655 and *E. coli* MG1655 ΔglyA in presence of metformin

Δ*glyA* cells were grown with glycine and serine supplements whereas parent strain was not given any supplements.

reduced folates of the cell. The interactions of osmolytes with one such folate pathway enzyme, DHPS, was further studied in Chapter 3. The effect of weak interactions of several osmolytes with the ligands of dihydropteroate synthase, as well as the effects of osmolytes on the enzyme itself were measured. Each osmolyte increase, or decreased, ligand binding in manner that was specific to the osmolyte and ligand; dependent upon the atom types with which the osmolyte preferentially interacts. Dihydropteroate synthase is a folate synthesis enzyme present in bacteria and serves as a major antibacterial drug target. Thus, the effect of osmolytes on sulfa drugs that affect DHPS were calculated and evaluated. We have used several biophysical, biochemical and computational technique to interpret and refine our understanding of weak interactions. We have explored how folate pathway enzymes behave in the midst of weak interactions and in the crowded cell in Chapter 4. In this chapter, we have connected the entire thesis to explain how osmotic stress affects cell growth and enzyme activity *in vivo*. These assays can be further extended in the future to be used to score for candidates affected by drugs.

5.5 References

[1] Tibbetts, A. S., and Appling, D. R. (2010) Compartmentalization of mammalian folate-mediated one-carbon metabolism, *Annu. Rev. Nutr. 30*, 57-81.

[2] Ducker, G. S., and Rabinowitz, J. D. (2017) One-carbon metabolism in health and disease, *J. Cell Metabol. 25*, 27-42.

[3] Cayley, S., and Record, M. T. (2003) Roles of cytoplasmic osmolytes, water, and crowding in the response of *Escherichia coli* to osmotic stress: biophysical basis of osmoprotection by glycine betaine, *Biochemistry 42*, 12596-12609.

[4] Chopra, S., Dooling, R. M., Horner, C. G., and Howell, E. E. (2008) A balancing act between net uptake of water during dihydrofolate binding and net release of water upon NADPH binding in R67 dihydrofolate reductase, *J. Biol. Chem. 283*, 4690-4698.

[5] Grubbs, J., Rahmanian, S., DeLuca, A., Padmashali, C., Jackson, M., Duff Jr, M. R., and Howell, E. E. (2011) Thermodynamics and solvent effects on substrate and cofactor binding in *Escherichia coli* chromosomal dihydrofolate reductase, *Biochemistry 50*, 3673-3685.

[6] Bhojane, P. P., Duff Jr, M. R., Bafna, K., Rimmer, G. P., Agarwal, P. K., and Howell, E. E. (2016) Aspects of weak interactions between folate and glycine betaine, *Biochemistry 55*, 6282-6294.

[7] Duff Jr, M. R., Grubbs, J., Serpersu, E., and Howell, E. E. (2012) Weak interactions between folate and osmolytes in solution, *Biochemistry 51*, 2309-2318.

[8] Sapir, L., and Harries, D. (2010) Linking trehalose self-association with binary aqueous solution equation of state, *J. Phys. Chem. B 115*, 624-634.

[9] Hong, J., Gierasch, L. M., and Liu, Z. (2015) Its preferential interactions with biopolymers account for diverse observed effects of trehalose, *Biophys. J. 109*, 144-153.

[10] Cayley, S., Lewis, B., and Record, M. (1992) Origins of the osmoprotective properties of betaine and proline in *Escherichia coli* K-12, *J. Bacteriol. 174*, 1586-1595.

[11] Chopra, S., Lynch, R., Kim, S.-H., Jackson, M., and Howell, E. E. (2006) Effects of temperature and viscosity on R67 dihydrofolate reductase catalysis, *Biochemistry 45*, 6596-6605.

[12] Nambiar, D., Berhane, T.-K., Shew, R., Schwarz, B., Duff, M. R., and Howell, E. E. (2018) In vivo Titration of Folate Pathway Enzymes, *Appl. Environ. Microbiol. 84*, e01139-01118.

[13] Kumar, R., and biophysics. (2009) Role of naturally occurring osmolytes in protein folding and stability, *Arch. Biochem. 491*, 1-6.

[14] Knowles, D., Shkel, I. A., Phan, N. M., Sternke, M., Lingeman, E., Cheng, X., Cheng, L., O'Connor, K., and Record, M. T. (2015) Chemical interactions of polyethylene glycols (PEGs) and glycerol with protein functional groups: applications to effects of PEG and glycerol on protein processes, *Biochemistry 54*, 3528-3542.

[15] Capp, M. W., Pegram, L. M., Saecker, R. M., Kratz, M., Riccardi, D., Wendorff, T., Cannon, J. G., and Record Jr, M. T. (2009) Interactions of the osmolyte glycine betaine with molecular surfaces in water: thermodynamics, structural interpretation, and prediction of m-values, *Biochemistry 48*, 10372-10379.

[16] Diehl, R. C., Guinn, E. J., Capp, M. W., Tsodikov, O. V., and Record Jr, M. T. (2013) Quantifying additive interactions of the osmolyte proline with individual functional groups of proteins: comparisons with urea and glycine betaine, interpretation of m-values, *Biochemistry 52*, 5997-6010.
[17] Peral, F., and Gallego, E. (1997) Self-association of imidazole and its methyl derivatives in aqueous solution. A study by ultraviolet spectroscopy, *J. Mol. Struct. 415*, 187-196.
[18] Simpson, A. (2001) Multidimensional solution state NMR of humic substances: a practical guide and review, *Soil Sci. 166*, 795-809.
[19] Winther, L. R., Qvist, J., and Halle, B. (2012) Hydration and mobility of trehalose in aqueous solution, *J. Phys. Chem. B 116*, 9196-9207.
[20] Leuner, C., and Dressman, J. (2000) Improving drug solubility for oral delivery using solid dispersions, *Eur. J. Pharm. Biopharm. 50*, 47-60.
[21] Craig, D. Q. (2002) The mechanisms of drug release from solid dispersions in water-soluble polymers, *Int. J. Pharm. 231*, 131-144.
[22] Babaoglu, K., Qi, J., Lee, R. E., and White, S. W. (2004) Crystal structure of 7, 8-dihydropteroate synthase from *Bacillus anthracis*: mechanism and novel inhibitor design, *Structure 12*, 1705-1717.
[23] Yun, M.-K., Wu, Y., Li, Z., Zhao, Y., Waddell, M. B., Ferreira, A. M., Lee, R. E., Bashford, D., and White, S. W. (2012) Catalysis and sulfa drug resistance in dihydropteroate synthase, *Science 335*, 1110-1114.
[24] Zhao, Y., Shadrick, W. R., Wallace, M. J., Wu, Y., Griffith, E. C., Qi, J., Yun, M.-K., White, S. W., and Lee, R. E. (2016) Pterin–sulfa conjugates as dihydropteroate synthase inhibitors and antibacterial agents, *Bioorg. Med. Chem. Lett. 26*, 3950-3954.
[25] Kwon, Y. K., Lu, W., Melamud, E., Khanam, N., Bognar, A., and Rabinowitz, J. D. (2008) A domino effect in antifolate drug action in *Escherichia coli*, *Nat. Chem. Biol. 4*, 602.
[26] Kast, P., Asif-Ullah, M., Jiang, N., and Hilvert, D. (1996) Exploring the active site of chorismate mutase by combinatorial mutagenesis and selection: the importance of electrostatic catalysis, *Proc. Natl. Acad. Sci. 93*, 5043-5048.
[27] Hermes, J. D., Blacklow, S. C., and Knowles, J. R. (1990) Searching sequence space by definably random mutagenesis: improving the catalytic potency of an enzyme, *Proc. Natl. Acad. Sci. 87*, 696-700.
[28] Hengge, R. (2009) Principles of c-di-GMP signalling in bacteria, *Nat. Rev. Microbiol. 7*, 263.
[29] O'Neal, L., Ryu, M.-H., Gomelsky, M., and Alexandre, G. (2017) Optogenetic manipulation of cyclic di-GMP (c-di-GMP) levels reveals the role of c-di-GMP in regulating aerotaxis receptor activity in *Azospirillum brasilense*, *J. Bacteriol. 199*, e00020-00017.
[30] Griffith, E. C., Wallace, M. J., Wu, Y., Kumar, G., Gajewski, S., Jackson, P., Phelps, G. A., Zheng, Z., Rock, C. O., and Lee, R. E. (2018) The Structural and Functional Basis for Recurring Sulfa Drug Resistance Mutations in *Staphylococcus aureus* Dihydropteroate Synthase, *Front. Microbiol. 9*.

[31] Cayley, S., Lewis, B. A., Guttman, H. J., and Record Jr, M. T. (1991) Characterization of the cytoplasm of *Escherichia coli* K-12 as a function of external osmolarity: implications for protein-DNA interactions in vivo, *J. Mol. Biol. 222*, 281-300.

[32] Gabel, S. A., Duff, M. R., Pedersen, L. C., DeRose, E. F., Krahn, J. M., Howell, E. E., and London, R. E. (2017) A structural basis for biguanide activity, *Biochemistry 56*, 4786-4798.

[33] Cabreiro, F., Au, C., Leung, K.-Y., Vergara-Irigaray, N., Cochemé, H. M., Noori, T., Weinkove, D., Schuster, E., Greene, N. D., and Gems, D. (2013) Metformin retards aging in *C. elegans* by altering microbial folate and methionine metabolism, *Cell 153*, 228-239.

VITA

Deepika Karunakaran Nambiar was born in Mumbai, India in the year 1985. She attended Children's Academy, Kandivali in Mumbai. She then obtained her Bachelor's degree in Microbiology from Sathaye College, University of Mumbai. After completing her Bachelor's program, she successfully completely a Master's degree in Microbiology from Bhavan's College, University of Mumbai. Upon completion of her Master's program, Deepika worked as an intern at Unilever, Bangalore for 6 months and as a Junior Research Fellow at the Radiation Medicine Center, BARC for one year. Deepika then joined the University of Tennessee, Knoxville to pursue her doctoral degree in Biochemistry in the Biochemistry, Cellular and Molecular Biology department. She has interned in Unilever, Trumbull, USA in Summer 2019. Upon completion of her doctoral degree, she plans to pursue research in an industry.